

(NASA-CR-179077) WIND TUNNEL TEST IA300  
ANALYSIS AND RESULTS, VOLUME 1 Interim  
Report (Lockheed Missiles and Space Co.)  
128 p Avail: NTIS HC A07/MF A01 CSCL 01A

N87-21858

Unclassified  
G3/02 0071139

# WIND TUNNEL TEST IA300 ANALYSIS AND RESULTS

VOLUME I - <sup>INTERIM</sup> ~~FINAL~~ REPORT

January 1987

Contract NAS8-33807

Prepared for

**NATIONAL AERONAUTICS AND SPACE ADMINISTRATION  
MARSHALL SPACE FLIGHT CENTER, AL 35812**

by

P.B. Kelley

W.B. Beaufait

L.L. Kitchens

J.P. Pace

 **Lockheed**  
*Missiles & Space Company, Inc.*  
Huntsville Engineering Center  
4800 Bradford Drive, Huntsville, AL 35807

FOREWORD

This final report presents the results of work performed by personnel of the Aerodynamics Systems Group of Lockheed's Huntsville Engineering Center for NASA-MSFC under Contract NAS8-33807. The NASA Contracting Officer's Representative and technical monitor for this contract was Mr. Charlie C. Dill, Jr., to whom the authors are grateful for his valuable assistance, direction, and contributions to the successful completion of this study.

This report is presented in three volumes as follows:

Volume I - Final Report

Volume II - Appendix A

Volume III - Appendixes B, C, D, E

## CONTENTS

<u>Section</u>		<u>Page</u>
	FOREWORD	ii
1	INTRODUCTION	1-1
2	WIND TUNNEL MODEL	2-1
3	TEST PROGRAM	3-1
4	MODEL NOZZLE CALIBRATION	4-1
5	PLUME SIMULATION	5-1
6	DATA ANALYSIS AND INTEGRATION MODEL	6-1
6.1	Orbiter Base	6-4
6.2	OMS Pods	6-9
6.3	Body Flap	6-9
6.4	Orbiter Forebody	6-9
6.5	Wing and Elevons	6-21
6.6	Vertical Tail	6-21
6.7	SRB Base Pressure	6-34
6.8	SRB Forebody	6-34
6.9	ET Base	6-34
6.10	ET Forebody	6-51
7	ANALYSIS OF TEST RESULTS	7-1
8	TEST RESULTS INTEGRATION	8-1
9	REFERENCES	9-1

Appendices

A	Data Listings	A-1
B	Longitude vs Mach (-4, 0), ( $C_N$ , $C_M$ )	B-1
C	Gimbal Effects at $M = 0.9, 1.1, 1.25$	C-1
D	Longitude vs Alpha, ( $C_N$ , $C_M$ )	D-1
E	Latitude vs Beta, ( $C_Y$ , $C_{YN}$ , $C_L$ )	E-1

~~PRECEDED PAGE BLANK NOT FILMED~~

## LIST OF TABLES

<u>Table</u>		<u>Page</u>
3-1	IA300 Cold Flow Test Configurations	3-3
4-1	TWT-680 Nozzle Configuration	4-1
4-2	TWT-583 Nozzle Configuration	4-3
5-1	Ascent Trajectory and SRB-SSME Chamber Pressure	5-12
6-1	Effective Area Modeling of Taps for Orbiter Forebody	6-7
6-2	OMS Pod (Left Side)	6-11
6-3	Effective Area Used for Pressure Integration	6-15
6-4	Effective Area Modeling Representative Locations	6-23
6-5	Effective Area Modeling of Taps for Right Orbiter Wing	6-29
6-6	Effective Area Modeling of Taps for Vertical Tail	6-40
6-7	Effective Area Modeling of Taps for SRB Base	6-44
6-8	Effective Area Modeling of Taps for Left Orbiter Forebody	6-46
6-9	Effective Area Modeling of Taps for ET Base	6-50
6-10	Effective Area Modeling of Taps for ET Forebody	6-59

## LIST OF FIGURES

<u>Figure</u>		<u>Page</u>
2-1	Launch Configuration	2-2
2-2	Orbiter Configuration	2-3
2-3	External Tank (General Arrangement)	2-4
2-4	Solid Rocket Booster (General Arrangement)	2-5
2-5a	Single Strut Configuration	2-6
2-5b	Dual Strut Configuration	2-7
2-6	Nozzle Dimensions	2-8
2-7	IA300 Orbiter Fuselage Pressure Instrumentation	2-10
2-8	Orbiter Body Flap Pressure Instrumentation	2-11
2-9	Orbiter Base Pressure Instrumentation	2-12
2-10	IA300 Orbiter Wing Pressure Instrumentation	2-13
2-11	Orbiter SSME Nozzle Pressure Instrumentation	2-14
2-12	OMS Engine Nozzle Pressure Instrumentation	2-15
2-13	IA300 Vertical Tail Pressure Instrumentation	2-16
2-14	External Tank Pressure Instrumentation	2-17
2-15	IA300 External Tank Base Pressure Instrumentation	2-18
2-16	IA300 SRB Pressure Instrumentation	2-19
2-17	IA300 SRB Aft Skirt Pressure Instrumentation	2-20
4-1	TWT-680 Test Results	4-2
4-2	TWT-683 Test Results (Configurations 63 and 64)	4-4
4-3	TWT-683 Test Results (Configurations 61 and 62)	4-5

~~PRECEDING PAGE BLANK NOT FILMED~~

## LIST OF FIGURES (Continued)

<u>Figure</u>		<u>Page</u>
5-1	IA300 SSME/SRB Chamber Pressure vs Base Pressures for SRB, ET, and Orbiter	5-2
5-2	Comparison of Base Pressure for IA300 Nominal SSME/SRB Power Levels	5-3
5-3	SSME Similarity Parameter (Configuration 61)	5-4
5-4	SSME Similarity Parameter (Configuration 62)	5-5
5-5	SSME Similarity Parameter (Configuration 63)	5-6
5-6	SSME Similarity Parameter (Configuration 64)	5-7
5-7	SSME Mach Numbers (Configuration 61)	5-8
5-8	SSME Mach Numbers (Configuration 62)	5-9
5-9	SSME Mach Numbers (Configuration 63)	5-10
5-10	SSME Mach Numbers (Configuration 64)	5-11
5-11	Total Envelope of all Orbiter Flight Base Pressures (STS 1-5)	5-13
5-12	Total Envelope of all ET Flight Base Pressures (STS 1-5)	5-14
5-13	Total Envelope of all SRB Flight Base Pressures (STS 1-5)	5-15
6-1a	Plume Flowfield Areas	6-2
6-1b	Sample of Data Set Listing	6-3
6-2	IA300 Orbiter Base Pressure Instrumentation	6-5
6-3	Orbiter Base Relative Areas	6-6
6-4	Comparison of Base Pressure Instrumentations	6-8
6-5	OMS Pod Areas	6-10
6-6	Orbiter Body Flap Pressure Instrumentation	6-12
6-7a	Upper Body Flap Areas	6-13
6-7b	Lower Body Flap Areas	6-14
6-8	Orbiter Forebody Pressure Instrumentation	6-16
6-9a	Sample Analysis Plots ( $M_\infty = 0.60; 0.80; 0.90$ )	6-17
6-9b	Sample Analysis Plots ( $M_\infty = 0.95; 1.05; 1.10$ )	6-18
6-10	Sample Analysis Plots ( $M_\infty = 0.60; 0.80; 0.90$ )	6-19
6-11	Power $\Delta C_p$ Along Orbiter Fuselage	6-20
6-12	Orbiter Forebody Effective Area Modeling	6-22
6-13	Orbiter Wing Pressure Instrumentation Layout	6-25
6-14	Orbiter Wing Pressure Integration	6-26
6-15	Wing Pressure Evaluation	6-27
6-16	Wing Pressure Instrumentation Areas	6-28
6-17	Wing and Elevon Force and Moment Sign Convention	6-32
6-18	IA300 Vertical Tail Instrumentation	6-33
6-19a	Power $\Delta C_p$ , Nominal Power, Mach 0.8	6-35
6-19b	Power $\Delta C_p$ , High Power, Mach 0.9	6-36
6-19c	Power, $\Delta C_p$ , Nominal Power, Mach 1.25	6-37
6-19d	Power, $\Delta C_p$ , High Power, Mach 1.25	6-38

~~PRECEDING PAGE BLANK NOT FILMED~~

## LIST OF FIGURES (Concluded)

<u>Figure</u>		<u>Page</u>
6-20	Vertical Tail Pressure Integration	6-39
6-21	Vertical Tail Force and Moment Sign Convention	6-41
6-22	SRB Base Instrumentation Layout	6-42
6-23	SRB Base Effective Area	6-43
6-24	IA300 SRB Pressure Instrumentation	6-45
6-25	ET Base Instrumentation Layout	6-48
6-26	ET Base Effective Area Modeling	6-49
6-27	ET Forebody Instrumentation Layout	6-52
6-28a	IA300 ET Rings - Forebody ( $\Delta C_{p,pwr} \times 100$ )	6-53
6-28b	IA300 ET Rings - Forebody ( $\Delta C_{p,pwr} \times 100$ )	6-54
6-28c	IA300 ET Rings - Forebody ( $\Delta C_{p,pwr} \times 100$ )	6-55
6-28d	IA300 ET Rings - Forebody ( $\Delta C_{p,pwr} \times 100$ )	6-56
6-29a	ET Power Delta - Dual Strut ( $\Delta C_p \times 100$ )	6-57
6-29b	ET Power Delta - Dual Strut, 35 deg Nozzle ( $\Delta C_p \times 100$ )	6-58
7-1	Comparison of Orbiter Normal Force Coefficient Plume Increments with Flight Extracted Data	7-2
7-2	Comparison of Orbiter Wing Normal Force Coefficient Plume Increments with Flight Extracted Data	7-3
7-3	Comparison of Orbiter Wing Hinge Moment Coefficient Plume Increments with Flight Extracted Data	7-4
7-4	SSLV and Element Normal Force Coefficient Characteristics (With and Without Plume Increments)	7-6
7-5	Comparison of ET Normal Force Coefficient Plume Increments (With Flight Extracted Data)	7-7
7-6	Orbiter Pitching Moment Coefficient Plume Increments	7-9
8-1	Sample of Data Listing	8-2
8-2	Sample of Analysis Plots in Appendix B	8-4
8-3	Sample of Analysis Plots in Appendix C	8-5
8-4	Sample of Analysis Plots in Appendix D	8-6
8-5	Sample of Analysis Plots in Appendix E	8-7

## 1. INTRODUCTION

This document presents the analysis and interpretation of wind tunnel pressure data from Space Shuttle wind tunnel test IA300. The primary objective of the test was to determine the effects of the SSME and SRB plumes on the integrated vehicle forebody pressure distributions, the elevon hinge moments, and wing loads. The results of this test will be combined with flight test results to form a new data base to be employed in the IVBC-3 airloads analysis. A secondary objective was to obtain solid plume data for correlation with the results of gaseous plume tests.

Wind tunnel test IA300 was a transonic test of a 0.01-scale model of the Space Shuttle Launch Vehicle (SSLV). The wind tunnel test was conducted in the 11 x 11-foot section of the NASA-Ames Research Center Unitary Plan Wind Tunnel during January and February 1983. Pressure data were obtained over portions of the entire wind tunnel model. The instrumentation consisted of surface pressure taps on the Orbiter, external tank and SRB strain gages on the Orbiter wing and elevons.

Air was used as a simulant gas to develop the model exhaust plumes. A portion of the test was devoted to testing at various power levels. Data from the power level portion was used in conjunction with flight base pressures to evaluate nominal power levels to be used during the investigation of changes in model attitude, elevon deflection and nozzle gimbal angle.

The plume induced aerodynamic loads were developed for the Space Shuttle base areas and forebody areas. A computer code was developed to integrate the pressure data. Using simplified geometrical models of the Space Shuttle elements and components. The pressure data were integrated to develop plume induced force and moment coefficients that can be combined

with a power-off data base to develop a power-on data base. The base areas include the Orbiter base including nozzles, ET base, and SRB base. The forebody includes the Orbiter areas forward of the base, including the body flap, wings and elevons, and ET and SRB areas forward of the base.

A math model of the plume induced aerodynamic characteristics was developed for a range of Mach numbers to match the forebody aerodynamic math model. The base aerodynamic characteristics are presented in terms of forces and moments versus attitude for the mission 3A reference trajectory. Total vehicle base and forebody aerodynamic characteristics are presented in terms of aerodynamic coefficient increments for Mach numbers 0.6 to 1.4. Element and component base and forebody aerodynamic increments are also presented for Mach numbers 0.6 to 1.4. These Mach numbers are compatible with defined forebody aerodynamic characteristics except for Mach 1.4. Base and forebody plume induced data are provided at Mach 1.4 since this was the highest Mach number for which data were available from the IA300 test.

## 2. WIND TUNNEL MODEL

The IA300 wind tunnel model was a 0.01-scale model (75-OTS) of the Space Shuttle Launch Vehicle configuration (Fig. 2-1). This model was essentially the same as was used for an earlier plume test, IA138, conducted in 1977. The Orbiter model was the 140C model configuration (Fig. 2-2) which generally represents the OV101 Orbiter mold lines. The External Tank model (Fig. 2-3) had all the significant protuberances and interstage hardware of the Light Weight Tank. The SRB models (Fig. 2-4) did not have the forward separation motors and TVC pod on the aft skirt modeled. Details of the model configuration are obtainable from the pretest report (Ref. 1).

The model was supported by two strut configurations as shown in Figs. 2-5a and 2-5b. In the dual strut configuration, the vertical tail is replaced by a dorsal strut supporting the Orbiter and housing the instrumentation as well as the high pressure air flow passages. This configuration allowed the interstage area between the Orbiter and ET to be simulated with minimum strut interference. The single strut configuration was used in order to measure the pressures on the upper fuselage, upper wing, and vertical tail with minimum strut interference.

The nozzles for both the Space Shuttle Main Engine (SSME) and Solid Rocket Boosters (SRBs) were conical nozzles as shown schematically in Fig. 2-6. Two different wall angles, 22 deg and 35 deg, were used for the SSME nozzles. The SRB nozzles used only the 35 deg wall angle. Calibration data for the nozzles are presented in Section 4. Details of the nozzle configurations can be obtained from the pretest report (Ref. 1) and the nozzle calibration report (Ref. 2).

The Orbiter was instrumented with 216 surface pressure taps distributed over the fuselage left wing, vertical tail and body flap. The right wing was

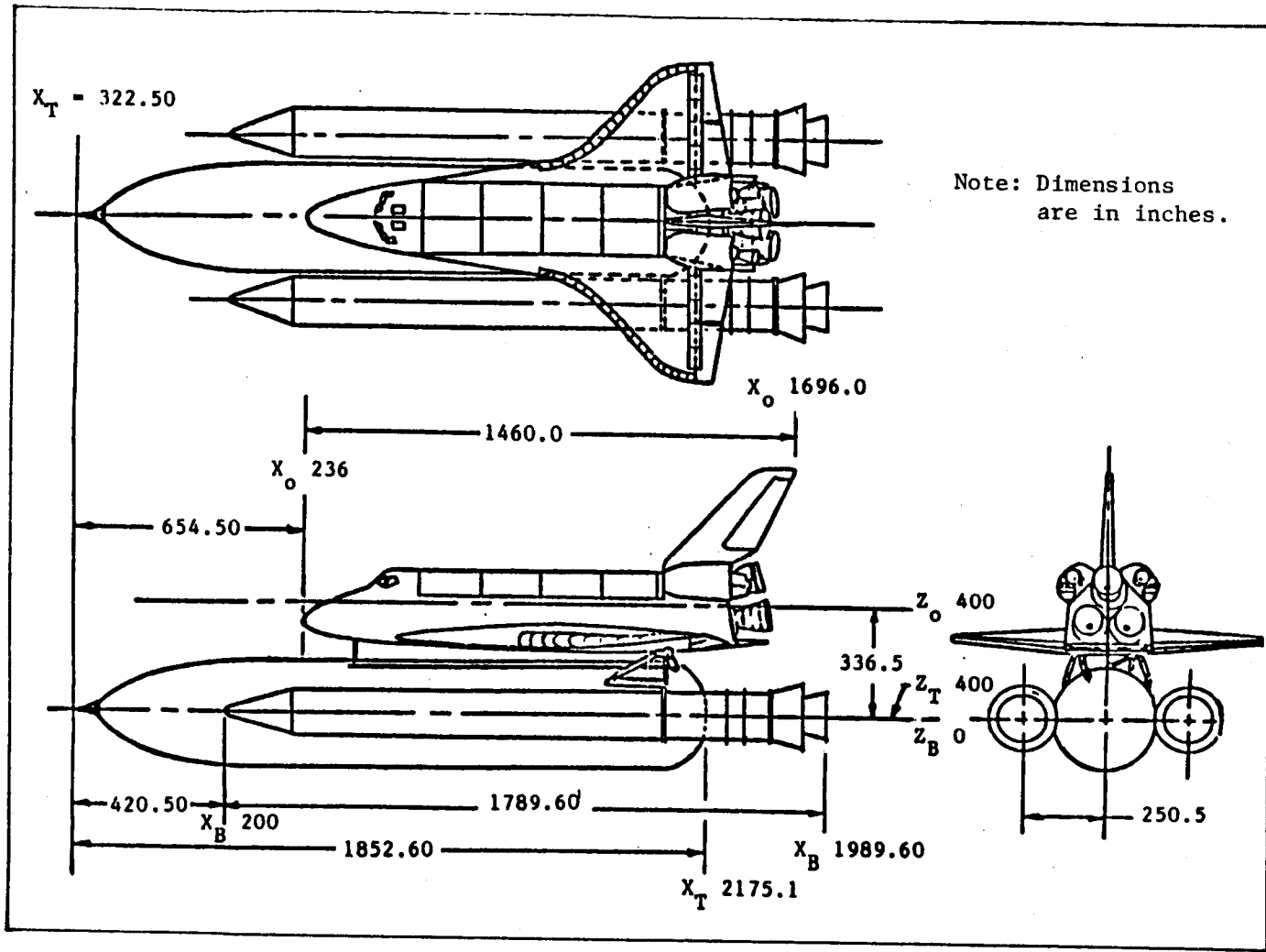


Fig. 2-1 Launch Configuration

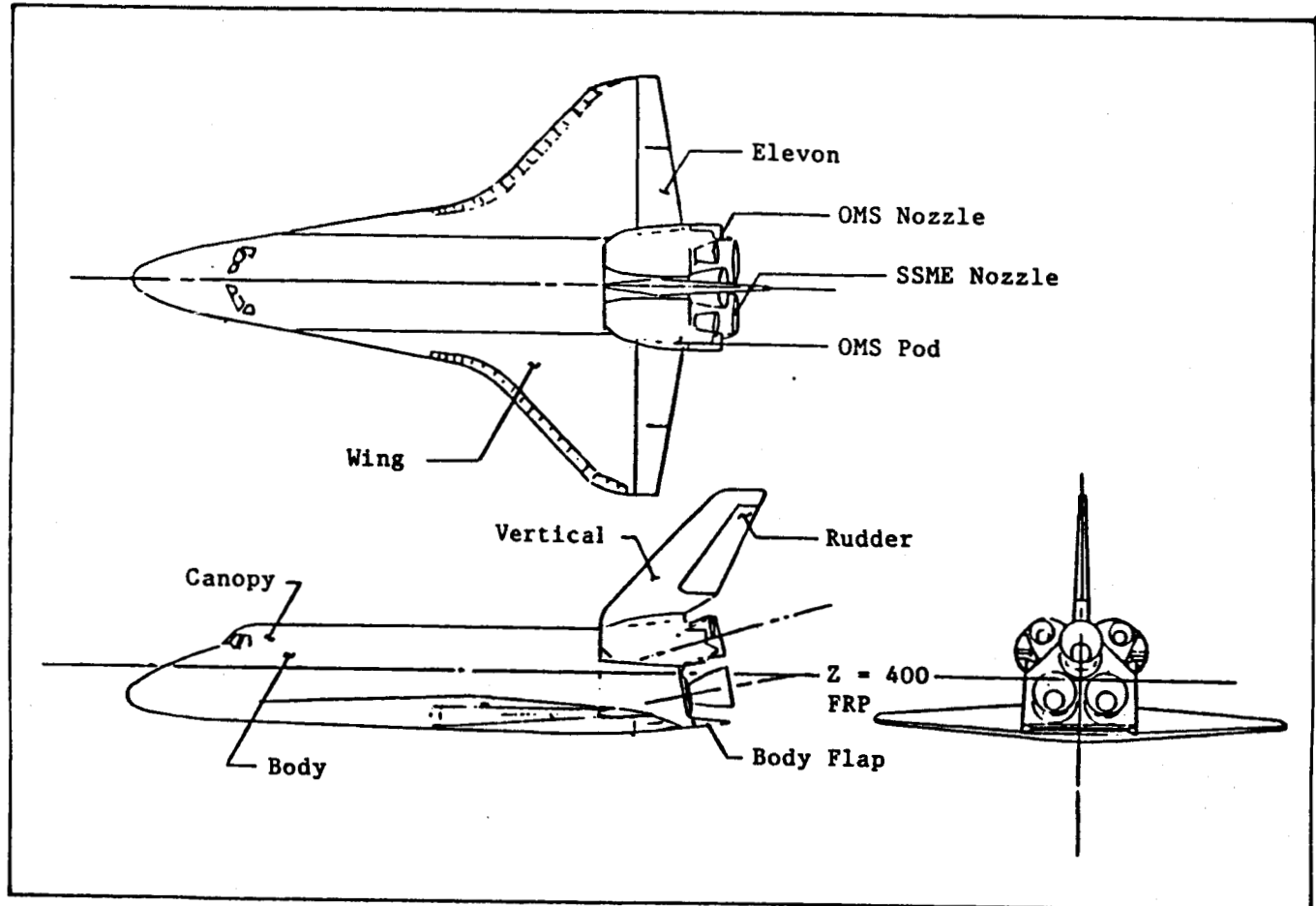


Fig. 2-2 Orbiter Configuration

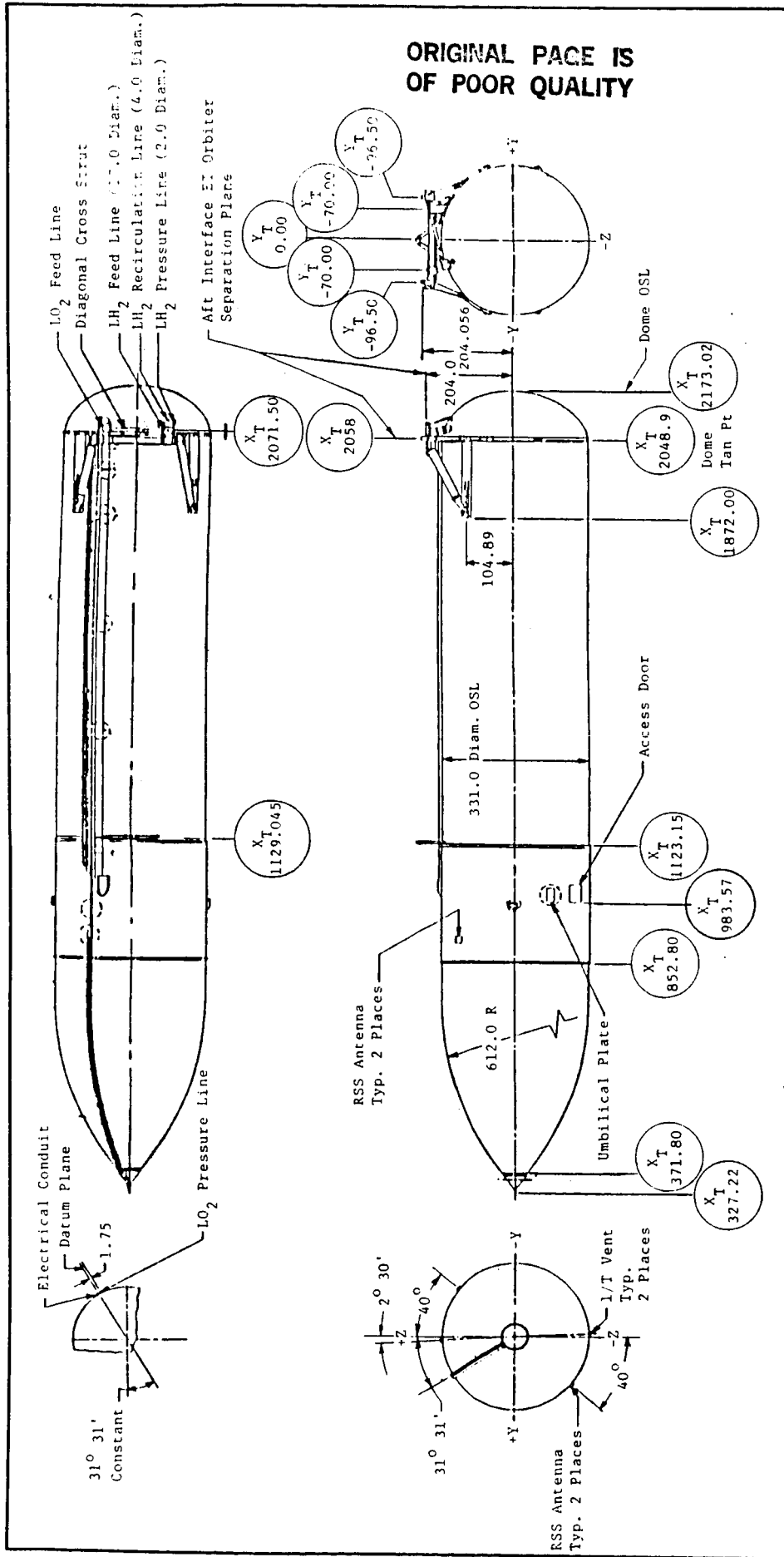


Fig. 2-3 External Tank (General Arrangement)

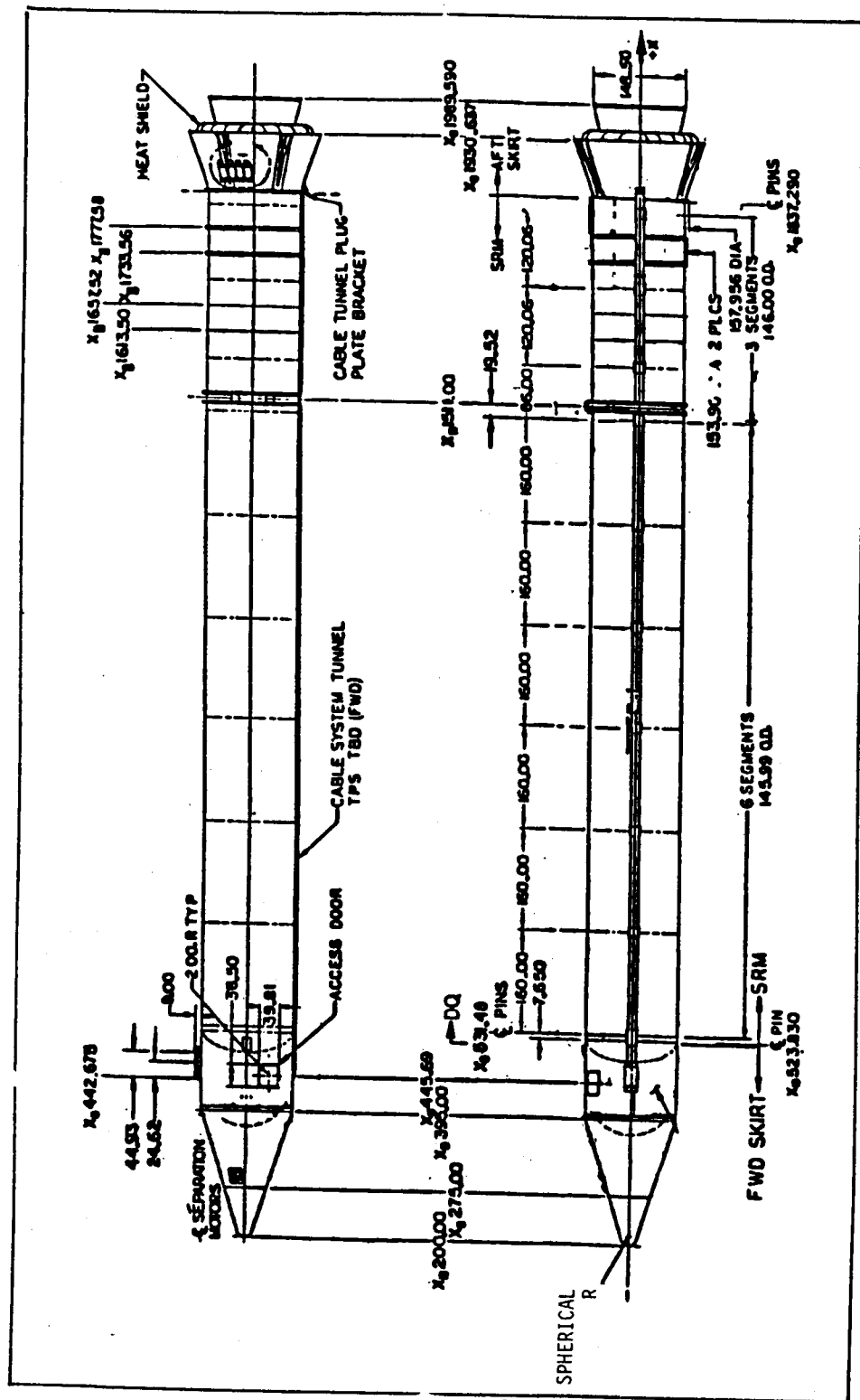


Fig. 2-4 Solid Rocket Booster (General Arrangement)

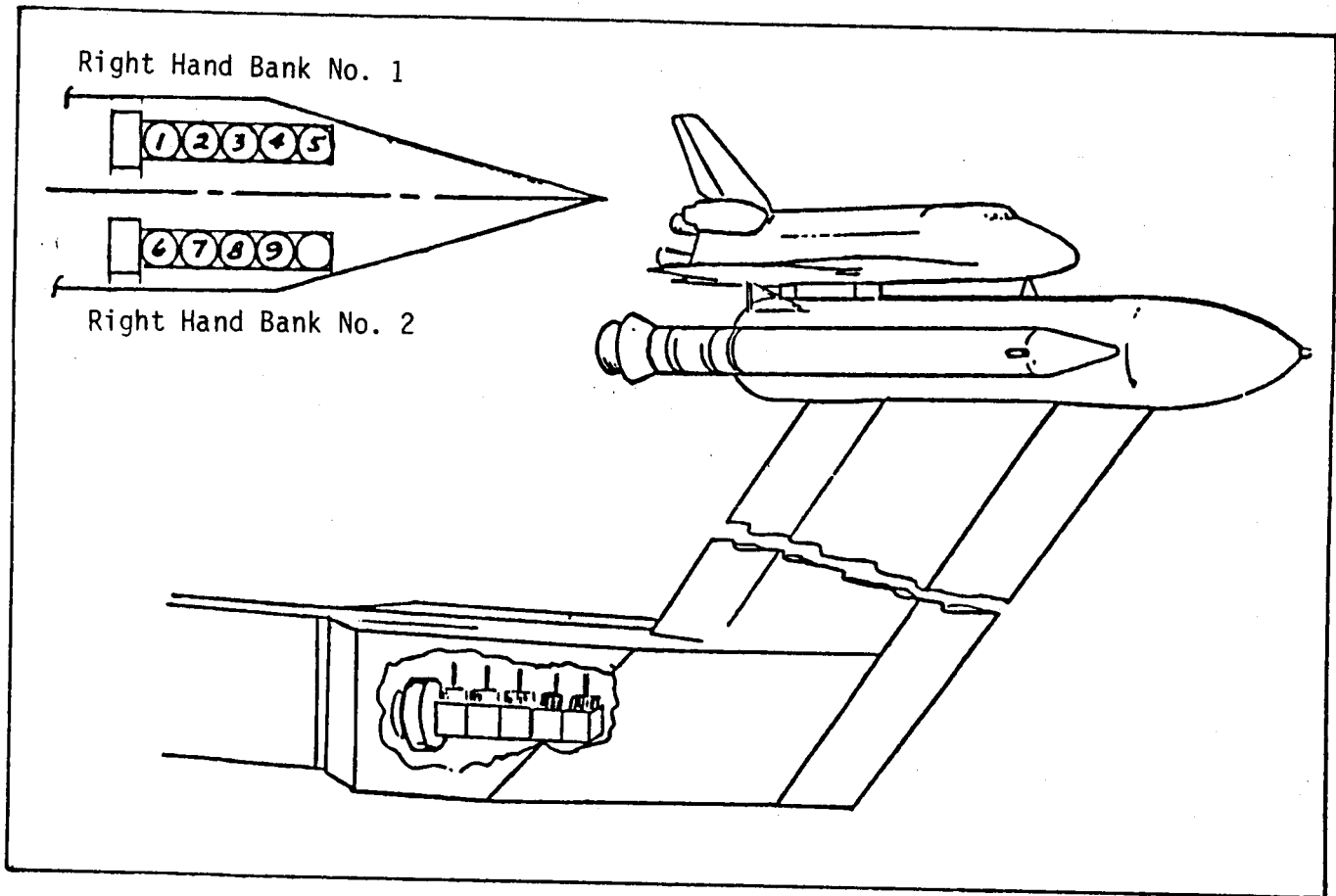


Fig. 2-5a Single Strut Configuration

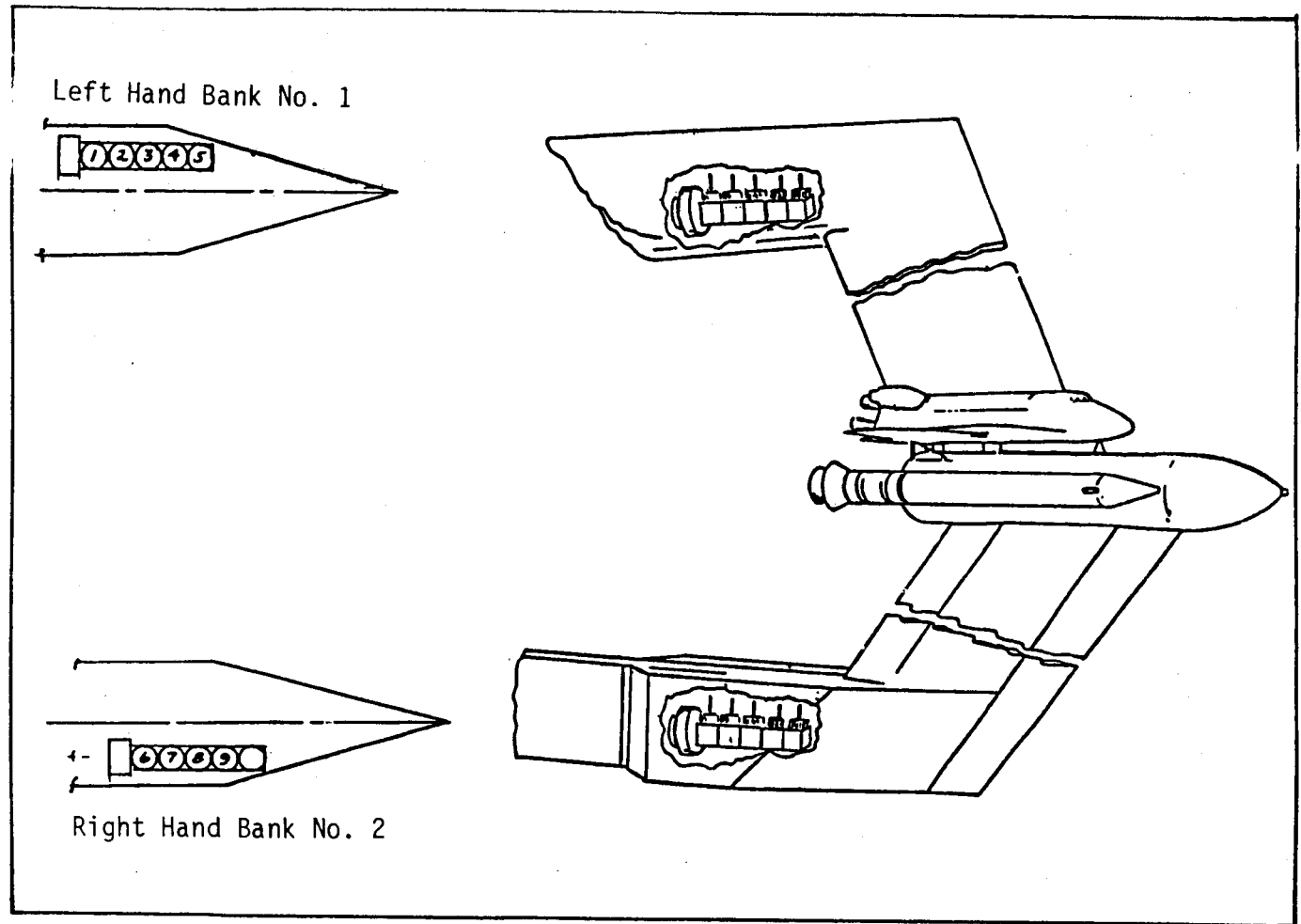
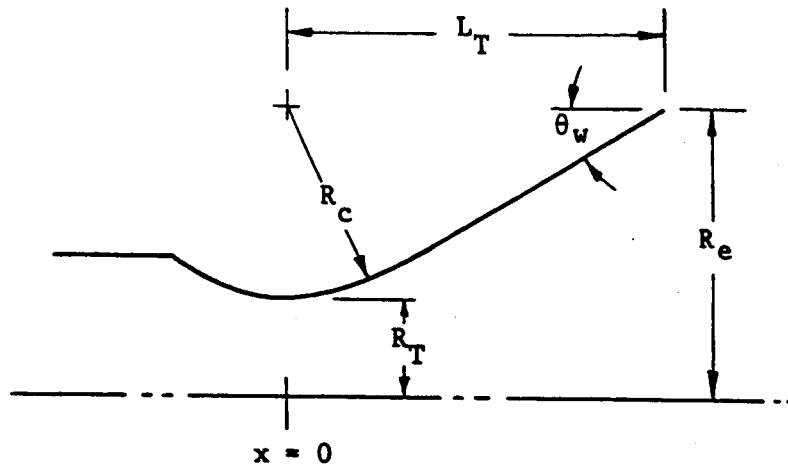


Fig. 2-5b Dual Strut Configuration



SSME ( $Re = .4536$  in.)

$\theta_w$ (deg)	$R_T$ (in.)	$Re/R_T$	$L_T$ (in.)
35	.2207	2.0554	.4022
22	.2035	2.2290	.6586

SRB ( $Re = .7283$  in.)

$\theta_w$ (deg)	$R_T$ (in.)	$Re/R_T$	$L_T$ (in.)
35	.3526	2.0655	0.6477
22	.2035	2.2290	1.0573

All Nozzles Conical.

$R_c/T_T = 1.0$  for All Nozzles.

Fig. 2-6 Nozzle Dimensions

gauged to obtain wing shear, root bending moment, and torsion moment data. The inboard and outboard elevons on the right wing were separately gauged to obtain hinge moment data. The wing and elevon gages were operational only during the early portions of the test and did not provide consistent data through the IA300 test.

The flow-through SSME and (SRB) nozzles were capable of being set at various gimbal positions with six gimbal patterns investigated during the test. The inboard and outboard elevons were also set at various deflection angles and data obtained for three combinations of settings.

The complete pressure instrumentation layout for the IA300 test is shown in Figs. 2-7 through 2-17.

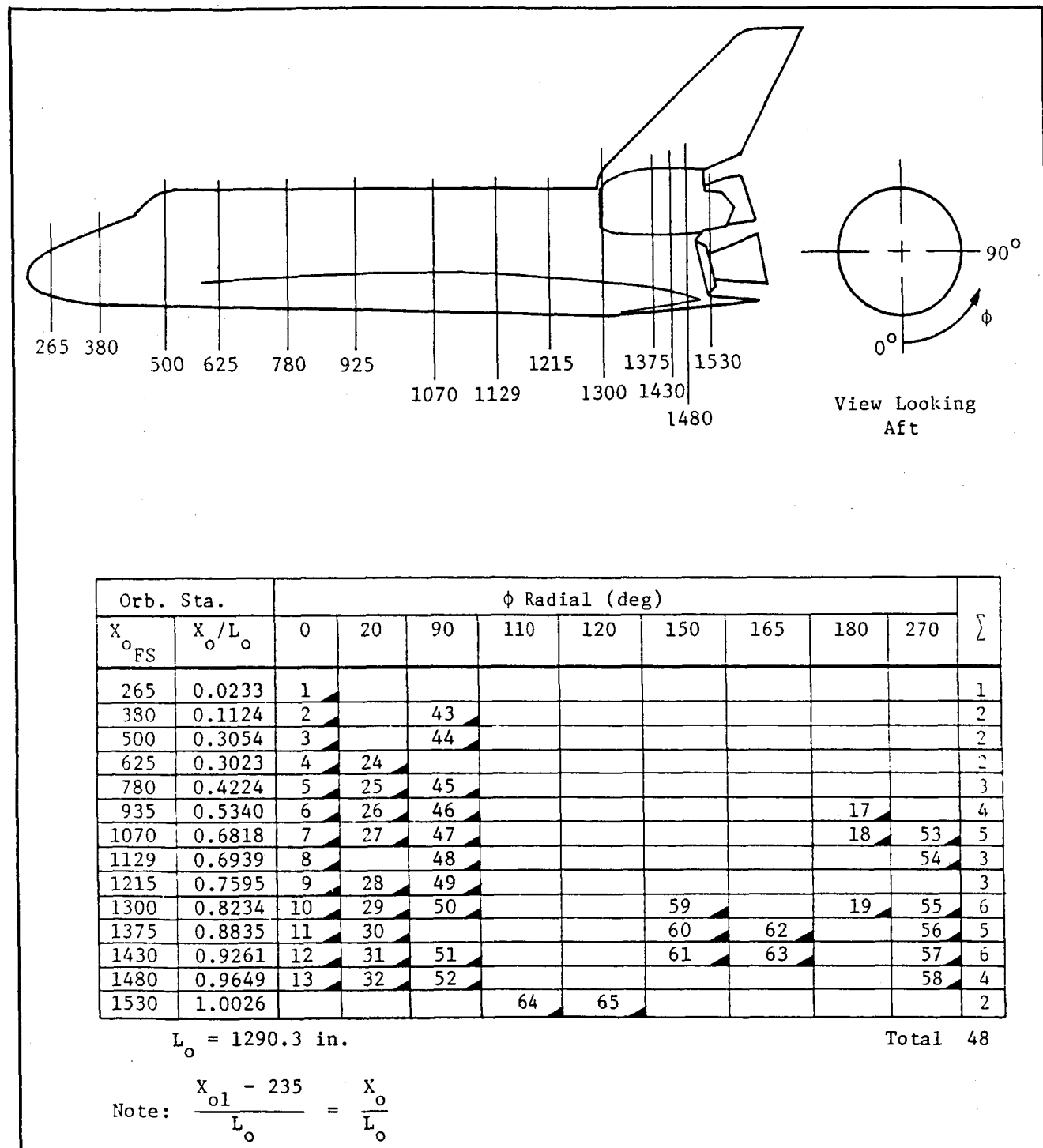


Fig. 2-7 IA300 Orbiter Fuselage Pressure Instrumentation

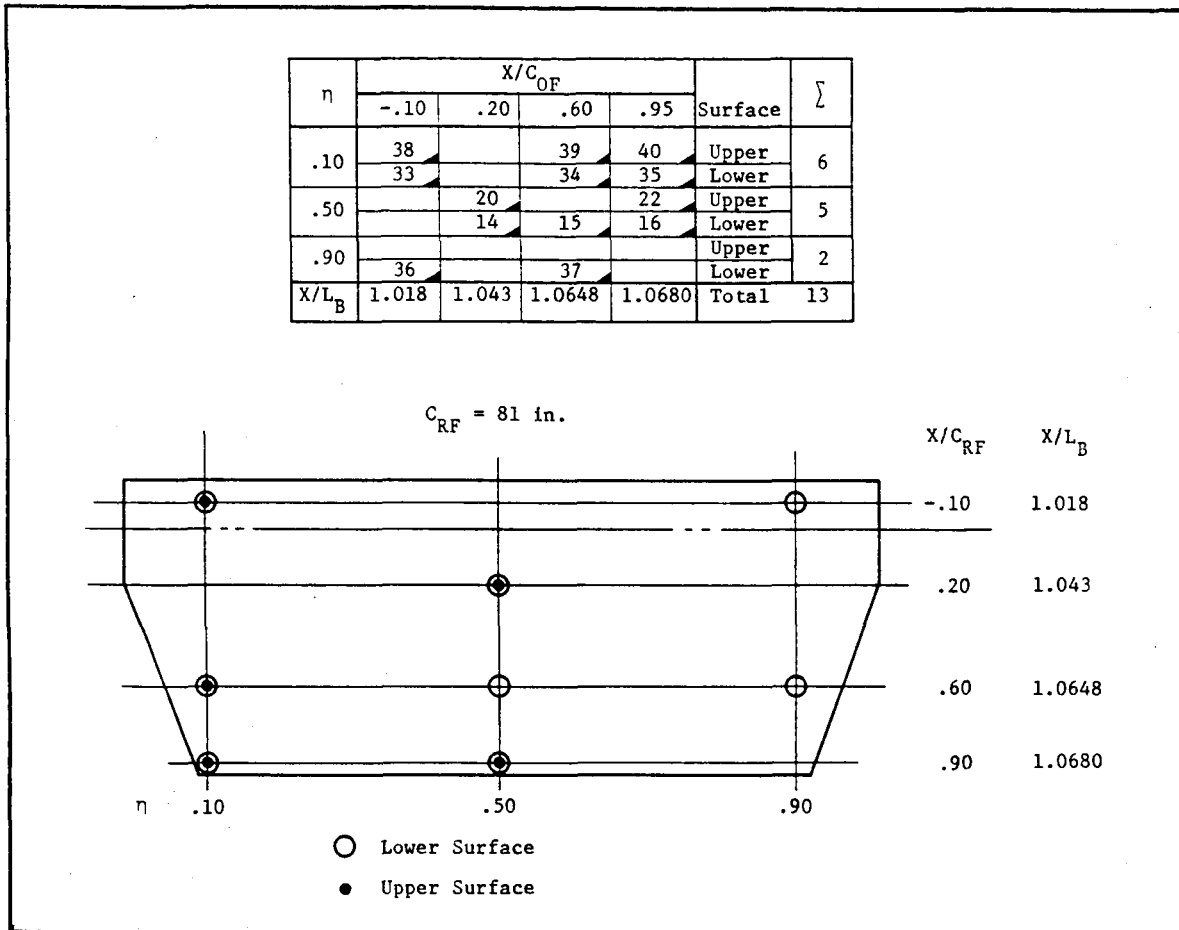


Fig. 2-8 Orbiter Body Flap Pressure Instrumentation

Tap	$Z_o$	$Y_o$
66	4.00	0
67	3.28	0
75	4.87	-0.49
76	4.12	-0.38
68	3.03	-0.26
77	4.25	-0.82
69	3.03	-0.89
73	4.32	-1.01
72	3.84	-1.00
71	3.50	-1.08
70	3.03	-1.24
80	5.14	-0.55
79	4.39	-1.07
78	4.65	-1.30
74	4.58	-0.68

Total 15 Taps

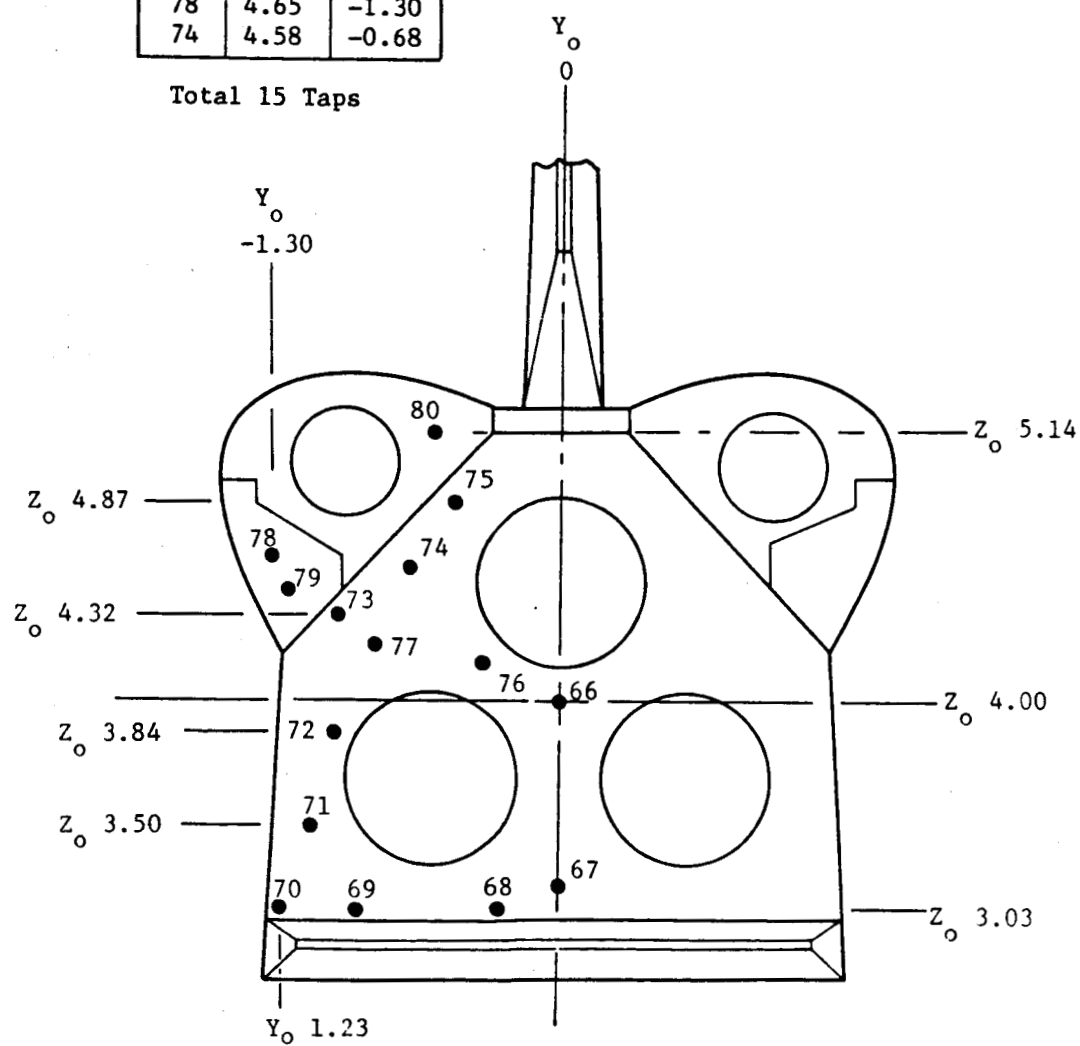


Fig. 2-9 Orbiter Base Pressure Instrumentation

ORIGINAL PAGE IS  
OF POOR QUALITY

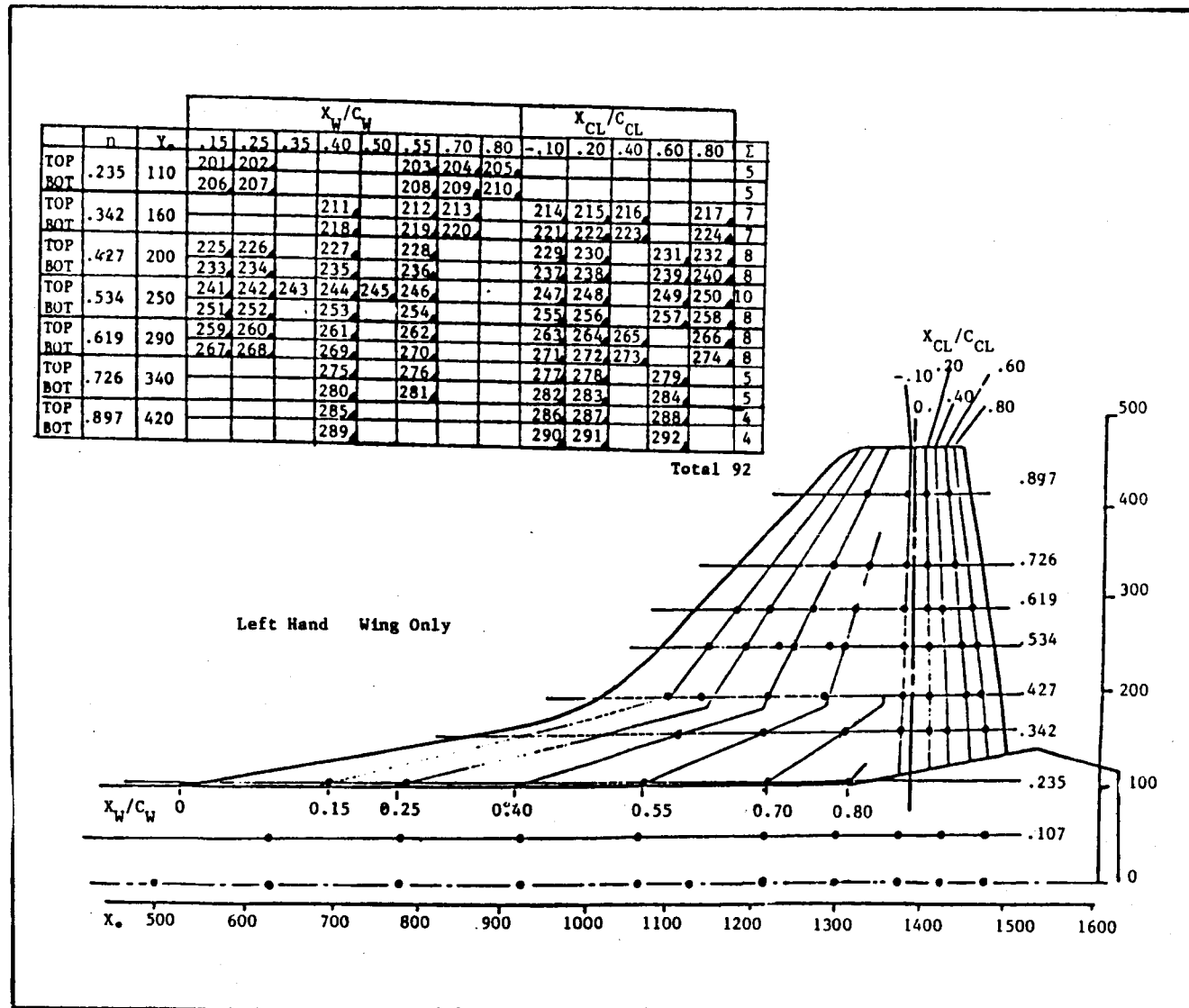


Fig. 2-10 IA300 Orbiter Wing Pressure Instrumentation

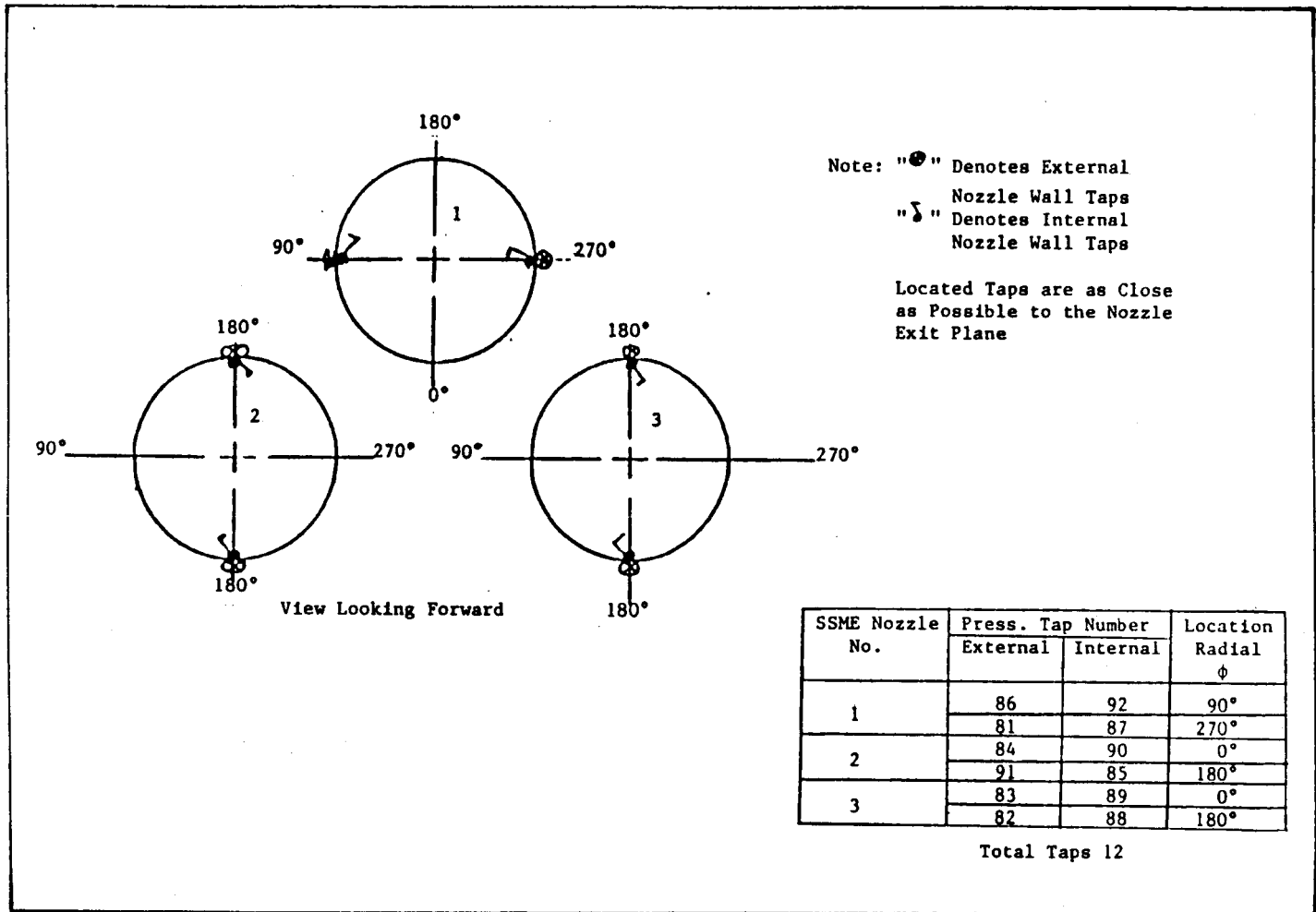


Fig. 2-11 Orbiter SSME Nozzle Pressure Instrumentation

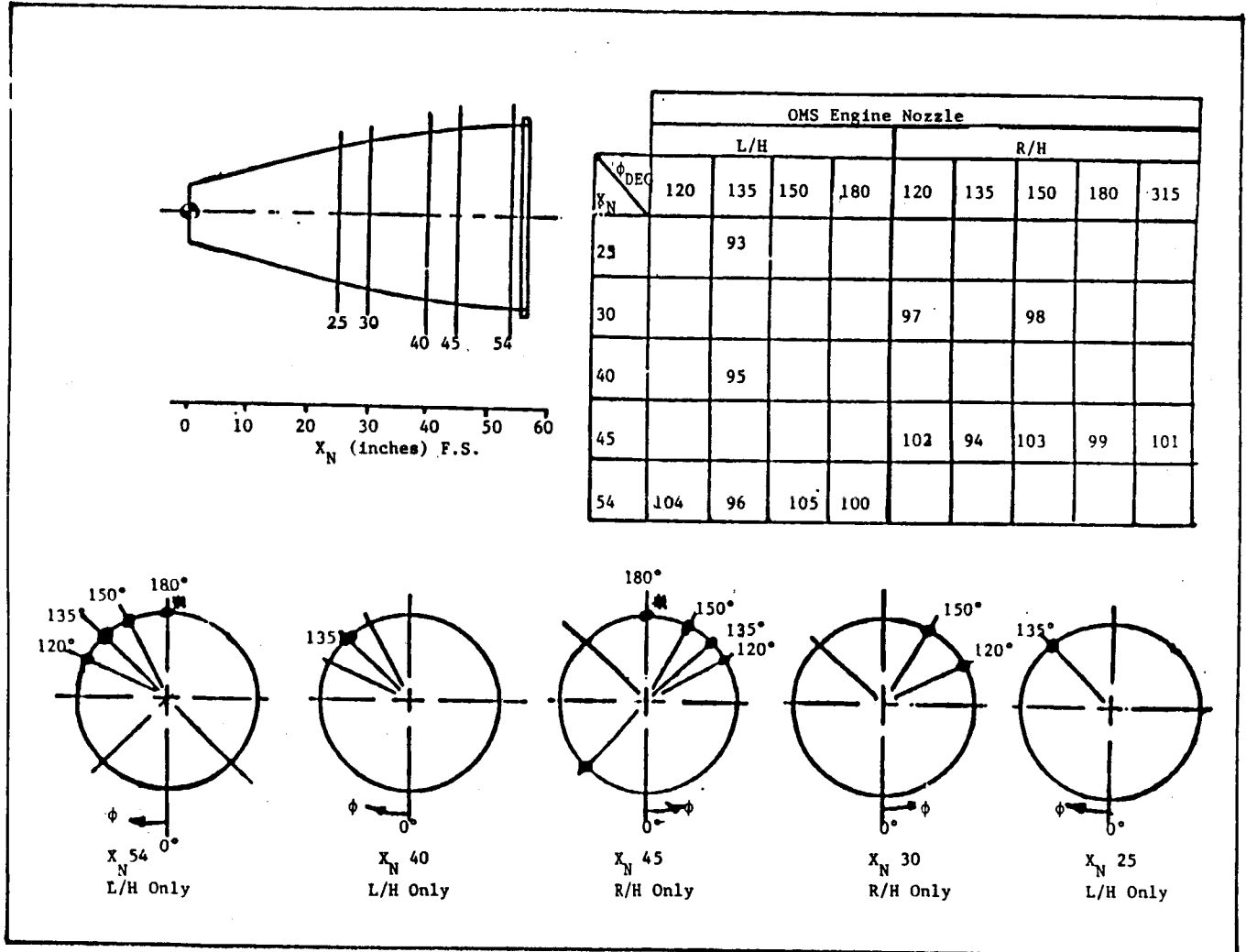


Fig. 2-12 OMS Engine Nozzle Pressure Instrumentation

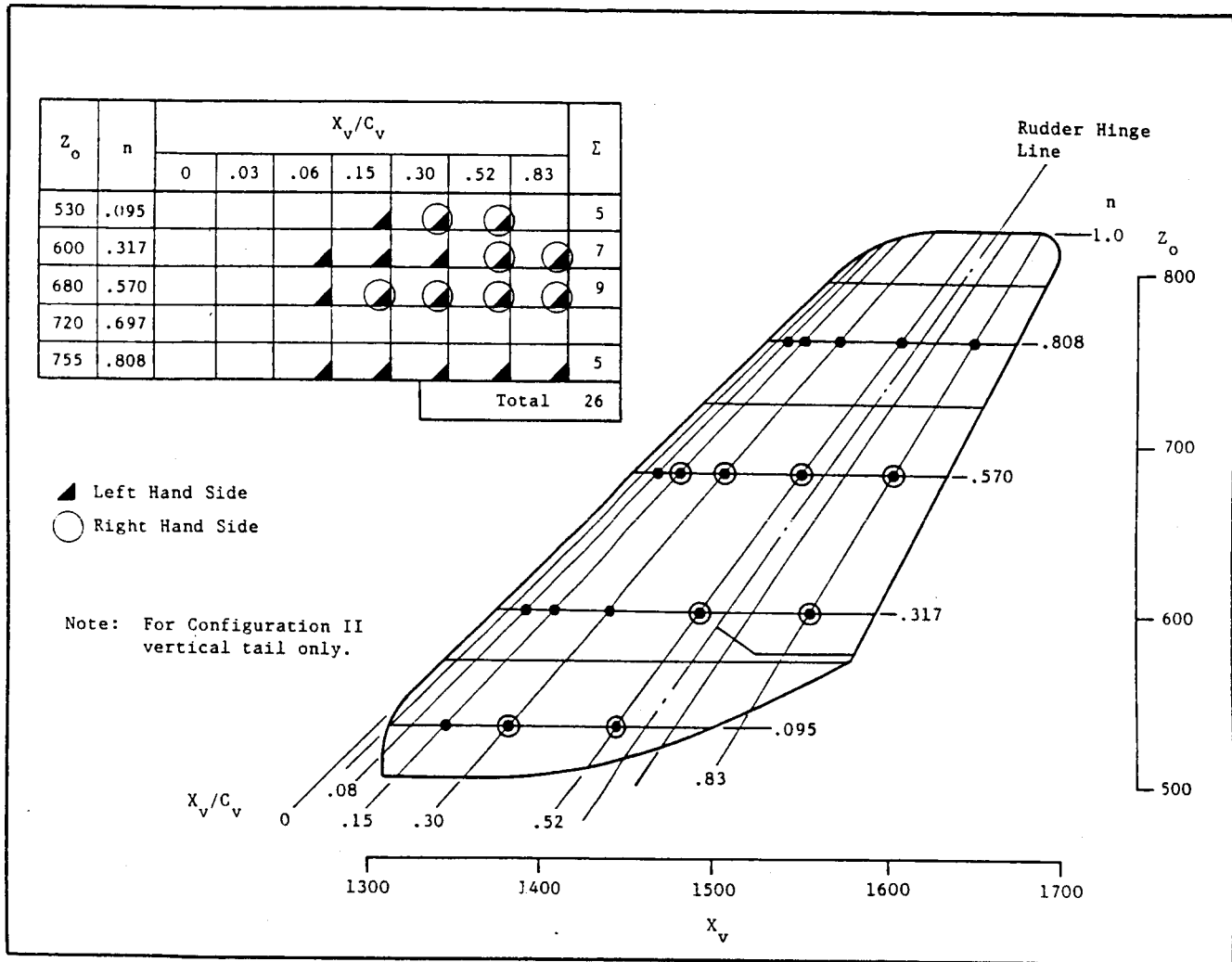
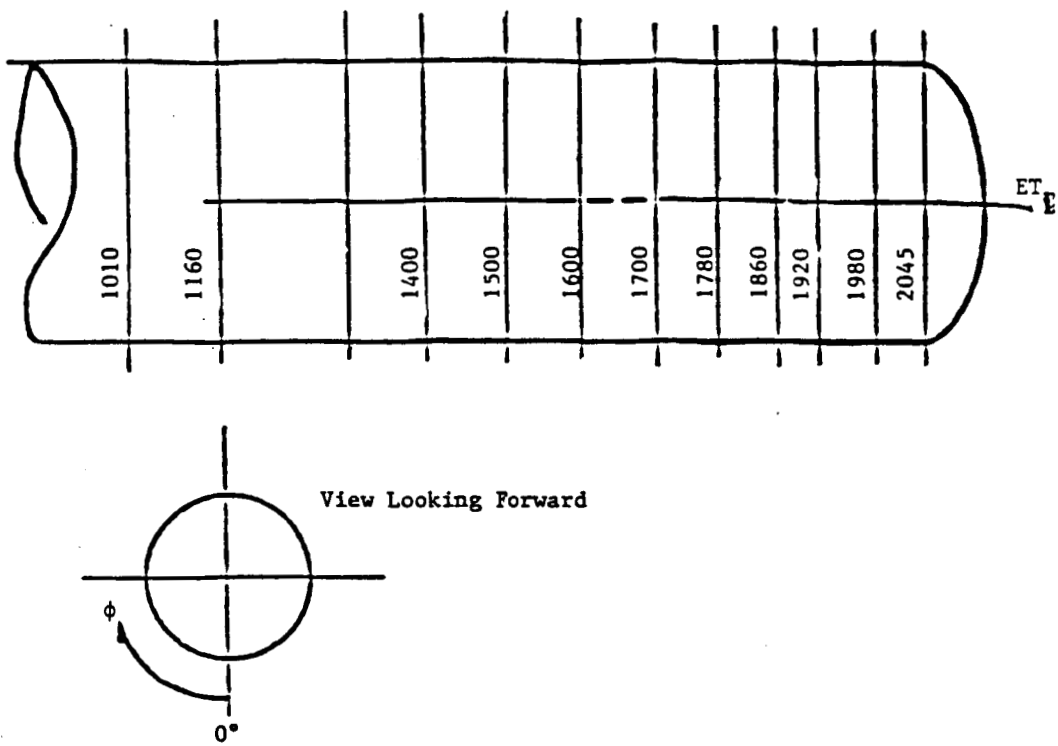


Fig. 2-13 IA300 Vertical Tail Pressure Instrumentation



$X_T / l_T$	ET STA	$\phi$ Radial Location (deg)												$\Sigma$
		0	25	30	60	85	90	112.5	139	153.5	165	180	195	
0.3699	1010													3
0.4511	1160													3
0.5812	1400													3
0.6353	1500													3
0.6896	1600													1
0.7437	1700													1
0.7871	1780													8
0.8304	1860													9
0.8629	1920													6
0.8954	1980													10
0.9306	2054													10

$$X_{T_0} = 327.22$$

$$l_T = 1845.8$$

Fig. 2-14 External Tank Pressure Instrumentation

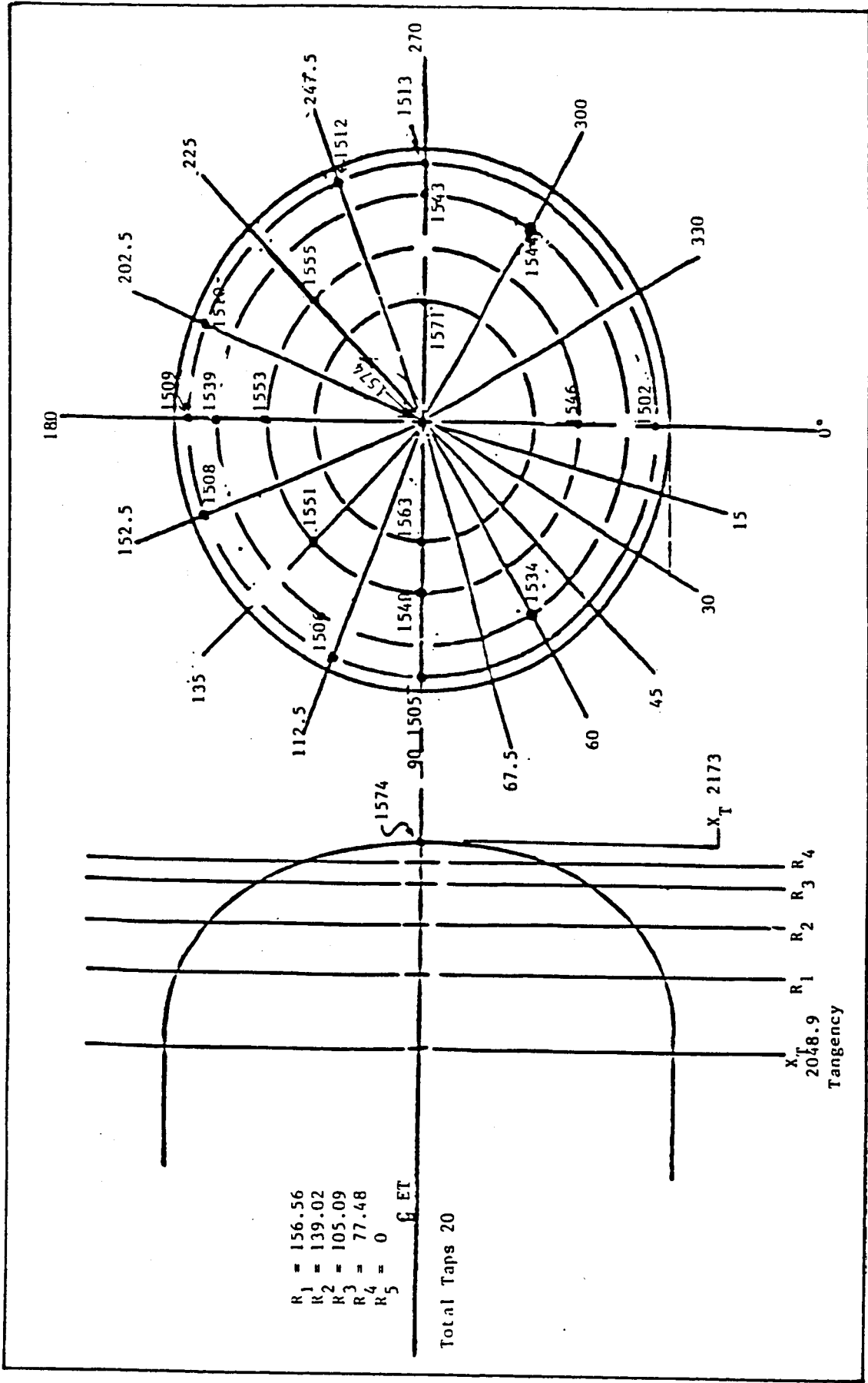


Fig. 2-15 IA300 External Tank Base Pressure Instrumentation

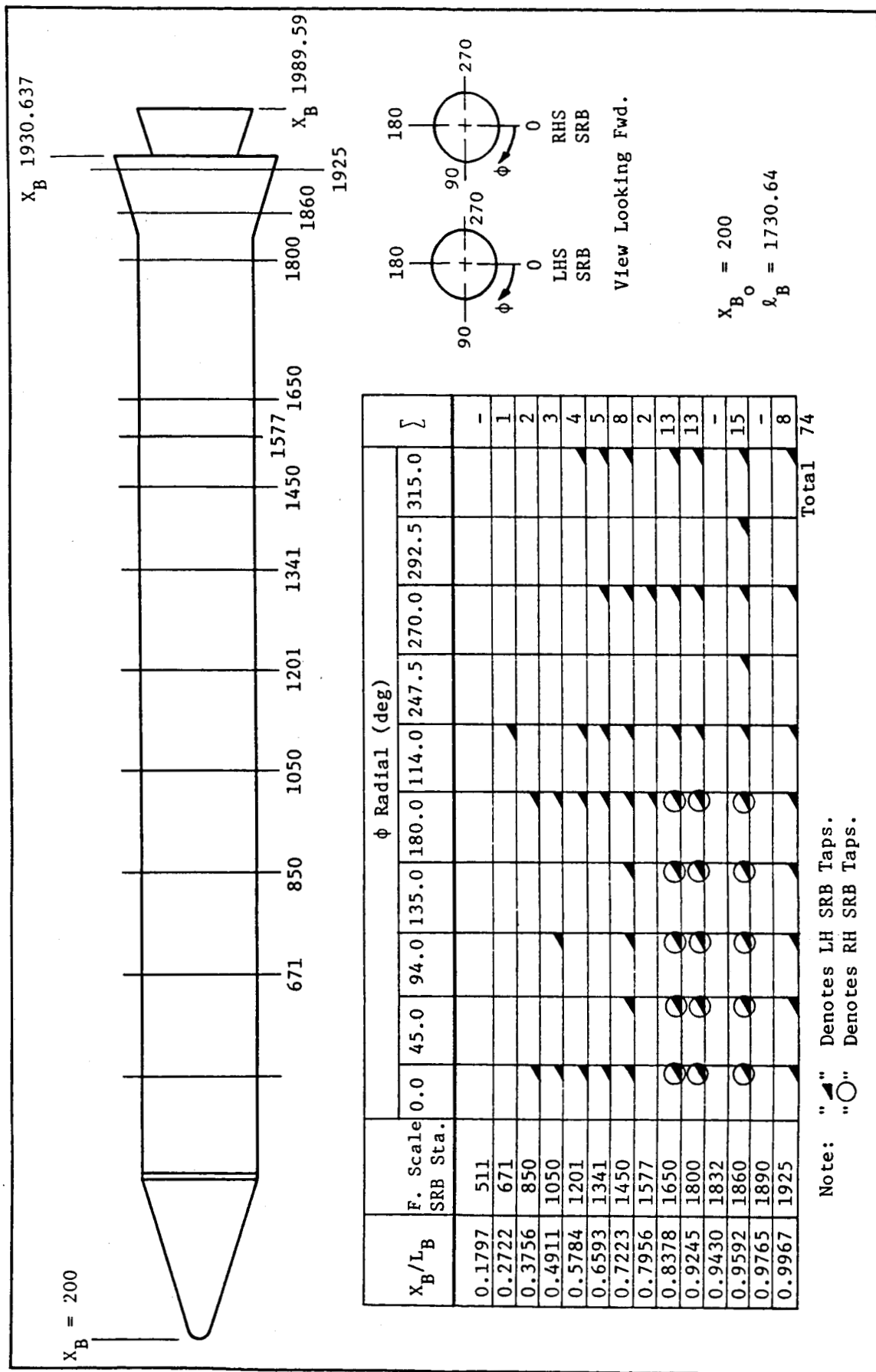


Fig. 2-16 IA300 SRB Pressure Instrumentation

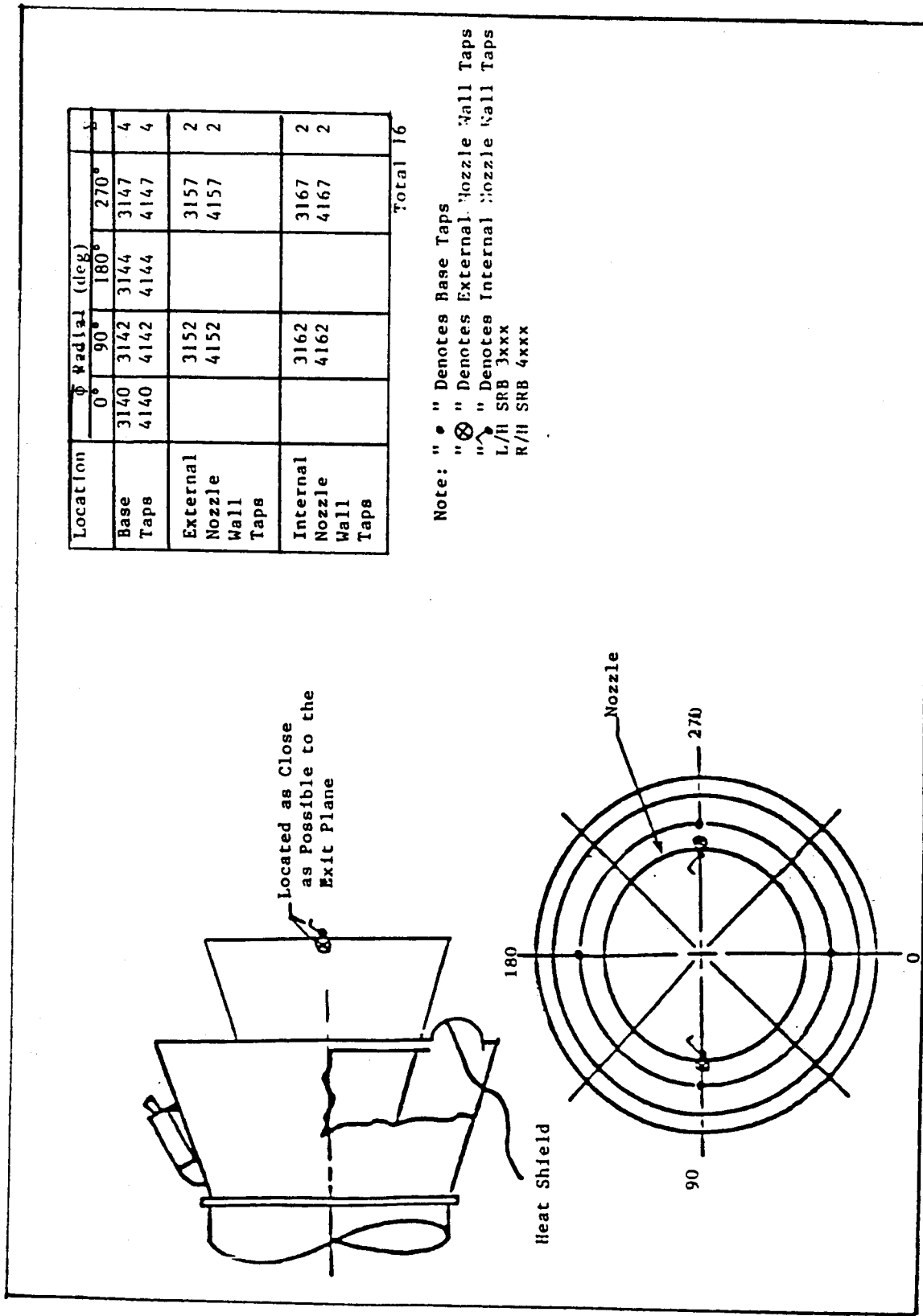


Fig. 2-17 IA300 SRB Aft Skirt Pressure Instrumentation

### 3. TEST PROGRAM

The IA300 wind tunnel test program consisted of a power variation phase at near flight attitude where the chamber pressure of the SSME and SRB model nozzles were varied in an attempt to match flight base pressures on the Orbiter, ET and SRB. Then, in subsequent phases of the test, the chamber pressures were set at a nominal power level based on the best match of these base pressures to the flight values. Elevon deflections, nozzle gimbal settings, and attitude variations were run at the selected nominal power levels.

Base pressure data from the power variations were evaluated at the test site to define the nominal model chamber pressures required to match flight base pressure. Section 5 provides a discussion of the correlation of the flight base pressure and plume simulation. The power variation phase was conducted at -4 deg angle of attack and zero angle of sideslip for a series of Mach numbers from 0.6 to 1.4. These conditions generally approximated the attitudes for the range of flight base pressure data used for the plume simulation.

Following the power variations, the selected nominal power levels were set as the model was tested over a range of attitudes and configurations (dual/single strut, elevon deflections, and gimbal angles). Data were obtained at angles of attack of -8, -4, 0, and +4 deg. The angles of sideslip were 0, and  $\pm 4$  deg.

At the completion of the cold flow portion of the test, solid plume simulations replaced the cold-flow nozzles and the final testing was conducted using the solid plumes. This report does not address the solid plume portion of the IA300 test.

Table 3-1 lists all the variations and configurations tested during the cold flow portion of the IA300 test. The top portion of the table indicates which Mach numbers were tested for each configuration. Below the Mach number columns, the table lists the various attitudes, elevon deflection and gimbal configurations for each Mach number tested.

Three inboard/outboard elevon deflections were tested during the cold-flow portion of the test, 10/9, 10/5, and 8/9. Over the Mach range tested, these deflections provided as close a match as possible to the Schedule 6 duty cycle while providing sufficient data to develop inboard and outboard elevon variations effects.

The gimbal configurations tested during the IA300 test consisted of six different gimbal patterns including the nominal gimbal for both the SSME and SRB followed by variations from the nominal setting.

ORIGINAL PAGE IS  
OF POOR QUALITY

Table 3-1 IA300 COLD FLOW TEST CONFIGURATIONS

## IA300 TEST PROGRAM

## Gimbal - SRB/SSME

IA300	Dual Strut 22° SSME	Dual Strut 35° SSME	Single Strut 35° SSME	Single Strut Solid Plume
0.60	•			
0.80	•	•	•	•
0.90	•	•	•	•
0.95	•	•	•	•
Mach No.	1.05	•	•	•
	1.10	•	•	•
	1.15	•	•	•
	1.25	•	•	•
	1.30	•	•	•
	1.40	•	•	•
Power	Var	•		
	Nom	•	•	•
Alpha	-4	•		
	Var	•	•	•
Beta	0	•		
	Var	•	•	•
Elev.	10/9	•		
	8/9		•	
	10/5	•	•	•
Gimbal (SRB/Orb)	N/N	•	•	•
	N/2			
	N/-5			
	2/N	•		
	2/2		•	
	2/-5		•	
Plume (SSME/SRB)	C <sub>1</sub> /B <sub>1</sub>			•
	C <sub>2</sub> /B <sub>1</sub>			•
	C <sub>2</sub> /B <sub>2</sub>			•
X	2.5			•
	4.5			•
	6.25			•

#### 4. MODEL NOZZLE CALIBRATION

Two model nozzle tests were conducted in the NASA-MSFC 14-Inch Transonic Wind Tunnel (TWT) to verify and calibrate the nozzles designed to produce flight base pressure coefficients during the IA300 test. In the first test, TWT-680, six nozzle configurations were tested to ensure that each nozzle design would produce full flow and the desired exit flow conditions. The six nozzle configurations tested are shown in Table 4-1.

Table 4-1 TWT-680 NOZZLE CONFIGURATIONS

Nozzle No.	Throat Radius (in.)	Length (in.)	Wall Angle (deg)	Exit Plane Diam. (in.)
10	.355	1.052	30	1.814
11	.355	0.900	35	1.814
12	.375	0.426	35	1.182
13	.375	0.684	35	1.542
14	.375	0.891	35	1.832
15	.375	0.613	40	1.550

The results of TWT-680 indicated that each of the nozzles tested exhibited full flow characteristics. Figure 4-1 shows the actual results of one nozzle compared to method-of-characteristics (MOC) predictions. Additional details of these results are available in Ref. 2.

For the second test, TWT-683, the following components were tested:  
 (1) one SRB nozzle, (2) part of the actual 0.01-scale SRB model flow system;  
 (3) two sets of nozzles; and (4) with the aft section of the fuselage. The nozzle dimensional data are listed in Table 4-2.

NOZZLE WALL PRESSURES  
MOC vs MSFC (TWT-680)

THETAW	$R_T$	Re/RT	LT/RT	
SSME 35 Deg	.3547	2.5577	2.5399	-11 Nozzle
PC = 1222 psi (MOC)    RC = RT				
Run 48 O	Run 49 X	Run 50 +		
PC = 1647	PC = 1650	PC = 1651		PC/PINF

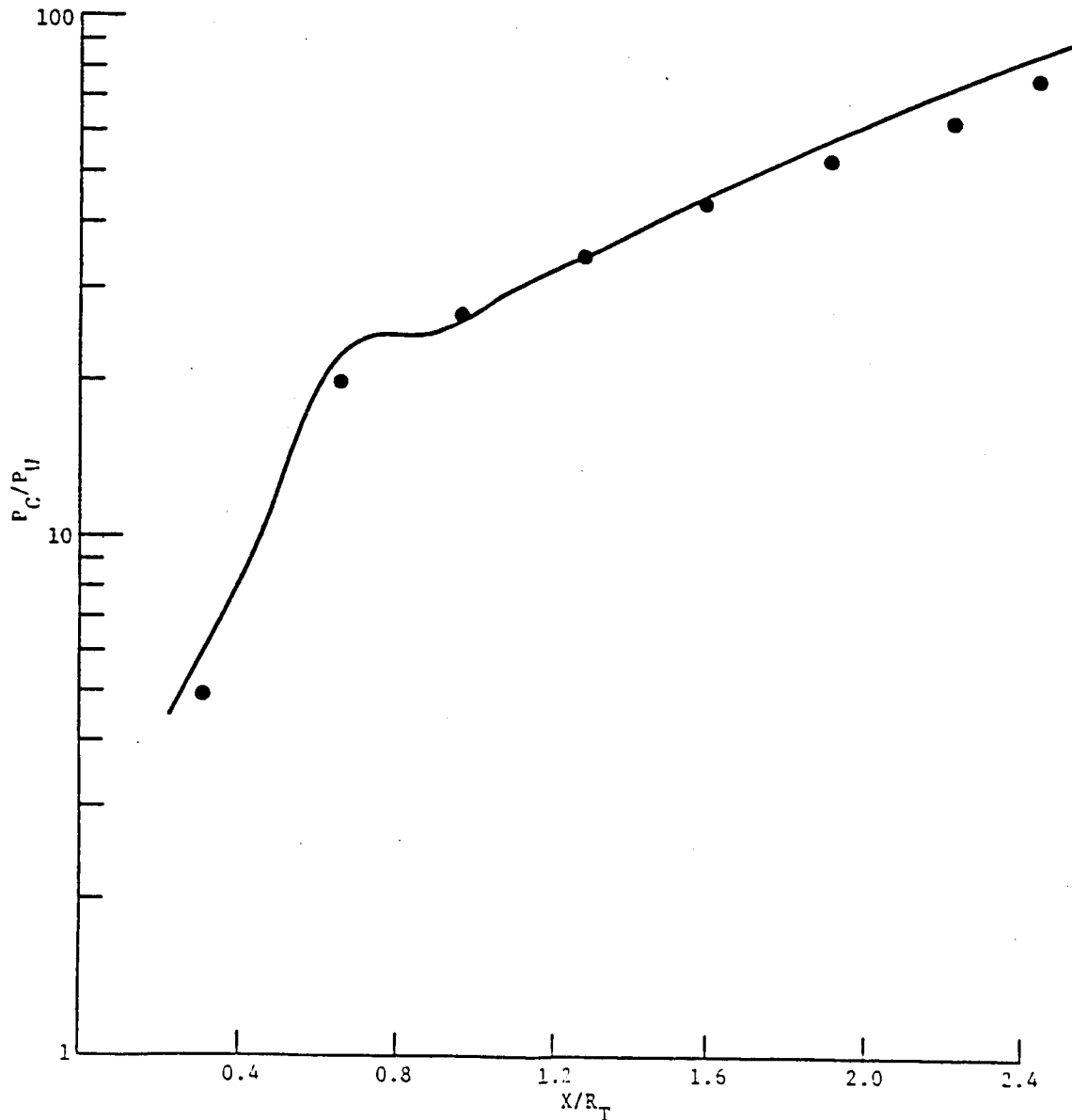


Fig. 4-1 TWT-680 Test Results

Table 4-2 TWT-683 NOZZLE CONFIGURATIONS

Nozzle	Throat Area	Wall Angle
SRB	.0027123 ft <sup>2</sup>	35 deg
SRB Set 1	.003187 ft <sup>2</sup>	35 deg
SSME Set 2	.002711 ft <sup>2</sup>	22 deg

TWT-683 was conducted to verify the 0.01-scale nozzle fabrication and performance and to verify the adequacy of the IA300 model flow system.

Each nozzle in the TWT-683 contained four pressure taps, two internal and two external, located near the nozzle exit plane.

The results of TWT-683 compared to MOC results for various chamber pressures are shown in Figs. 4-2 and 4-3 for the 22 deg and 35 deg SSME nozzles, respectively. Additional details of the TWT-683 results are available in Ref. 2.

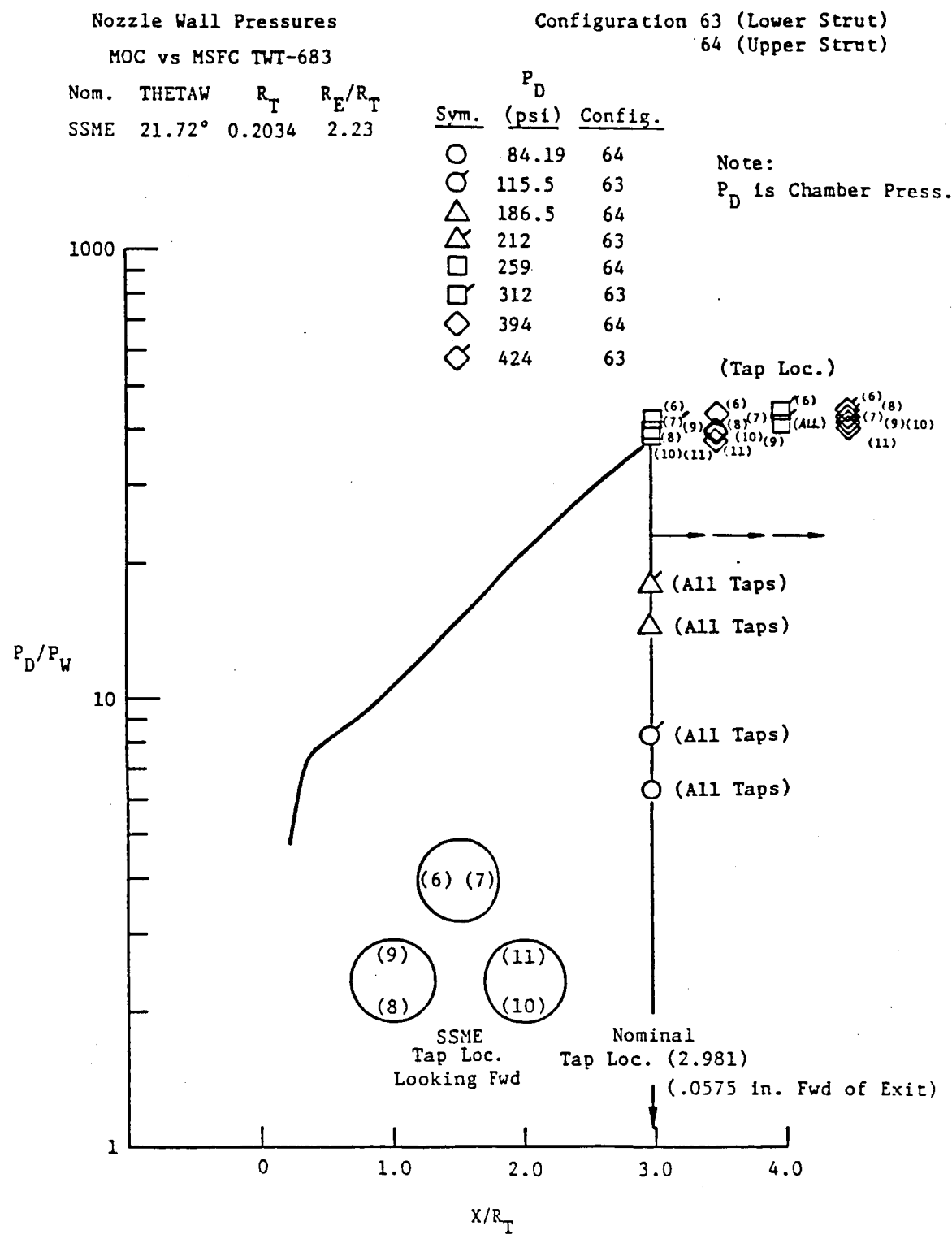


Fig. 4-2 TWT-683 Test Results (Configurations 63 and 64)

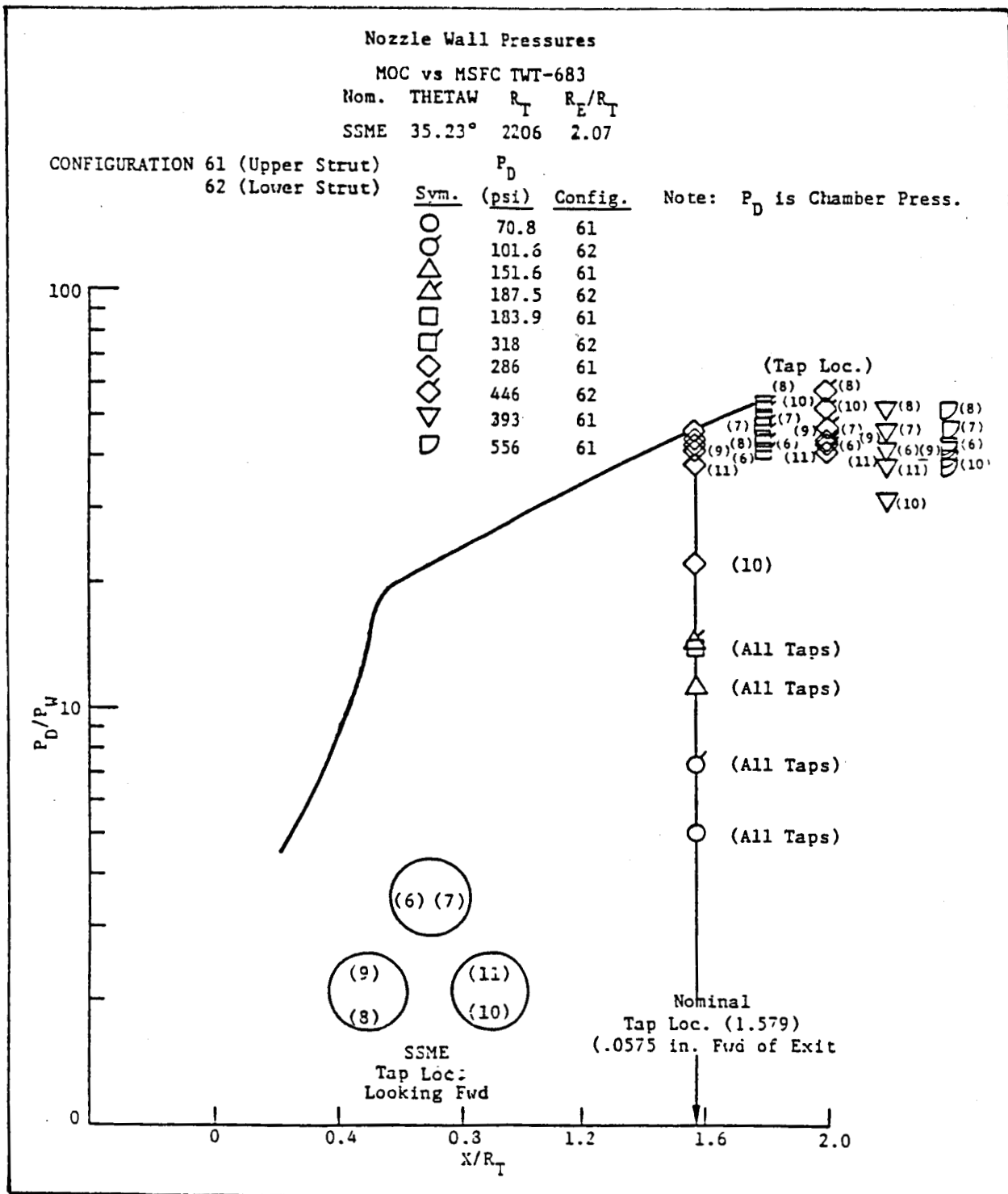


Fig. 4-3 TWT-683 Test Results (Configurations 61 and 62)

## 5. PLUME SIMULATION

The Space Shuttle plumes were simulated using cold air flowing through the IA300 model nozzles. The model plume characteristics required for the IA300 test were determined from the best match of the model base pressure environment to the base pressure environment developed from the first five Shuttle test flights. This was the criterion for determining the nominal chamber pressures for the SSME and SRB plumes. Power variations were run varying the SSME and SRB chamber pressure. The Orbiter and ET base pressures were measured and plotted versus SRB/SSME chamber pressure to establish the nominal power level as shown in Fig. 5-1. The nominal power level was determined where the model base pressure curve crossed into the flight base pressure envelope. The base pressure for the selected nominal power level was then plotted versus Mach number as shown in Fig. 5-2.

The plume similarity parameter (SP) used for each flow through nozzle in the IA300 test was

$$SP = \frac{M_j \delta_j}{M_e^{0.25} \gamma}$$

The results of the nozzle calibration test, TWT-683, for the SSME similarity parameter,  $M_e$  and  $M_j$  are shown in Figs. 5-3 through 5-10.

The prototype plume characteristics are a function of the motor chamber pressure and altitude and are therefore dependent on the ascent trajectory. The Mission 3A ascent trajectory characteristics were used as a reference trajectory. These reference characteristics that influence the prototype plume characteristics are presented in Table 5-1.

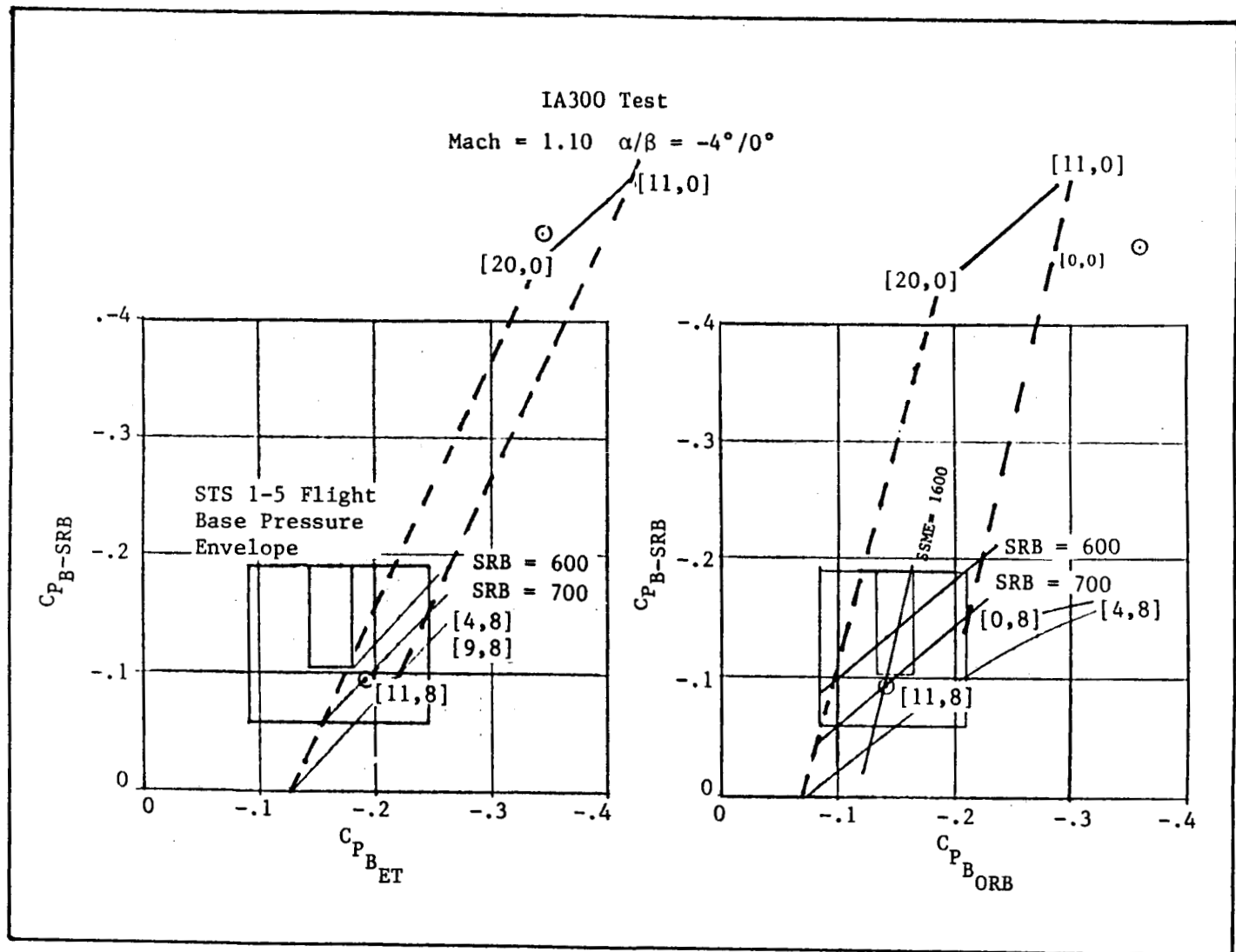


Fig. 5-1 IA300 SSME/SRB Chamber Pressures vs Base Pressures for SRB, ET, and Orbiter

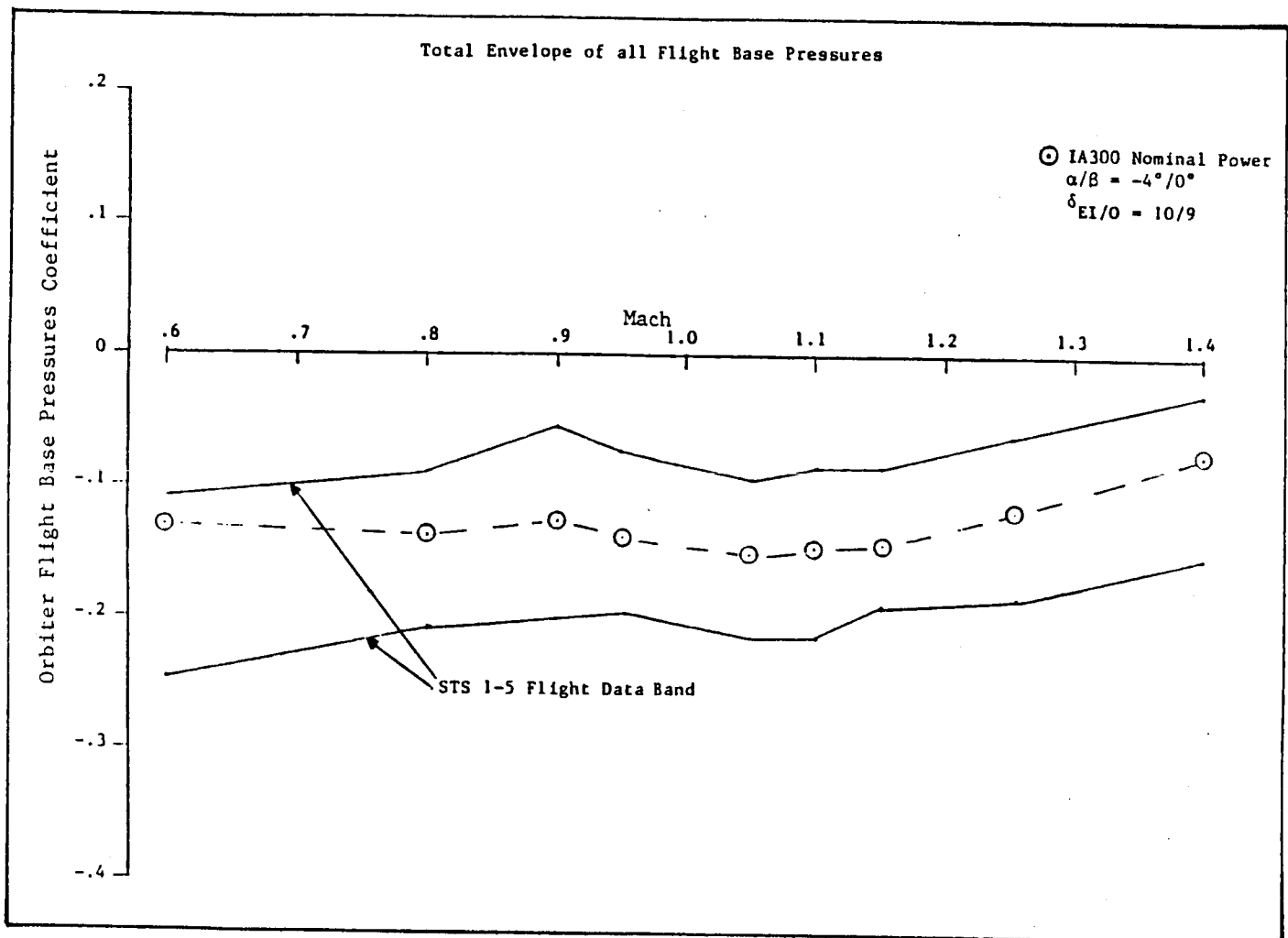


Fig. 5-2 Comparison of Base Pressure for IA300 Nominal SSME/SRB Power Levels

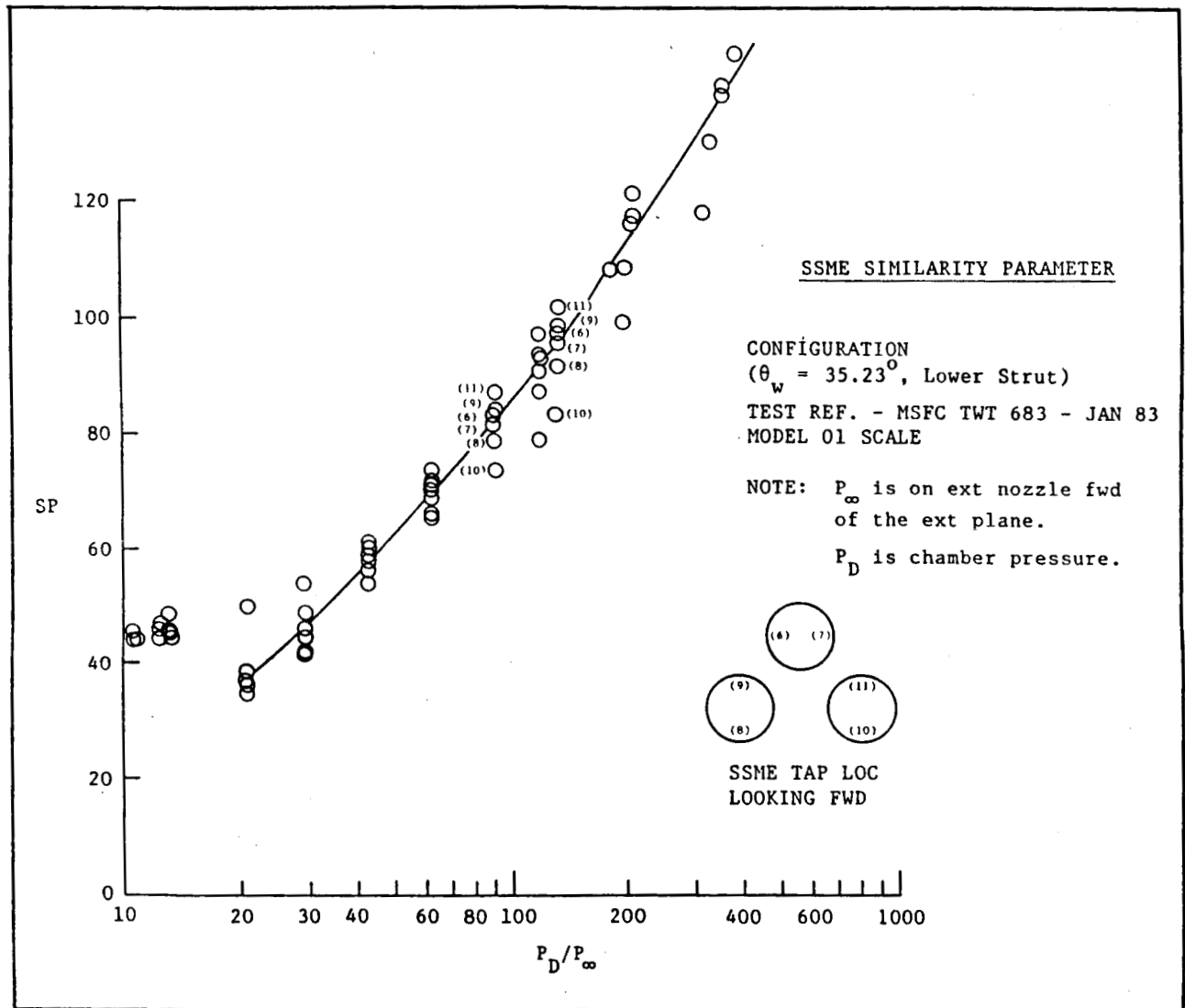


Fig. 5-3 SSME Similarity Parameter (Configuration 61)

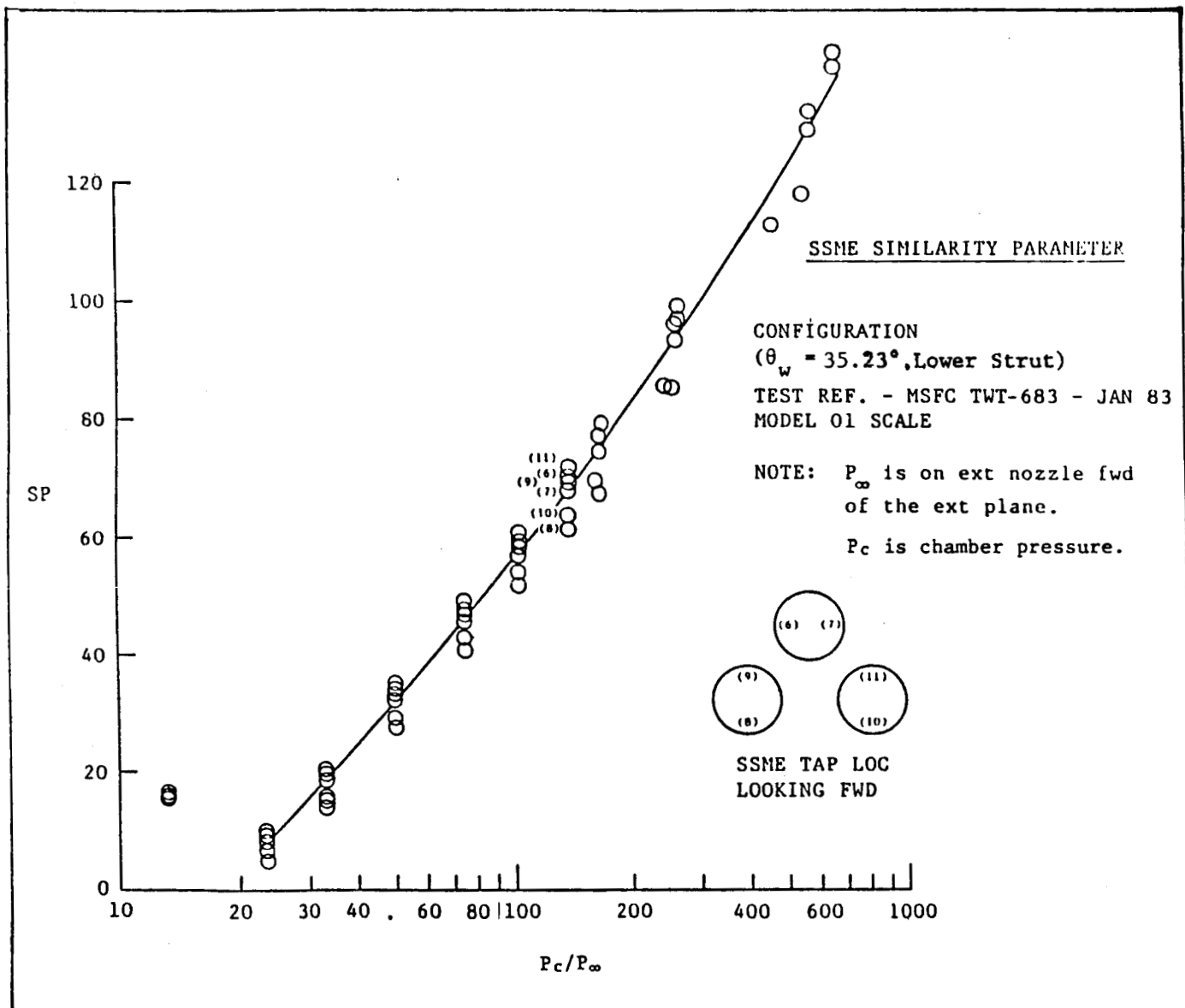


Fig. 5-4 SSME Similarity Parameter (Configuration 62)

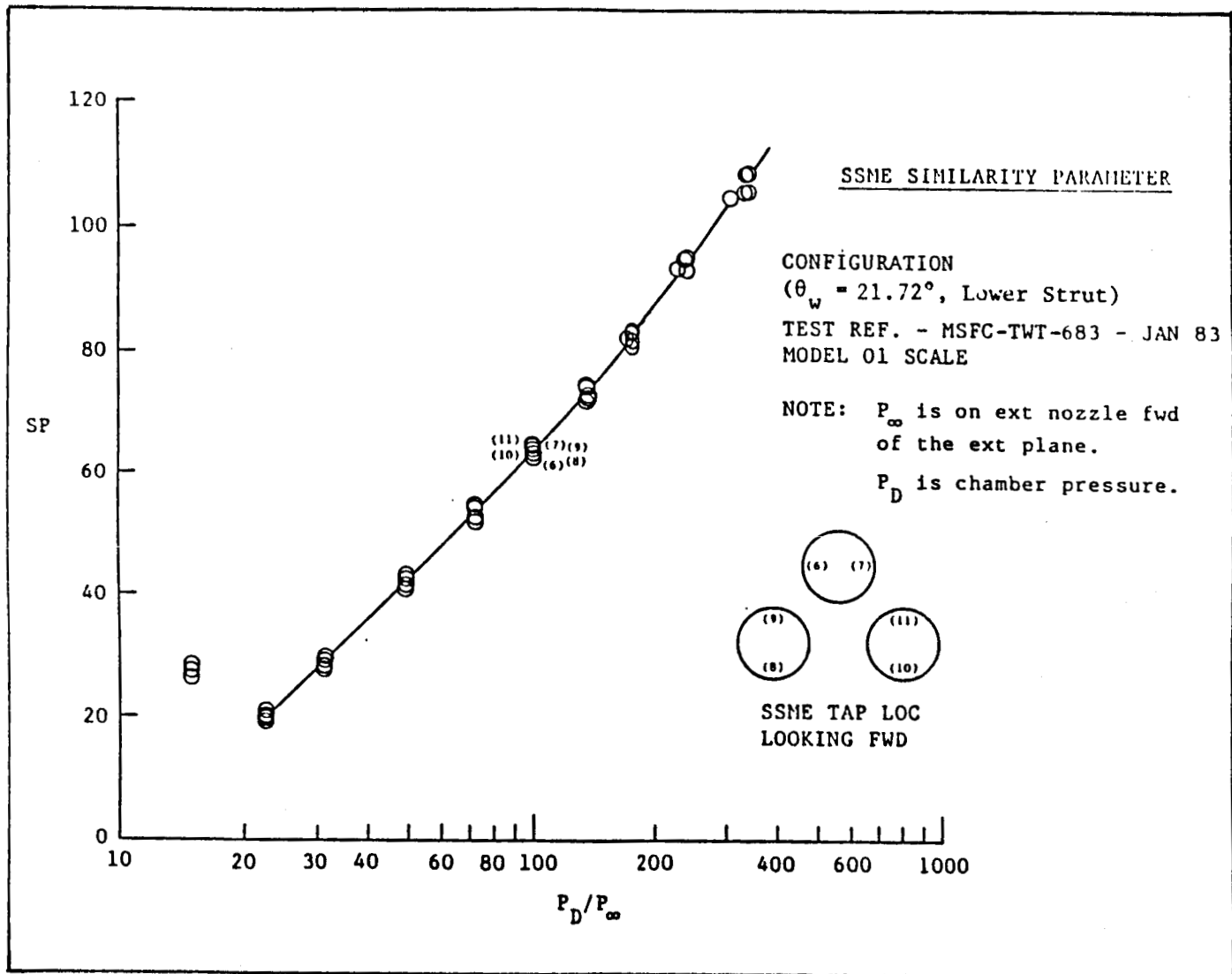


Fig. 5-5 SSME Similarity Parameter (Configuration 63)

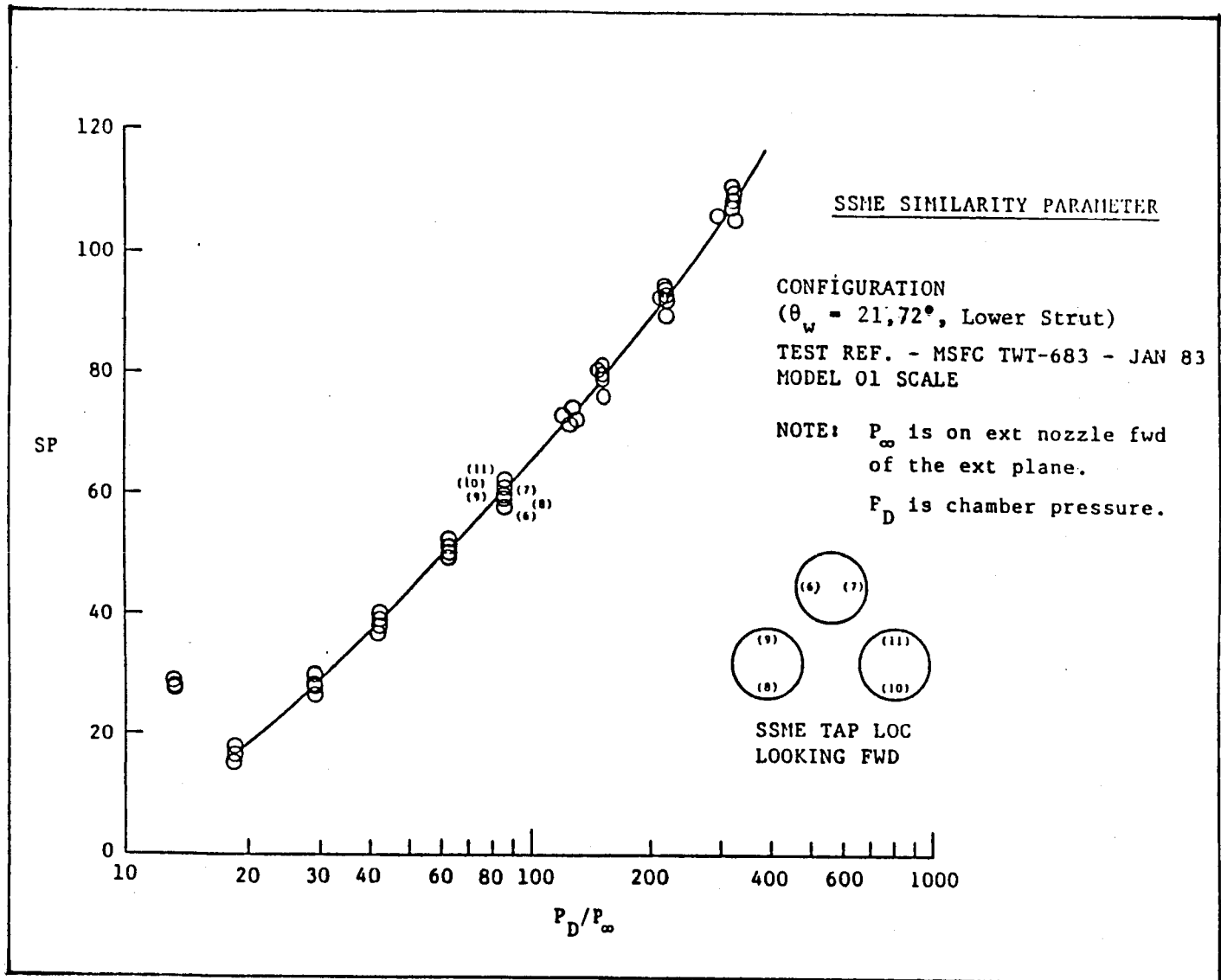


Fig. 5-6 SSME Similarity Parameter (Configuration 64)

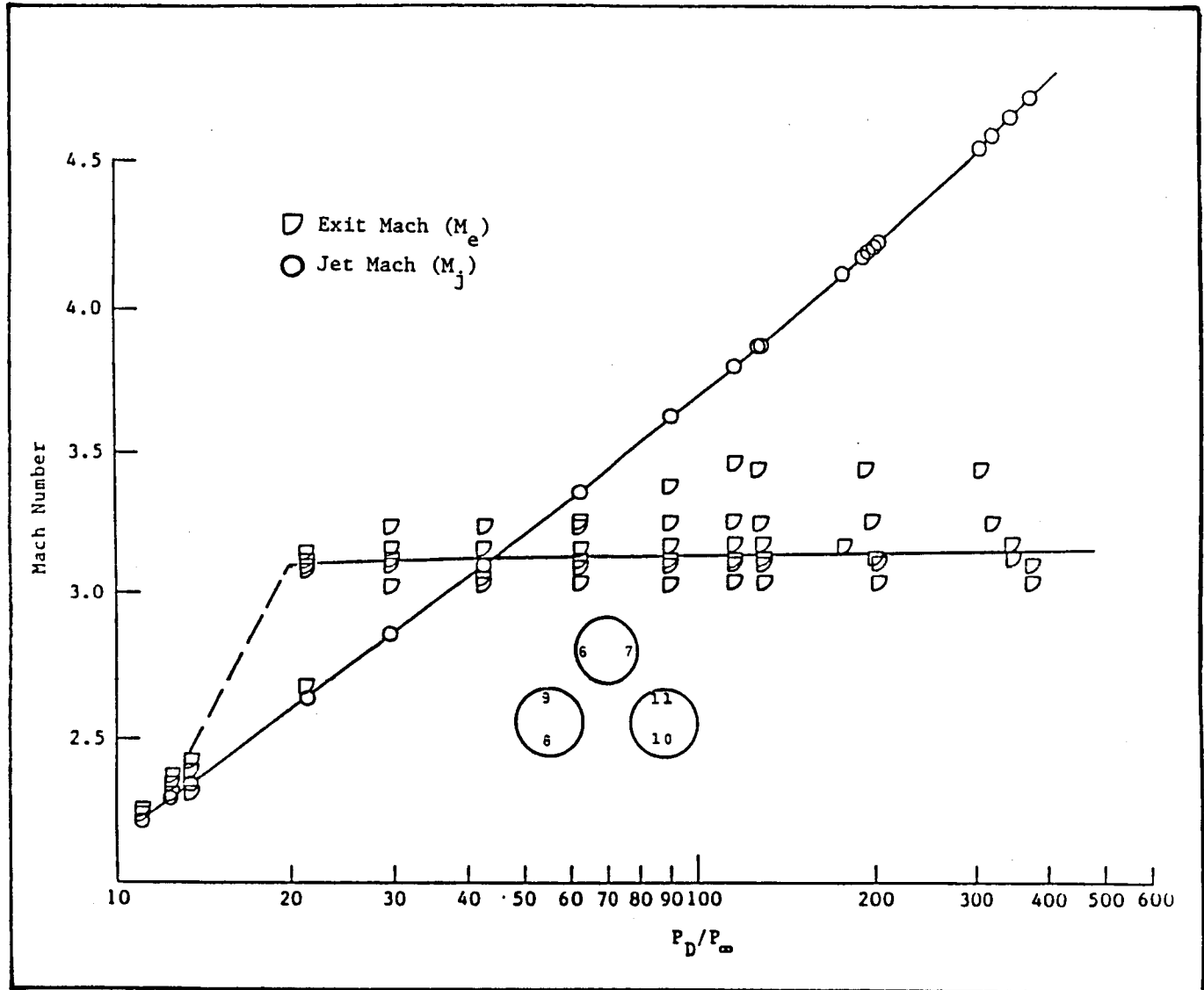


Fig. 5-7 SSME Mach Numbers (Configuration 61)

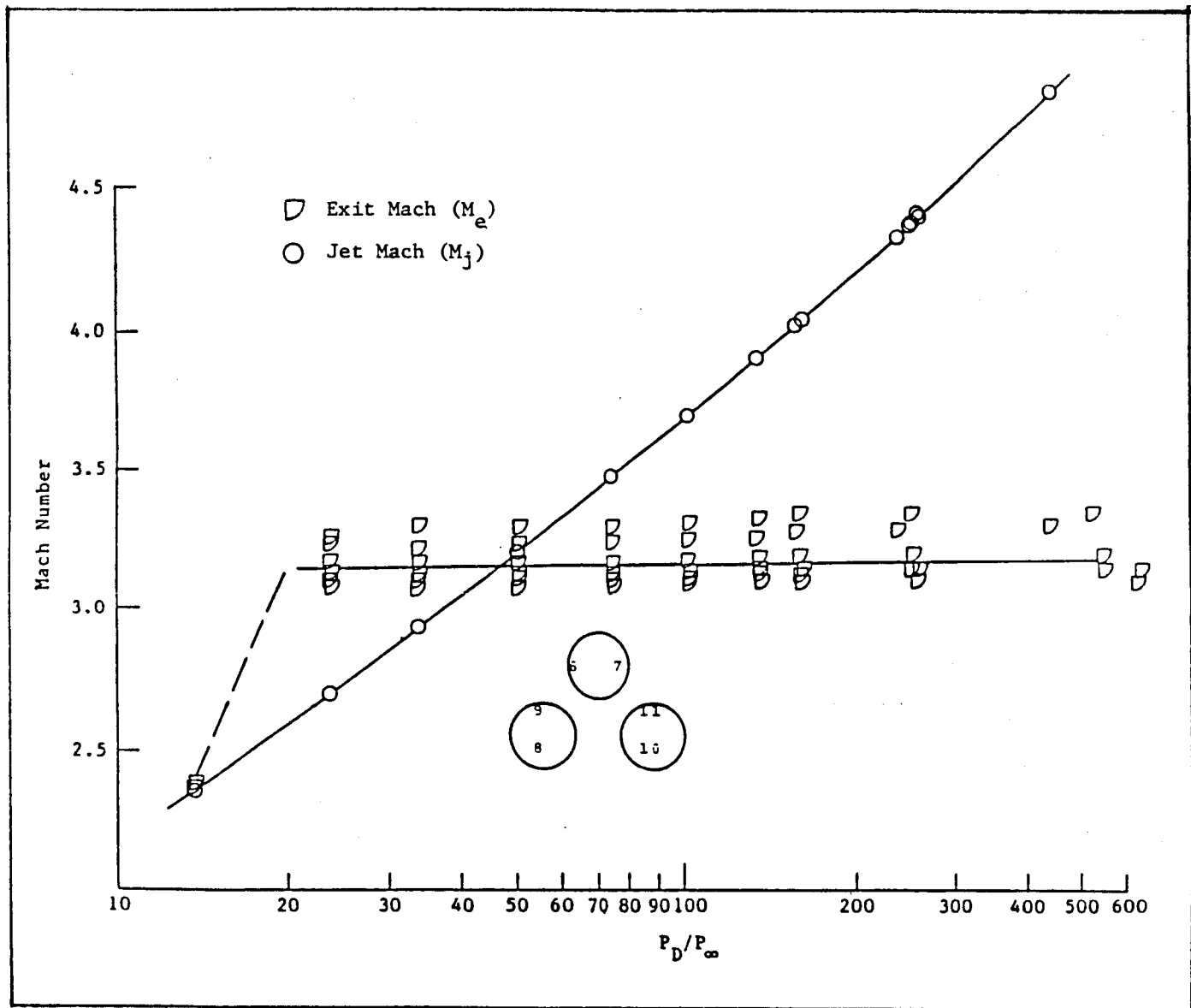


Fig. 5-8 SSME Mach Numbers (Configuration 62)

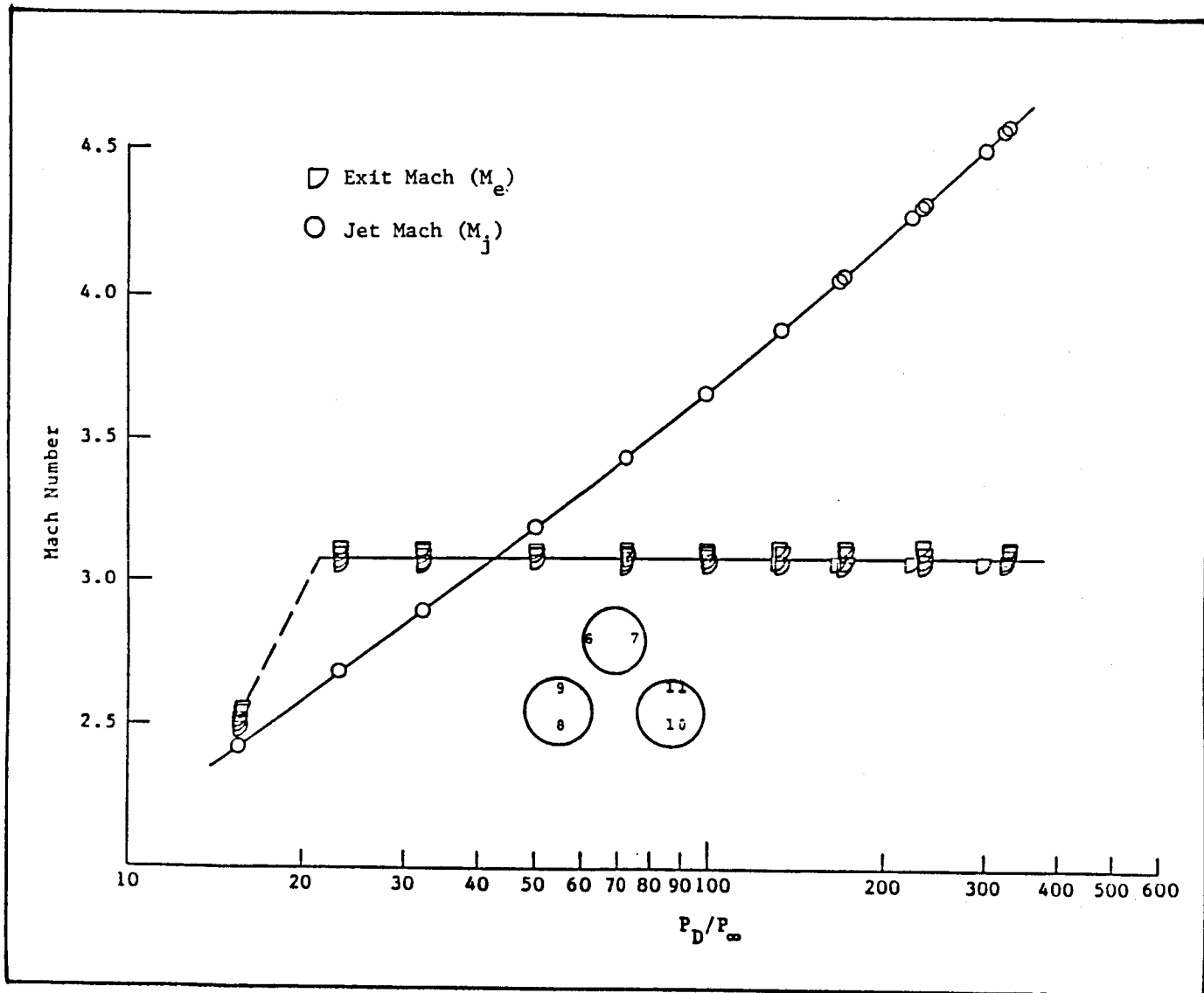


Fig. 5-9 SSME Mach Numbers (Configuration 63)

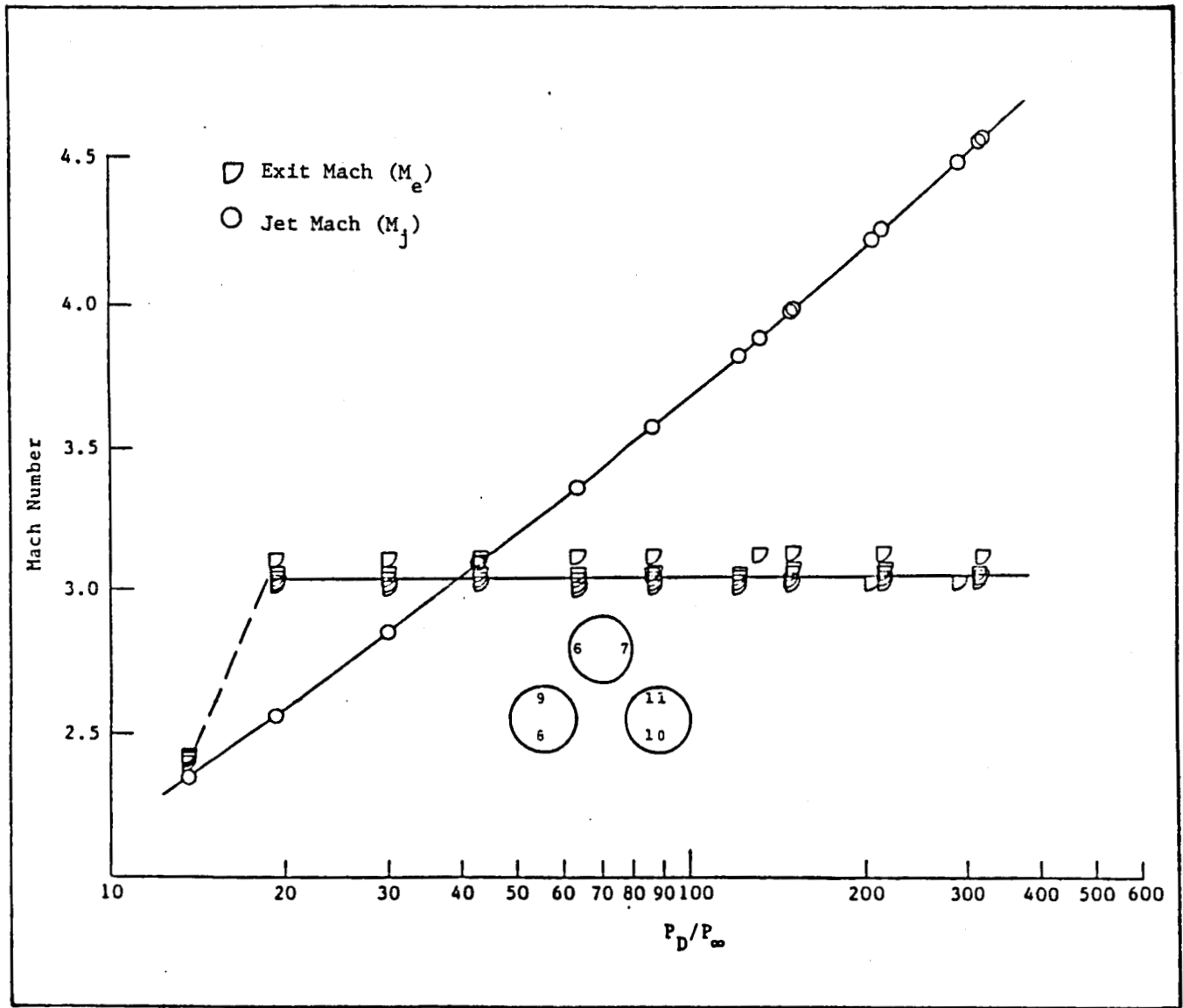


Fig. 5-10 SSME Mach Numbers (Configuration 64)

Table 5-1 ASCENT TRAJECTORY AND SRB - SSME CHAMBER PRESSURE

Time	Mach No.	P (psia)	q (psf)	$P_D$ SRB (psia)	SSME Throttle, %
31.0	0.6	10.41	375.5	697	109.0
40.4	0.8	8.09	526.0	628	88.4
44.8	0.9	7.02	574.2	601	88.4
47.0	0.95	6.51	592.5	592	88.4
51.2	1.05	5.56	617.4	580	88.4
53.2	1.10	5.13	626.4	586	88.4
55.0	1.15	4.76	633.5	584	88.4
58.3	1.25	4.11	642.8	586	88.4
62.9	1.40	3.29	649.5	603	109.0

The results of the IA300 power variations in matching the Orbiter, ET, and SRB flight base pressures are shown as the selected nominal power level in Figs. 5-11 through 5-13. These figures show that the nominal power level matched the Orbiter and ET base pressures throughout the Mach range. However, the SRB base pressures were generally on the high side of the flight base pressure envelope. These results were generally the same as was observed in the MSFC TWT-675 solid plume test.

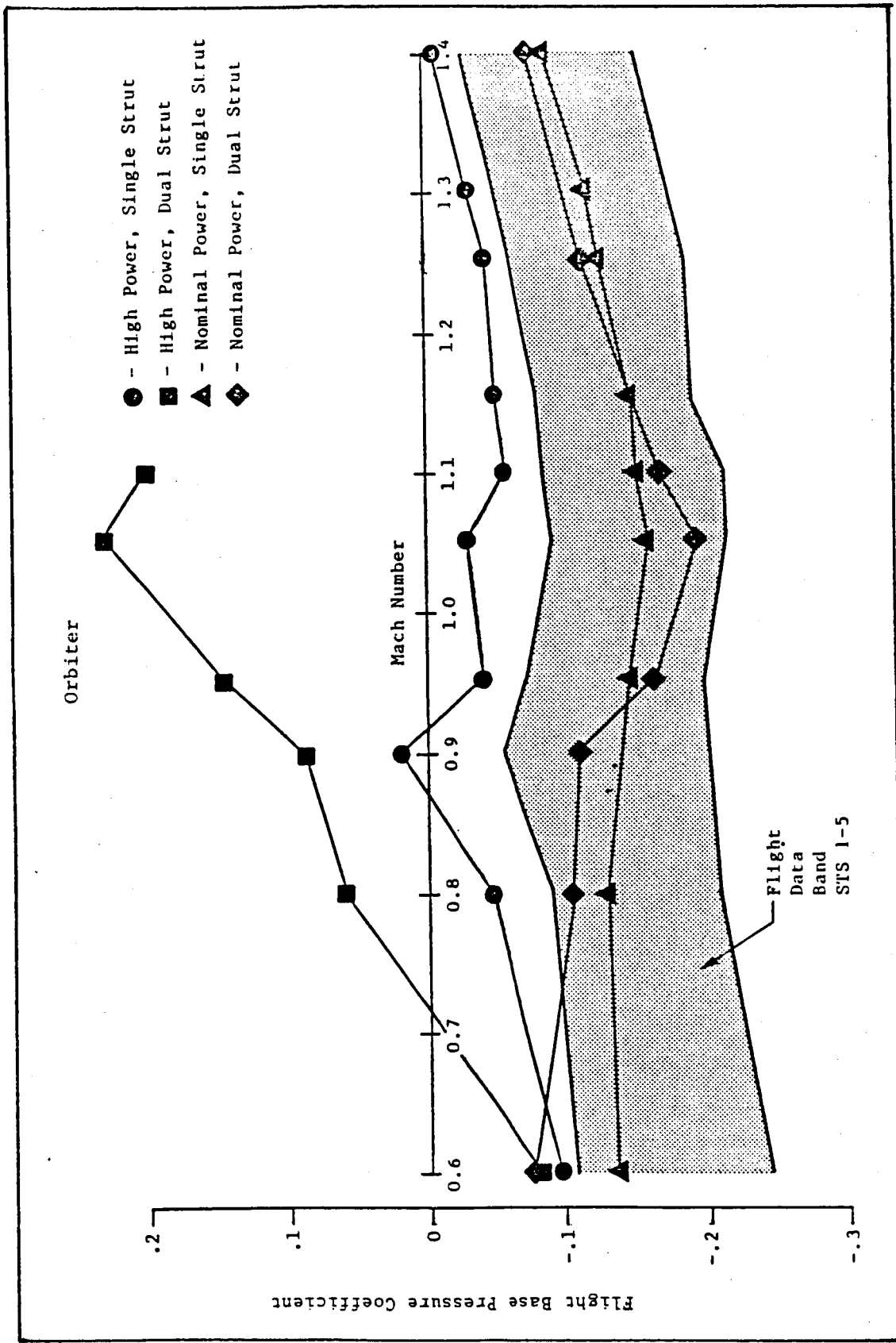


Fig. 5-11 Total Envelope of All Orbiter Flight Base Pressures (STS 1-5)

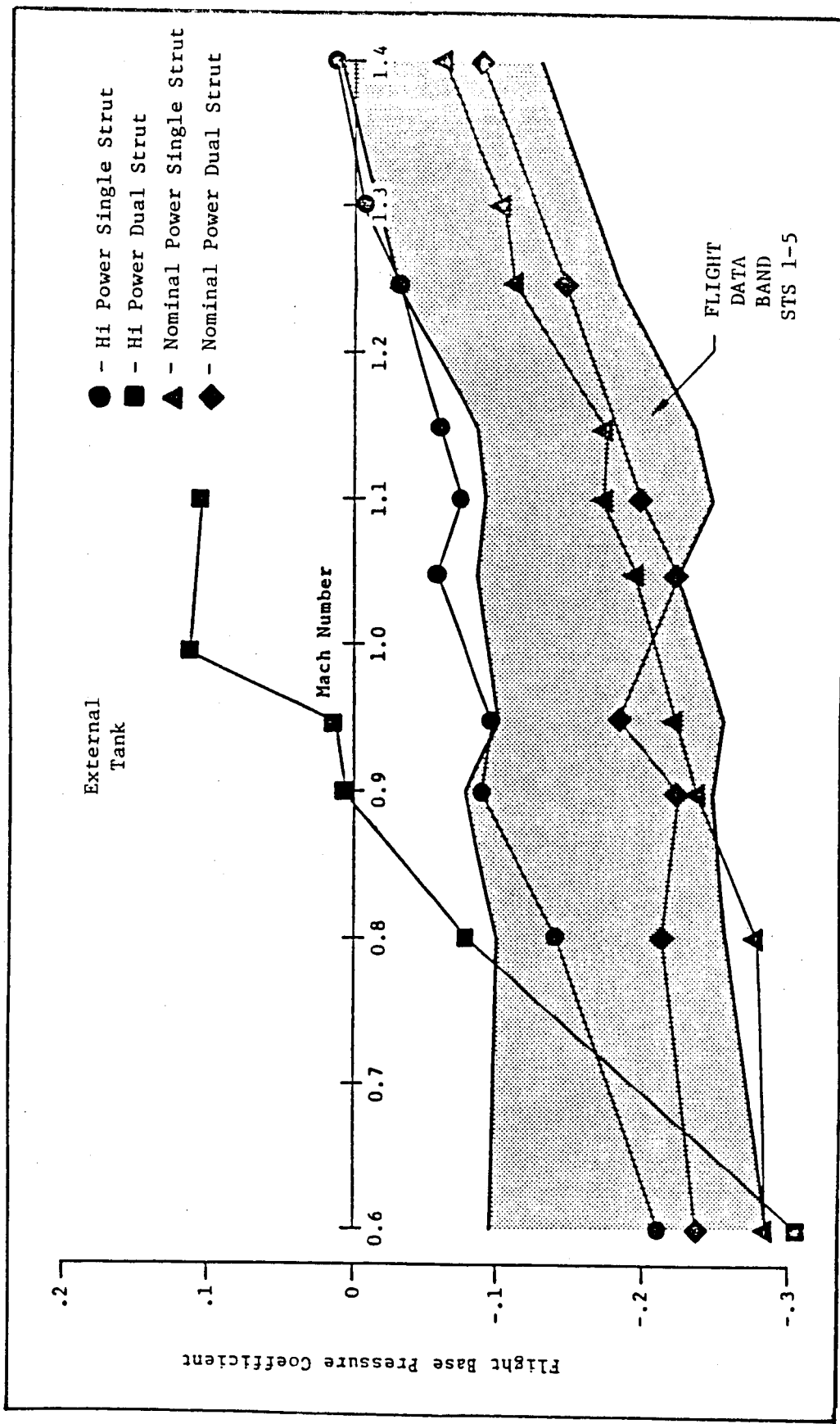


Fig. 5-12 Total Envelope of All ET Flight Base Pressures (STS 1-5)

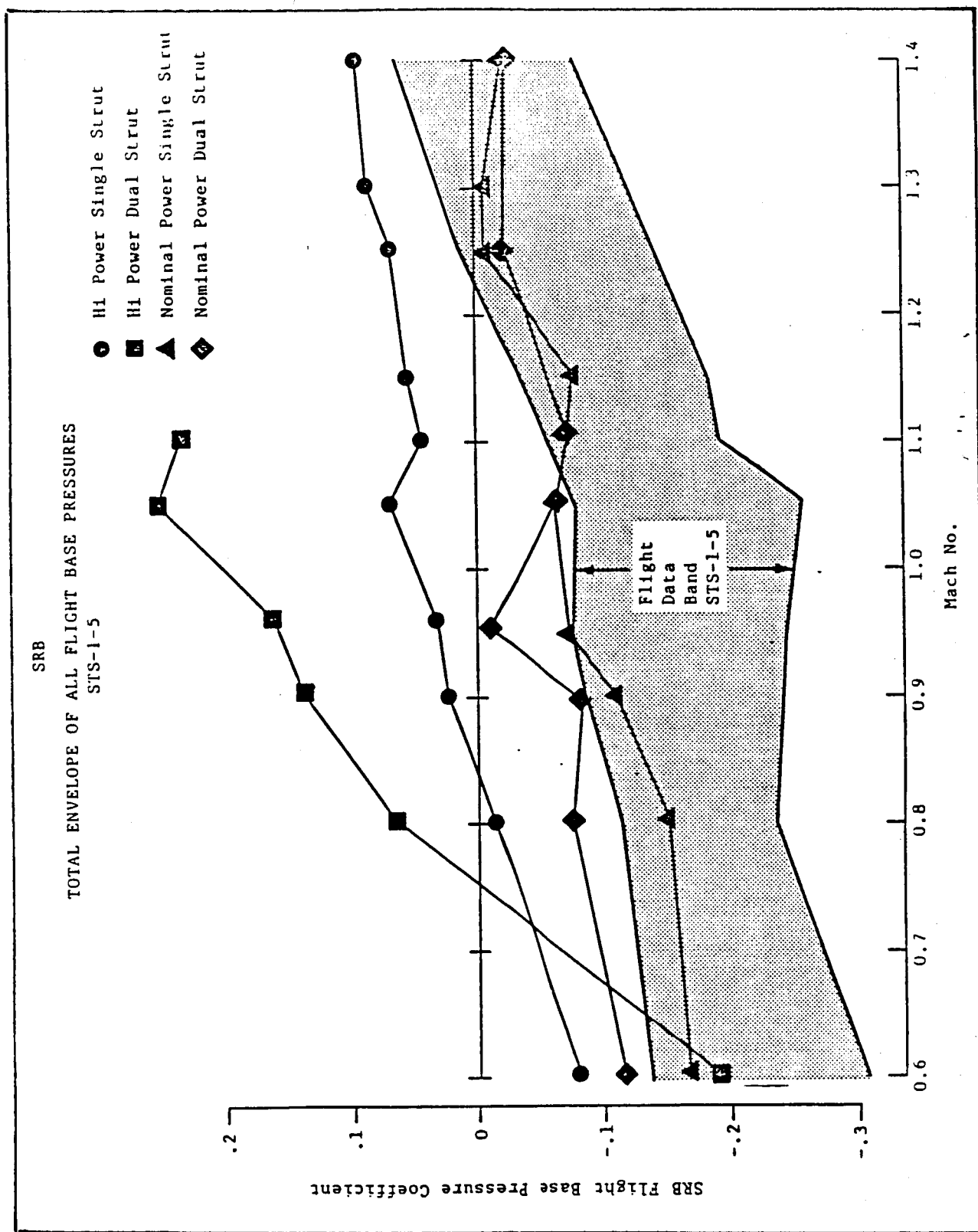


Fig. 5-13 Total Envelope of All SRB Flight Base Pressures (STS 1-5)

## 6. DATA ANALYSIS AND INTEGRATION MODEL

The analysis of the IA300 plume induced aerodynamic characteristics was performed using different pressure data over different portions of the vehicle. This type of analysis was similar to that used for the IA119/IA138 analysis (Ref. 3). The two types of pressure data used were power-on pressure coefficients to evaluate the base forces and moments and power-delta pressure coefficients ( $\Delta C_p = C_{p_{\text{power-on}}} - C_{p_{\text{power-off}}}$ ) to evaluate the change in forebody aerodynamic characteristics. The location on the Space Shuttle vehicle where these two types of pressure data were used is shown in Fig. 6-1a.

The data analysis procedure required power-on, power-off and power-delta pressure coefficients from the IA300 DATAMAN tapes. Both power-on pressure coefficients and power-delta pressure coefficients were required to evaluate the plume effects from the IA300 test. Each data set on the DATAMAN tape contained all the interpolated alpha and beta conditions that were run for a particular elevon and gimbal configuration. Figure 6-1b shows a sample of the data sets that were used to determine the power delta pressure coefficients or pressure coefficients for each component in the pressure integration. This table lists the component, the power-on and power-off data set identifier, the strut configuration (dual or single), the starting address for each data set and the range of pressure taps in each data set. Similar data sheets were used for each Mach number, elevon configuration, and gimbal configuration. These data sheets were used to develop a pressure integration data file for each case integrated.

The next phase of the analysis consisted of developing a computer model for performing the pressure integration. This was accomplished by dividing the total Shuttle vehicle into various elements and modeling these elements in such a manner so as to provide an accurate representation of the actual

ORIGINAL PAGE IS  
OF POOR QUALITY

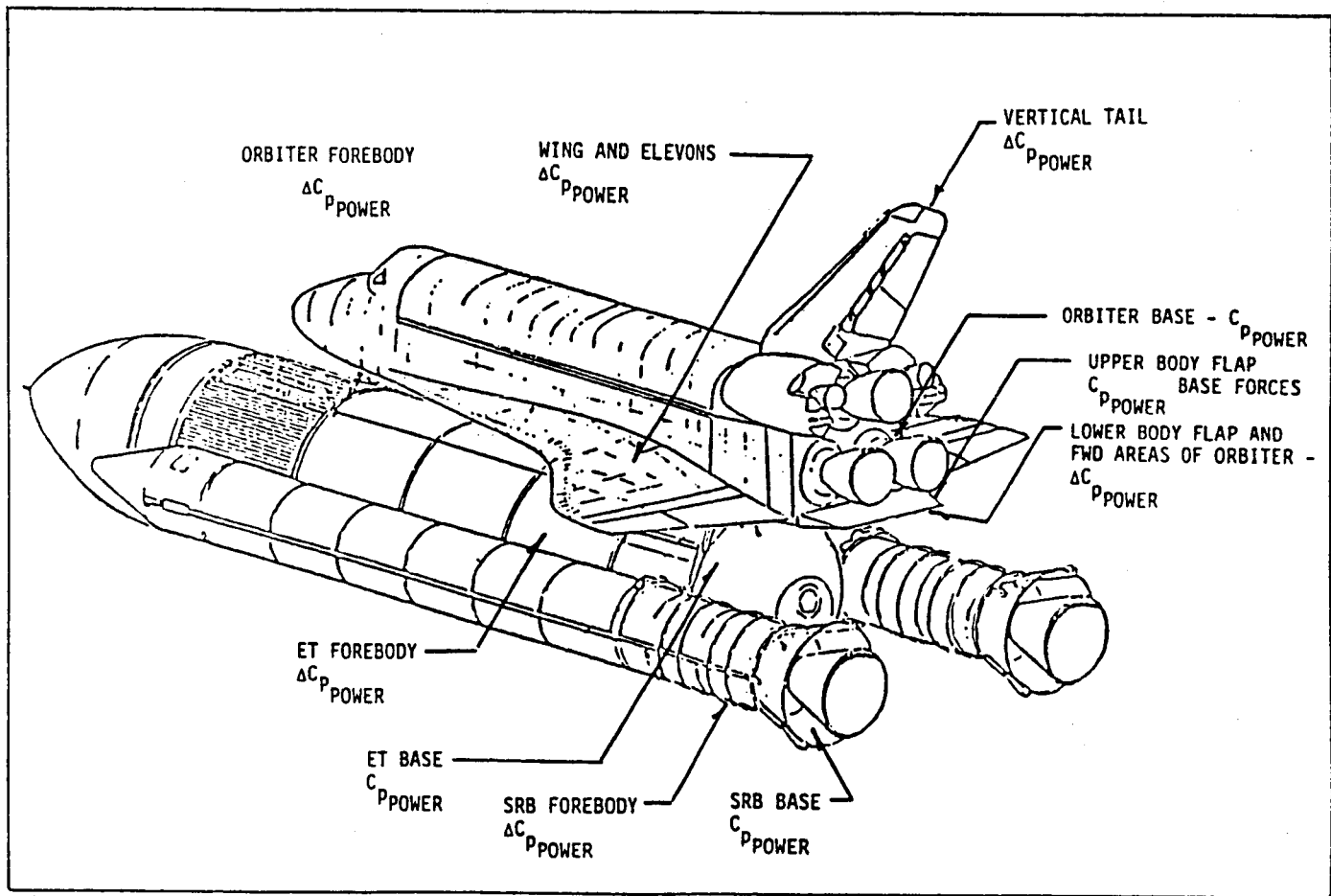


Fig. 6-1a Plume Flowfield Areas

Data Base for PDP Integration

MACH	0.6
IB-ELV	10
OB-ELV	9
SSMEGIM	C1
SRB GIM	B1
SSMENOZ	4.5"
SRB NOZ	

Component Description Data Sets	Strut	Press	Starting Address	Ending Address	Starting Taps	Ending Taps
Orbiter Fuse. Bottom A**371 - A**99	DS	$\Delta C_P$	46678	29097	1	32
Orbiter Fuse. Top A**371 - A**99	SS	$\Delta C_P$	46678	29097	43	58
Upper Body Flap B**371	DS	$C_P$	64774		38	22
Lower Body Flap C**371 - C**99	DS	$\Delta C_P$	95262	814 4	33	16
Orbiter Base Bottom D**371	SS	$C_P$	61107		66	73
Orbiter Base Top D**371	DS	$C_P$	61107		74	80
Upper Wing E**371 - E**99	SS	$\Delta C_P$	138972	123413	201	288
Lower Wing F**371 - F**99	DS	$C_P$	82200	66291	206	292
SSME Noz. Int. G**371	SS	$C_P$	56309		92	88
Left OMS Noz. I*371	SS	$C_P$	68455		104	100
Right OMS Noz. J**371	SS	$C_P$	88129		97	101
Left Vert. Tail K**371 - K**99	SS	$\Delta C_P$	28950	20486	406	426
Right Vert. Tail L**371 - L**99	SS	$\Delta C_P$	46184	37726	418	421
External Tank M**371 - M**99	DS	$\Delta C_P$	130496	108620	1901	2019
ET Base N**371	DS	$C_P$	65401		1502	1544
Left SRB O**371 - O**99	DS	$\Delta C_P$	105135	84319	3020	3139
Left SRB Base P**371	DS	$C_P$	63887		3140	3147
Left SRB Noz. Int. Q**371	DS	$C_P$	55601		3162	3167
Right SRB S**371 - S**99	DS	$\Delta C_P$	86748	72944	4080	4114
Right SRB Base T**371	DS	$C_P$	68005		4140	4147
Right SRB Noz. Int. U**371	DS	$C_P$	85743		4162	4167

Fig. 6-1b Sample of Data Set Listings

external pressure environment over the complete vehicle. Each of the elements discussed in the following paragraphs were modeled into discrete areas to which pressure measurements were assigned using the pressure tap identification numbers from the test. Prior to developing the discrete area models, an analysis was made of the spatial extent of the plume effects on the model. A portion of these analyses is presented in the discussion of each of the integration model elements.

The following paragraphs present a brief discussion of the analysis and modeling techniques used to evaluate the plume induced aerodynamic characteristics.

#### 6.1 ORBITER BASE

The Orbiter base includes the base heat shield, upper body flap area, OMS pod base projected area, and vertical tail base. Orbiter base pressure instrumentation on IA300 was limited to one side of the orbiter base and one OMS pod as shown in Fig. 6-2. A schematic of the projected areas assigned to each pressure tap on the Orbiter base is shown in Fig. 6-3. The nozzle exit area projections on the base heat shield were excluded from the total base area as shown in the figure. Table 6-1 lists the full scale projected areas for the orbiter base along with their location, size, and tap number used for integration. Single strut pressure data were used for the lower half of the base and dual strut data for the upper half. This was necessary since various pressure taps on the upper portion of the base were not functional during the single strut part of the IA300 test. Figure 6-4 shows a comparison of the base taps for both the dual and single strut portions of the test. As can be seen from this figure, using base pressure data from the single strut configuration would not provide adequate base pressure data for the upper portion of the Orbiter base.

Tap No.	$Z_o$	$Y_o$
66	4.00	0.0
67	3.28	0.0
75	4.87	-0.49
76	4.12	-0.38
68	3.03	-0.26
77	4.25	-0.26
69	3.03	-0.89
73	4.32	-1.01
72	3.84	-1.00
71	3.50	-1.08

Tap No.	$Z_o$	$Y_o$
70	3.03	-1.24
80	5.14	-0.55
79	4.39	-1.07
78	4.65	-1.30
74	4.58	-0.68

Total 15 Taps

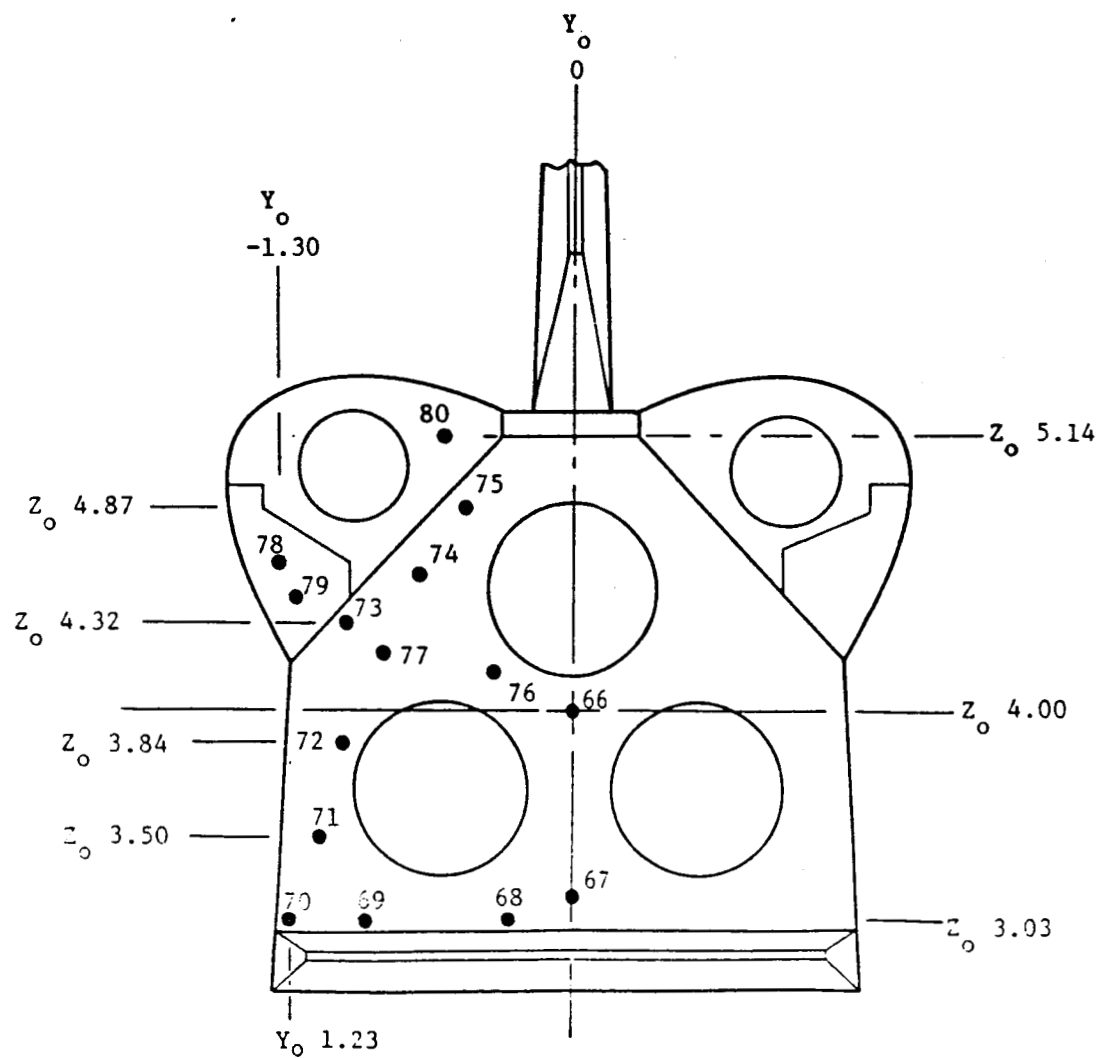


Fig. 6-2 IA300 Orbiter Base Pressure Instrumentation

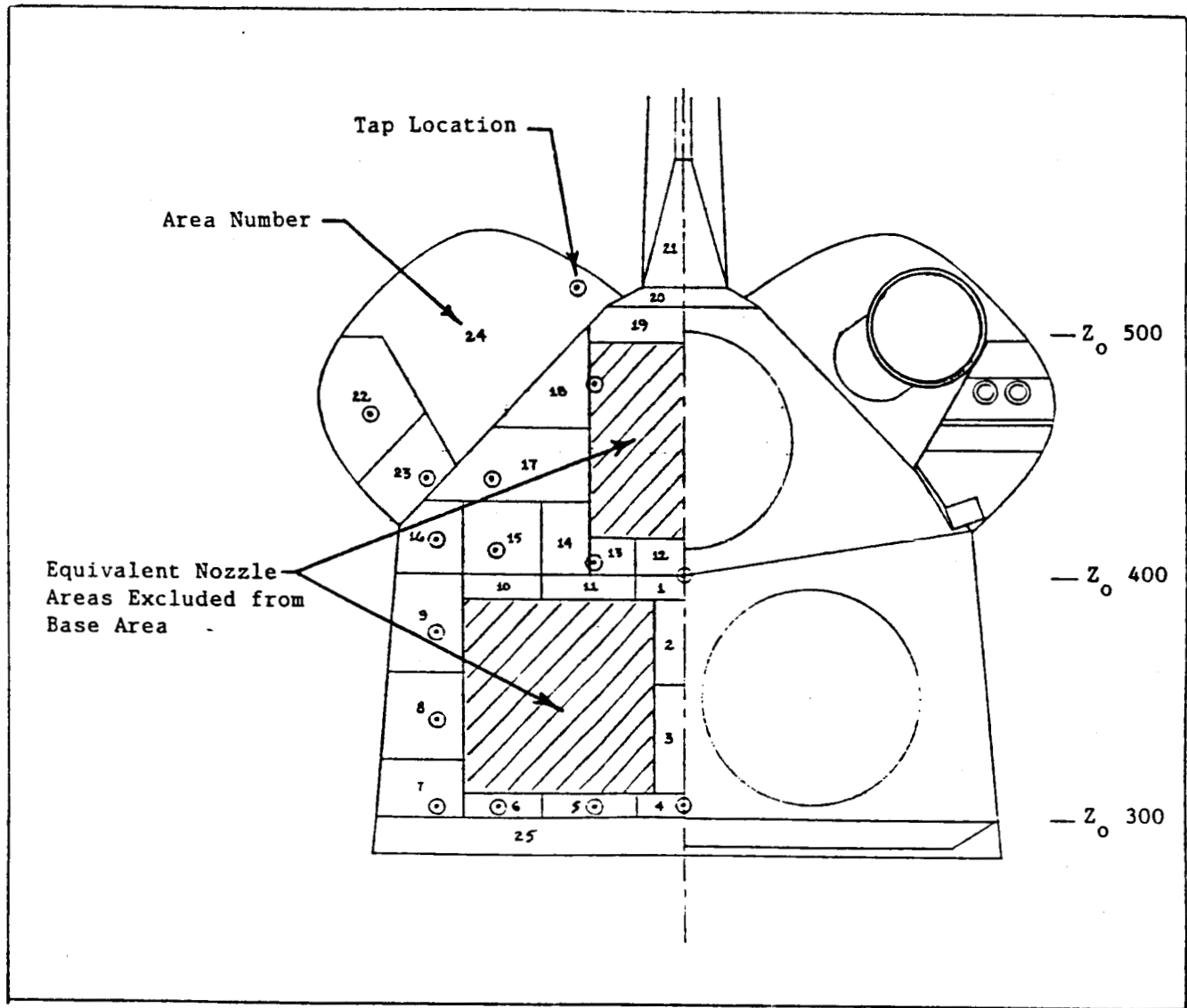


Fig. 6-3 Orbiter Base Relative Areas

Table 6-1 EFFECTIVE AREA MODELING OF TAPS FOR ORBITER FOREBODY

BODY	TAP #/FUNC.	AREA SQ.FT.	X	Y	Z	THETA	PHI
764. ORBITER BASE	66	1.3898	2238.98	-10.00	731.50	80.0	0.0
765. ORBITER BASE	66	1.3898	2238.98	10.00	731.50	80.0	0.0
766. ORBITER BASE	66	3.3330	2243.28	-6.00	706.50	80.0	0.0
767. ORBITER BASE	66	3.3330	2243.28	6.00	706.50	80.0	0.0
768. ORBITER BASE	67	3.3330	2250.20	-6.00	666.50	80.0	0.0
769. ORBITER BASE	67	3.3330	2250.20	6.00	666.50	80.0	0.0
770. ORBITER BASE	67	1.6670	2254.70	-10.00	640.50	80.0	0.0
771. ORBITER BASE	67	1.6670	2254.70	10.00	640.50	80.0	0.0
772. ORBITER BASE	68	3.3330	2254.70	-40.00	640.50	80.0	0.0
773. ORBITER BASE	68	3.3330	2254.70	40.00	640.50	80.0	0.0
774. ORBITER BASE	69	2.6670	2254.70	-76.00	640.50	80.0	0.0
775. ORBITER BASE	69	2.6670	2254.70	76.00	640.50	80.0	0.0
776. ORBITER BASE	70	6.3198	2253.50	-109.00	647.50	80.0	0.0
777. ORBITER BASE	70	6.3198	2253.50	109.00	647.50	80.0	0.0
778. ORBITER BASE	71	8.1250	2248.10	-108.00	678.50	80.0	0.0
779. ORBITER BASE	71	8.1250	2248.10	108.00	678.50	80.0	0.0
780. ORBITER BASE	72	8.1940	2241.50	-107.00	716.50	80.0	0.0
781. ORBITER BASE	72	8.1940	2241.50	107.00	716.50	80.0	0.0
782. ORBITER BASE	77	2.2220	2238.98	-75.00	731.50	80.0	0.0
783. ORBITER BASE	77	2.2220	2238.98	75.00	731.50	80.0	0.0
784. ORBITER BASE	76	2.7780	2238.90	-40.00	731.50	80.0	0.0
785. ORBITER BASE	76	2.7780	2238.90	40.00	731.50	80.0	0.0
786. ORBITER BASE	66	2.2220	2235.80	-10.00	744.50	74.0	0.0
787. ORBITER BASE	66	2.2220	2235.80	10.00	744.50	74.0	0.0
788. ORBITER BASE	76	2.2220	2235.80	-30.00	744.50	74.0	0.0
789. ORBITER BASE	76	2.2220	2235.80	30.00	744.50	74.0	0.0
790. ORBITER BASE	76	4.1670	2233.90	-50.00	751.50	74.0	0.0
791. ORBITER BASE	76	4.1670	2233.90	50.00	751.50	74.0	0.0
792. ORBITER BASE	77	6.2500	2233.90	-75.00	751.50	74.0	0.0
793. ORBITER BASE	77	6.2500	2233.90	75.00	751.50	74.0	0.0
794. ORBITER BASE	73	5.6700	2234.40	-103.00	749.50	74.0	0.0
795. ORBITER BASE	73	5.6700	2234.40	103.00	749.50	74.0	0.0
796. ORBITER BASE	(*73'+76')/2*	11.5170	2225.90	-62.00	780.50	74.0	0.0
797. ORBITER BASE	(*73'+76')/2*	11.5170	2225.90	62.00	780.50	74.0	0.0
798. ORBITER BASE	(*73'+76')/2*	5.6800	2217.30	-53.00	811.50	74.0	0.0
799. ORBITER BASE	(*73'+76')/2*	5.6800	2217.30	53.00	811.50	74.0	0.0
800. ORBITER BASE	80	3.7190	2209.60	-16.00	839.50	74.0	0.0
801. ORBITER BASE	80	3.7190	2209.60	16.00	839.50	74.0	0.0
802. ORBITER BASE	80	1.4170	2206.70	-13.00	850.00	74.0	0.0
803. ORBITER BASE	80	1.4170	2206.70	13.00	850.00	74.0	0.0
804. ORBITER BASE	80	3.9720	2248.08	-37.00	875.00	155.0	0.0
805. ORBITER BASE	80	3.9720	2249.00	37.00	875.00	155.0	0.0
806. ORBITER BASE	78	9.9000	2301.00	-130.00	801.50	90.0	0.0
807. ORBITER BASE	78	9.9000	2301.00	130.00	801.50	90.0	0.0
808. ORBITER BASE	79	6.7500	2301.00	-115.00	778.50	90.0	0.0
809. ORBITER BASE	79	6.7500	2301.00	115.00	778.50	90.0	0.0
810. ORBITER BASE	80	33.5000	2250.30	-68.00	826.50	90.0	0.0
811. ORBITER BASE	80	33.5000	2250.30	68.00	826.50	90.0	0.0
812. ORBITER BASE	22	11.2300	2254.00	-64.00	628.50	0.0	0.0
813. ORBITER BHSE	22	11.2300	2254.00	64.00	628.50	0.0	0.0
814. ORBITER BASE	65	8.1160	2271.00	-144.00	822.50	44.0	270.0
815. ORBITER BASE	65	8.1160	2271.00	144.00	822.50	44.0	90.0
816. ORBITER BASE	64	23.9500	2279.00	-130.00	770.50	150.0	270.0
817. ORBITER BASE	64	23.9500	2279.00	130.00	778.50	150.0	90.0
818. ORBITER BASE	73	40.0000	2251.00	-74.00	802.50	136.0	90.0
819. ORBITER BHSE	73	40.0000	2251.00	74.00	802.50	136.0	270.0
820. ORBITER BASE	40	8.0200	2343.00	-88.00	623.50	0.0	0.0
821. ORBITER BASE	40	8.0200	2343.00	88.00	623.50	0.0	0.0
822. ORBITER BASE	22	8.7500	2343.00	-38.00	623.50	0.0	0.0
823. ORBITER BASE	22	8.7500	2343.00	38.00	623.50	0.0	0.0
824. ORBITER BHSE	39	27.6000	2301.00	-95.00	623.50	0.0	0.0
825. ORBITER BASE	39	27.6000	2301.00	95.00	623.50	0.0	0.0
826. ORBITER BASE	20	25.0000	2303.00	-30.00	623.50	0.0	0.0
827. ORBITER BHSE	20	25.0000	2303.00	30.00	623.50	0.0	0.0
828. ORBITER BASE	20	12.7400	2266.00	-66.00	623.50	0.0	0.0
829. ORBITER BHSE	20	12.7400	2266.00	66.00	623.50	0.0	0.0

\*Tap weighted area averaging.

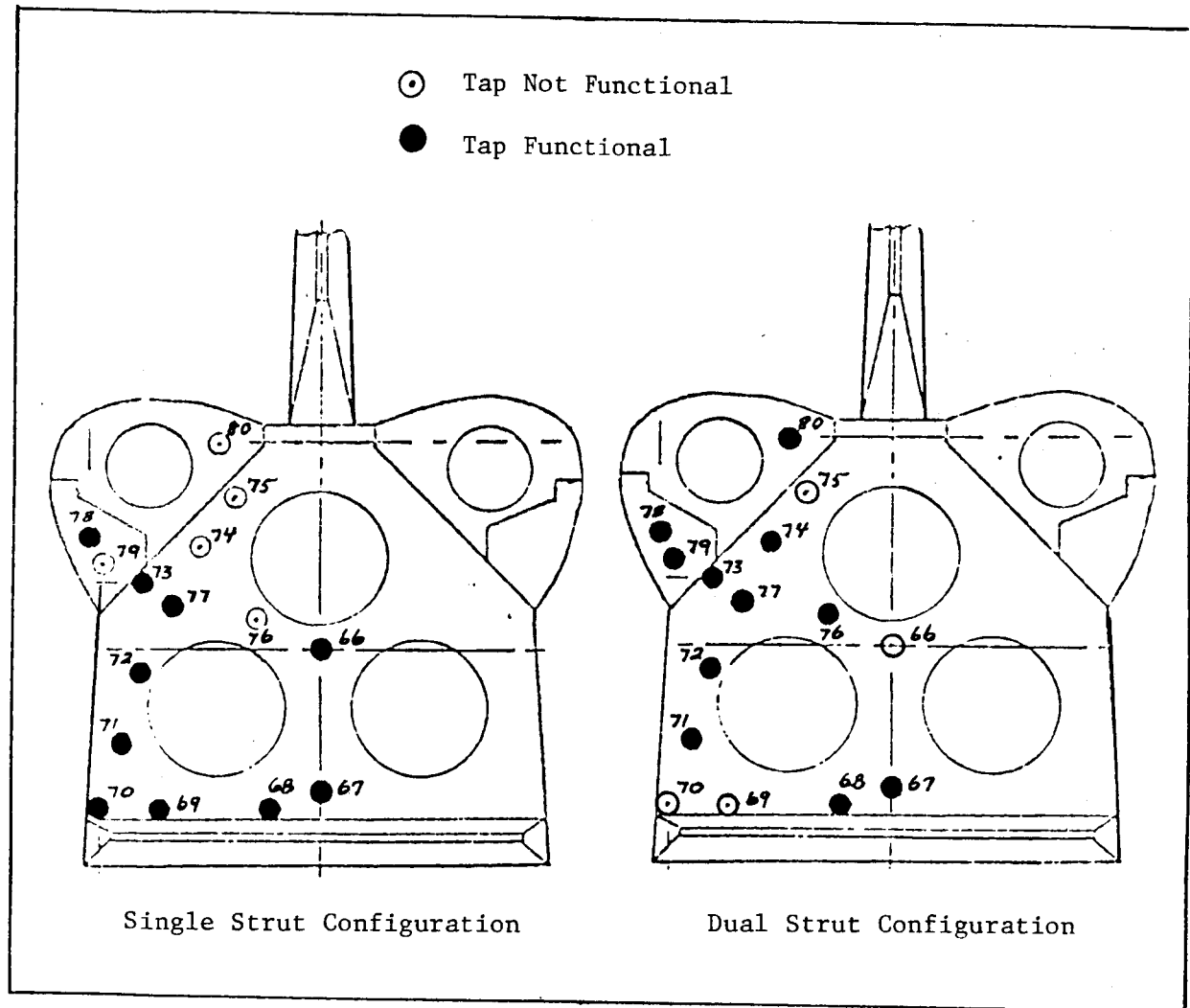


Fig. 6-4 Comparison of Base Pressure Instrumentation

## 6.2 OMS PODS

The OMS pods were analyzed using the effective areas and orientation as shown in Fig. 6-5. The areas shown in this figure are tabulated in Table 6-2. These forebody area values are projected areas from the orientation shown in Fig. 6-5. The angles shown are at the centroid of each area measured clockwise from the Y axis. Proximity Orbiter base pressures were used for the overhang area.

## 6.3 BODY FLAP

The Orbiter body flap instrumentation and effective areas for the base, are shown in Figs. 6-6, 6-7a and 6-7b, respectively. The effective areas that were used for pressure integration are listed in Table 6-3. The upper and aft surfaces of the body flap are included on the Orbiter base while lower surface is included in the Orbiter forebody.

## 6.4 ORBITER FOREBODY

The Orbiter forebody pressure instrumentation layout from the Pretest Report (Ref. 1) is shown in Fig. 6-8. The forebody plume induced aerodynamic characteristics were evaluated using power delta Cp values. Evaluation of the power delta Cp values showed that the forebody power effects were as far forward as the forward attach strut on the underside of the Orbiter and to the vicinity of the glove leading edge/fuselage junction on the side of the Orbiter. Figures 6-9a, 6-9b, and 6-10 show a sample of the analysis plots for several Mach numbers at two stations aft of the forward attach strut. These plots reflect the maximum power setting for the SSME and SRB along with the power variations of the SRB and SSME, respectively. Figure 6-11 represents the power delta Cp along the side of the Orbiter fuselage and indicates an incremental pressure of +0.015 forward of the glove fuselage junction at some Mach numbers.

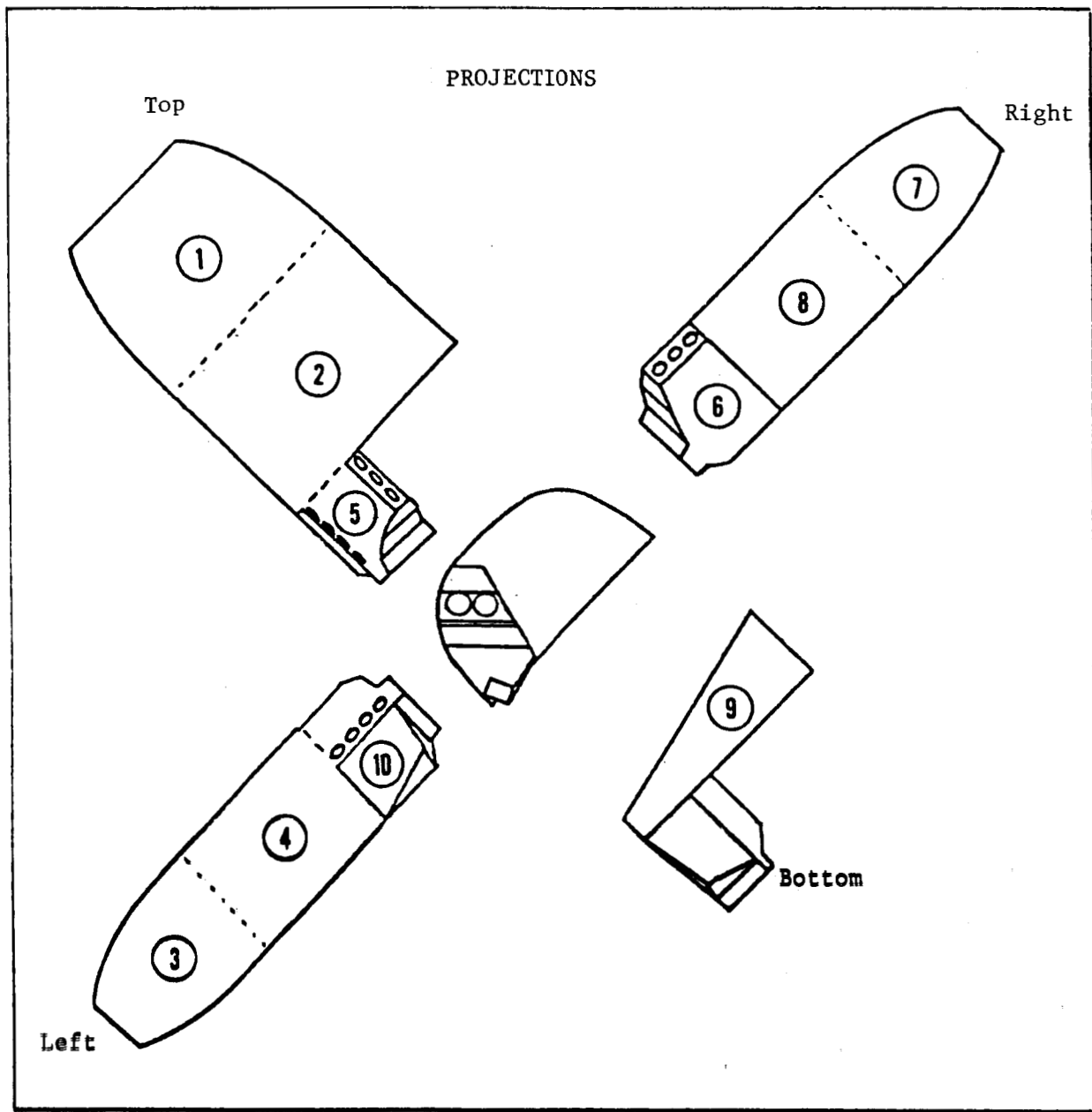


Fig. 6-5 OMS Pod Areas

Table 6-2 OMS POD (LEFT SIDE)

Area	X <sub>0</sub>	Y <sub>0</sub>	Z <sub>0</sub>	$\theta$ (deg)	Area (ft <sup>2</sup> )	Tap No.
1	1365	-122	513	134	48.560	60
2	1460	-122	513	134	83.986	61
3	1365	-135	438	47	27.344	51
4	1460	-135	438	47	43.944	51
5	1530	-144	486	134	8.116	65
6	1538	-138	442	47	23.958	64
7	1365	-52	522	30	27.344	62
8	1460	-52	522	30	43.944	63
9	1510	-74	466	134	40.00	73
10	1538	-110	470	47	23.958	80

Note: OMS pod overhang (duplicate of Area 6 from top side).

$\eta$	X/C <sub>OF</sub>				Surface	{
	-.10	.20	.60	.95		
.10	38		39	40	Upper	6
	33		34	35	Lower	
.50		20		22	Upper	5
		14	15	16	Lower	
.90		36			Upper	2
			37		Lower	
X/L <sub>B</sub>	1.018	1.043	1.0648	1.0680	Total	13

$C_{RF} = 81$  in.

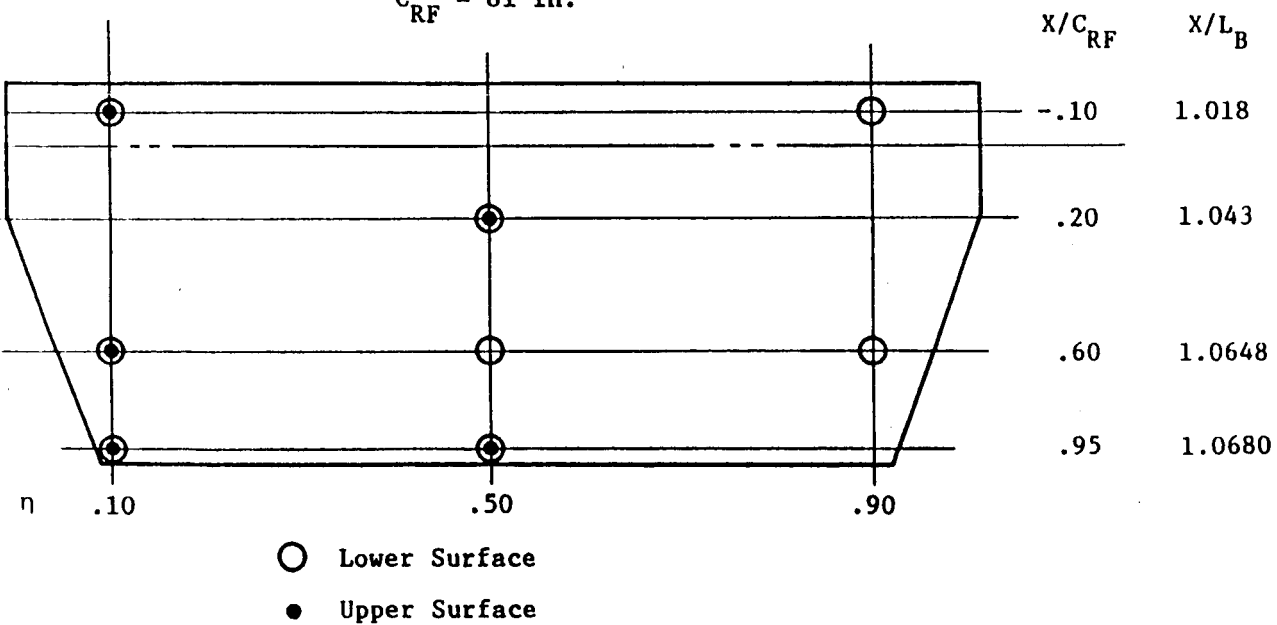


Fig. 6-6 Orbiter Body Flap Pressure Instrumentation

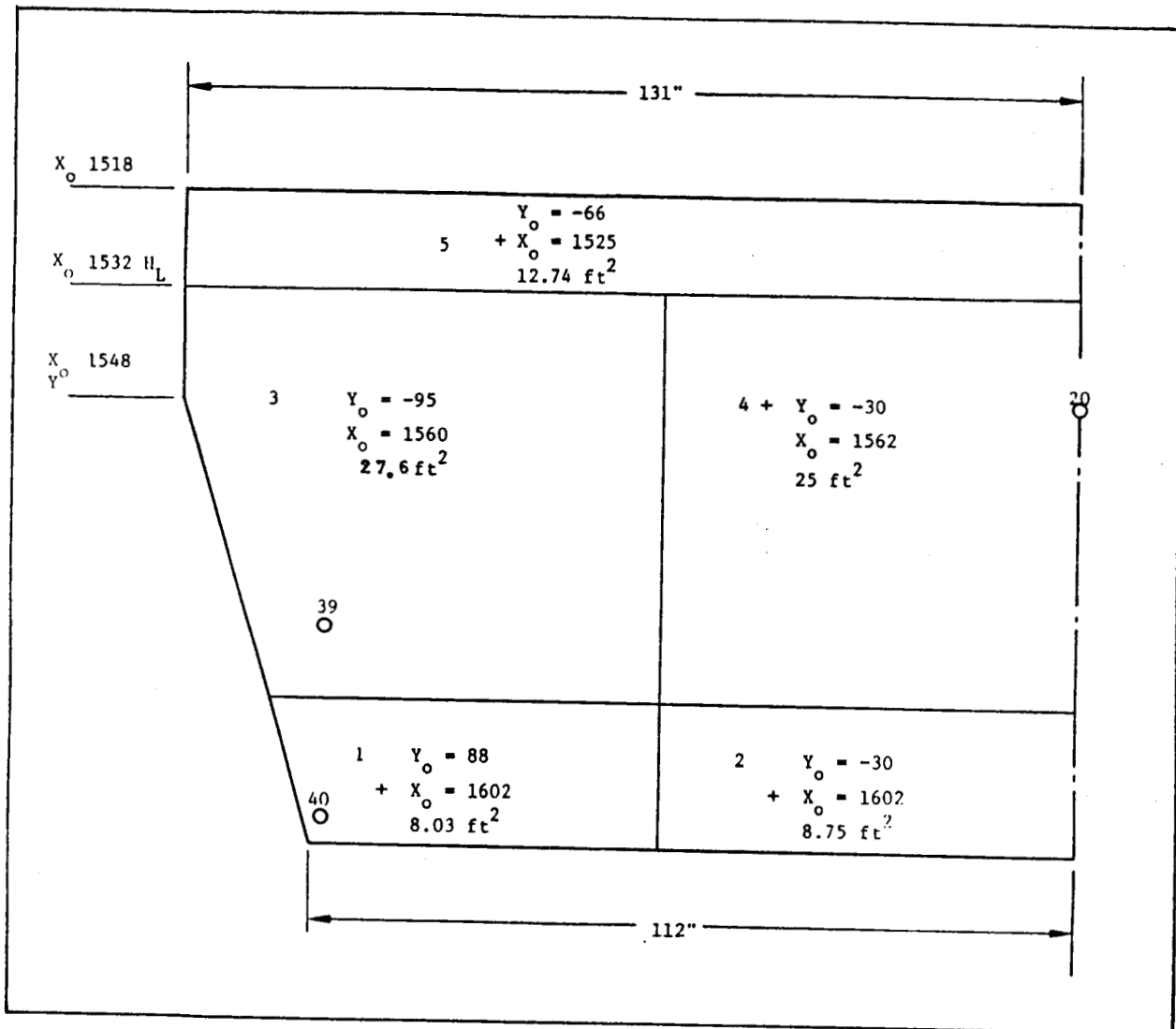


Fig. 6-7a Upper Body Flap Areas

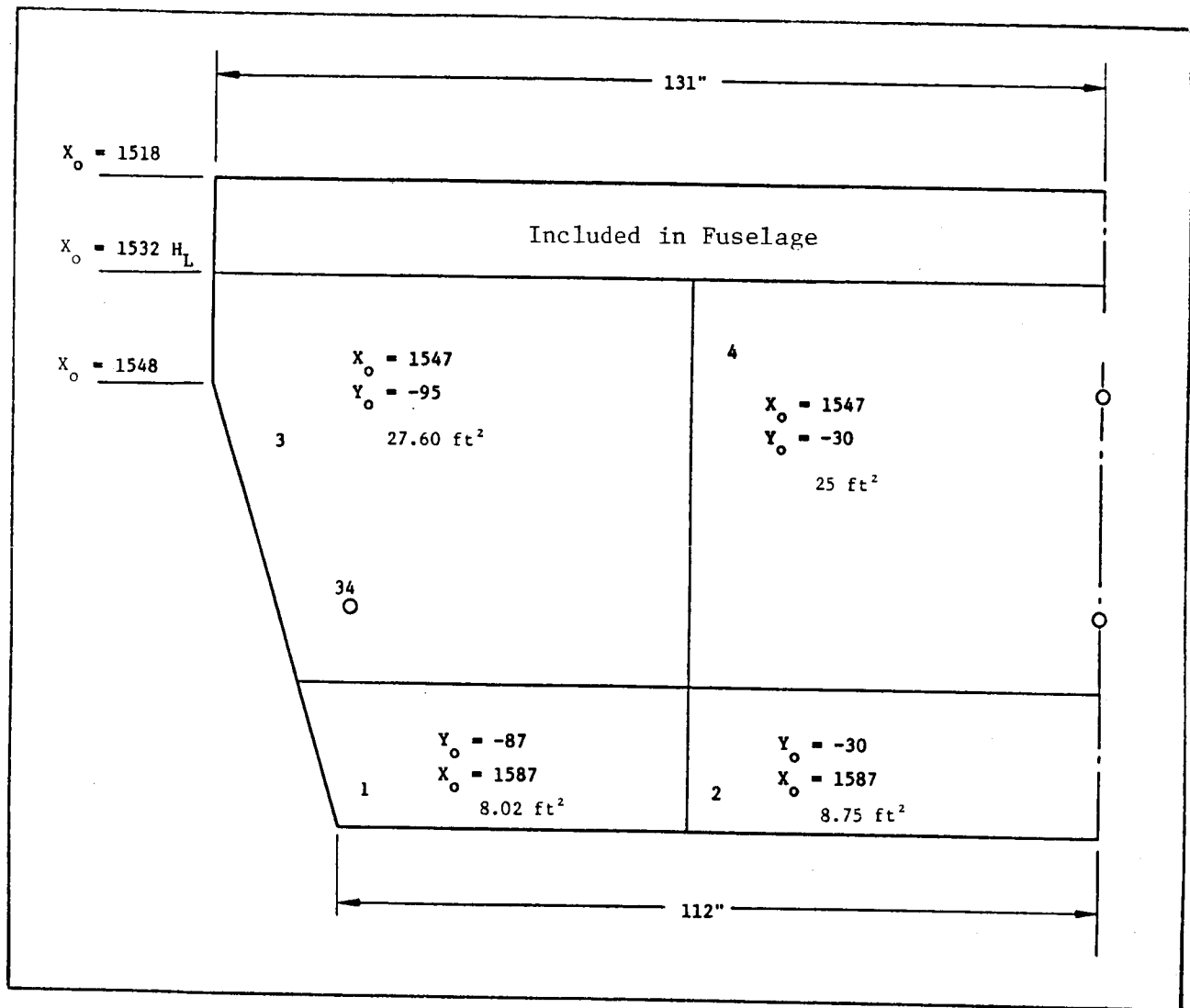
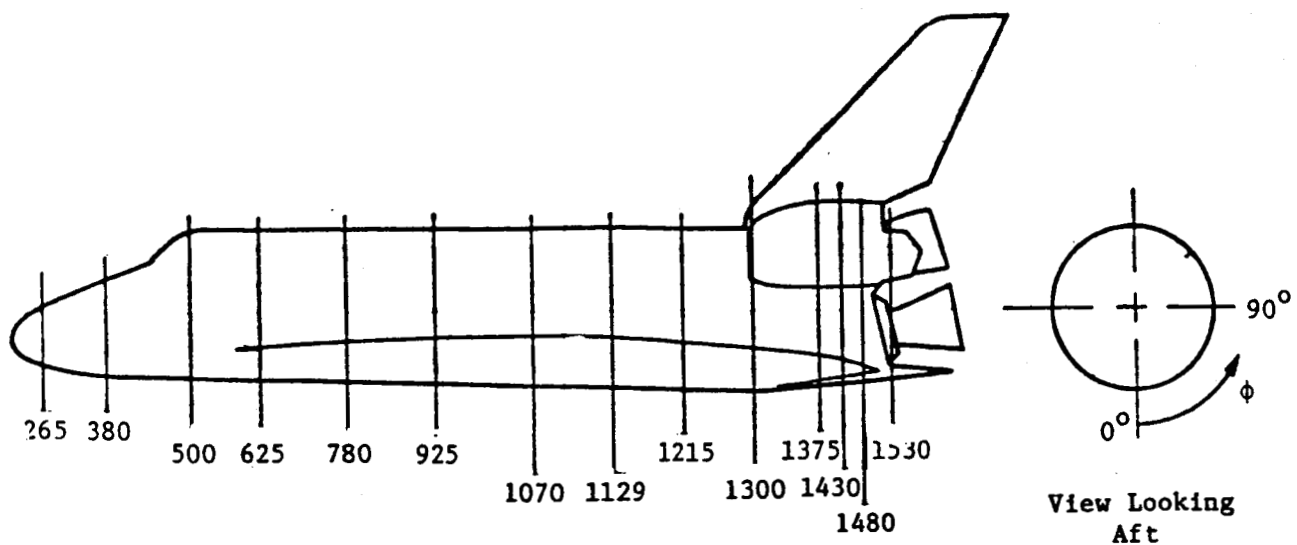


Fig. 6-7b Lower Body Flap Areas

Table 6-3 EFFECTIVE AREAS USED FOR PRESSURE INTEGRATION

Area No.	X <sub>o</sub>	Y <sub>o</sub>	Z <sub>o</sub>	Area (ft <sup>2</sup> )	Tap No.
1	1602	-88	288	8.02	40
2	1602	-30	288	8.75	40
3	1560	-95	288	27.60	39 Upper
4	1562	-30	288	25.00	20
5	1525	-66	288	12.74	20
1	1587	-87	288	8.02	34
2	1587	-30	288	8.75	15 Lower
3	1547	-95	288	27.60	34
4	1547	-30	288	25.00	14



Orb. Sta.		$\phi$ Radial (deg)									$\sum$
$X_o$ FS	$X_o / L_o$	0	20	90	110	120	150	165	180	270	
265	-0.0233	1									1
380	0.1124	2		43							2
500	0.3054	3		44							2
625	0.3023	4	24								2
780	0.4224	5	25	45							3
935	0.5340	6	26	46					17		4
1070	0.6818	7	27	47					18	53	5
1129	0.6939	8		48						54	3
1215	0.7595	9	28	49							3
1300	0.8234	10	29	50			59		19	55	6
1375	0.8835	11	30			60	62			56	5
1430	0.9261	12	31	51		61	63			57	6
1480	0.9649	13	32	52						58	4
1530	1.0026				64	65					2

$$L_o = 1290.3 \text{ in.}$$

Total 48

Note: 
$$\frac{X_{o1}}{L_o} = \frac{X_o}{L_o}$$

Fig. 6-8 Orbiter Forebody Pressure Instrumentation

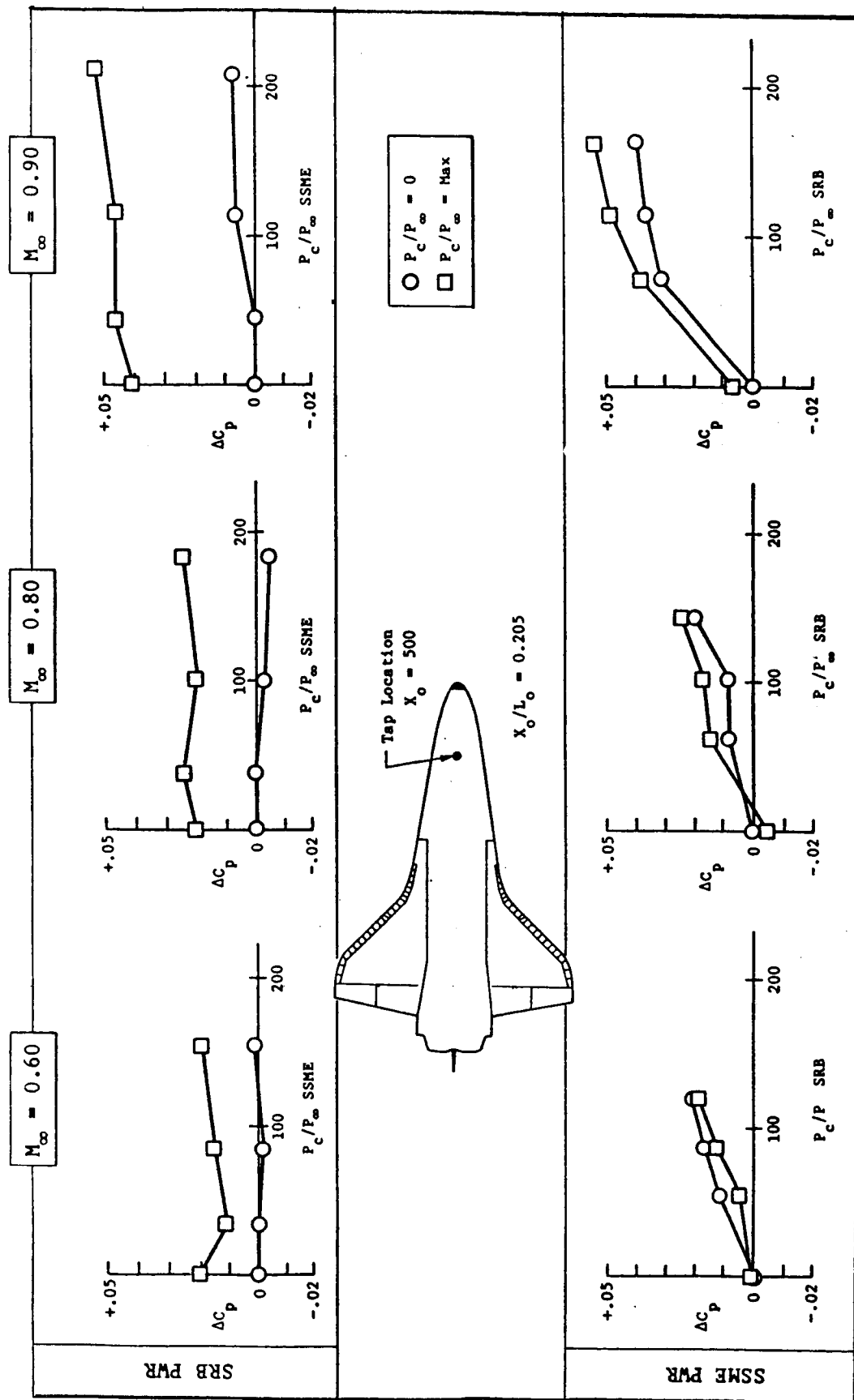


Fig. 6-9a Sample Analysis Plots ( $M_\infty = 0.60; 0.80; 0.90$ )

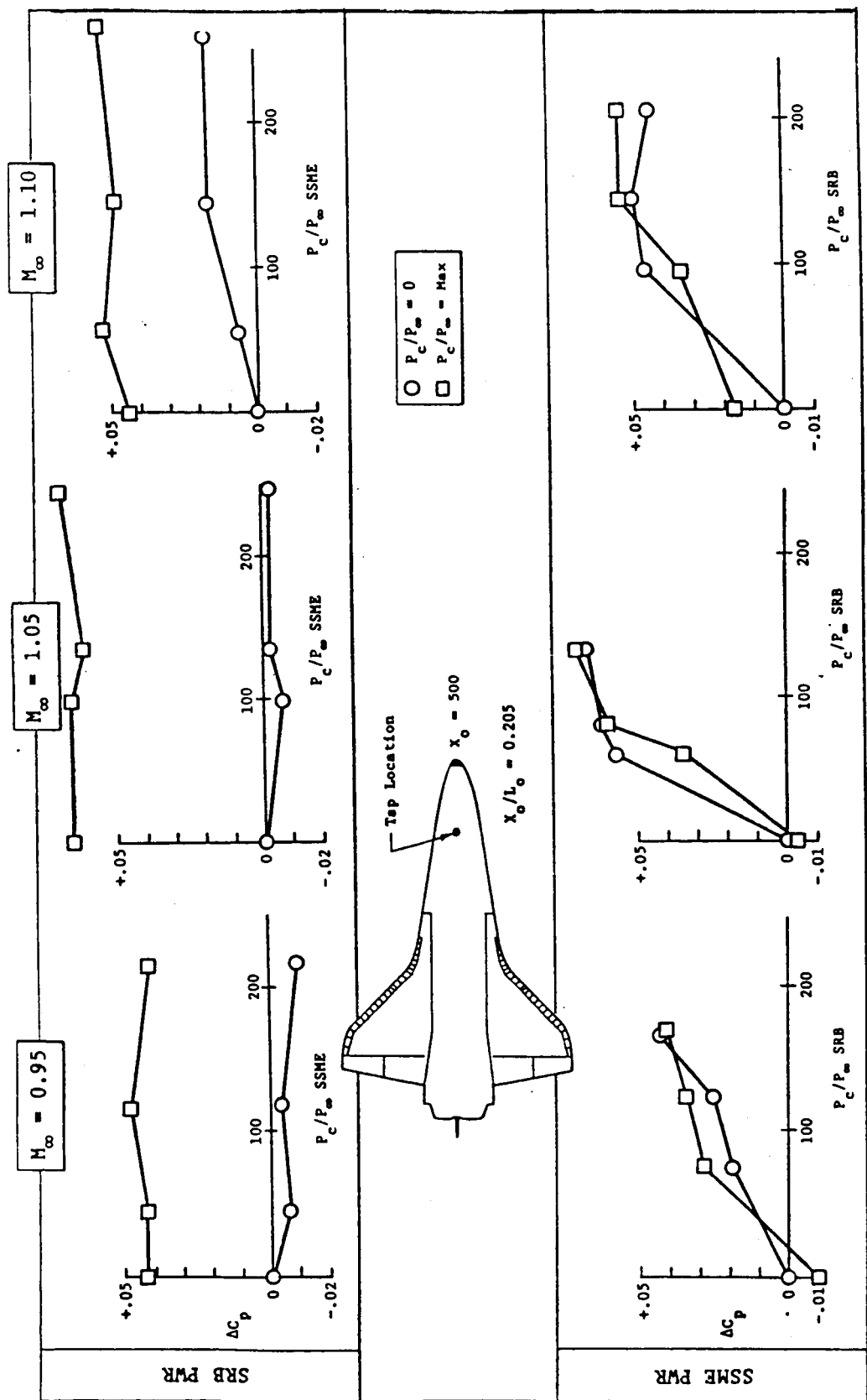
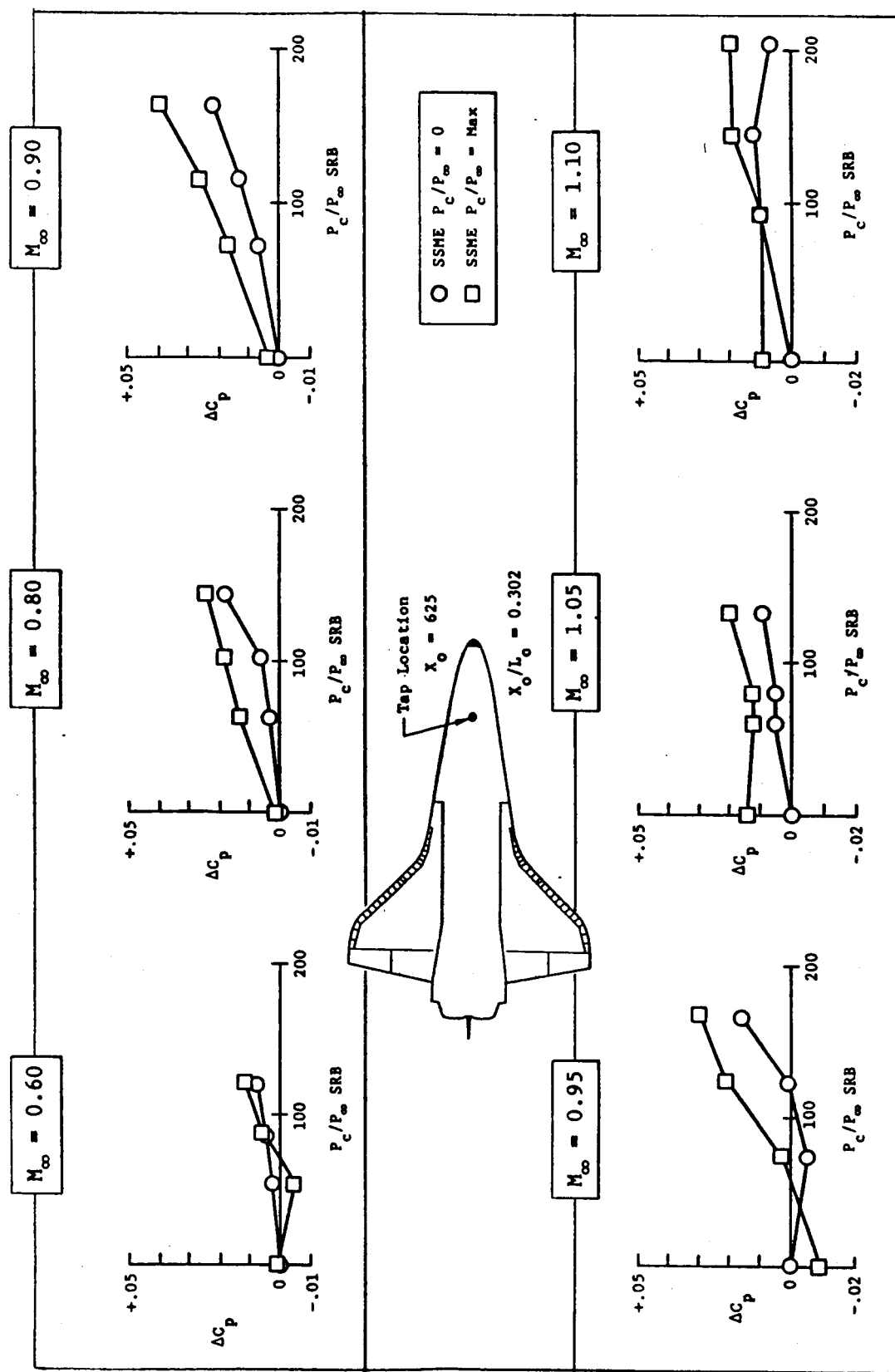
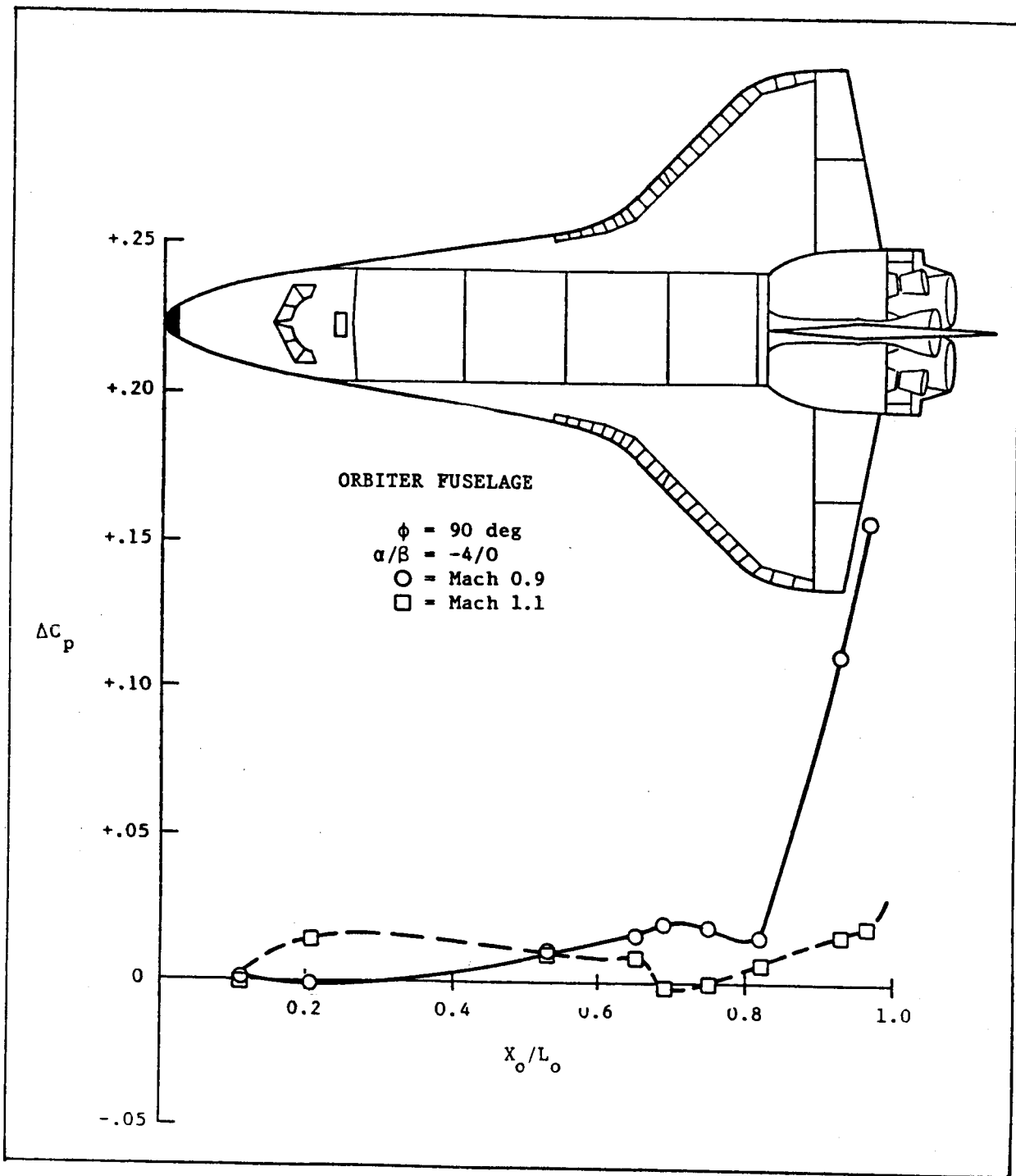


Fig. 6-9b Sample Analysis Plots ( $H_{\infty} = 0.95$ ; 1.05; 1.10)

Fig. 6-10 Sample Analysis Plots ( $M_\infty = 0.60; 0.80; 0.90$ )

Fig. 6-11 Power  $\Delta C_p$  Along Orbiter Fuselage

As a result of this analysis almost the entire Orbiter was modeled for the forebody pressure integration. Figure 6-12 shows the effective area modeling for the Orbiter forebody. These areas and their representative locations are listed in Table 6-4. The table also lists the pressure tap or weighted combination of pressure taps that were assigned to each area for the pressure integration. The weighted combination of taps was determined by analysis of pressure tap data in adjacent areas with the resulting weighted area averaging a function of the spatial location of the taps used and the integration area analyzed. The first six areas listed in the table do not have a pressure tap assigned for integration. This indicates that these areas were subsequently deleted from the area model because of insufficient pressure data.

#### 6.5 WING AND ELEVONS

The wing pressure instrumentation layout is presented in Fig. 6-13. The wing power delta pressures were evaluated at the high power levels and nominal power levels to determine the wing spatial content of the plume effects. An example of the evaluation at the nominal power level is shown in Figs. 6-14 and 6-15 for Mach 0.9 for the upper and lower wing surface. As can be seen from these figures, subsonically, the plume effects covered the entire Orbiter wing. In the transonic region, the spatial extent of the plume effects was somewhat smaller and generally limited to the aft portion of the wing and inboard elevon. For the pressure integration, the entire Orbiter wing was modeled as shown in Fig. 6-16. The areas, location and tap numbers assigned to each area are shown in Table 6-5. The sign convention used for the wing plume induced aerodynamic characteristics is presented in Fig. 6-17.

#### 6.6 VERTICAL TAIL

The vertical tail pressure instrumentation is shown in Fig. 6-18. Power delta Cp's were evaluated for both the maximum and nominal SSME/SRB

Table 6-4 EFFECTIVE AREA MODELING REPRESENTATIVE LOCATIONS

BODY	TAP #/FUNC.	AREA SQ.FT.	X	Y	Z	THETA	PHI
502. ORB. FBDY	0	41.6667	1296.00	0.00	836.50	0.0	0.0
503. ORB. FBDY	0	29.5139	1296.00	-50.00	836.50	0.0	0.0
504. ORB. FBDY	0	29.5139	1296.00	50.00	836.50	0.0	0.0
505. ORB. FBDY	0	83.3333	1441.00	0.00	836.50	0.0	0.0
506. ORB. FBDY	0	83.3333	1441.00	-60.00	836.50	0.0	0.0
507. ORB. FBDY	0	83.3333	1441.00	60.00	836.50	0.0	0.0
508. ORB. FBDY	(.5*18')*	83.3333	1641.00	0.00	836.50	0.0	0.0
509. ORB. FBDY	(.5*18')*	83.3333	1641.00	-60.00	836.50	0.0	0.0
510. ORB. FBDY	(.5*18')*	83.3333	1641.00	60.00	836.50	0.0	0.0
511. ORB. FBDY	18	83.3333	1841.00	0.00	836.50	0.0	0.0
512. ORB. FBDY	18	83.3333	1841.00	-60.00	836.50	0.0	0.0
513. ORB. FBDY	18	83.3333	1841.00	60.00	836.50	0.0	0.0
514. ORB. FBDY	59	45.8333	1996.00	0.00	836.50	0.0	0.0
515. ORB. FBDY	59	45.8333	1996.00	-60.00	836.50	0.0	0.0
516. ORB. FBDY	59	45.8333	1996.00	60.00	836.50	0.0	0.0
517. ORB. FBDY	62	11.7188	2096.00	-15.50	844.00	6.4	180.0
518. ORB. FBDY	62	11.7188	2096.00	15.50	844.00	6.4	180.0
519. ORB. FBDY	63	4.5139	2171.00	-20.00	849.00	6.4	180.0
520. ORB. FBDY	63	4.5139	2171.00	20.00	849.00	6.4	180.0
521. ORB. FBDY	44	43.4028	1136.00	-78.00	676.50	90.0	256.0
522. ORB. FBDY	44	43.4028	1136.00	78.00	676.50	90.0	184.0
523. ORB. FBDY	44	74.2108	1286.00	-102.00	741.50	90.0	264.0
524. ORB. FBDY	44	74.2108	1286.00	102.00	741.50	90.0	96.0
525. ORB. FBDY	44	49.3024	1266.00	-100.00	676.50	90.0	264.0
526. ORB. FBDY	44	49.3024	1266.00	100.00	676.50	90.0	96.0
527. ORB. FBDY	(*44'*.*7)+(*46'*.*3)*	103.1184	1411.00	-106.00	761.50	90.0	276.0
528. ORB. FBDY	(*44'*.*7)+(*46'*.*3)*	103.1184	1411.00	106.00	761.50	90.0	98.0
529. ORB. FBDY	281	39.8412	1411.00	-106.00	686.50	90.0	276.0
530. ORB. FBDY	281	39.8412	1411.00	106.00	686.50	90.0	98.0
531. ORB. FBDY	46	87.8416	1531.00	-106.00	761.50	90.0	276.0
532. ORB. FBDY	46	87.8416	1531.00	106.00	761.50	90.0	98.0
533. ORB. FBDY	282	29.9460	1531.00	-106.00	686.50	90.0	276.0
534. ORB. FBDY	282	29.9460	1531.00	106.00	686.50	90.0	98.0
535. ORB. FBDY	46	109.3608	1671.00	-106.00	761.50	90.0	276.0
536. ORB. FBDY	46	109.3608	1671.00	106.00	761.50	90.0	98.0
537. ORB. FBDY	46	36.4560	1671.00	-106.00	691.50	90.0	276.0
538. ORB. FBDY	46	36.4560	1671.00	106.00	691.50	90.0	98.0
539. ORB. FBDY	47	72.9120	1791.00	-106.00	761.50	90.0	276.0
540. ORB. FBDY	47	72.9120	1791.00	106.00	761.50	90.0	98.0
541. ORB. FBDY	283	24.3048	1791.00	-106.00	691.50	90.0	276.0
542. ORB. FBDY	283	24.3048	1791.00	106.00	691.50	90.0	98.0
543. ORB. FBDY	48	57.2680	1878.50	-106.00	761.50	90.0	276.0
544. ORB. FBDY	48	57.2800	1878.50	106.00	761.50	90.0	98.0
545. ORB. FBDY	(*48'*.*4)+(*203'*.*4)+(*204'*.*2)*	19.5308	1878.50	-106.00	686.50	90.0	276.0
546. ORB. FBDY	(*48'*.*4)+(*203'*.*4)+(*204'*.*2)*	19.5308	1878.50	106.00	686.50	90.0	98.0
547. ORB. FBDY	(.6*50')+(.4*48')*	62.4960	1953.50	-106.00	756.50	90.0	276.0
548. ORB. FBDY	(.6*50')+(.4*48')*	62.4960	1953.50	106.00	756.50	90.0	98.0
549. ORB. FBDY	284	19.5308	1953.50	-106.00	676.50	90.0	276.0
550. ORB. FBDY	284	19.5308	1953.50	106.00	676.50	90.0	98.0
551. ORB. FBDY	50	52.0000	2021.00	-106.00	756.50	90.0	276.0
552. ORB. FBDY	50	52.0000	2021.00	106.00	756.50	90.0	98.0
553. ORB. FBDY	285	17.0720	2021.00	-106.00	671.50	90.0	276.0
554. ORB. FBDY	285	17.0720	2021.00	106.00	671.50	90.0	98.0
555. ORB. FBDY	(*58'*.*5)+(*51'*.*5)*	60.9336	2116.00	-112.00	719.00	87.4	265.2
556. ORB. FBDY	(*58'*.*5)+(*51'*.*5)*	60.9336	2116.00	112.00	719.00	87.4	94.8

\* Weighted area averaging.

(Continued)

Table 6-4 (Concluded)

BODY	TAP #/FUNC.	AREA SQ.FT.	X	Y	Z	THETA	PHI
557. ORB. FBDY	(*.51*.3)+(*.205*.7)*	43.4434	2116.00	-114.00	661.50	67.4	264.0
558. ORB. FBDY	(*.51*.3)+(*.205*.7)*	43.4434	2116.00	114.00	661.50	87.4	96.0
559. ORB. FBDY	52	27.0816	2211.00	-120.00	719.00	03.6	265.2
560. ORB. FBDY	52	27.0816	2211.00	120.00	719.00	83.6	94.8
561. ORB. FBDY	52	24.3040	2216.00	-124.00	661.50	82.8	264.0
562. ORB. FBDY	52	24.3040	2216.00	124.00	661.50	82.8	96.0
563. ORB. FBDY	24	83.7500	1366.00	-65.00	606.50	160.0	0.0
564. ORB. FBDY	24	83.7500	1366.00	65.00	606.50	180.0	0.0
565. ORB. FBDY	25	83.7500	1516.00	-65.00	606.50	160.0	0.0
566. ORB. FBDY	25	83.7500	1516.00	65.00	606.50	180.0	0.0
567. ORB. FBDY	26	83.7500	1666.00	-65.00	601.50	100.0	0.0
568. ORB. FBDY	26	83.7500	1666.00	65.00	601.50	160.0	0.0
569. ORB. FBDY	7	83.7500	1816.00	-65.00	599.00	180.0	0.0
570. ORB. FBDY	7	83.7500	1816.00	65.00	599.00	180.0	0.0
571. ORB. FBDY	(*.9*.5+*.205*.5)*	62.0130	1948.50	-65.00	596.50	180.0	0.0
572. ORB. FBDY	(*.9*.5+*.205*.5)*	62.0130	1948.50	65.00	596.50	180.0	0.0
573. ORB. FBDY	10	34.9200	2035.50	-65.00	596.50	160.0	0.0
574. ORB. FBDY	10	34.9200	2035.50	65.00	596.50	160.0	0.0
575. ORB. FBDY	11	43.9200	2103.50	-67.50	596.50	100.0	0.0
576. ORB. FBDY	11	43.9200	2103.50	67.50	596.50	100.0	0.0
577. ORB. FBDY	(.3*12)+(3*30)+(4*32)*	40.7990	2171.00	-70.00	601.50	173.5	0.0
578. ORB. FBDY	(.3*12)+(3*30)+(4*32)*	40.7990	2171.00	70.00	601.50	173.5	0.0
579. ORB. FBDY	32	47.4610	2238.50	-72.50	609.00	173.5	0.0
580. ORB. FBDY	32	47.4610	2238.50	72.50	609.00	173.5	0.0
581. ORB. FBDY	1	27.3400	1023.50	0.00	641.50	161.0	100.0
582. ORB. FBDY	(.5*1)+(5*3)*	43.4920	1128.50	0.00	621.50	174.0	180.0
583. ORB. FBDY	3	34.7220	1241.00	0.00	611.50	160.0	0.0
584. ORB. FBDY	4	52.0040	1366.00	0.00	606.50	100.0	0.0
585. ORB. FBDY	5	52.0040	1516.00	0.00	606.50	100.0	0.0
586. ORB. FBDY	6	52.0040	1666.00	0.00	601.50	180.0	0.0
587. ORB. FBDY	7	34.7220	1791.00	0.00	599.00	180.0	0.0
588. ORB. FBDY	8	28.6460	1893.50	0.00	596.50	160.0	0.0
589. ORB. FBDY	9	26.0420	1966.00	0.00	596.50	180.0	0.0
590. ORB. FBDY	10	21.7020	2035.50	0.00	596.50	100.0	0.0
591. ORB. FBDY	11	26.0420	2103.50	0.00	596.50	100.0	0.0
592. ORB. FBDY	12	21.7020	2171.00	0.00	601.50	173.5	0.0
593. ORB. FBDY	60	48.5600	2106.00	-122.00	849.50	44.0	270.0
594. ORB. FBDY	60	48.5600	2106.00	122.00	849.50	44.0	90.0
595. ORB. FBDY	61	83.9860	2201.00	-122.00	849.50	44.0	270.0
596. ORB. FBDY	61	83.9860	2201.00	122.00	849.50	44.0	90.0
597. ORB. FBDY	51	27.3440	2106.00	-135.00	774.50	150.0	270.0
598. ORB. FBDY	51	27.3440	2106.00	135.00	774.50	150.0	90.0
599. ORB. FBDY	51	43.9440	2201.00	-135.00	774.50	150.0	270.0
600. ORB. FBDY	51	43.9440	2201.00	135.00	774.50	150.0	90.0
601. ORB. FBDY	62	27.3440	2106.00	-52.00	858.50	43.0	90.0
602. ORB. FBDY	62	27.3440	2106.00	52.00	858.50	43.0	270.0
603. ORB. FBDY	63	43.9440	2201.00	-52.00	858.50	43.0	90.0
604. ORB. FBDY	63	43.9440	2201.00	52.00	858.50	43.0	270.0
605. ORB. FBDY	80	23.9500	2279.00	-110.00	806.50	46.0	90.0
606. ORB. FBDY	80	23.9500	2279.00	110.00	806.50	46.0	270.0
607. ORB. FBDY	13	23.4360	2238.50	0.00	609.00	173.5	0.0

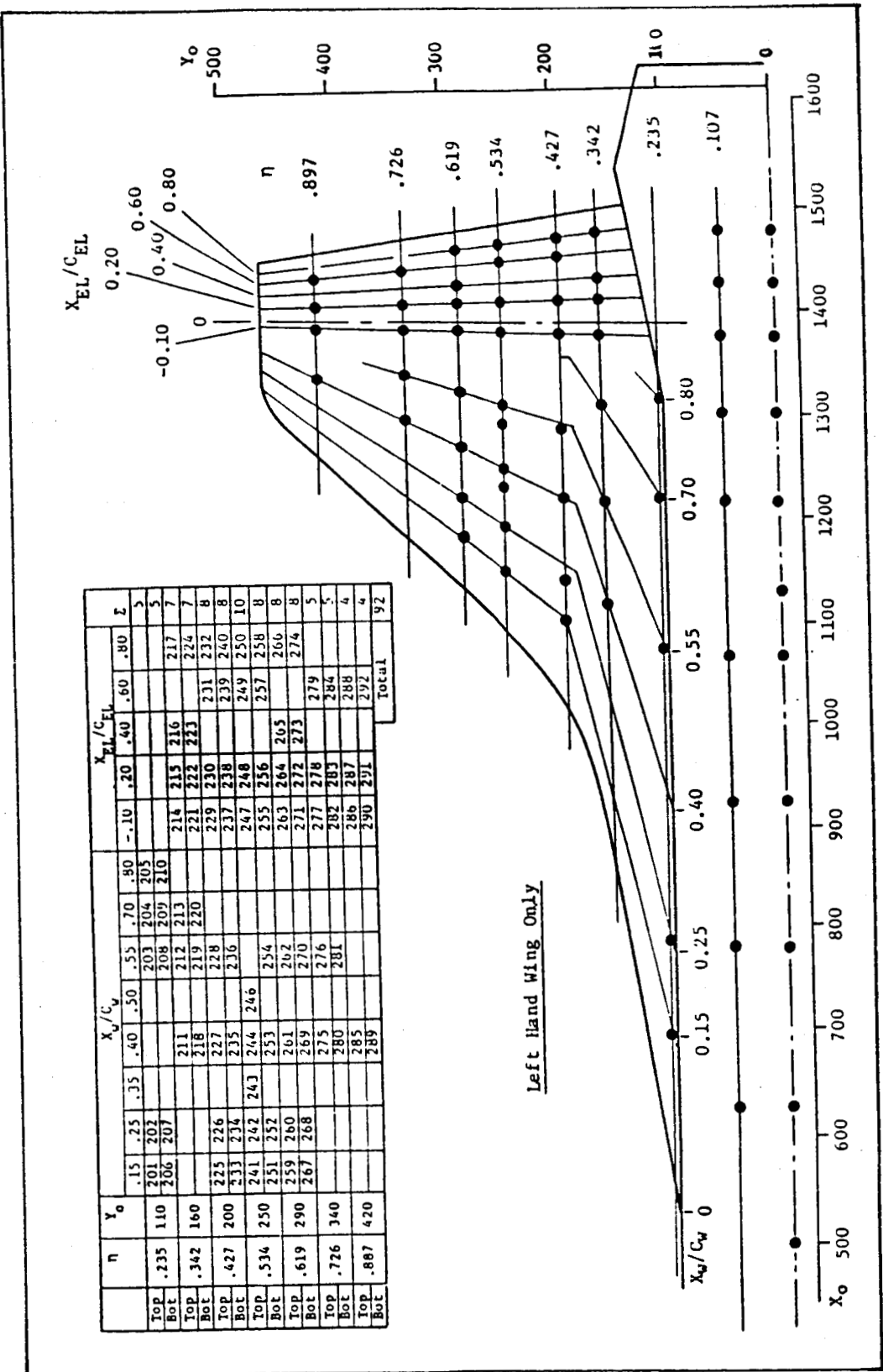


Fig. 6-13 Orbiter Wing Pressure Instrumentation Layout

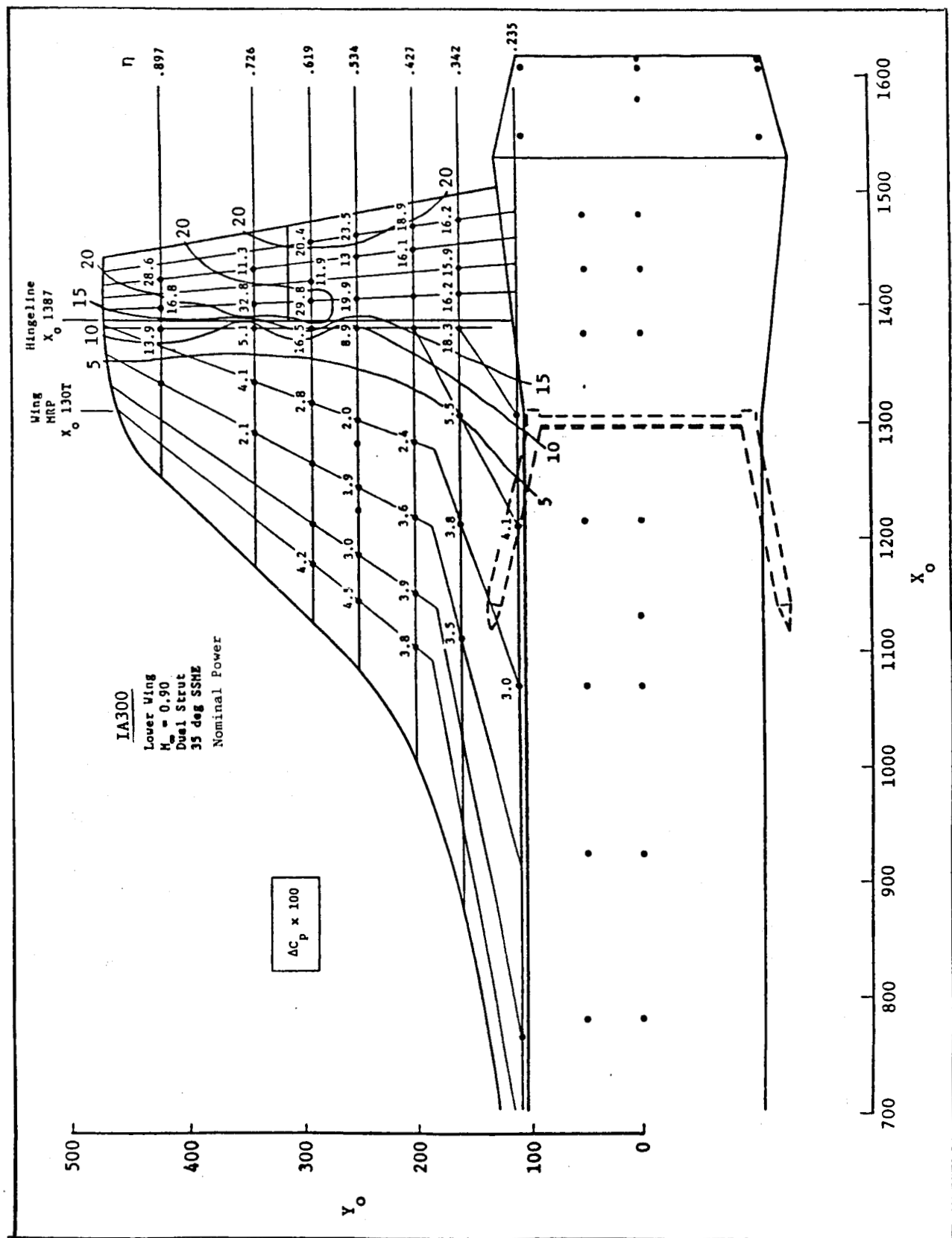


Fig. 6-14 Orbiter Wing Pressure Integration

ORIGINAL PAGE IS  
OF POOR QUALITY

LMSC-HEC TR D951415

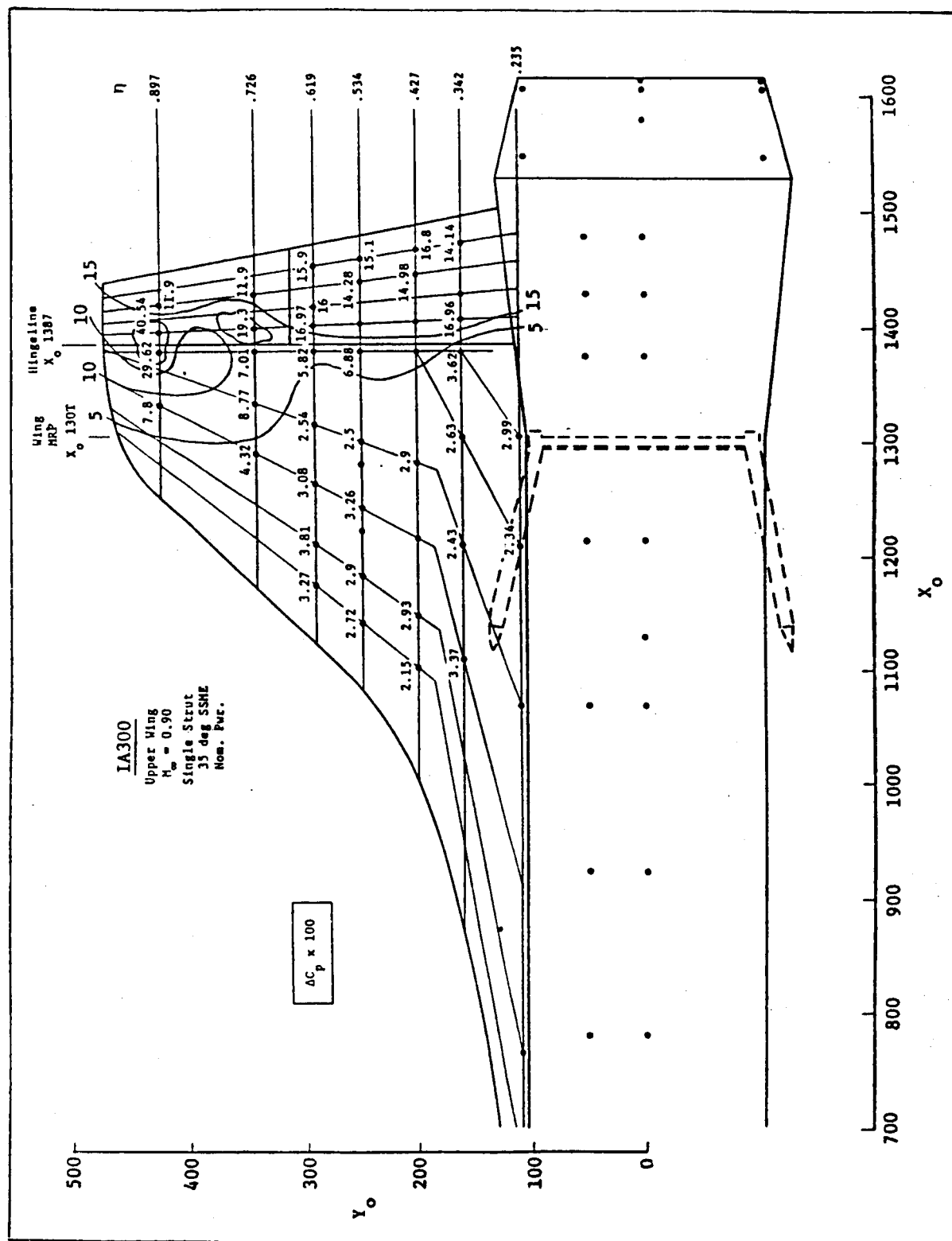


Fig. 6-15 Wing Pressure Evaluation

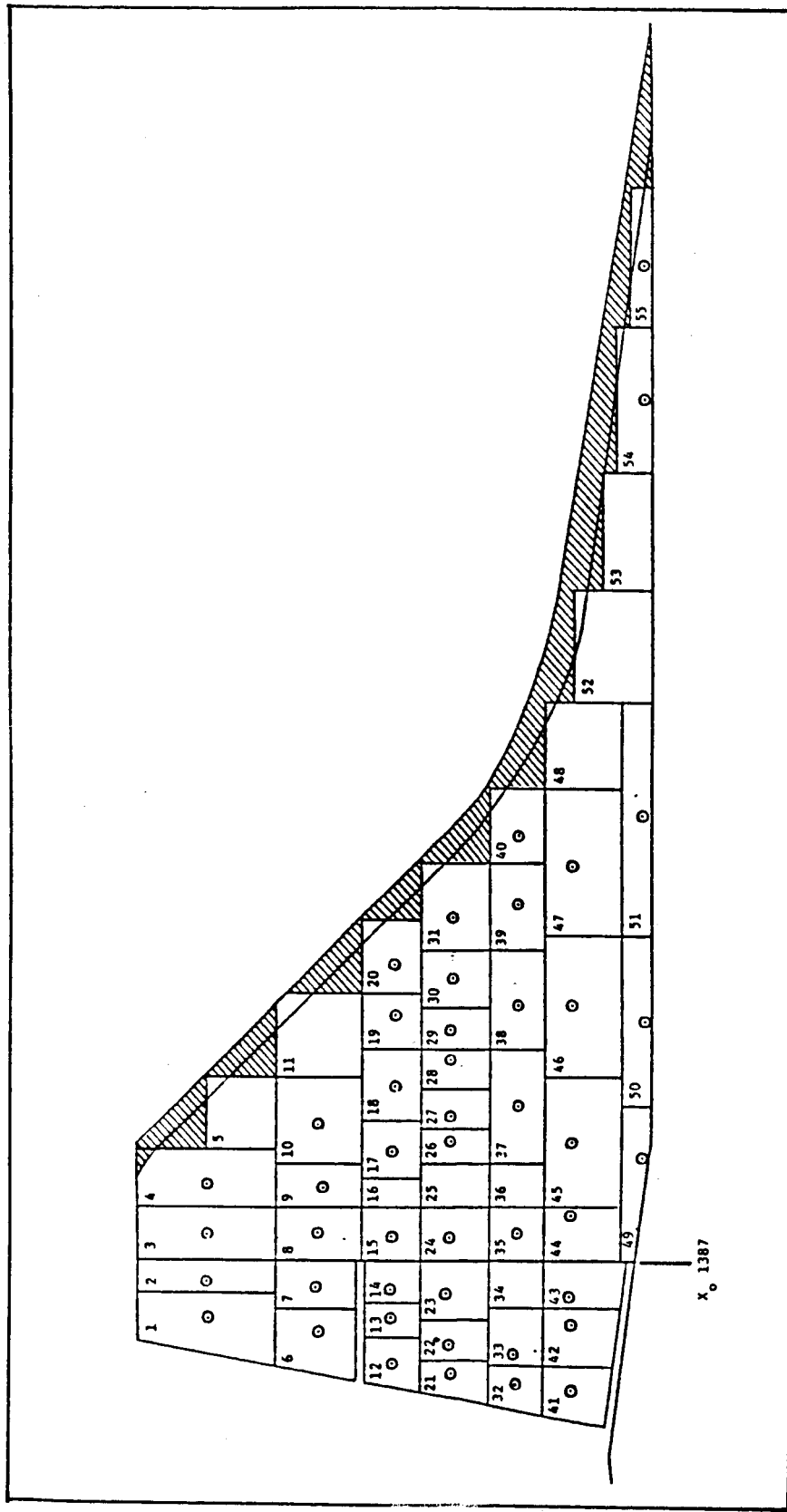


Fig. 6-16 Wing Pressure Instrumentation Areas

Table 6-5 EFFECTIVE AREA MODELING OF TAPS FOR RIGHT ORBITER WING

BODY	TAP #/FUNC.	AREA SQ.FT.	X	Y	Z	THETA	PHI
394. RIGHT WING	281	9.7220	1431.00	-113.00	636.50	0.0	0.0
395. RIGHT WING	286	9.7220	1431.00	-113.00	636.50	180.0	0.0
396. RIGHT WING	202	16.6670	1531.00	-118.00	636.50	0.0	0.0
397. RIGHT WING	25	16.6670	1531.00	-118.00	636.50	180.0	0.0
398. RIGHT WING	202	18.0890	1621.00	-123.00	636.50	0.0	0.0
399. RIGHT WING	(.5*25)+(1.5*26)*	18.0890	1621.00	-123.00	636.50	100.0	0.0
400. RIGHT WING	(.5*202)+(1.5*203)*	30.0000	1701.00	-133.00	636.50	0.0	0.0
401. RIGHT WING	26	30.0000	1701.00	-133.00	636.50	180.0	0.0
402. RIGHT WING	203	22.2200	1821.00	-116.00	636.50	0.0	0.0
403. RIGHT WING	208	22.2200	1821.00	-116.00	636.50	180.0	0.0
404. RIGHT WING	204	16.6670	1961.00	-116.00	636.50	0.0	0.0
405. RIGHT WING	209	16.6670	1961.00	-116.00	636.50	180.0	0.0
406. RIGHT WING	205	12.0830	2061.00	-116.00	636.50	0.0	0.0
407. RIGHT WING	210	12.0830	2061.00	-116.00	636.50	180.0	0.0
408. RIGHT WING	203	22.5000	1771.00	-154.00	636.50	0.0	0.0
409. RIGHT WING	208	22.5000	1771.00	-154.00	636.50	180.0	0.0
410. RIGHT WING	211	37.5000	1851.00	-154.00	636.50	0.0	0.0
411. RIGHT WING	218	37.5000	1851.00	-154.00	636.50	180.0	0.0
412. RIGHT WING	212	37.5000	1951.00	-154.00	636.50	0.0	0.0
413. RIGHT WING	219	37.5000	1951.00	-154.00	636.50	180.0	0.0
414. RIGHT WING	213	33.7500	2046.00	-154.00	636.50	0.0	0.0
415. RIGHT WING	228	33.7500	2046.00	-154.00	636.50	180.0	0.0
416. RIGHT WING	214	13.8750	2109.00	-154.00	636.50	0.0	0.0
417. RIGHT WING	221	13.8750	2109.00	-154.00	636.50	180.0	0.0
418. RIGHT WING	225	13.0890	1026.00	-200.00	636.50	0.0	0.0
419. RIGHT WING	233	13.0890	1826.00	-200.00	636.50	180.0	0.0
420. RIGHT WING	226	16.6670	1081.00	-200.00	636.50	0.0	0.0
421. RIGHT WING	234	16.6670	1881.00	-200.00	636.50	180.0	0.0
422. RIGHT WING	(.212*.7)+(.243*.3)*	19.4440	1996.00	-200.00	636.50	0.0	0.0
423. RIGHT WING	235	19.4440	1996.00	-200.00	636.50	180.0	0.0
424. RIGHT WING	228	22.2220	2021.00	-200.00	636.50	0.0	0.0
425. RIGHT WING	236	22.2220	2021.00	-200.00	636.50	180.0	0.0
426. RIGHT WING	213	0.3330	2076.00	-200.00	636.50	0.0	0.0
427. RIGHT WING	220	0.3330	2076.00	-200.00	636.50	180.0	0.0
428. RIGHT WING	214	18.2700	2109.00	-200.00	636.50	0.0	0.0
429. RIGHT WING	221	18.2700	2109.00	-200.00	636.50	180.0	0.0
430. RIGHT WING	241	20.8330	1881.00	-245.00	636.50	0.0	0.0
431. RIGHT WING	251	20.8330	1881.00	-245.00	636.50	180.0	0.0
432. RIGHT WING	242	13.8890	1931.00	-245.00	636.50	0.0	0.0
433. RIGHT WING	252	13.8890	1931.00	-245.00	636.50	100.0	0.0
434. RIGHT WING	243	10.4170	1966.00	-245.00	636.50	0.0	0.0
435. RIGHT WING	253	10.4170	1966.00	-245.00	636.50	100.0	0.0
436. RIGHT WING	244	9.7220	1995.00	-245.00	636.50	0.0	0.0
437. RIGHT WING	253	9.7220	1995.00	-245.00	636.50	180.0	0.0
438. RIGHT WING	245	9.7220	2023.00	-245.00	636.50	0.0	0.0
439. RIGHT WING	254	9.7220	2023.00	-245.00	636.50	160.0	0.0
440. RIGHT WING	246	0.3330	2049.00	-245.00	636.50	0.0	0.0
441. RIGHT WING	254	0.3330	2049.00	-245.00	636.50	100.0	0.0
442. RIGHT WING	(.247*.7)+(.246*.3)*	10.4170	2076.00	-245.00	636.50	0.0	0.0
443. RIGHT WING	(.255*.7)+(.254*.3)*	10.4170	2076.00	-245.00	636.50	100.0	0.0
444. RIGHT WING	247	12.8470	2109.00	-245.00	636.50	0.0	0.0
445. RIGHT WING	255	12.8470	2109.00	-245.00	636.50	180.0	0.0
446. RIGHT WING	259	13.8090	1916.00	-290.00	636.50	0.0	0.0
447. RIGHT WING	267	13.8090	1916.00	-290.00	636.50	180.0	0.0
448. RIGHT WING	260	11.1110	1961.00	-290.00	636.50	0.0	0.0
449. RIGHT WING	252	11.1110	1961.00	-290.00	636.50	160.0	0.0
450. RIGHT WING	261	13.8890	2006.00	-290.00	636.50	0.0	0.0
451. RIGHT WING	(.253*.7)+(.280*.3)*	13.8890	2006.00	-290.00	636.50	180.0	0.0
452. RIGHT WING	262	11.1110	2051.00	-290.00	636.50	0.0	0.0
453. RIGHT WING	270	11.1110	2051.00	-290.00	636.50	160.0	0.0
454. RIGHT WING	(.263*.5)+(.262*.5)*	5.5560	2091.00	-290.00	636.50	0.0	0.0
455. RIGHT WING	(.270*.5)+(.271*.5)*	5.5560	2091.00	-290.00	636.50	160.0	0.0
456. RIGHT WING	263	10.2780	2109.00	-290.00	636.50	0.0	0.0
457. RIGHT WING	271	10.2780	2109.00	-290.00	636.50	180.0	0.0
458. RIGHT WING	(.280*.5)*	25.0000	1917.00	-340.00	636.50	0.0	0.0
459. RIGHT WING	(.267*.5)*	25.0000	1917.00	-340.00	636.50	160.0	0.0
460. RIGHT WING	275	25.0000	2031.00	-340.00	636.50	0.0	0.0
461. RIGHT WING	280	25.0000	2031.00	-340.00	636.50	100.0	0.0
462. RIGHT WING	276	12.5000	2076.00	-340.00	636.50	0.0	0.0
463. RIGHT WING	281	12.5000	2076.00	-340.00	636.50	160.0	0.0
464. RIGHT WING	(.275*.5)*	17.3610	2026.00	-395.00	636.50	0.0	0.0
465. RIGHT WING	(.260*.5)*	17.3610	2026.00	-395.00	636.50	100.0	0.0
466. RIGHT WING	285	25.6660	2071.00	-410.00	636.50	0.0	0.0
467. RIGHT WING	289	26.6660	2071.00	-410.00	636.50	100.0	0.0
468. RIGHT WING	286	24.6660	2109.00	-410.00	636.50	0.0	0.0
469. RIGHT WING	290	24.6660	2109.00	-410.00	636.50	100.0	0.0

\*Weighted area averaging.

(Continued)

Table 6-5 (Continued)

BODY	TAP #/FUNC.	AREA SQ.FT.	X	Y	Z	THETR	PHI
656. LEFT WING	201	9.7228	1431.00	113.00	636.50	0.0	0.0
657. LEFT WING	206	9.7228	1431.00	113.00	636.50	180.0	0.0
658. LEFT WING	202	16.6678	1531.00	118.00	636.50	0.0	0.0
659. LEFT WING	23	16.6678	1531.00	118.00	636.50	180.0	0.0
660. LEFT WING	202	10.6690	1621.00	123.00	636.50	0.0	0.0
661. LEFT WING	(.5*25')+(.5*26')- *	18.6598	1621.00	123.00	636.50	160.0	0.0
662. LEFT WING	(.5*282')+(.5*283') *	38.8888	1701.00	133.00	636.50	0.0	0.0
663. LEFT WING	26	30.8888	1701.00	133.00	636.50	180.0	0.0
664. LEFT WING	203	22.2208	1821.00	116.00	636.50	0.0	0.0
665. LEFT WING	208	22.2208	1821.00	116.00	636.50	180.0	0.0
666. LEFT WING	204	16.6678	1961.00	116.00	636.50	0.0	0.0
667. LEFT WING	209	16.6678	1961.00	116.00	636.50	180.0	0.0
668. LEFT WING	205	12.0838	2061.00	116.00	636.50	0.0	0.0
669. LEFT WING	210	12.0838	2061.00	116.00	636.50	160.0	0.0
670. LEFT WING	203	22.5000	1771.00	154.00	636.50	0.0	0.0
671. LEFT WING	208	22.5000	1771.00	154.00	636.50	160.0	0.0
672. LEFT WING	211	37.5088	1851.00	154.00	636.50	0.0	0.0
673. LEFT WING	218	37.5088	1851.00	154.00	636.50	180.0	0.0
674. LEFT WING	212	37.5088	1951.00	154.00	636.50	0.0	0.0
675. LEFT WING	219	37.5088	1951.00	154.00	636.50	160.0	0.0
676. LEFT WING	213	33.7500	2046.00	154.00	636.50	0.0	0.0
677. LEFT WING	220	33.7500	2046.00	154.00	636.50	160.0	0.0
678. LEFT WING	214	13.8750	2109.00	154.00	636.50	0.0	0.0
679. LEFT WING	221	13.0750	2109.00	154.00	636.50	160.0	0.0
680. LEFT WING	225	13.0898	1626.00	208.00	636.50	0.0	0.0
681. LEFT WING	233	13.0898	1626.00	208.00	636.50	180.0	0.0
682. LEFT WING	226	16.6678	1681.00	208.00	636.50	0.0	0.0
683. LEFT WING	234	16.6678	1681.00	208.00	636.50	180.0	0.0
684. LEFT WING	(*212*.7)+(*243*.3) *	19.4448	1956.00	208.00	636.50	0.0	0.0
685. LEFT WING	235	19.4448	1956.00	208.00	636.50	180.0	0.0
686. LEFT WING	228	22.2220	2021.00	208.00	636.50	0.0	0.0
687. LEFT WING	236	22.2220	2021.00	208.00	636.50	180.0	0.0
688. LEFT WING	213	0.3330	2076.00	208.00	636.50	0.0	0.0
689. LEFT WING	228	0.3330	2076.00	208.00	636.50	180.0	0.0
690. LEFT WING	214	10.2780	2109.00	208.00	636.50	0.0	0.0
691. LEFT WING	221	10.2768	2109.00	208.00	636.50	180.0	0.0
692. LEFT WING	241	20.8330	1681.00	245.00	636.50	0.0	0.0
693. LEFT WING	251	20.8330	1681.00	245.00	636.50	180.0	0.0
694. LEFT WING	242	13.8898	1931.00	245.00	636.50	0.0	0.0
695. LEFT WING	252	13.8898	1931.00	245.00	636.50	180.0	0.0
696. LEFT WING	243	10.4170	1956.00	245.00	636.50	0.0	0.0
697. LEFT WING	253	10.4170	1956.00	245.00	636.50	180.0	0.0
698. LEFT WING	244	9.7220	1995.00	245.00	636.50	0.0	0.0
699. LEFT WING	253	9.7220	1995.00	245.00	636.50	180.0	0.0
700. LEFT WING	243	9.7220	2023.00	245.00	636.50	0.0	0.0
701. LEFT WING	254	9.7220	2023.00	245.00	636.50	180.0	0.0
702. LEFT WING	246	0.3330	2049.00	245.00	636.50	0.0	0.0
703. LEFT WING	254	0.3330	2049.00	245.00	636.50	180.0	0.0
704. LEFT WING	(*247*.7)+(*246*.3) *	10.4170	2076.00	245.00	636.50	0.0	0.0
705. LEFT WING	(*255*.7)+(*254*.3) *	10.4170	2076.00	245.00	636.50	180.0	0.0
706. LEFT WING	247	12.8470	2109.00	245.00	636.50	0.0	0.0
707. LEFT WING	255	12.8470	2109.00	245.00	636.50	180.0	0.0
708. LEFT WING	259	13.0090	1916.00	290.00	636.50	0.0	0.0
709. LEFT WING	267	13.0090	1916.00	290.00	636.50	180.0	0.0
710. LEFT WING	260	11.1110	1961.00	290.00	636.50	0.0	0.0
711. LEFT WING	252	11.1110	1961.00	290.00	636.50	180.0	0.0
712. LEFT WING	261	13.0090	2006.00	290.00	636.50	0.0	0.0
713. LEFT WING	(*253*.7)+(*200*.3)*	13.0090	2006.00	290.00	636.50	180.0	0.0
714. LEFT WING	262	11.1110	2051.00	290.00	636.50	0.0	0.0
715. LEFT WING	270	11.1110	2051.00	290.00	636.50	180.0	0.0
716. LEFT WING	(*263*.5)+(*262*.5)*	-5.5560	2081.00	340.00	636.50	0.0	0.0
717. LEFT WING	(*270*.5)+(*271*.5)*	5.5560	2081.00	340.00	636.50	180.0	0.0
718. LEFT WING	263	10.2760	2109.00	340.00	636.50	0.0	0.0
719. LEFT WING	271	10.2760	2109.00	340.00	636.50	180.0	0.0
720. LEFT WING	(*260*.5)*	25.0000	1917.00	340.00	636.50	0.0	0.0
721. LEFT WING	(*267*.5)*	25.0000	1917.00	340.00	636.50	180.0	0.0
722. LEFT WING	275	25.0000	2031.00	340.00	636.50	0.0	0.0
723. LEFT WING	280	25.0000	2031.00	340.00	636.50	180.0	0.0
724. LEFT WING	276	12.5000	2076.00	340.00	636.50	0.0	0.0
725. LEFT WING	281	12.5000	2076.00	340.00	636.50	180.0	0.0
726. LEFT WING	(*275*.5)*	17.3610	2026.00	395.00	636.50	0.0	0.0
727. LEFT WING	(*208*.5)*	17.3610	2026.00	395.00	636.50	180.0	0.0
728. LEFT WING	285	26.6660	2071.00	410.00	636.50	0.0	0.0
729. LEFT WING	289	26.6660	2071.00	410.00	636.50	180.0	0.0
730. LEFT WING	286	24.6660	2109.00	410.00	636.50	0.0	0.0
731. LEFT WING	290	24.6660	2109.00	410.00	636.50	180.0	0.0

(Continued)

Table 6-5 (Concluded)

BODY	TAP #/FUNC.	AREA SQ.FT.	X	Y	Z	THETA	PHI
732. LEFT IELV	215	12.0330	2145.00	-154.00	636.50	0.0	0.0
733. LEFT IELV	(*215*.7)+(*217*.3)*	14.1670	2181.00	-154.00	636.50	0.0	0.0
734. LEFT IELV	217	11.4060	2219.00	*154.00	636.50	0.0	0.0
735. LEFT IELV-	231	9.1670	2145.00	-200.00	636.50	0.0	0.0
736. LEFT IELV	231	11.1110	2181.00	-200.00	636.50	0.0	0.0
737. LEFT IELV	232	8.0550	2215.00	-200.00	636.50	0.0	0.0
738. LEFT IELV	249	14.2360	2149.00	-245.00	636.50	0.0	0.0
739. LEFT IELV	249	9.7220	2183.00	-245.00	636.50	0.0	0.0
740. LEFT IELV	250	12.1530	2209.00	-245.00	636.50	0.0	0.0
741. LEFT IELV	264	7.6530	2141.00	-290.00	636.50	0.0	0.0
742. LEFT IELV-	265	6.3330	2170.00	-290.00	636.50	0.0	0.0
743. LEFT IELV	266	8.9720	2197.00	-290.00	636.50	0.0	0.0
744. LEFT OELV	278	12.8330	2145.00	-340.00	636.50	0.0	0.0
745. LEFT OELV	279	17.1110	2181.00	-340.00	636.50	0.0	0.0
746. LEFT OELV-	207	15.3330	2139.00	-410.00	636.50	0.0	0.0
747. LEFT OELV	208	27.3330	2169.00	-410.00	636.50	0.0	0.0
748. LEFT IELV	222	12.8330	2145.00	-154.00	636.50	180.0	0.0
749. LEFT IELV	223	14.1670	2181.00	-154.00	636.50	180.0	0.0
750. LEFT IELV	224	11.4860	2219.00	-154.00	636.50	180.0	0.0
751. LEFT IELV	222	9.1670	2145.00	-200.00	636.50	180.0	0.0
752. LEFT IELV	239	11.1110	2181.00	-200.00	636.50	180.0	0.0
753. LEFT IELV	240	8.0550	2215.00	-200.00	636.50	180.0	0.0
754. LEFT IELV	256	14.2360	2149.00	-245.00	636.50	180.0	0.0
755. LEFT IELV	257	9.7220	2183.00	-245.00	636.50	180.0	0.0
756. LEFT IELV-	258	12.1530	2209.00	-245.00	636.50	180.0	0.0
757. LEFT IELV	272	7.6530	2141.00	-290.00	636.50	180.0	0.0
758. LEFT IELV	273	6.3330	2170.00	-290.00	636.50	180.0	0.0
759. LEFT IELV	274	8.9720	2197.00	-290.00	636.50	180.0	0.0
760. LEFT OELV	283	12.8330	2145.00	-340.00	636.50	180.0	0.0
761. LEFT OELV	284	17.1110	2181.00	-340.00	636.50	180.0	0.0
762. LEFT OELV	291	15.3330	2139.00	-410.00	636.50	180.0	0.0
763. LEFT OELV	292	27.3330	2169.00	-410.00	636.50	180.0	0.0
470. RIGHT IELV	215	12.0330	2145.00	154.00	636.50	0.0	0.0
471. RIGHT IELV	(*215*.7)+(*217*.3)*	14.1670	2181.00	154.00	636.50	0.0	0.0
472. RIGHT IELV	217	11.4060	2219.00	154.00	636.50	0.0	0.0
473. RIGHT IELV	231	9.1670	2145.00	200.00	636.50	0.0	0.0
474. RIGHT IELV	231	11.1110	2181.00	200.00	636.50	0.0	0.0
475. RIGHT IELV	232	8.0550	2215.00	200.00	636.50	0.0	0.0
476. RIGHT IELV	249	14.2360	2149.00	245.00	636.50	0.0	0.0
477. RIGHT IELV	249	9.7220	2183.00	245.00	636.50	0.0	0.0
478. RIGHT IELV	250	12.1530	2209.00	245.00	636.50	0.0	0.0
479. RIGHT IELV	264	7.6530	2141.00	290.00	636.50	0.0	0.0
480. RIGHT IELV	265	6.3330	2170.00	290.00	636.50	0.0	0.0
481. RIGHT IELV	266	8.9720	2197.00	290.00	636.50	0.0	0.0
482. RIGHT OELV	278	12.8330	2145.00	340.00	636.50	0.0	0.0
483. RIGHT OELV	279	17.1110	2181.00	340.00	636.50	0.0	0.0
484. RIGHT OELV	287	15.3330	2139.00	410.00	636.50	0.0	0.0
485. RIGHT OELV	289	27.3330	2169.00	410.00	636.50	0.0	0.0
486. RIGHT IELV	222	12.8330	2145.00	154.00	636.50	180.0	0.0
487. RIGHT IELV	223	14.1670	2181.00	154.00	636.50	180.0	0.0
488. RIGHT IELV	224	11.4060	2219.00	154.00	636.50	180.0	0.0
489. RIGHT IELV	222	9.1670	2145.00	200.00	636.50	180.0	0.0
490. RIGHT IELV	239	11.1110	2181.00	200.00	636.50	180.0	0.0
491. RIGHT IELV	240	8.0550	2215.00	200.00	636.50	180.0	0.0
492. RIGHT IELV	256	14.2360	2149.00	245.00	636.50	180.0	0.0
493. RIGHT IELV	257	9.7220	2183.00	245.00	636.50	180.0	0.0
494. RIGHT IELV	258	12.1530	2209.00	245.00	636.50	180.0	0.0
495. RIGHT IELV	272	7.6530	2141.00	290.00	636.50	180.0	0.0
496. RIGHT IELV	273	6.3330	2170.00	290.00	636.50	180.0	0.0
497. RIGHT IELV	274	8.9720	2197.00	290.00	636.50	180.0	0.0
498. RIGHIT OELV	283	12.0330	2145.00	340.00	636.50	180.0	0.0
499. RIGHT OELV	284	17.1110	2181.00	340.00	636.50	180.0	0.0
500. RIGHT OELV	291	15.3330	2139.00	410.00	636.50	180.0	0.0
501. RIGHT OELV	292	27.3330	2169.00	410.00	636.50	180.0	0.0

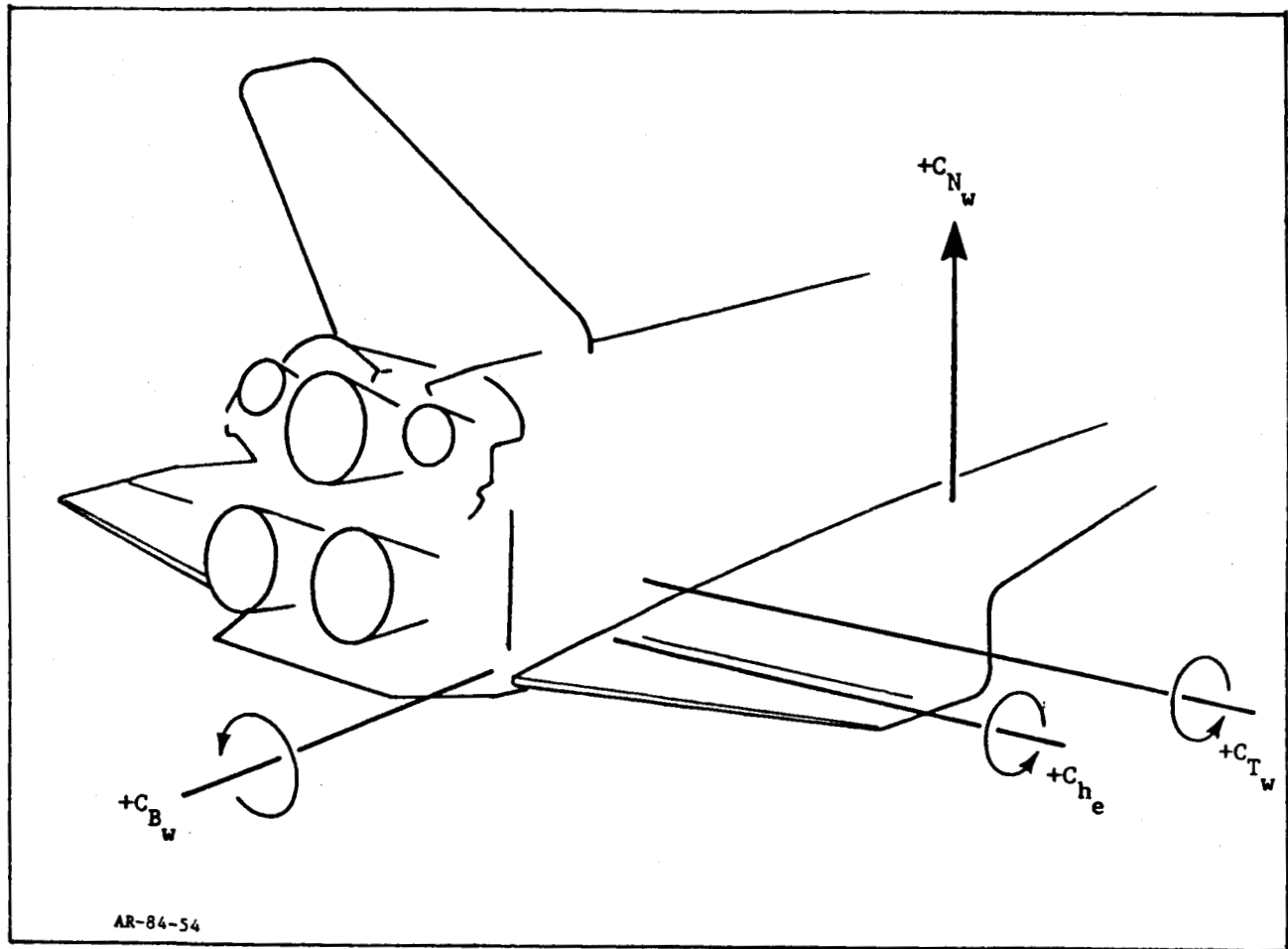


Fig. 6-17 Wing and Elevon Force and Moment Sign Convention

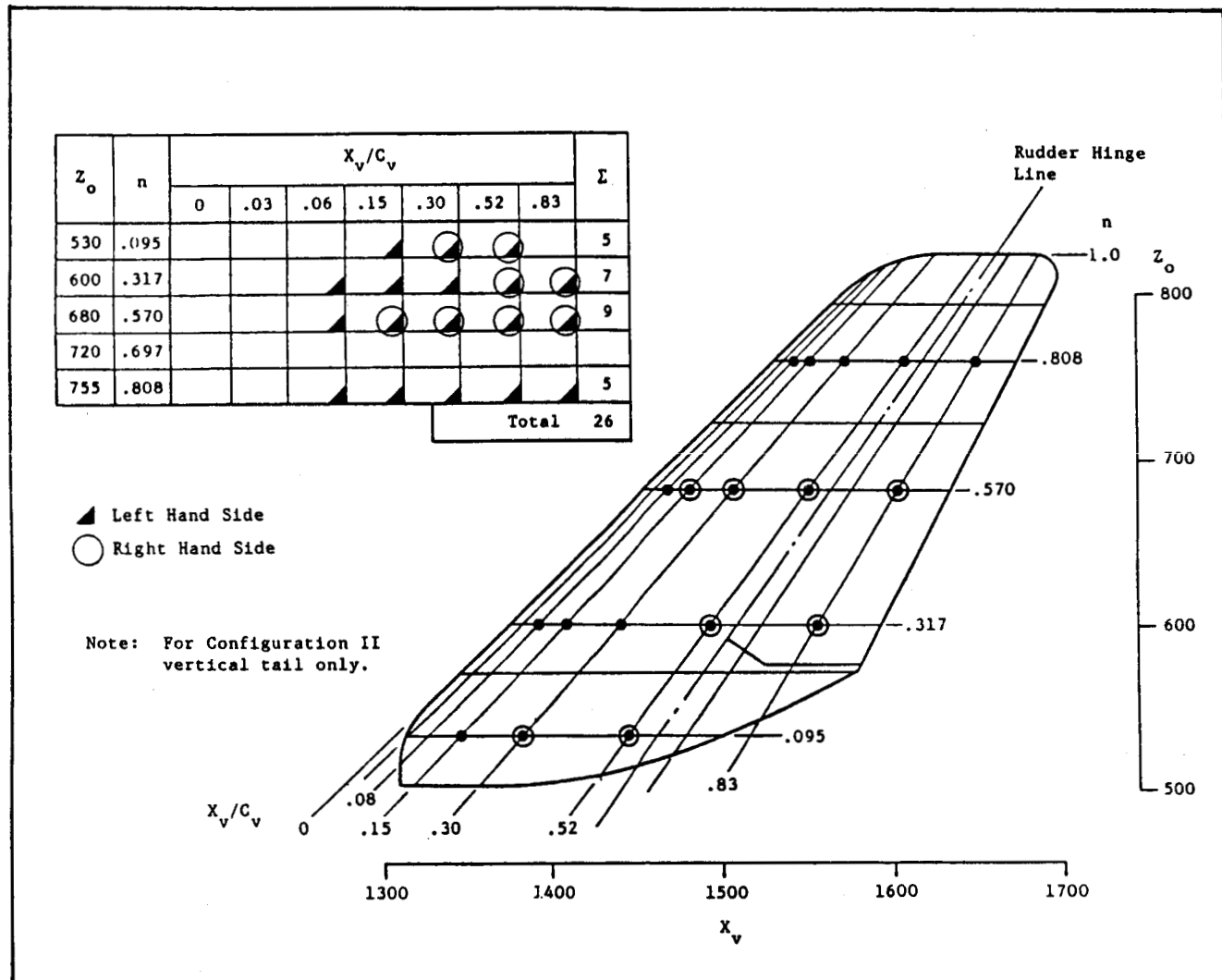


Fig. 6-18 IA300 Vertical Tail Instrumentation

power levels as presented in Figs. 6-19a through 6-19d in the subsonic and transonic Mach regimes. These figures indicate that for the higher Mach numbers, the plume effects at both power levels were generally limited to the aft portion of the vertical tail, extending along the entire span. Subsonically, however, the plume effects encompassed the complete vertical tail.

For the pressure integration, the complete vertical tail was modeled as shown in Fig. 6-20. Each of the areas shown in this figure are listed in Table 6-6 along with the assigned pressure tap numbers that were used for the integration. The sign convention used for computing the vertical tail forces and moments is shown in Fig. 6-21.

#### 6.7 SRB BASE PRESSURE

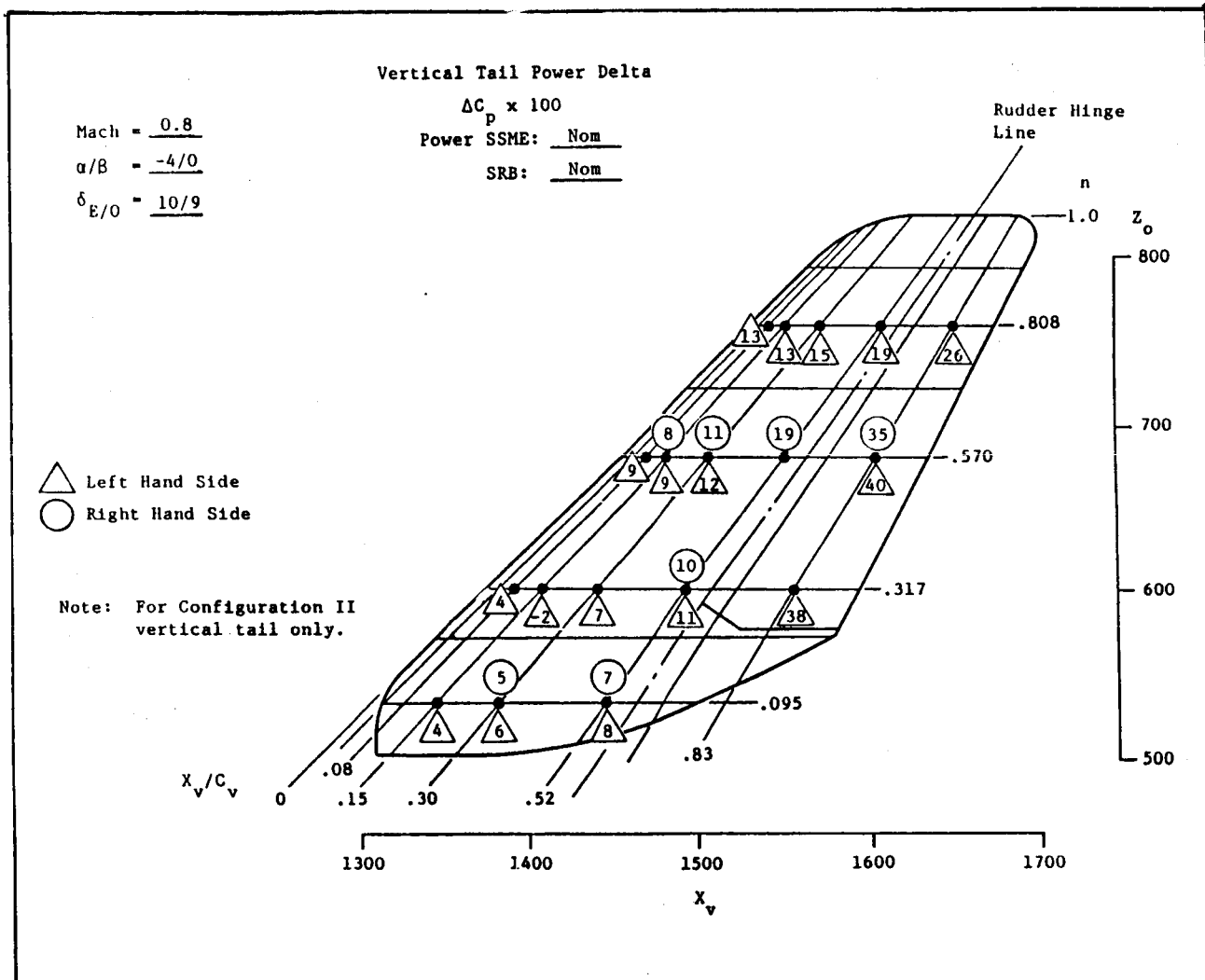
The SRB base instrumentation layout from Ref. 1 is shown in Fig. 6-22. The effective area model for the SRB base is shown in Fig. 6-23. Table 6-7 lists the effective areas and the pressure tap assigned to each area.

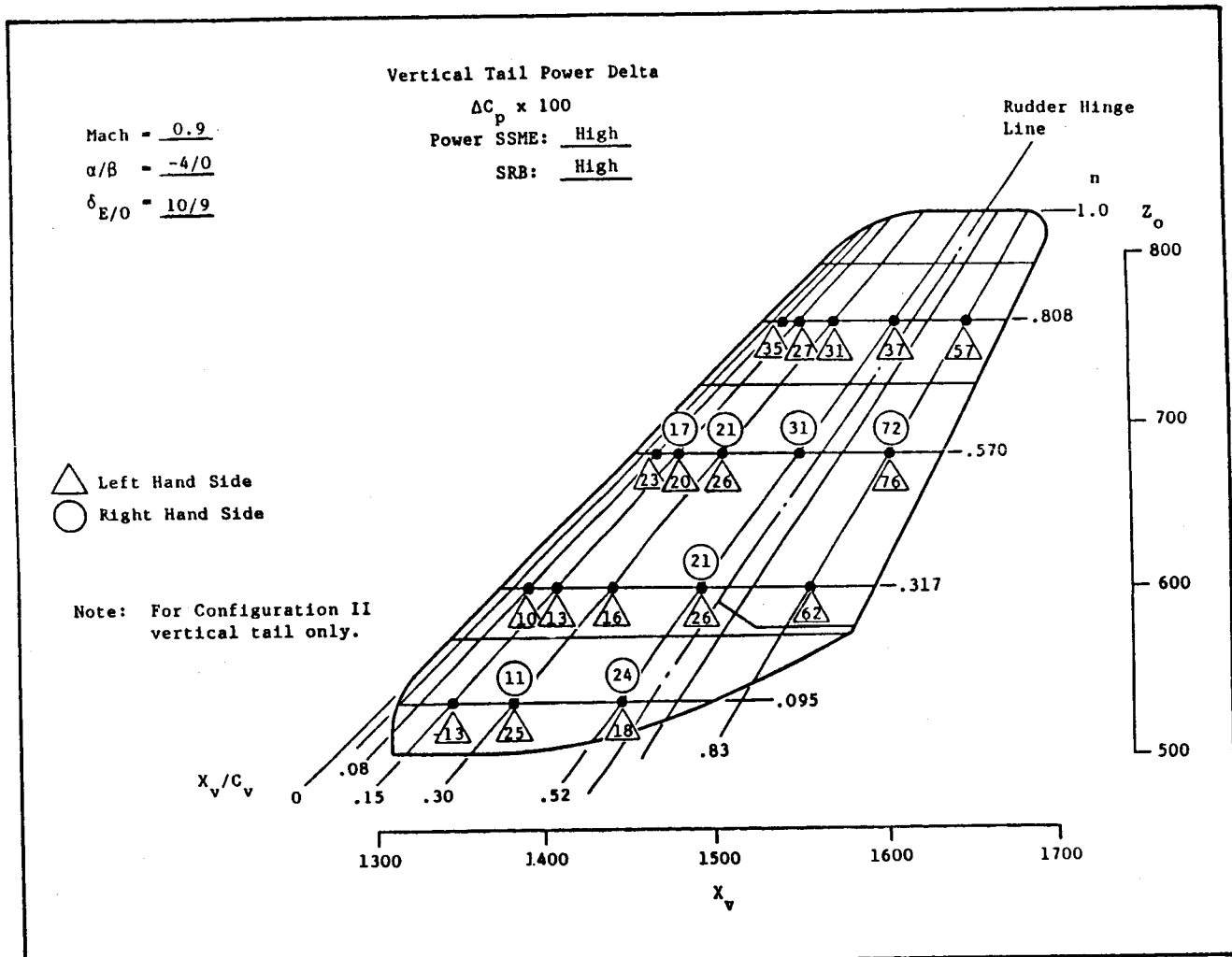
#### 6.8 SRB FOREBODY

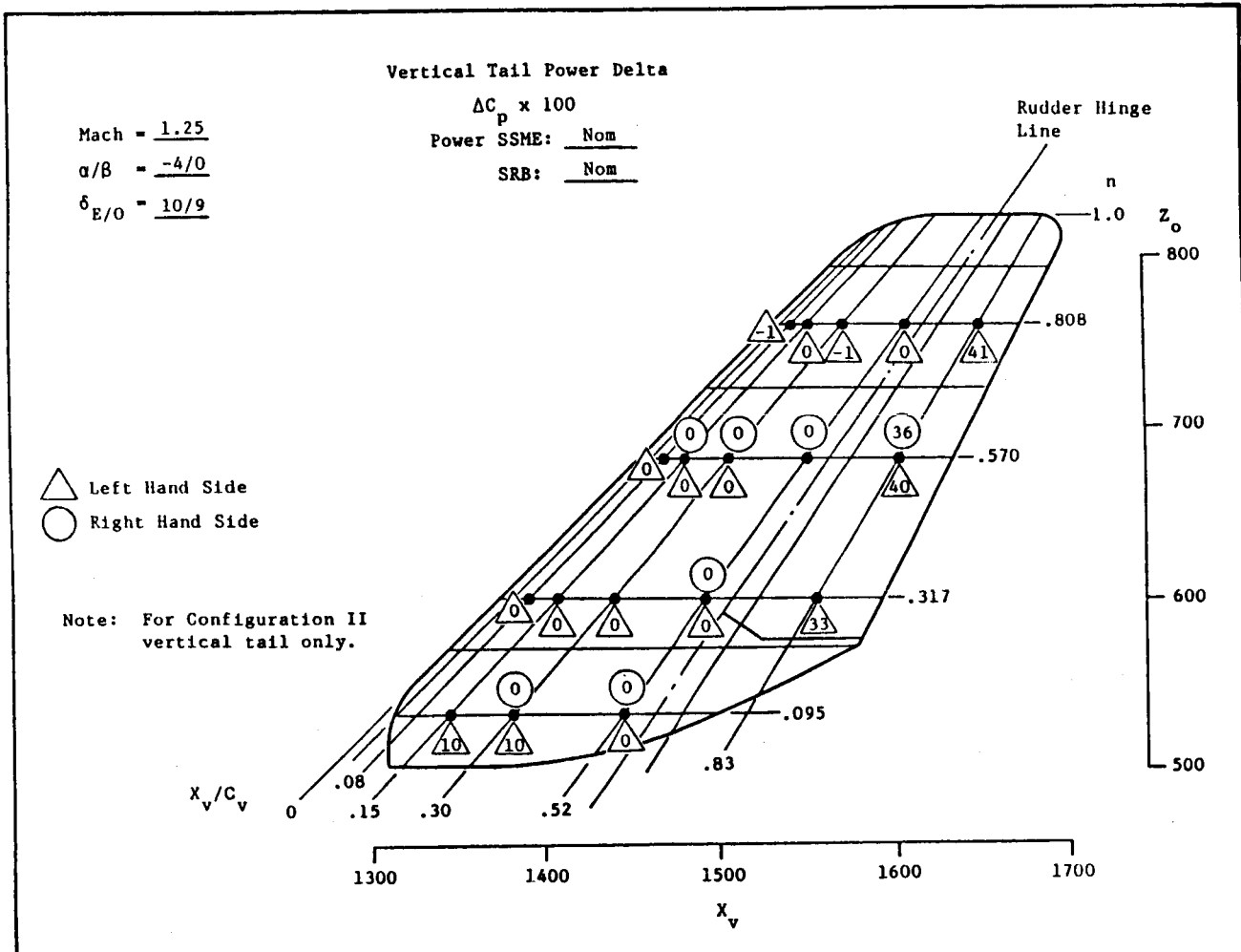
The SRB forebody instrumentation layout from Ref. 1 is shown in Fig. 6-24 and the pressure integration effective areas listed in Table 6-8.

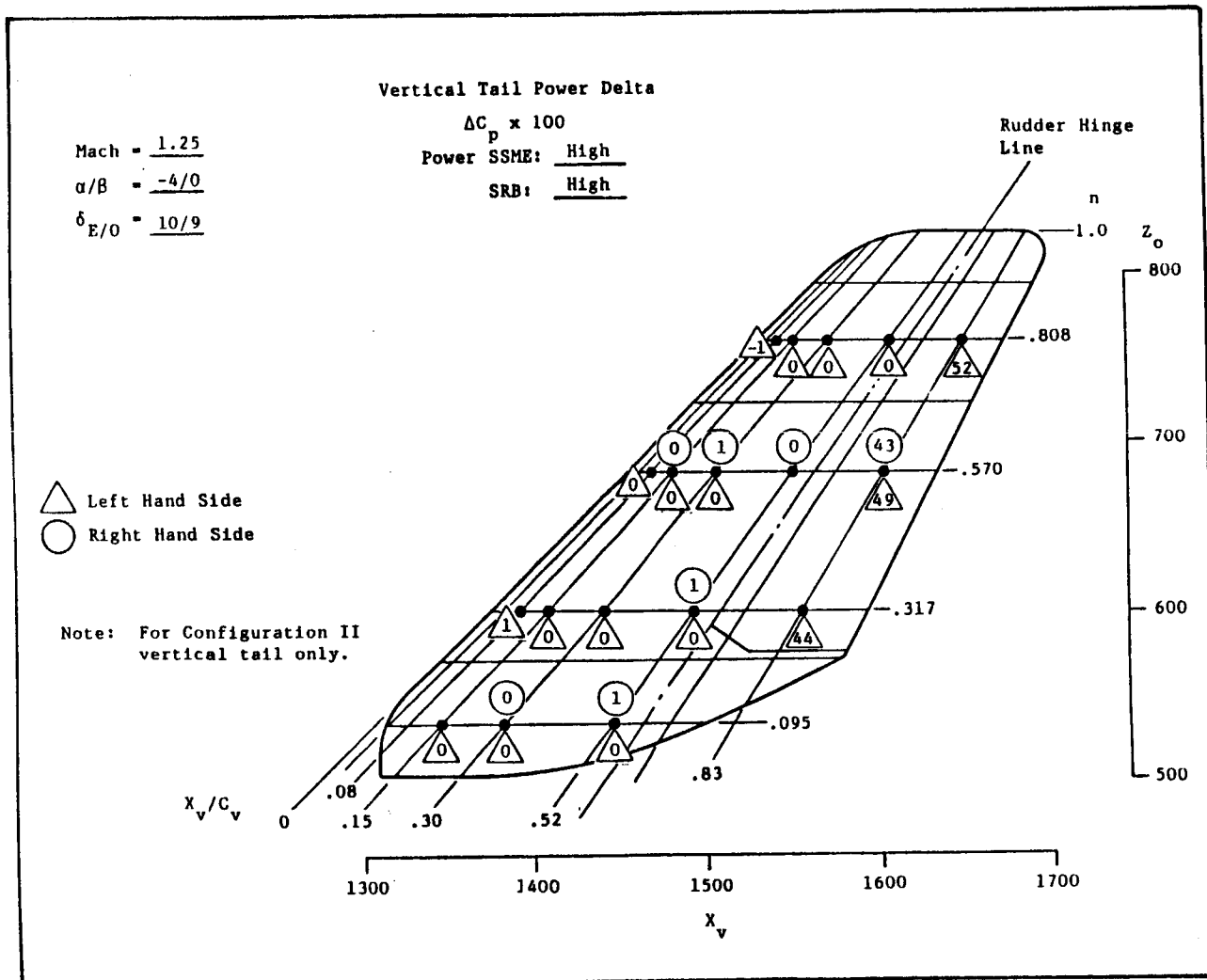
#### 6.9 ET BASE

The ET base instrumentation layout from Ref. 1 is shown in Fig. 6-25. The effective area model for the ET base is shown in Fig. 6-26. Table 6-9 lists each of the pressure integration areas along with their pressure tap assignments.

Fig. 6-19a Power  $\Delta C_p$ , Nominal Power, Mach 0.8

Fig. 6-19b Power  $\Delta C_p$ , High Power, Mach 0.9

Fig. 6-19c Power  $\Delta C_p$ , Nominal Power, Mach 1.25

Fig. 6-19d Power  $\Delta C_p$ , High Power, Mach 1.25

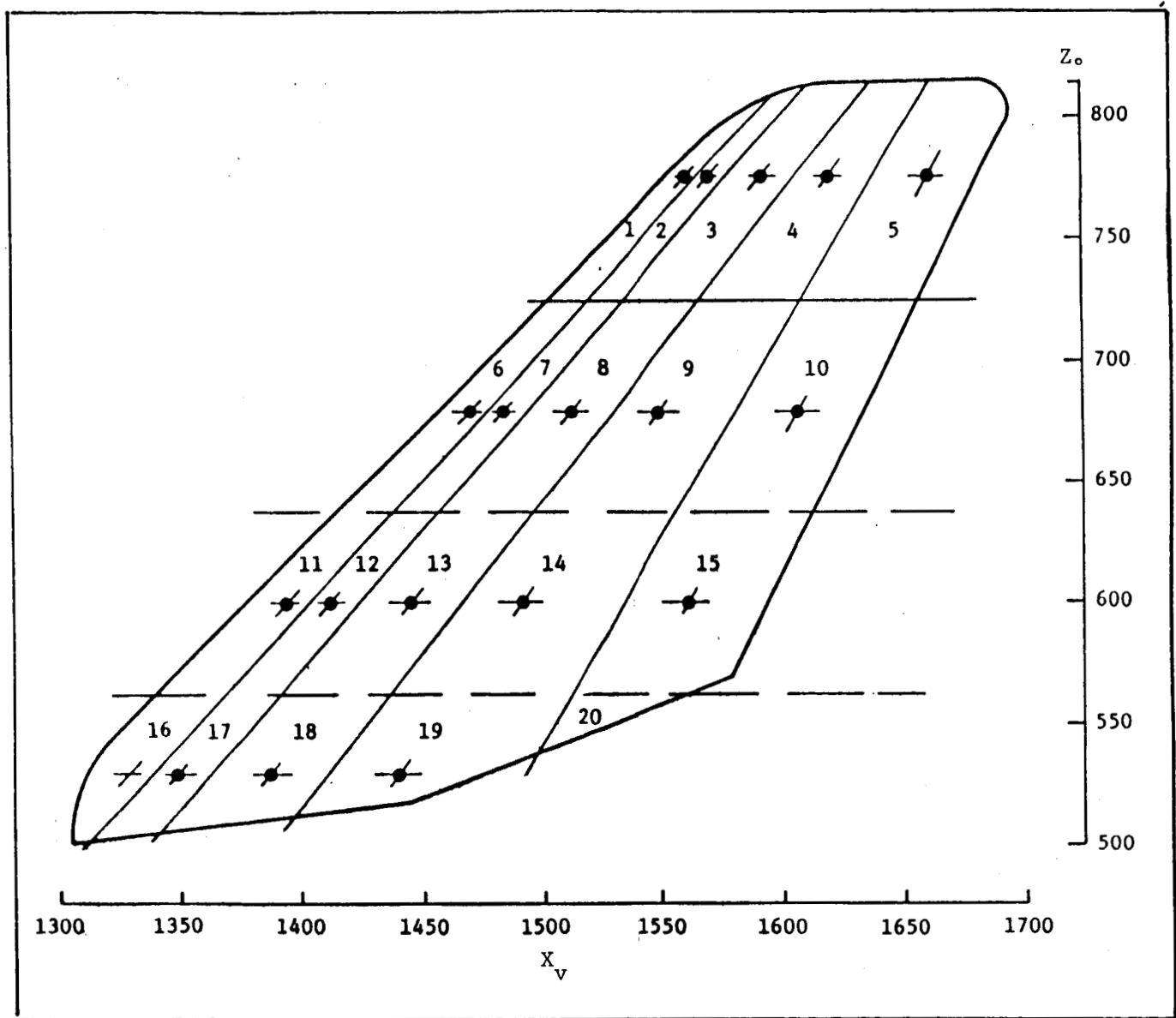


Fig. 6-20 Vertical Tail Pressure Integration

Table 6-6 EFFECTIVE AREA MODELING OF TAPS FOR VERTICAL TAIL

BODY	TAP #/FUNC.	AREA SQ.FT.	X	Y	Z	THETA	PHI
608. VERT. TAIL	423	6.7450	2301.00	0.00	1088.50	90.0	270.0
609. VERT. TAIL	423	6.7450	2301.00	0.00	1088.50	90.0	90.0
610. VERT. TAIL	423	7.8542	2313.50	0.00	1088.50	90.0	270.0
611. VERT. TAIL	423	7.8542	2313.50	0.00	1088.50	90.0	90.0
612. VERT. TAIL	424	17.9072	2320.00	0.00	1088.50	90.0	270.0
613. VERT. TAIL	424	17.9072	2320.00	0.00	1088.50	90.0	90.0
614. VERT. TAIL	425	20.3734	2361.00	0.00	1088.50	90.0	270.0
615. VERT. TAIL	425	20.3734	2361.00	0.00	1088.50	90.0	90.0
616. VERT. TAIL	426	27.7094	2399.00	0.00	1088.50	90.0	270.0
617. VERT. TAIL	426	27.7094	2399.00	0.00	1088.50	90.0	90.0
618. VERT. TAIL	414	11.3932	2209.00	0.00	1013.50	90.0	270.0
619. VERT. TAIL	414	11.3932	2209.00	0.00	1013.50	90.0	90.0
620. VERT. TAIL	414	10.6337	2224.00	0.00	1013.50	90.0	270.0
621. VERT. TAIL	414	10.6337	2224.00	0.00	1013.50	90.0	90.0
622. VERT. TAIL	415	22.1708	2252.00	0.00	1013.50	90.0	270.0
623. VERT. TAIL	415	22.1708	2252.00	0.00	1013.50	90.0	90.0
624. VERT. TAIL	415	31.2934	2296.00	0.00	1013.50	90.0	270.0
625. VERT. TAIL	415	31.2934	2296.00	0.00	1013.50	90.0	90.0
626. VERT. TAIL	417	32.3568	2346.00	0.00	1013.50	90.0	270.0
627. VERT. TAIL	417	32.3568	2346.00	0.00	1013.50	90.0	90.0
628. VERT. TAIL	407	13.2813	2138.00	0.00	933.50	90.0	270.0
629. VERT. TAIL	407	13.2813	2138.00	0.00	933.50	90.0	90.0
630. VERT. TAIL	407	11.0677	2156.00	0.00	933.50	90.0	270.0
631. VERT. TAIL	407	11.0677	2156.00	0.00	933.50	90.0	90.0
632. VERT. TAIL	408	22.2656	2106.00	0.00	933.50	90.0	270.0
633. VERT. TAIL	408	22.2656	2106.00	0.00	933.50	90.0	90.0
634. VERT. TAIL	409	35.1563	2239.00	0.00	933.50	90.0	270.0
635. VERT. TAIL	409	35.1563	2239.00	0.00	933.50	90.0	90.0
636. VERT. TAIL	410	31.2500	2302.00	0.00	933.50	90.0	270.0
637. VERT. TAIL	410	31.2500	2302.00	0.00	933.50	90.0	90.0
638. VERT. TAIL	401	10.6745	2076.00	0.00	873.50	90.0	270.0
639. VERT. TAIL	401	10.6745	2076.00	0.00	873.50	90.0	90.0
640. VERT. TAIL	401	10.6510	2091.00	0.00	863.50	90.0	270.0
641. VERT. TAIL	401	10.6510	2091.00	0.00	863.50	90.0	90.0
642. VERT. TAIL	402	18.2292	2124.00	0.00	873.50	90.0	270.0
643. VERT. TAIL	402	18.2292	2124.00	0.00	873.50	90.0	90.0
644. VERT. TAIL	403	22.0189	2189.00	0.00	876.50	90.0	270.0
645. VERT. TAIL	403	22.0189	2189.00	0.00	876.50	90.0	90.0
646. VERT. TAIL	410	7.2891	2262.00	0.00	863.50	90.0	270.0
647. VERT. TAIL	410	7.2891	2262.00	0.00	863.50	90.0	90.0

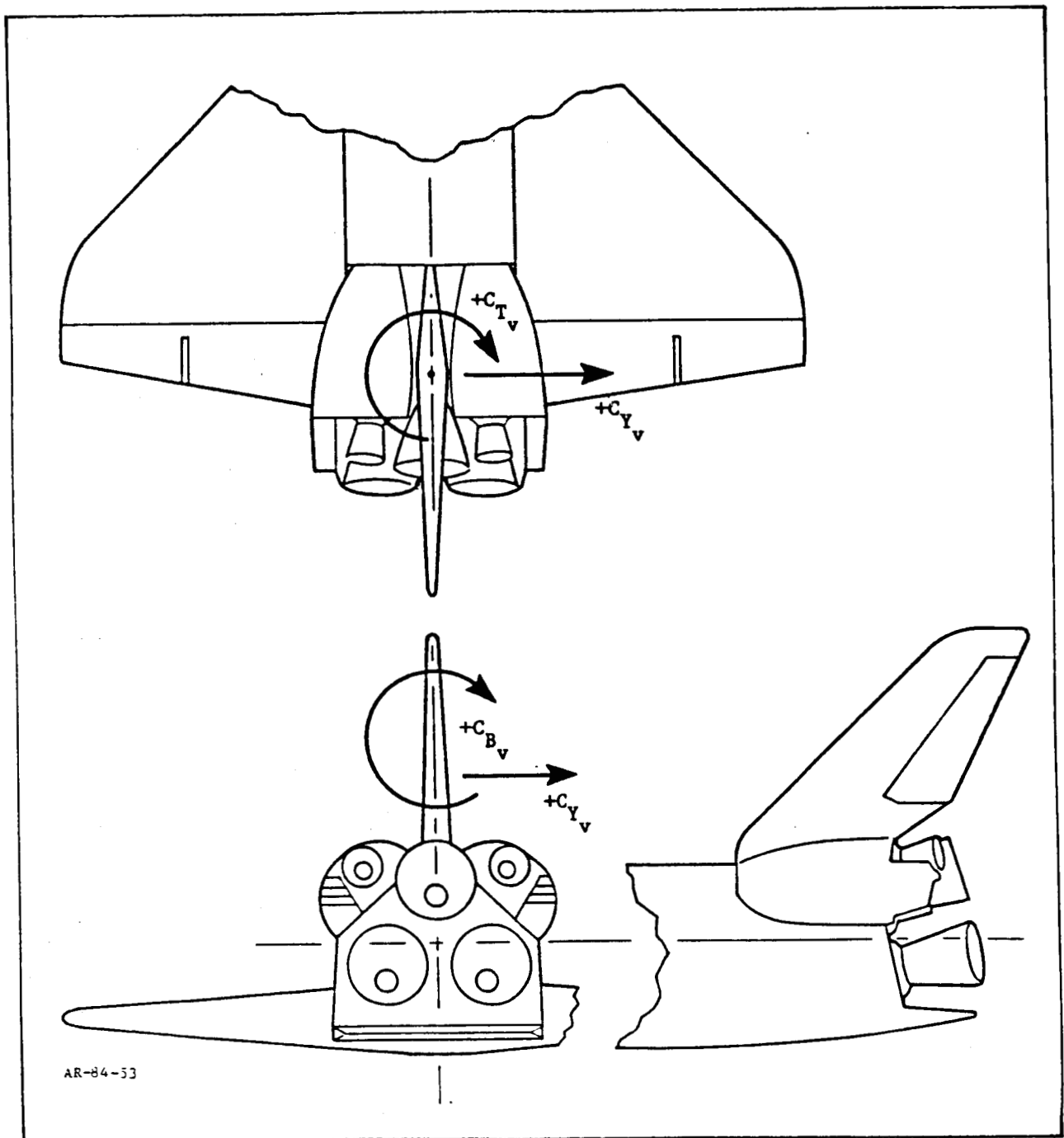


Fig. 6-21 Vertical Tail Force and Moment Sign Convention

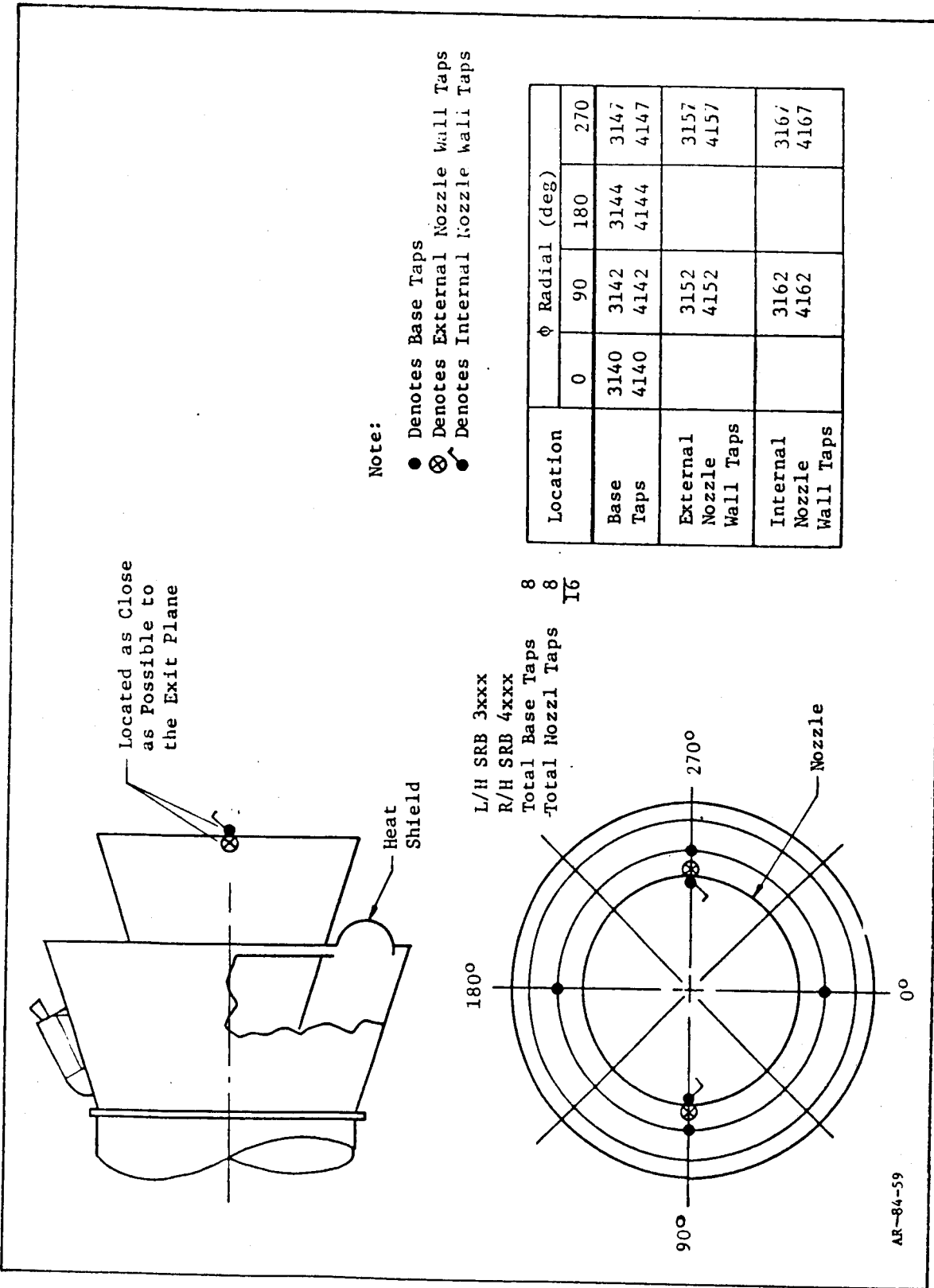


Fig. 6-22 SRB Base Instrumentation Layout

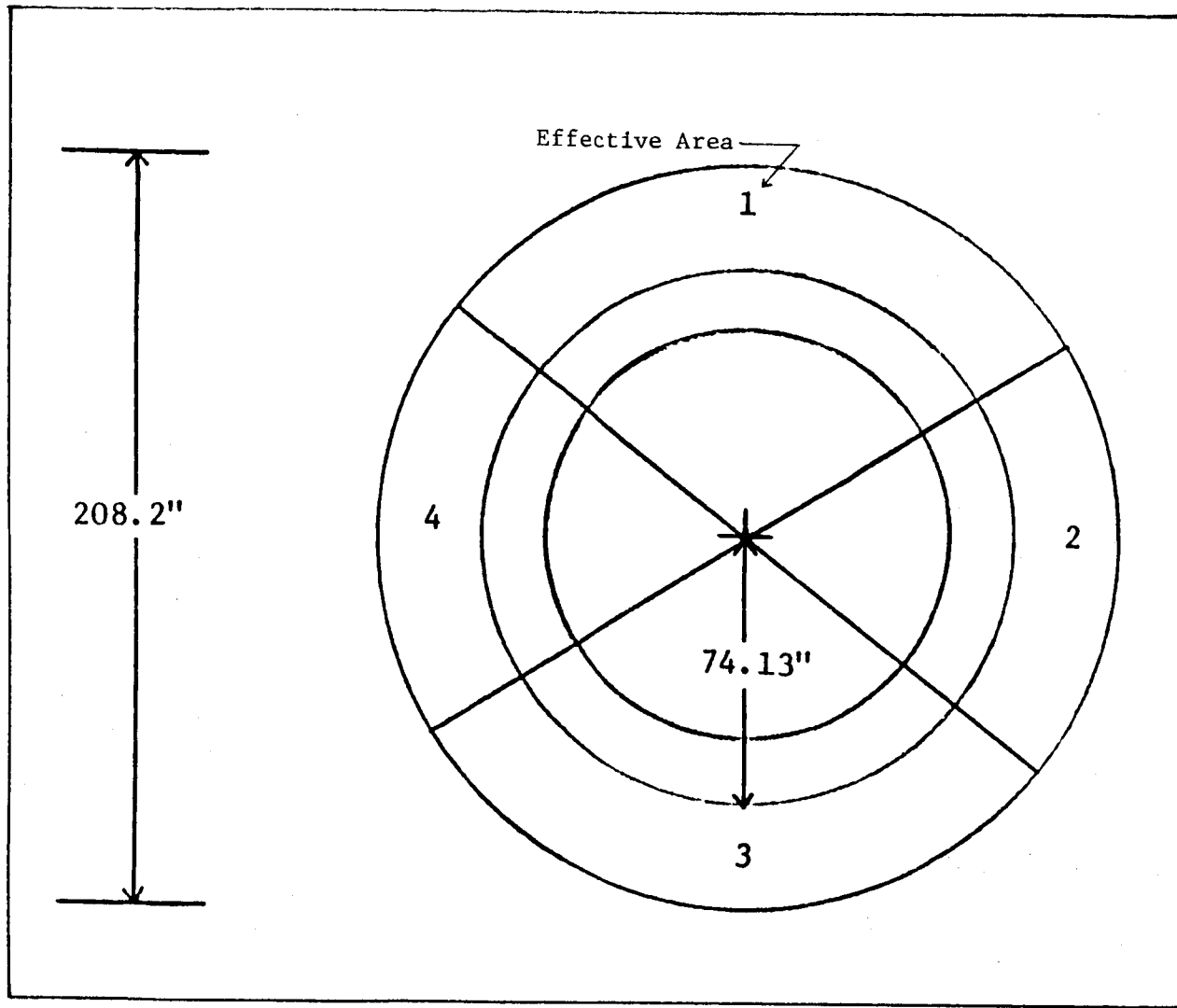


Fig. 6-23 SRB Base Effective Area

Table 6-7 EFFECTIVE AREA MODELING OF TAPS FOR SRB BASE

BODY	TAP #/FUNC.	AREA SQ.FT.	X	Y	Z	THETA	PHI
73. L. SRB BASE	3140	29.9360	2470.50	-250.50	310.89	90.0	0.0
74. L. SRB BASE	3142	29.9360	2470.50	-339.61	400.00	90.0	0.0
75. L. SRB BASE	3144	29.9360	2470.50	-250.50	489.11	90.0	0.0
76. L. SRB BASE	3147	29.9360	2470.50	-161.38	400.00	90.0	0.0
<hr/>							
149. R. SRB BASE	3140	29.9360	2470.50	250.50	310.89	90.0	0.0
150. R. SRB BASE	3142	29.9360	2470.50	339.61	400.00	90.0	0.0
151. R. SRB BASE	3144	29.9360	2470.50	250.50	489.11	90.0	0.0
152. R. SRB BASE	3147	29.9360	2470.50	161.38	400.00	90.0	0.0

ORIGINAL PAGE IS  
OF POOR QUALITY

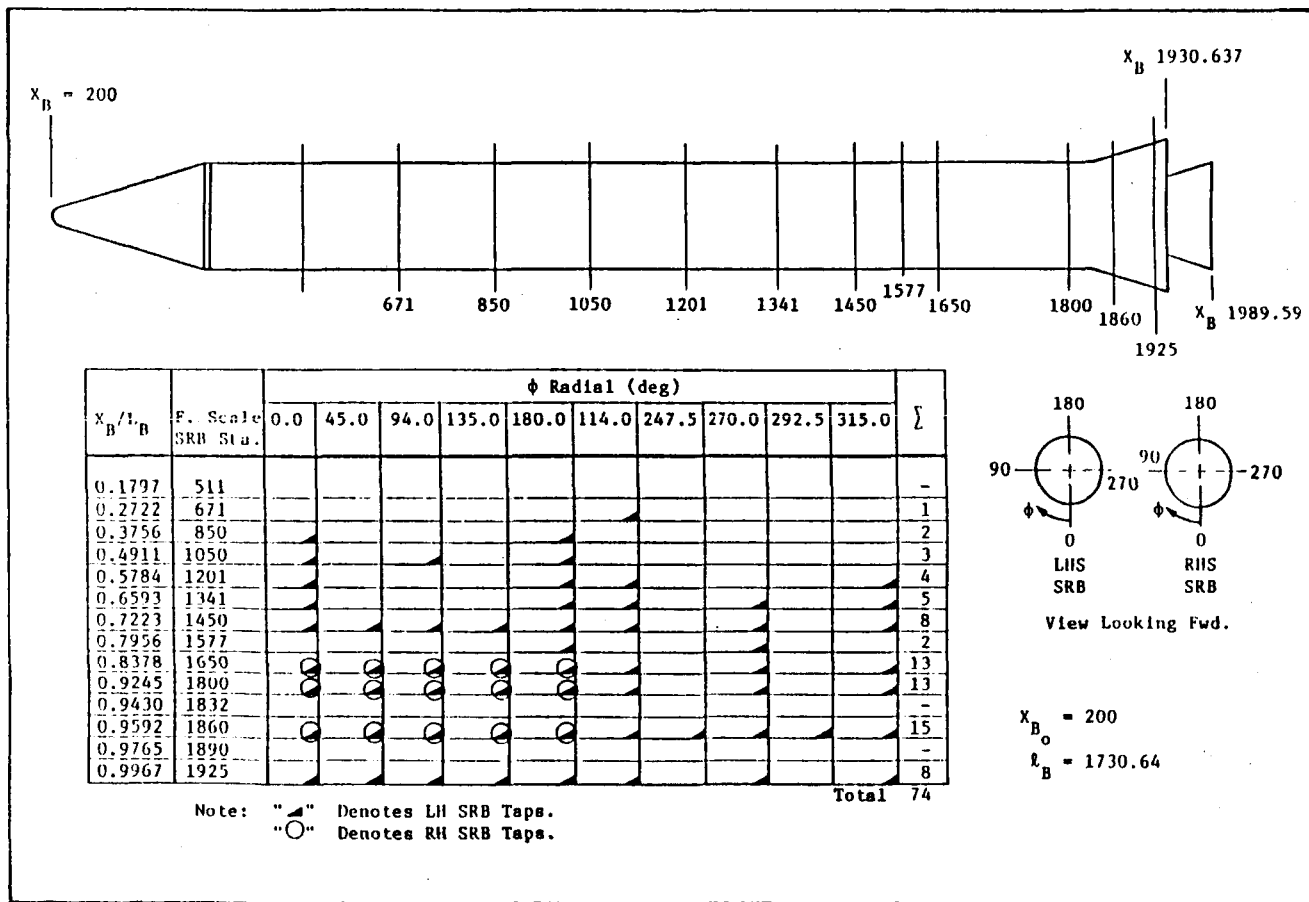


Fig. 6-24 IA300 SRB Pressure Instrumentation

Table 6-8 EFFECTIVE AREA MODELING OF TAPS FOR LEFT ORBITER FOREBODY

BODY	TAP #/FUNC.	AREA SQ.FT.	X	Y	Z	THETR	PHI
1. L. SRB FBODY.	(“3059”*,.17)*	69.6770	1405.50	-250.50	327.19	180.0	270.0
2. L. SRB FBODY.	(“3061”*,.17)*	69.6770	1405.50	-301.98	348.52	135.0	270.0
3. L. SRB FBODY.	(“3062”*,.17)*	69.6770	1405.50	-323.31	400.00	90.0	270.0
4. L. SRB FBODY.	(“3063”*,.17)*	69.6770	1405.50	-381.98	451.48	45.0	270.0
5. L. SRB FBODY.	(“3024”)	69.6770	1405.50	-250.50	472.81	8.0	90.0
6. L. SRB FBODY.	(“3065”*,.17)*	69.6770	1405.50	-199.82	451.48	45.0	90.0
7. L. SRB FBODY.	(“3057”*,.17)*	69.6770	1405.50	-177.69	400.00	90.0	90.0
8. L. SRB FBODY.	(“3059”*,.17)*	69.6770	1405.50	-199.82	348.52	135.0	90.0
9. L. SRB FBODY.	(“3059”*,.5) *	69.6770	1500.50	-250.50	327.19	180.0	270.0
10. L. SRB FBODY.	(“3061”*,.43)*	69.6770	1500.50	-301.98	349.52	135.0	270.0
11. L. SRB FBODY.	3032	69.6770	1500.50	-323.31	400.00	90.0	270.0
12. L. SRB FBODY.	(“3063”*,.43)*	69.6770	1500.50	-381.98	451.48	45.0	270.0
13. L. SRB FBODY.	3034	69.6770	1500.50	-250.50	472.81	0.0	90.0
14. L. SRB FBODY.	(“3045”*,.52)*	69.6770	1500.50	-199.82	451.48	45.0	90.0
15. L. SRB FBODY.	(“3057”*,.52)*	69.6770	1500.50	-177.69	400.00	90.0	90.0
16. L. SRB FBODY.	(“3059”*,.5)*	69.6770	1500.50	-199.82	348.52	135.0	90.0
17. L. SRB FBODY.	(“3059”*,.83)*	59.7200	1743.00	-250.50	327.19	180.0	270.0
18. L. SRB FBODY.	(“3061”*,.7)*	59.7200	1743.00	-301.98	349.52	135.0	270.0
19. L. SRB FBODY.	(“3062”*,.7)*	59.7200	1743.00	-323.31	400.00	90.0	270.0
20. L. SRB FBODY.	(“3063”*,.7)*	59.7200	1743.00	-301.98	451.48	45.0	270.0
21. L. SRB FBODY.	3044	59.7200	1743.00	-250.50	472.81	0.0	90.0
22. L. SRB FBODY.	3045	59.7200	1743.00	-199.82	451.48	45.0	90.0
23. L. SRB FBODY.	(“3057”*,.83)*	59.7200	1743.00	-177.69	400.00	90.0	90.0
24. L. SRB FBODY.	(“3059”*,.83)*	59.7200	1743.00	-199.82	348.52	135.0	90.0
25. L. SRB FBODY.	3050	49.7700	1800.50	-250.50	327.19	180.0	270.0
26. L. SRB FBODY.	(“3061”*,.8)*	49.7700	1800.50	-301.98	349.52	135.0	270.0
27. L. SRB FBODY.	(“3062”*,.8)*	49.7700	1800.50	-323.31	400.00	90.0	270.0
28. L. SRB FBODY.	(“3063”*,.8)*	49.7700	1800.50	-301.98	451.48	45.0	270.0
29. L. SRB FBODY.	3054	49.7700	1800.50	-250.50	472.81	0.0	90.0
30. L. SRB FBODY.	3055	49.7700	1800.50	-199.82	451.48	45.0	90.0
31. L. SRB FBODY.	3057	49.7700	1800.50	-177.69	400.00	90.0	90.0
32. L. SRB FBODY.	3059	49.7700	1800.50	-199.82	349.52	135.0	90.0
33. L. SRB FBODY.	3060	59.7200	2018.00	-250.50	327.19	180.0	270.0
34. L. SRB FBODY.	3061	59.7200	2018.00	-301.98	349.52	135.0	270.0
35. L. SRB FBODY.	3062	59.7200	2018.00	-323.31	400.00	90.0	270.0
36. L. SRB FBODY.	3063	59.7200	2018.00	-301.98	451.48	45.0	270.0
37. L. SRB FBODY.	3065	59.7200	2018.00	-250.50	472.81	0.0	90.0
38. L. SRB FBODY.	3065	59.7200	2018.00	-199.82	451.48	45.0	90.0
39. L. SRB FBODY.	3067	59.7200	2018.00	-177.69	400.00	90.0	90.0
40. L. SRB FBODY.	3069	59.7200	2018.00	-199.82	349.52	135.0	90.0
41. L. SRB FBODY.	3080	69.6770	2100.50	-250.50	327.19	180.0	270.0
42. L. SRB FBODY.	3081	69.6770	2100.50	-301.98	451.48	45.0	90.0
43. L. SRB FBODY.	3082	69.6770	2100.50	-323.31	400.00	90.0	270.0
44. L. SRB FBODY.	3082	69.6770	2100.50	-301.98	451.48	45.0	270.0
45. L. SRB FBODY.	3005	69.6770	2100.50	-250.50	472.81	0.0	90.0
46. L. SRB FBODY.	3085	69.6770	2100.50	-199.82	451.48	45.0	90.0
47. L. SRB FBODY.	3087	69.6770	2100.50	-177.69	400.00	90.0	90.0
48. L. SRB FBODY.	3089	69.6770	2100.50	-199.82	348.52	135.0	90.0
49. L. SRB FBODY.	3090	44.7900	2324.25	-250.50	327.19	180.0	270.0
50. L. SRB FBODY.	3091	44.7900	2324.25	-301.98	348.52	135.0	270.0
51. L. SRB FBODY.	3092	44.7900	2324.25	-323.31	400.00	90.0	270.0
52. L. SRB FBODY.	3093	44.7900	2324.25	-301.98	451.48	45.0	270.0
53. L. SRB FBODY.	3095	44.7900	2324.25	-250.50	472.81	0.0	90.0
54. L. SRB FBODY.	3095	44.7900	2324.25	-199.82	451.48	45.0	90.0
55. L. SRB FBODY.	3097	44.7900	2324.25	-177.69	400.00	90.0	90.0
56. L. SRB FBODY.	3099	44.7900	2324.25	-199.82	348.52	135.0	90.0
57. L. SRB SKIRT	3110	21.0000	2403.00	-250.50	334.50	161.0	100.0
58. L. SRB SKIRT	3111	21.0000	2403.00	-296.76	353.74	132.0	244.0
59. L. SRB SKIRT	3112	21.0000	2403.00	-315.92	400.00	90.0	251.0
60. L. SRB SKIRT	3113	21.0000	2403.00	-296.76	446.26	48.0	244.0
61. L. SRB SKIRT	3114	21.0000	2403.00	-250.50	465.42	19.0	180.0
62. L. SRB SKIRT	3115	21.0000	2403.00	-204.24	446.26	40.0	116.0
63. L. SRB SKIRT	3117	21.0000	2403.00	-185.00	400.00	90.0	109.0
64. L. SRB SKIRT	3119	21.0000	2403.00	-204.24	353.74	132.0	116.0
65. L. SRB SKIRT	3130	25.1600	2468.00	-250.50	355.74	161.0	180.0
66. L. SRB SKIRT	3131	25.1600	2468.00	-281.79	360.71	132.0	244.0
67. L. SRB SKIRT	3132	25.1600	2468.00	-294.76	400.00	90.0	251.0
68. L. SRB SKIRT	3133	25.1600	2468.00	-281.79	431.29	43.0	244.0
69. L. SRB SKIRT	3134	25.1600	2468.00	-250.50	444.26	19.0	180.0
70. L. SRB SKIRT	3135	25.1600	2468.00	-219.21	431.29	40.0	116.0
71. L. SRB SKIRT	3137	25.1600	2468.00	-206.24	400.00	90.0	109.0
72. L. SRB SKIRT	3139	25.1600	2468.00	-219.21	360.71	132.0	116.0

(Continued)

\* Tap averaging.

Table 6-8 (Concluded)

BODY	TAP #/FUNC.	AREA 50.FT.	X	Y	Z	THETA	PHI
77. R. SRB FBDY.	(“3059”*.17)*	69.6770	1405.50	250.50	327.19	160.0	90.0
78. R. SRB FBDY.	(“3061”*.17)*	69.6770	1405.50	301.98	349.52	135.0	90.0
79. R. SRB FBDY.	(“3062”*.17)*	69.6770	1405.50	323.31	400.00	90.0	90.0
80. R. SRB FBDY.	(“3063”*.17)*	69.6770	1405.50	301.98	451.48	45.0	90.0
81. R. SRB FBDY.	(“3024”)	69.6770	1405.50	250.50	472.81	0.0	270.0
82. R. SRB FBDY.	(“3065”*.17)*	69.6770	1405.50	199.02	451.48	45.0	270.0
83. R. SRB FBDY.	(“3057”*.17)*	69.6770	1405.50	177.69	400.00	90.0	270.0
84. R. SRB FBDY.	(“3059”*.17)*	69.6770	1405.50	199.02	348.52	135.0	270.0
85. R. SRB FBDY.	(“3059”*.5)*	69.6770	1580.50	250.50	327.19	160.0	90.0
86. R. SRB FBDY.	(“3061”*.43)*	69.6770	1580.50	301.98	348.52	135.0	90.0
87. R. SRB FBDY.	3032	69.6770	1580.50	323.31	400.00	90.0	90.0
88. R. SRB FBDY.	(“3063”*.43)*	69.6770	1580.50	301.98	451.48	45.0	90.0
89. R. SRB FBDY.	3034	69.6770	1580.50	250.50	472.81	0.0	270.0
90. R. SRB FBDY.	(“3045”*.52)*	69.6770	1580.50	199.02	451.48	45.0	270.0
91. R. SRB FBDY.	(“3057”*.52)*	69.6770	1580.50	177.69	400.00	90.0	270.0
92. R. SRB FBDY.	(“3059”*.5)*	69.6770	1580.50	199.02	348.52	135.0	270.0
93. R. SRB FBDY.	(“3059”*.83)*	59.7200	1743.00	250.50	327.19	160.0	90.0
94. R. SRB FBDY.	(“3061”*.7)*	59.7200	1743.00	301.98	343.52	135.0	90.0
95. R. SRB FBDY.	(“3062”*.7)*	59.7200	1743.00	323.31	400.00	90.0	90.0
96. R. SRB FBDY.	(“3063”*.7)*	59.7200	1743.00	301.98	451.48	45.0	90.0
97. R. SRB FBDY.	3044	59.7200	1743.00	250.50	472.81	0.0	270.0
98. R. SRB FBDY.	3045	59.7200	1743.00	199.02	451.48	45.0	270.0
99. R. SRB FBDY.	(“3057”*.83)*	59.7200	1743.00	177.69	400.00	90.0	270.0
100. R. SRB FBDY.	(“3059”*.83)*	59.7200	1743.00	199.02	348.52	135.0	270.0
101. R. SRB FBDY.	3050	49.7700	1890.50	250.50	327.19	160.0	90.0
102. R. SRB FBDY.	(“3061”*.8)*	49.7700	1890.50	301.98	348.52	135.0	90.0
103. R. SRB FBDY.	(“3062”*.8)*	49.7700	1890.50	323.31	400.00	90.0	90.0
104. R. SRB FBDY.	(“3063”*.8)*	49.7700	1890.50	301.98	451.48	45.0	90.0
105. R. SRB FBDY.	3054	49.7700	1890.50	250.50	472.81	0.0	270.0
106. R. SRB FBDY.	3055	49.7700	1890.50	199.02	451.48	45.0	270.0
107. R. SRB FBDY.	3057	49.7700	1890.50	177.69	400.00	90.0	270.0
108. R. SRB FBDY.	3059	49.7700	1890.50	199.02	348.52	135.0	270.0
109. R. SRB FBDY.	3060	59.7200	2018.00	250.50	327.19	160.0	90.0
110. R. SRB FBDY.	3061	59.7200	2018.00	301.98	348.52	135.0	90.0
111. R. SRB FBDY.	3062	59.7200	2018.00	323.31	400.00	90.0	90.0
+12. R. SRB FBDY.	3063	59.7200	2018.00	301.98	451.48	45.0	90.0
113. R. SRB FBDY.	3065	59.7200	2018.00	250.50	472.81	0.0	270.0
114. R. SRB FBDY.	3065	59.7200	2018.00	199.02	451.48	45.0	270.0
115. R. SRB FBDY.	3067	59.7200	2018.00	177.69	400.00	90.0	270.0
116. R. SRB FBDY.	3069	59.7200	2018.00	199.02	348.52	135.0	270.0
117. R. SRB FBDY.	3090	69.6770	2100.50	250.50	327.19	160.0	90.0
118. R. SRB FBDY.	3091	69.6770	2100.50	301.98	343.52	135.0	90.0
119. R. SRB FBDY.	3092	69.6770	2100.50	323.31	400.00	90.0	90.0
120. R. SRB FBDY.	3092	69.6770	2100.50	301.98	451.48	45.0	90.0
121. R. SRB FBDY.	3095	69.6770	2100.50	250.50	472.81	0.0	270.0
122. R. SRB FBDY.	3095	69.6770	2100.50	199.02	451.48	45.0	270.0
123. R. SRB FBDY.	3097	69.6770	2100.50	177.69	400.00	90.0	270.0
124. R. SRB FBDY.	3099	69.6770	2100.50	199.02	348.52	135.0	270.0
125. R. SRB FBDY.	3099	44.7900	2324.25	250.50	327.19	160.0	90.0
126. R. SRB FBDY.	3091	44.7900	2324.25	301.98	343.52	135.0	90.0
127. R. SRB FBDY.	3092	44.7900	2324.25	323.31	400.00	90.0	90.0
128. R. SRB FBDY.	3093	44.7900	2324.25	301.98	451.48	45.0	90.0
129. R. SRB FBDY.	3095	44.7900	2324.25	250.50	472.81	0.0	270.0
130. R. SRB FBDY.	3095	44.7900	2324.25	199.02	451.48	45.0	270.0
131. R. SRB FBDY.	3097	44.7900	2324.25	177.69	400.00	90.0	270.0
132. R. SRB FBDY.	3099	44.7900	2324.25	199.02	348.52	135.0	270.0
133. R. SRB SKIRT	3110	21.0000	2403.00	250.50	334.58	161.0	180.0
134. R. SRB SKIRT	3111	21.0000	2403.00	296.76	353.74	132.0	110.0
135. R. SRB SKIRT	3112	21.0000	2403.00	315.92	400.00	98.0	109.0
136. R. SRB SKIRT	3113	21.0000	2403.00	296.76	446.26	48.0	116.0
137. R. SRB SKIRT	3114	21.0000	2403.00	250.50	465.42	19.0	160.0
138. R. SRB SKIRT	3115	21.0000	2403.00	204.24	446.26	43.0	244.0
139. R. SRB SKIRT	3117	21.0000	2403.00	185.08	400.00	90.0	251.0
140. R. SRB SKIRT	3119	21.0000	2403.00	204.24	353.74	132.0	244.0
141. R. SRB SKIRT	3130	25.1800	2460.00	250.50	355.74	161.0	180.0
142. R. SRB SKIRT	3131	25.1800	2460.00	291.79	368.71	132.0	116.0
143. R. SRB SKIRT	3132	25.1800	2460.00	294.76	400.00	90.0	109.0
144. R. SRB SKIRT	3133	25.1800	2460.00	281.79	431.29	48.0	116.0
145. R. SRB SKIRT	3134	25.1800	2460.00	250.50	444.26	19.0	100.0
146. R. SRB SKIRT	3135	25.1800	2460.00	219.21	431.29	48.0	244.0
147. R. SRB SKIRT	3137	25.1600	2460.00	206.24	400.00	90.0	251.0
148. R. SRB SKIRT	3139	25.1800	2460.00	219.21	368.71	132.0	244.0

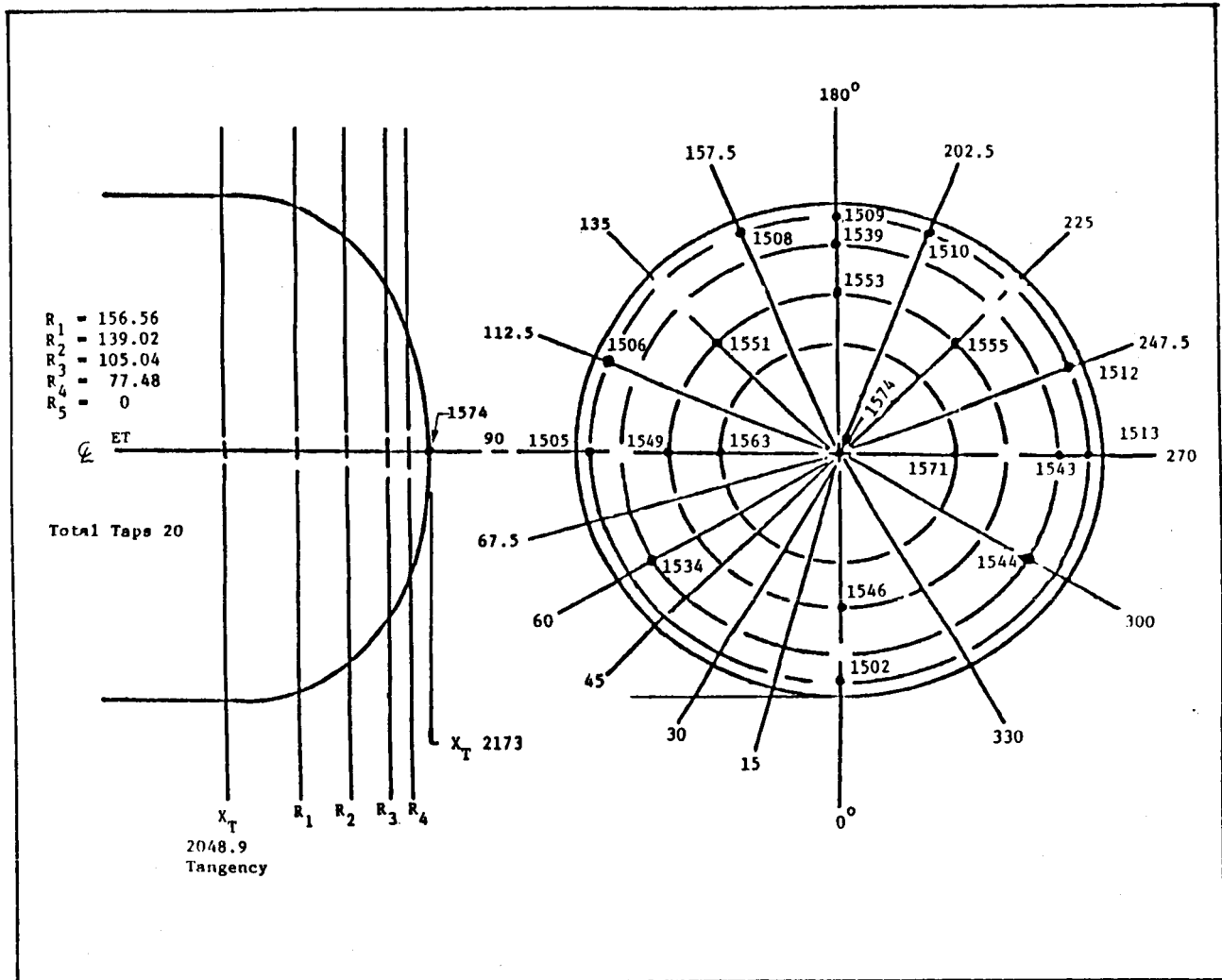


Fig. 6-25 ET Base Instrumentation Layout

C-2

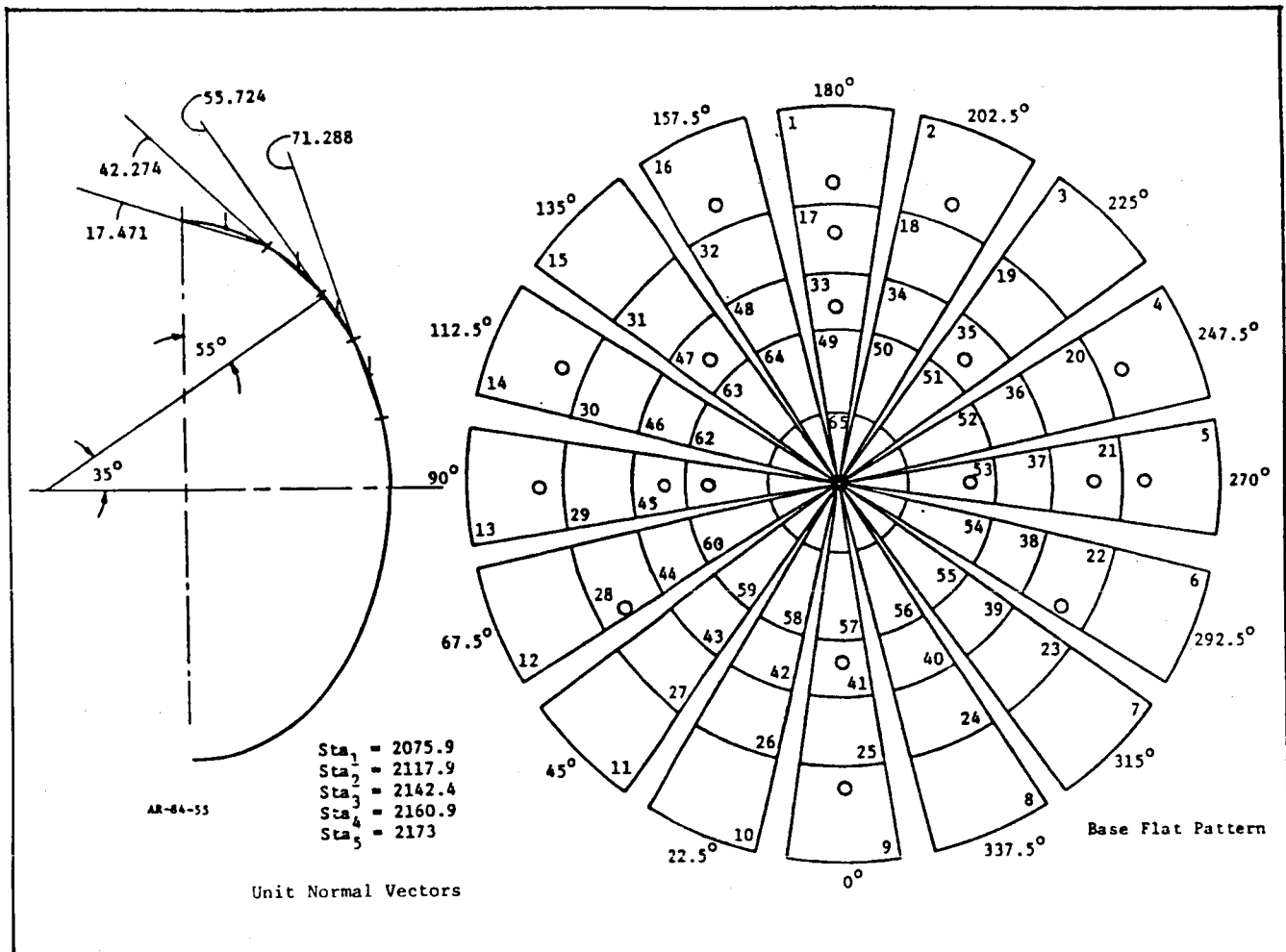


Fig. 6-26 ET Base Effective Area Modeling

Table 6-9 EFFECTIVE AREA MODELING OF TAPS FOR ET BASE

BODY	TAP #/FUNC.	AREA SQ.FT.	X	Y	Z	THETA	PHI
329. E.T. BASE	1502	18.5400	2075.90	0.00	238.46	162.3	0.0
330. E.T. BASE	1502	18.5400	2075.90	-61.82	250.76	151.6	-58.1
331. E.T. BASE	1502	18.5400	2075.90	-114.22	285.78	132.3	-65.7
332. E.T. BASE	1534	18.5400	2075.90	-149.24	338.18	111.4	-70.9
333. E.T. BASE	1505	18.5400	2075.90	-161.54	400.00	90.0	-72.3
334. E.T. BASE	1506	18.5400	2075.90	-149.24	461.82	68.6	-70.9
335. E.T. BASE	(1506+1508)/2*	18.5400	2075.90	-114.22	514.22	47.7	-65.7
336. E.T. BASE	1500	18.5400	2075.90	-61.82	549.24	20.4	-50.1
337. E.T. BASE	1509	18.5400	2075.90	0.00	561.54	17.7	0.0
338. E.T. BASE	1510	18.5400	2075.90	61.82	549.24	20.4	50.1
339. E.T. BASE	(1510+1512)/2*	18.5400	2075.90	114.22	514.22	47.7	65.7
340. E.T. BASE	1512	18.5400	2075.90	149.24	461.82	68.6	70.9
341. E.T. BASE	1513	18.5400	2075.90	161.54	400.00	90.0	72.3
342. E.T. BASE	1534	18.5400	2075.90	149.24	338.18	111.4	70.9
343. E.T. BASE	1502	18.5400	2075.90	114.22	285.78	132.3	65.7
344. E.T. BASE	1502	18.5400	2075.90	61.82	250.76	151.6	50.1
345. E.T. BASE	1534	14.2250	2117.90	8.00	262.44	137.7	0.0
346. E.T. BASE	1534	14.2250	2117.90	-52.64	272.91	133.1	-22.8
347. E.T. BASE	1534	14.2250	2117.90	-97.27	302.73	121.5	-37.9
348. E.T. BASE	1534	14.2250	2117.90	-127.09	347.36	106.4	-45.5
349. E.T. BASE	1549	14.2250	2117.90	-137.56	400.00	90.0	-47.7
350. E.T. BASE	1549	14.2250	2117.90	-127.09	452.64	73.6	-45.5
351. E.T. BASE	1551	14.2250	2117.90	-97.27	497.27	58.5	-37.9
352. E.T. BASE	1551	14.2250	2117.90	-52.64	527.89	46.9	-22.8
353. E.T. BASE	1539	14.2250	2117.90	8.00	537.56	42.3	0.0
354. E.T. BASE	1543	14.2250	2117.90	52.64	527.89	46.9	22.8
355. E.T. BASE	1543	14.2250	2117.90	97.27	497.27	58.5	37.9
356. E.T. BASE	1543	14.2250	2117.90	127.09	452.64	73.6	45.5
357. E.T. BASE	1543	14.2250	2117.90	137.56	400.00	90.0	47.7
358. E.T. BASE	1534	14.2250	2117.90	127.09	347.36	106.4	45.5
359. E.T. BASE	1534	14.2250	2117.90	97.27	302.73	121.5	37.9
360. E.T. BASE	1534	14.2250	2117.90	52.64	272.91	133.1	22.8
361. E.T. BASE	1546	9.8590	2142.40	8.00	291.10	124.3	0.0
362. E.T. BASE	1546	9.8590	2142.40	-41.64	299.46	121.3	-14.6
363. E.T. BASE	1546	9.8590	2142.40	-76.95	323.05	113.5	-25.7
364. E.T. BASE	1549	9.8590	2142.40	-100.54	358.36	102.4	-32.2
365. E.T. BASE	1549	9.8590	2142.40	-108.82	400.00	90.0	-34.3
366. E.T. BASE	1549	9.8590	2142.40	-100.54	441.64	77.6	-32.2
367. E.T. BASE	1551	9.8590	2142.40	-76.95	476.95	66.5	-25.7
368. E.T. BASE	1553	9.8590	2142.40	-41.64	500.54	58.7	-14.6
369. E.T. BASE	1553	9.8590	2142.40	8.00	508.82	55.7	0.0
370. E.T. BASE	1553	9.8590	2142.40	41.64	508.54	58.7	14.6
371. E.T. BASE	1555	9.8590	2142.40	76.95	476.95	66.5	25.7
372. E.T. BASE	1555	9.8590	2142.40	100.54	441.64	77.6	32.2
373. E.T. BASE	(1555+1543)/2*	9.8590	2142.40	108.82	400.00	90.0	34.3
374. E.T. BASE	1546	9.8590	2142.40	100.54	358.36	102.4	32.2
375. E.T. BASE	1546	9.8590	2142.40	76.95	323.05	113.5	25.7
376. E.T. BASE	1546	9.8590	2142.40	41.64	299.46	121.3	14.6
377. E.T. BASE	(1546+1574)/2*	9.1237	2160.90	8.00	320.72	109.7	0.0
378. E.T. BASE	1563	9.1237	2160.90	-27.20	354.15	107.2	-7.4
379. E.T. BASE	1563	9.1237	2160.90	-50.40	349.60	103.1	-13.5
380. E.T. BASE	1563	9.1237	2160.90	-65.85	372.72	97.1	-17.4
381. E.T. BASE	1563	9.1237	2160.90	-71.28	400.00	90.0	-18.7
382. E.T. BASE	(1563+1574)/2*	9.1237	2160.90	-65.85	427.28	82.9	-17.4
383. E.T. BASE	(1551+1574)/2*	9.1237	2160.90	-50.40	450.40	76.9	-13.5
384. E.T. BASE	(1553+1574)/2*	9.1237	2160.90	-27.20	465.85	72.8	-7.4
385. E.T. BASE	(1553+1574)/2*	9.1237	2160.90	8.00	471.20	71.3	0.0
386. E.T. BASE	(1553+1574)/2*	9.1237	2160.90	27.20	465.65	72.3	7.4
387. E.T. BASE	(1555+1574)/2*	9.1237	2160.90	50.40	450.40	76.9	13.5
388. E.T. BASE	(1571+1574)/2*	9.1237	2160.90	65.85	427.20	62.9	17.4
389. E.T. BASE	1571	9.1237	2160.90	71.20	400.00	90.0	18.7
390. E.T. BASE	(1571+1574)/2*	9.1237	2160.90	65.85	372.72	97.1	17.4
391. E.T. BASE	(1571+1574)/2*	9.1237	2160.90	50.40	349.60	103.1	13.5
392. E.T. BASE	(1546+1574)/2*	9.1237	2160.90	27.20	354.15	107.2	7.4
393. E.T. BASE	1574	9.1237	2173.00	8.00	400.00	90.0	0.0

\* Tap averaging.

## 6.10 ET FOREBODY

The ET forebody instrumentation layout from Ref. 1 is shown in Fig. 6-27. Forebody plume effects were analyzed on the ET to determine the spatial extent of the plume on the ET. Figures 6-28a through 6-29b are included to show a portion of this analysis. Table 6-10 lists each of the pressure integration areas along with their pressure tap assignments.

Figures 6-28a through 6-28d show the  $\Delta C_p$  variations at select ET stations for the nominal and high-power setting for Mach 0.9 and 1.25. These figures indicate that the plume effects transonically were generally limited to the aft portion of the ET. Figures 6-29a and 6-29b show an example of the power-delta evaluation on top of the ET (between the Orbiter and the ET). This analysis indicated that the power effects were as far forward as the forward attached strut.

ORIGINAL PAGE IS  
OF POOR QUALITY

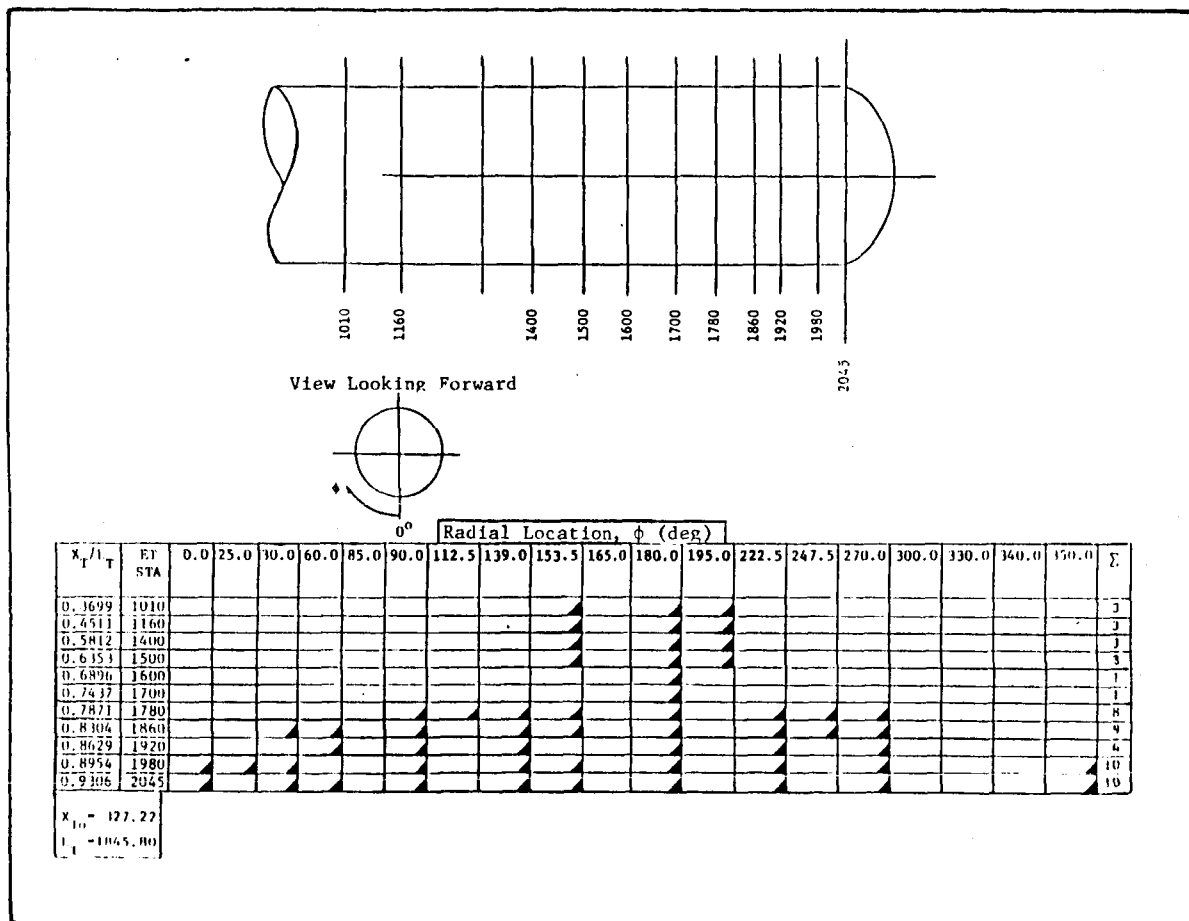


Fig. 6-27 ET Forebody Instrumentation Layout

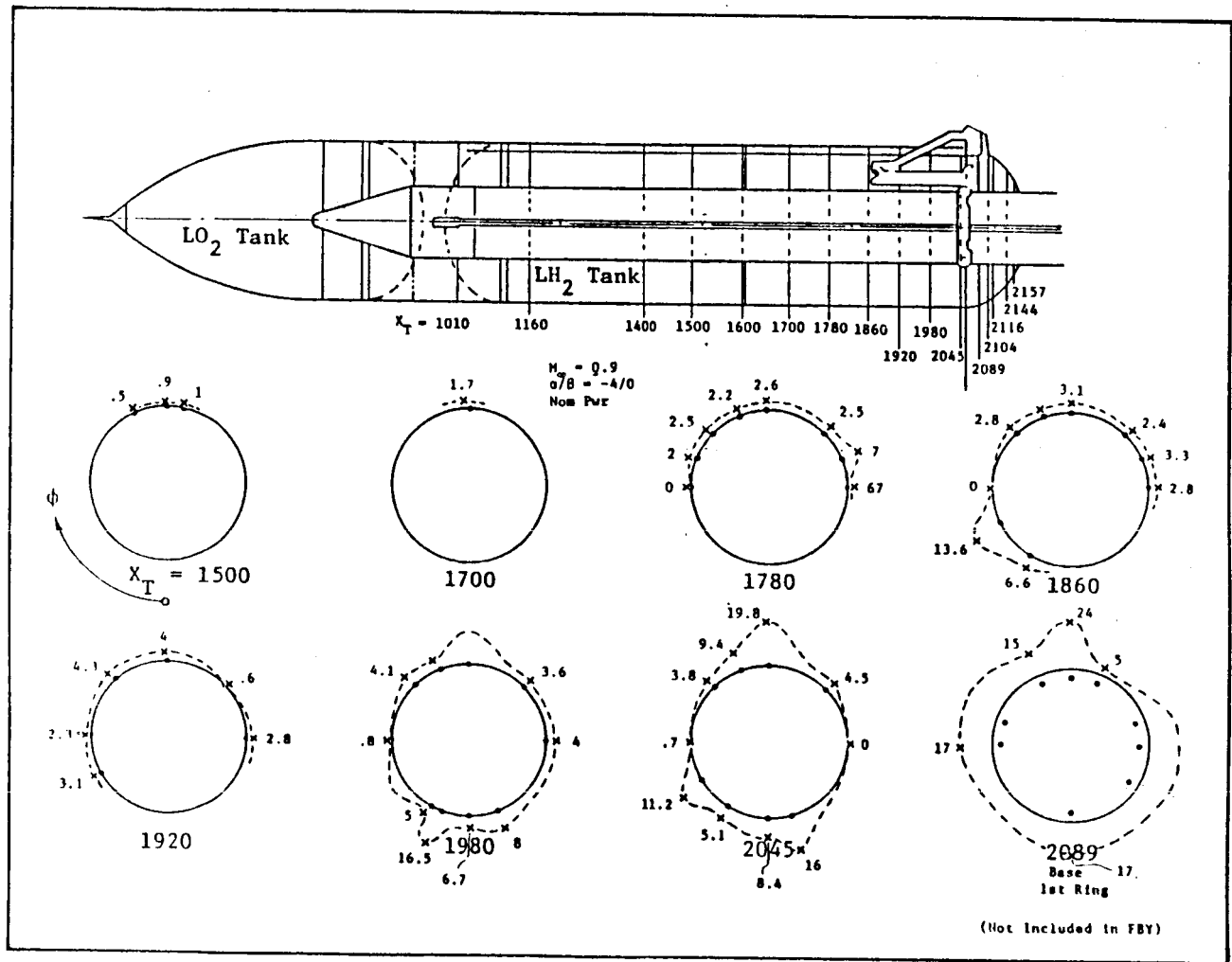


Fig. 6-28a IA300 ET Rings - Forebody ( $\Delta C_p$ <sub>pwr</sub>  $\times 100$ )

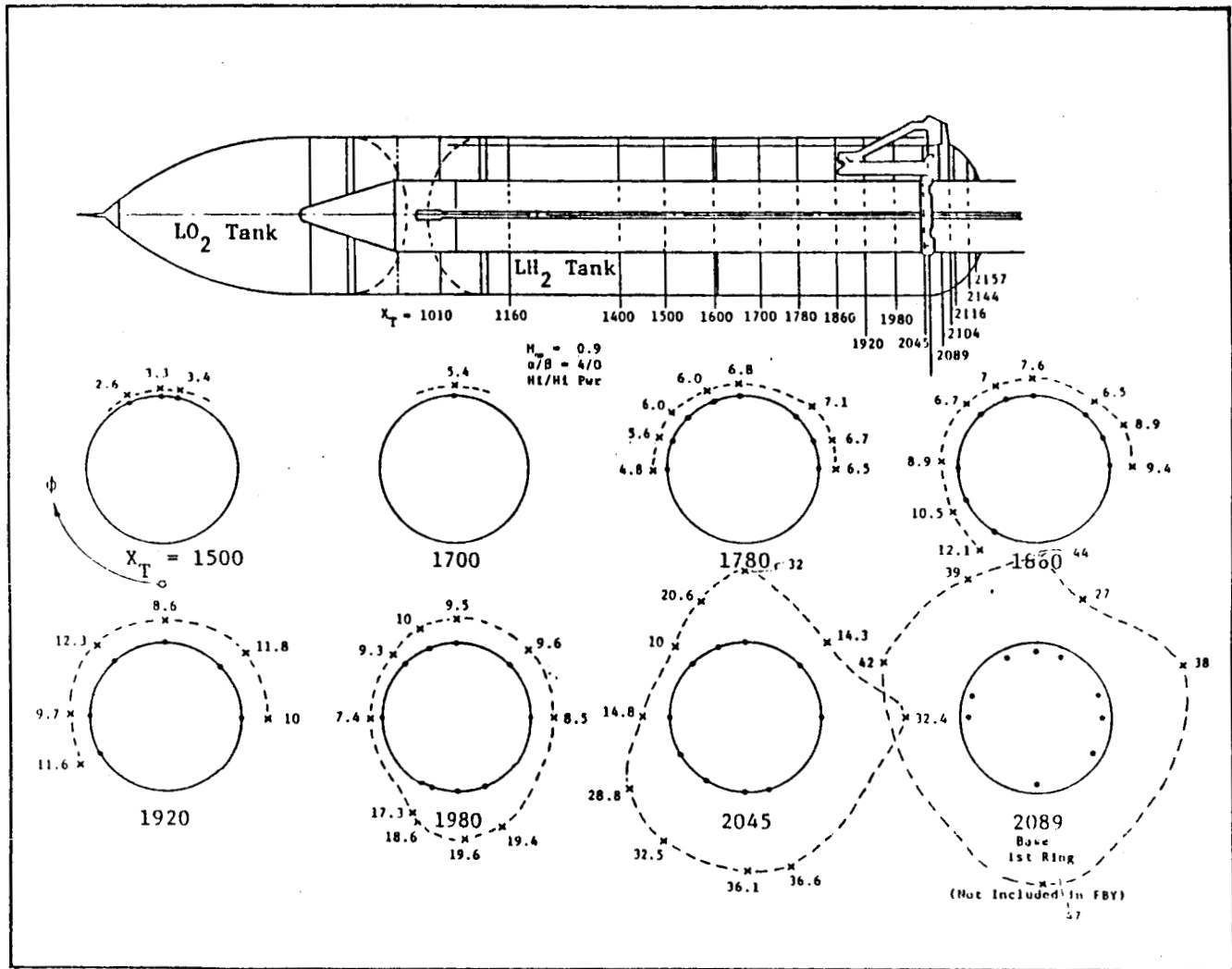


Fig. 6-28b IA300 ET Rings - Forebody ( $\Delta C_p \times 100$ )  
pwr

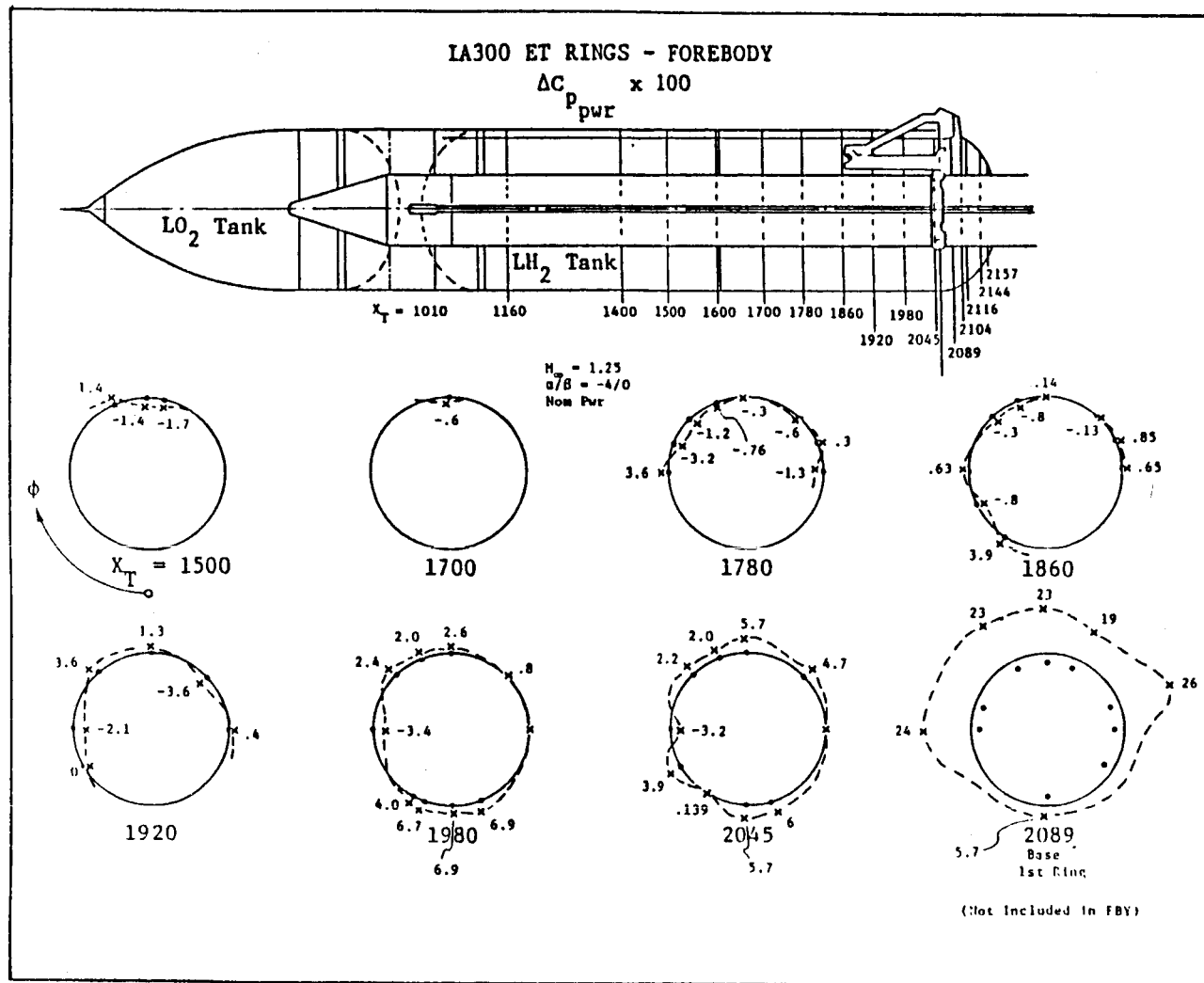


Fig. 6-28c IA300 ET Rings - Forebody ( $\Delta C_p \text{ pwr} \times 100$ )

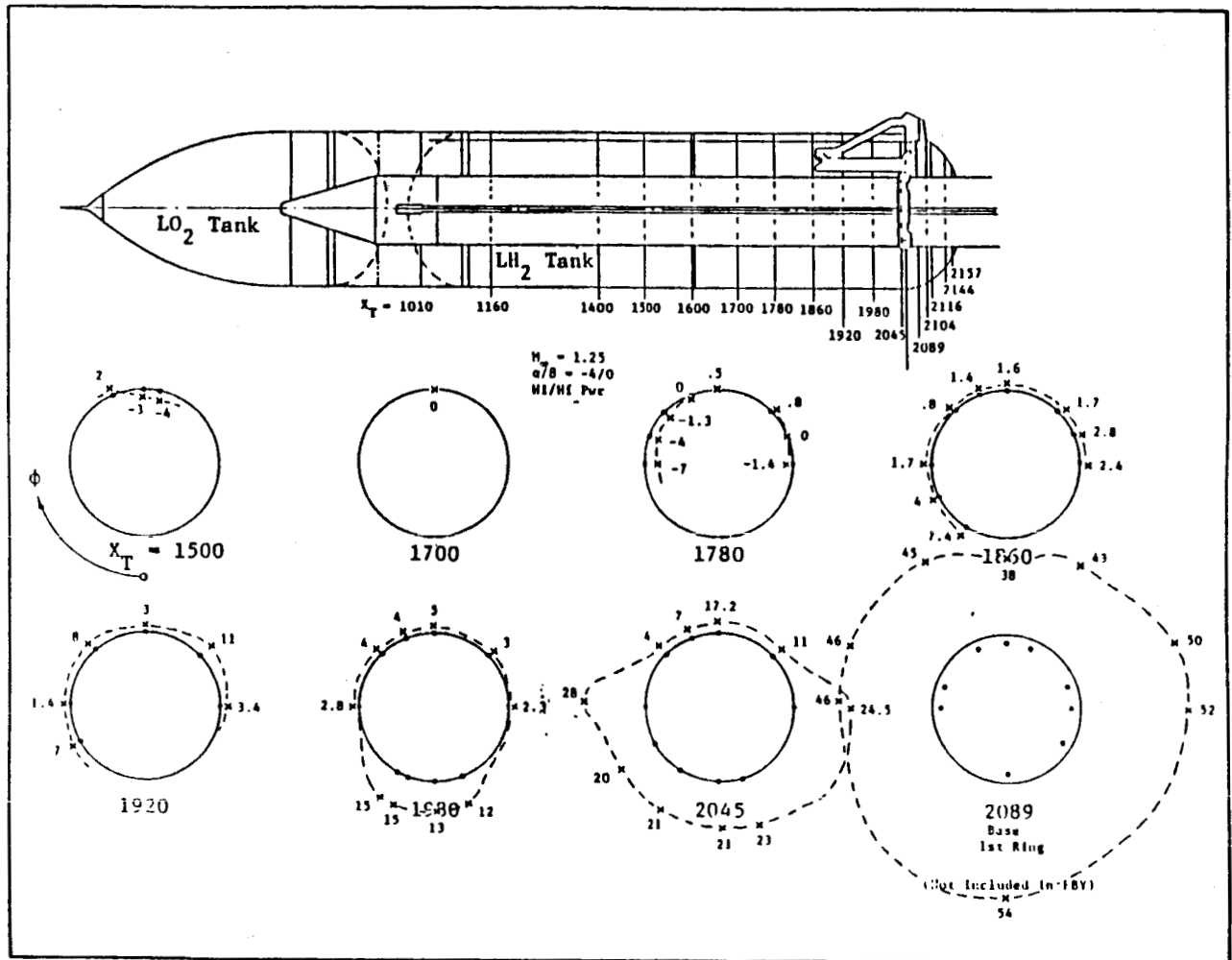


Fig. 6-28d IA300 ET Rings - Forebody ( $\Delta C_{P_{pwr}} \times 100$ )

ORIGINAL PAGE IS  
OF POOR QUALITY

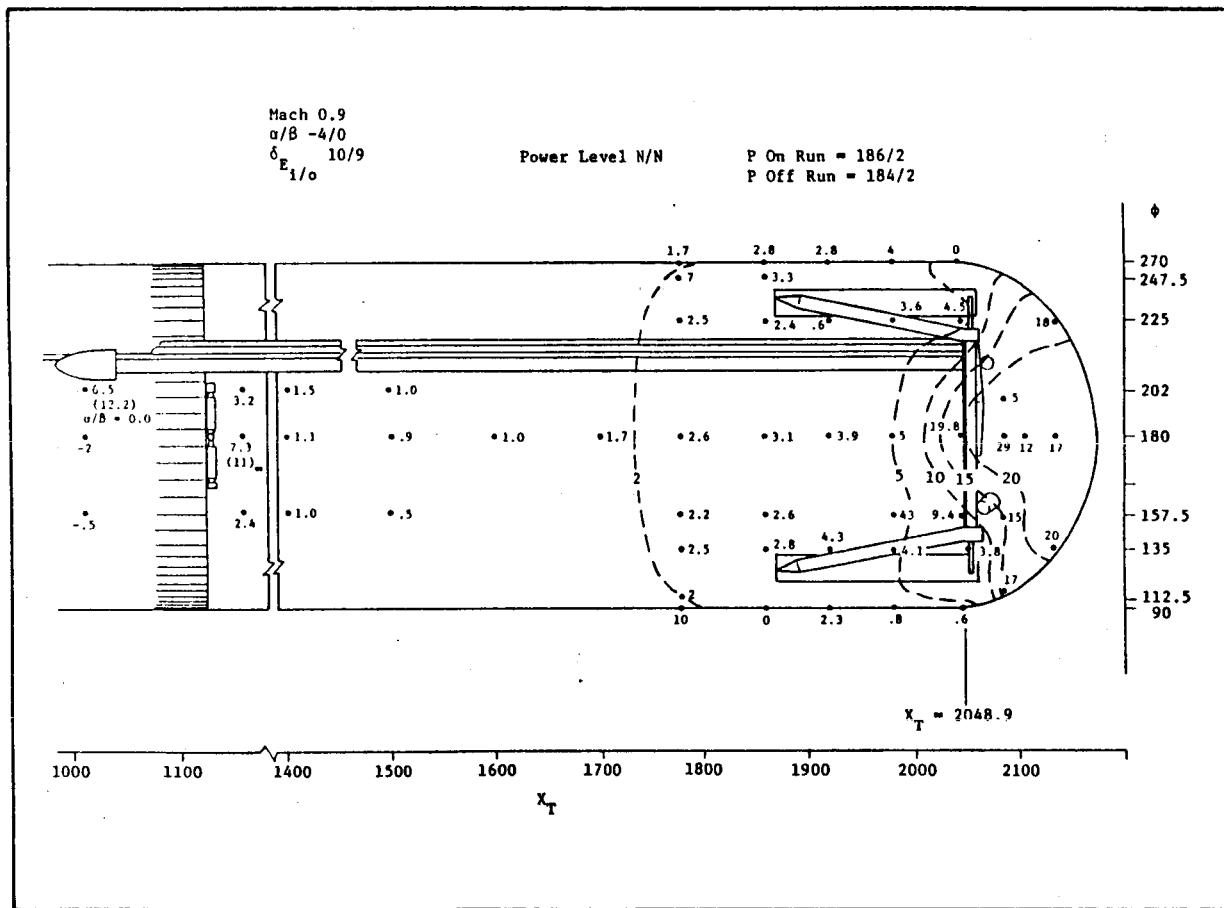


Fig. 6-29a ET Power Delta - Dual Strut ( $\Delta C_p \times 100$ )

ORIGINAL PAGE IS  
OF POOR QUALITY

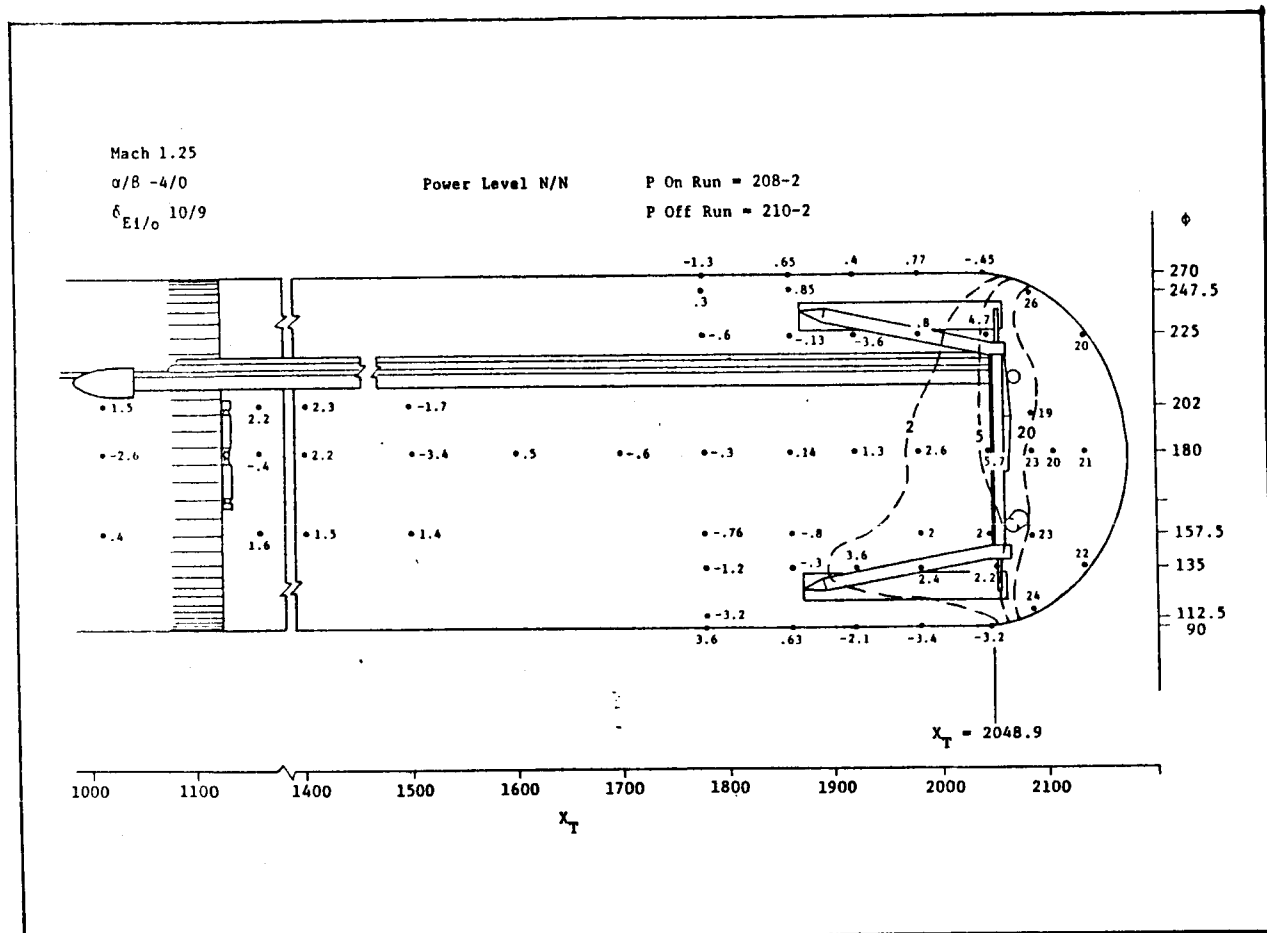


Fig. 6-29b ET Power Delta - Dual Strut, 35-deg Nozzle ( $\Delta C_p \times 100$ )

Table 6-10 EFFECTIVE AREA MODELING OF TAPS FOR ET FOREBODY

BODY	TAP #/FUNC.	AREA SQ.FT.	X	Y	Z	THETA	PHI
153. E.T. FBODY	(*1606'*.*1)*	79.4600	1010.00	0.00	234.50	180.0	270.0
154. E.T. FBODY	(*1606'*.*1)*	79.4600	1010.00	-63.33	247.10	157.5	270.0
155. E.T. FBODY	(*1606'*.*1)*	79.4600	1010.00	-117.03	282.97	135.0	270.0
156. E.T. FBODY	(*1606'*.*1)*	79.4600	1010.00	-152.90	336.67	112.5	270.0
157. E.T. FBODY	(*1606'*.*1)*	79.4600	1010.00	-165.50	400.00	90.0	270.0
158. E.T. FBODY	1009	79.4600	1010.00	-152.90	463.33	67.5	270.0
159. E.T. FBODY	1009	79.4600	1010.00	-117.03	517.03	45.0	270.0
160. E.T. FBODY	1009	79.4600	1010.00	-63.33	552.90	22.5	270.0
161. E.T. FBODY	1011	79.4600	1010.00	0.00	565.50	0.0	90.0
162. E.T. FBODY	1012	79.4600	1010.00	63.33	552.90	22.5	90.0
163. E.T. FBODY	(*1615'*.*005)*	79.4600	1010.00	117.03	517.03	45.0	90.0
164. E.T. FBODY	(*1615'*.*005)*	79.4600	1010.00	152.90	463.33	67.5	90.0
165. E.T. FBODY	(*1615'*.*005)*	79.4600	1010.00	165.50	400.00	90.0	90.0
166. E.T. FBODY	(*1615'*.*005)*	79.4600	1010.00	152.90	336.67	112.5	90.0
167. E.T. FBODY	(*1615'*.*005)*	79.4600	1010.00	117.03	282.97	135.0	90.0
168. E.T. FBODY	(*1615'*.*005)*	79.4600	1010.00	-63.33	247.10	157.5	90.0
169. E.T. FBODY	(*1606'*.*1)*	79.4600	1400.00	0.00	234.50	180.0	270.0
170. E.T. FBODY	(*1606'*.*1)*	79.4600	1400.00	-63.33	247.10	157.5	270.0
171. E.T. FBODY	(*1606'*.*1)*	79.4600	1400.00	-117.03	282.97	135.0	270.0
172. E.T. FBODY	(*1606'*.*1)*	79.4600	1400.00	-152.90	336.67	112.5	270.0
173. E.T. FBODY	(*1606'*.*1)*	79.4600	1400.00	-165.50	400.00	90.0	270.0
174. E.T. FBODY	1209	79.4600	1400.00	-152.90	463.33	67.5	270.0
175. E.T. FBODY	1209	79.4600	1400.00	-117.03	517.03	45.0	270.0
176. E.T. FBODY	1209	79.4600	1400.00	-63.33	552.90	22.5	270.0
177. E.T. FBODY	1211	79.4600	1400.00	0.00	565.50	0.0	90.0
178. E.T. FBODY	1212	79.4600	1400.00	63.33	552.90	22.5	90.0
179. E.T. FBODY	(*1615'*.*1)*	79.4600	1400.00	117.03	517.03	45.0	90.0
180. E.T. FBODY	(*1615'*.*1)*	79.4600	1400.00	152.90	463.33	67.5	90.0
181. E.T. FBODY	(*1615'*.*1)*	79.4600	1400.00	165.50	400.00	90.0	90.0
182. E.T. FBODY	(*1615'*.*05)*	79.4600	1400.00	152.90	336.67	112.5	90.0
183. E.T. FBODY	(*1615'*.*05)*	79.4600	1400.00	117.03	282.97	135.0	90.0
184. E.T. FBODY	(*1615'*.*05)*	79.4600	1400.00	63.33	247.10	157.5	90.0
185. E.T. FBODY	(*1606'*.*05)*	90.0000	1160.00	0.00	234.50	180.0	270.0
186. E.T. FBODY	(*1606'*.*05)*	90.0000	1160.00	-63.33	247.10	157.5	270.0
187. E.T. FBODY	(*1606'*.*05)*	90.0000	1160.00	-117.03	282.97	135.0	270.0
188. E.T. FBODY	(*1606'*.*05)*	90.0000	1160.00	-152.90	336.67	112.5	270.0
189. E.T. FBODY	(*1606'*.*05)*	90.0000	1160.00	-165.50	400.00	90.0	270.0
190. E.T. FBODY	(*1009'*.*5+*1209'*.*5)*	90.0000	1160.00	-152.90	463.33	67.5	270.0
191. E.T. FBODY	(*1009'*.*5+*1209'*.*5)*	90.0000	1160.00	-117.03	517.03	45.0	270.0
192. E.T. FBODY	(*1009'*.*5+*1209'*.*5)*	90.0000	1160.00	-63.33	552.90	22.5	270.0
193. E.T. FBODY	(*1011'*.*5+*1211'*.*5)*	90.0000	1160.00	0.00	565.50	0.0	90.0
194. E.T. FBODY	1112	90.0000	1160.00	63.33	552.90	22.5	90.0
195. E.T. FBODY	(*1615'*.*02)*	90.0000	1160.00	117.03	517.03	45.0	90.0
196. E.T. FBODY	(*1615'*.*02)*	90.0000	1160.00	152.90	463.33	67.5	90.0
197. E.T. FBODY	(*1615'*.*02)*	90.0000	1160.00	165.50	400.00	90.0	90.0
198. E.T. FBODY	(*1615'*.*01)*	90.0000	1160.00	152.90	336.67	112.5	90.0
199. E.T. FBODY	(*1615'*.*01)*	90.0000	1160.00	117.03	282.97	135.0	90.0
200. E.T. FBODY	(*1615'*.*01)*	90.0000	1160.00	63.33	247.10	157.5	90.0
201. E.T. FBODY	(*1606'*.*3)*	45.4000	1600.00	0.00	234.50	180.0	270.0
202. E.T. FBODY	(*1606'*.*3)*	45.4000	1600.00	-63.33	247.10	157.5	270.0
203. E.T. FBODY	(*1606'*.*3)*	45.4000	1600.00	-117.03	282.97	135.0	270.0
204. E.T. FBODY	(*1606'*.*3)*	45.4000	1600.00	-152.90	336.67	112.5	270.0
205. E.T. FBODY	(*1606'*.*3)*	45.4000	1600.00	-165.50	400.00	90.0	270.0
206. E.T. FBODY	1411	45.4000	1600.00	-152.90	463.33	67.5	270.0
207. E.T. FBODY	1411	45.4000	1600.00	-117.03	517.03	45.0	270.0
208. E.T. FBODY	1411	45.4000	1600.00	-63.33	552.90	22.5	270.0
209. E.T. FBODY	1411	45.4000	1600.00	0.00	565.50	0.0	90.0
210. E.T. FBODY	1312	45.4000	1600.00	63.33	552.90	22.5	90.0
211. E.T. FBODY	(*1613'*.*5)*	45.4000	1600.00	117.03	517.03	45.0	90.0
212. E.T. FBODY	(*1614'*.*5)*	45.4000	1600.00	152.90	463.33	67.5	90.0

(Continued)

\* Tap averaging.

Table 6-10 (Continued)

BODY	TAP #/FUNC.	AREA SQ.FT.	X	Y	Z	THETA	PHI
213. E.T. FBDY	("1615**.5) *	45.4000	1600.00	165.50	400.00	90.0	90.0
214. E.T. FBDY	("1615**.3) *	45.4000	1600.00	152.90	336.67	112.5	90.0
215. E.T. FBDY	("1615**.3) *	45.4000	1600.00	117.03	282.97	135.0	90.0
216. E.T. FBDY	("1615**.3) *	45.4000	1600.00	63.33	247.10	157.5	90.0
217. E.T. FBDY	("1606**.1) *	45.4000	1500.00	0.00	234.50	100.0	270.0
218. E.T. FBDY	("1606**.1) *	45.4000	1500.00	-63.33	247.10	157.5	270.0
219. E.T. FBDY	("1606**.1) *	45.4000	1500.00	-117.03	282.97	135.0	270.0
220. E.T. FBDY	("1606**.1) *	45.4000	1500.00	-152.90	336.67	112.5	270.0
221. E.T. FBDY	("1606**.1) *	45.4000	1500.00	-165.50	400.00	90.0	270.0
222. E.T. FBDY	1309	45.4000	1500.00	-152.90	463.33	67.5	270.0
223. E.T. FBDY	1309	45.4000	1500.00	-117.03	517.03	45.0	270.0
224. E.T. FBDY	1309	45.4000	1500.00	-63.33	552.90	22.5	270.0
225. E.T. FBDY	1311	45.4000	1500.00	0.00	565.50	0.0	90.0
226. E.T. FBDY	1312	45.4000	1500.00	63.33	552.90	22.5	90.0
227. E.T. FBDY	("1613**.2) *	45.4000	1500.00	117.03	517.03	45.0	90.0
228. E.T. FBDY	("1614**.2) *	45.4000	1500.00	152.90	463.33	67.5	90.0
229. E.T. FBDY	("1615**.2) *	45.4000	1500.00	165.50	400.00	90.0	90.0
230. E.T. FBDY	("1615**.1) *	45.4000	1500.00	152.90	336.67	112.5	90.0
231. E.T. FBDY	("1615**.1) *	45.4000	1500.00	117.03	282.97	135.0	90.0
232. E.T. FBDY	("1615**.1) *	45.4000	1500.00	63.33	247.10	157.5	90.0
233. E.T. FBDY	1606	34.0500	1700.00	0.00	234.50	100.0	270.0
234. E.T. FBDY	1606	34.0500	1700.00	-63.33	247.10	157.5	270.0
235. E.T. FBDY	1606	34.0500	1700.00	-117.03	282.97	135.0	270.0
236. E.T. FBDY	1606	34.0500	1700.00	-152.90	336.67	112.5	270.0
237. E.T. FBDY	1606	34.0500	1700.00	-165.50	400.00	90.0	270.0
238. E.T. FBDY	1607	34.0500	1700.00	-152.90	463.33	67.5	270.0
239. E.T. FBDY	1608	34.0500	1700.00	-117.03	517.03	45.0	270.0
240. E.T. FUDY	1609	34.0500	1700.00	-63.33	552.90	22.5	270.0
241. E.T. FBDY	1611	34.0500	1700.00	0.00	565.50	0.0	90.0
242. E.T. FBDY	("1611**.7)+("1312**.3) *	34.0500	1700.00	63.33	552.90	22.5	90.0
243. E.T. FBDY	1613	34.0500	1700.00	117.03	517.03	45.0	90.0
244. E.T. FBDY	1614	34.0500	1700.00	152.90	463.33	67.5	90.0
245. E.T. FBDY	1615	34.0500	1700.00	165.50	400.00	90.0	90.0
246. E.T. FBDY	1615	34.0500	1700.00	152.90	336.67	112.5	90.0
247. E.T. FBDY	1615	34.0500	1700.00	117.03	282.97	135.0	90.0
248. E.T. FBDY	1615	34.0500	1700.00	63.33	247.10	157.5	90.0
249. E.T. FBDY	("1606**.5) *	45.4000	1700.00	0.00	234.50	100.0	270.0
250. E.T. FBDY	("1606**.5) *	45.4000	1700.00	-63.33	247.10	157.5	270.0
251. E.T. FBDY	("1606**.5) *	45.4000	1700.00	-117.03	282.97	135.0	270.0
252. E.T. FBDY	("1606**.5) *	45.4000	1700.00	-152.90	336.67	112.5	270.0
253. E.T. FBDY	("1606**.8) *	45.4000	1700.00	-165.50	400.00	90.0	270.0
254. E.T. FBDY	("1607**.8) *	45.4000	1700.00	-152.90	463.33	67.5	270.0
255. E.T. FBDY	("1608**.8) *	45.4000	1700.00	-117.03	517.03	45.0	270.0
256. E.T. FBDY	("1609**.8) *	45.4000	1700.00	-63.33	552.90	22.5	270.0
257. E.T. FBDY	1511	45.4000	1700.00	0.00	565.50	0.0	90.0
258. E.T. FBDY	1312	45.4000	1700.00	63.33	552.90	22.5	90.0
259. E.T. FBDY	("1613**.8) *	45.4000	1700.00	117.03	517.03	45.0	90.0
260. E.T. FBDY	("1614**.8) *	45.4000	1700.00	152.90	463.33	67.5	90.0
261. E.T. FBDY	("1615**.8) *	45.4000	1700.00	165.50	400.00	90.0	90.0
262. E.T. FBDY	("1615**.5) *	45.4000	1700.00	152.90	336.67	112.5	90.0
263. E.T. FBDY	("1615**.5) *	45.4000	1700.00	117.03	282.97	135.0	90.0
264. E.T. FBDY	("1615**.5) *	45.4000	1700.00	63.33	247.10	157.5	90.0
265. E.T. FBDY	("1919**.7) *	22.7000	1920.00	0.00	234.50	100.0	270.0
266. E.T. FBDY	("1919**.7) *	22.7000	1920.00	-63.33	247.10	157.5	270.0
267. E.T. FBDY	("1919**.7) *	22.7000	1920.00	-117.03	282.97	135.0	270.0
268. E.T. FBDY	1004	22.7000	1920.00	-152.90	336.67	112.5	270.0
269. E.T. FBDY	1806	22.7000	1920.00	-165.50	400.00	90.0	270.0
270. E.T. FBDY	("1700**.5+1900**.5)*	22.7000	1920.00	-152.90	463.33	67.5	270.0
271. E.T. FBDY	("1700**.5+1900**.5)*	22.7000	1920.00	-117.03	517.03	45.0	270.0

\* Tap averaging.

(Continued)

Table 6-10 (Concluded)

BODY	TAP #/FUNC.	AREA 50.FT.	X	Y	Z	THETA	PHI
272. E.T. FBODY	(1708**.5+1908**.5)*	22.7000	1920.00	-63.33	552.90	22.5	270.0
273. E.T. FBODY	1811	22.7000	1920.00	0.00	555.50	0.0	90.0
274. E.T. FBODY	1811	22.7000	1920.00	63.33	552.90	22.5	90.0
275. E.T. FBODY	1813	22.7000	1920.00	117.03	517.03	45.0	90.0
276. E.T. FBODY	1815	22.7000	1920.00	152.90	463.33	67.5	90.0
277. E.T. FBODY	1815	22.7000	1920.00	165.50	400.00	90.0	90.0
278. E.T. FBODY	(1004+1815)/2 *	22.7000	1920.00	152.90	336.67	112.5	90.0
279. E.T. FBODY	(1919**.7)*	22.7000	1920.00	117.03	282.97	135.0	90.0
280. E.T. FBODY	(1919**.7)*	22.7000	1920.00	63.33	247.10	157.5	90.0
281. E.T. FBODY	1703	34.0500	1860.00	0.00	234.50	100.0	270.0
282. E.T. FBODY	1703	34.0500	1860.00	-63.33	247.10	157.5	270.0
283. E.T. FBODY	1703	34.0500	1860.00	-117.03	282.97	135.0	270.0
284. E.T. FBODY	1704	34.0500	1860.00	-152.90	336.67	112.5	270.0
285. E.T. FBODY	1706	34.0500	1860.00	-165.50	400.00	90.0	270.0
286. E.T. FBODY	1708	34.0500	1860.00	-152.90	463.33	67.5	270.0
287. E.T. FBODY	1700	34.0500	1860.00	-117.03	517.03	45.0	270.0
288. E.T. FBODY	1709	34.0500	1860.00	-63.33	552.90	22.5	270.0
289. E.T. FBODY	1711	34.0500	1860.00	0.00	555.50	0.0	90.0
290. E.T. FBODY	(1711**.8)+(1312**.2)*	34.0500	1860.00	63.33	552.90	22.5	90.0
291. E.T. FBODY	1713	34.0500	1860.00	117.03	517.03	45.0	90.0
292. E.T. FBODY	1714	34.0500	1860.00	152.90	463.33	67.5	90.0
293. E.T. FBODY	1715	34.0500	1860.00	165.50	400.00	90.0	90.0
294. E.T. FBODY	1704	34.0500	1860.00	152.90	336.67	112.5	90.0
295. E.T. FBODY	1704	34.0500	1860.00	117.03	282.97	135.0	90.0
296. E.T. FBODY	1703	34.0500	1860.00	63.33	247.10	157.5	90.0
297. E.T. FBODY	2019	17.2500	2045.00	0.00	234.50	100.0	270.0
298. E.T. FBODY	2003	17.2500	2045.00	-63.33	247.10	157.5	270.0
299. E.T. FBODY	2003	17.2500	2045.00	-117.03	282.97	135.0	270.0
300. E.T. FBODY	2004	17.2500	2045.00	-152.90	336.67	112.5	270.0
301. E.T. FBODY	2016	17.2500	2045.00	-165.50	400.00	90.0	270.0
302. E.T. FBODY	2000	17.2500	2045.00	-152.90	463.33	67.5	270.0
303. E.T. FBODY	2008	17.2500	2045.00	-117.03	517.03	45.0	270.0
304. E.T. FBODY	2009	17.2500	2045.00	-63.33	552.90	22.5	270.0
305. E.T. FBODY	2011	17.2500	2045.00	0.00	555.50	0.0	90.0
306. E.T. FBODY	2011	17.2500	2045.00	63.33	552.90	22.5	90.0
307. E.T. FBODY	2013	17.2500	2045.00	117.03	517.03	45.0	90.0
308. E.T. FBODY	2015	17.2500	2045.00	152.90	463.33	67.5	90.0
309. E.T. FBODY	2015	17.2500	2045.00	165.50	400.00	90.0	90.0
310. E.T. FBODY	2015	17.2500	2045.00	152.90	336.67	112.5	90.0
311. E.T. FBODY	2019	17.2500	2045.00	117.03	282.97	135.0	90.0
312. E.T. FBODY	2019	17.2500	2045.00	63.33	247.10	157.5	90.0
313. E.T. FBODY	1901	27.2400	1900.00	0.00	234.50	100.0	270.0
314. E.T. FBODY	1902	27.2400	1900.00	-63.33	247.10	157.5	270.0
315. E.T. FBODY	(1902**.7)*	27.2400	1900.00	-117.03	282.97	135.0	270.0
316. E.T. FBODY	(1902**.5)*	27.2400	1900.00	-152.90	336.67	112.5	270.0
317. E.T. FBODY	1906	27.2400	1900.00	-165.50	400.00	90.0	270.0
318. E.T. FBODY	1908	27.2400	1900.00	-152.90	463.33	67.5	270.0
319. E.T. FBODY	1908	27.2400	1900.00	-117.03	517.03	45.0	270.0
320. E.T. FBODY	1909	27.2400	1900.00	-63.33	552.90	22.5	270.0
321. E.T. FBODY	1911	27.2400	1900.00	0.00	555.50	0.0	90.0
322. E.T. FBODY	1911	27.2400	1900.00	63.33	552.90	22.5	90.0
323. E.T. FBODY	1913	27.2400	1900.00	117.03	517.03	45.0	90.0
324. E.T. FBODY	1913	27.2400	1900.00	152.90	463.33	67.5	90.0
325. E.T. FBODY	1915	27.2400	1900.00	165.50	400.00	90.0	90.0
326. E.T. FBODY	(1919**.5)*	27.2400	1900.00	152.90	336.67	112.5	90.0
327. E.T. FBODY	1919	27.2400	1900.00	117.03	282.97	135.0	90.0
328. E.T. FBODY	1919	27.2400	1900.00	63.33	247.10	157.5	90.0

\* Tap averaging.

## 7. ANALYSIS OF TEST RESULTS

The analysis of the plume induced forebody pressures showed that the spatial content included the entire wing and extended up to the region of the forward attach structure (see Section 6). The extent of the forebody plume induced pressure field for the original Space Shuttle Cold Flow Plume Test (IA119-IA138, Ref. 1) did not extend nearly this far forward on the vehicle. The magnitude of the plume induced pressure were not as large in test IA119 as they are in test IA300. The magnitude of the plume induced Orbiter forebody aerodynamic normal force (obtained by integrating the plume induced pressures) is presented in Fig. 7-1. Also presented in the figure are flight extracted increments that are the difference between flight extracted aerodynamic data and, pre-STS-1 predicted characteristics. Also presented in the figure are test results from a solid plume test, TWT-675. Note in the figure that the IA300 and TWT-675 test results show similar trends although the IA300 test results are slight higher than the TWT-675 results. The best match of the flight extracted results occurs using the IA300 test results with the SSME & SRB nozzles gimbaled in a similar fashion as the flight vehicle. The plume induced Orbiter wing normal force coefficient data are presented in Fig. 7-2 and compared with flight extracted results. Comparison of the IA300 results with the flight extracted results show a favorable comparison. The wing inboard elevon hinge moment coefficient comparison is presented in Fig. 7-3. The wing hinge moment plume induced aerodynamic characteristics were used as an indicator for the spatial content of the plume induced phenomenon. Although the figure shows a lack of correlation in the subsonic flight regime (IA300 test results show a negative increment compared to positive flight results), the subsonic values would require higher fidelity modeling of the elevon, flipper door, and hinge line geometric characteristics. The data scatter near Mach 1.0 is not of concern and is due to wind tunnel shock reflection problems. The excellent

ORIGINAL PAGE IS  
OF POOR QUALITY

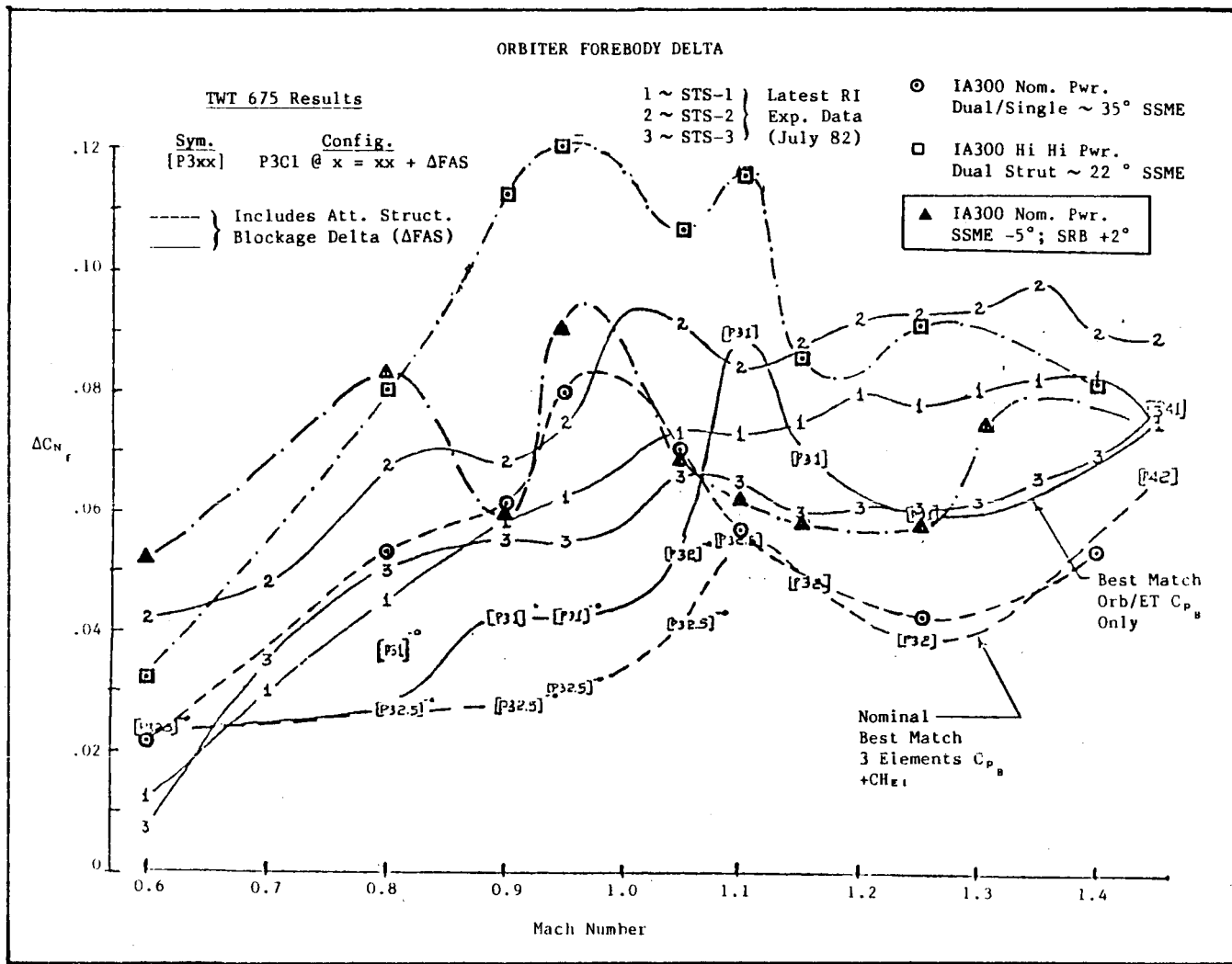


Fig. 7-1 Comparison of Orbiter Normal Force Coefficient Plume Increments with Flight Extracted Data

ORIGINAL PAGE IS  
OF POOR QUALITY

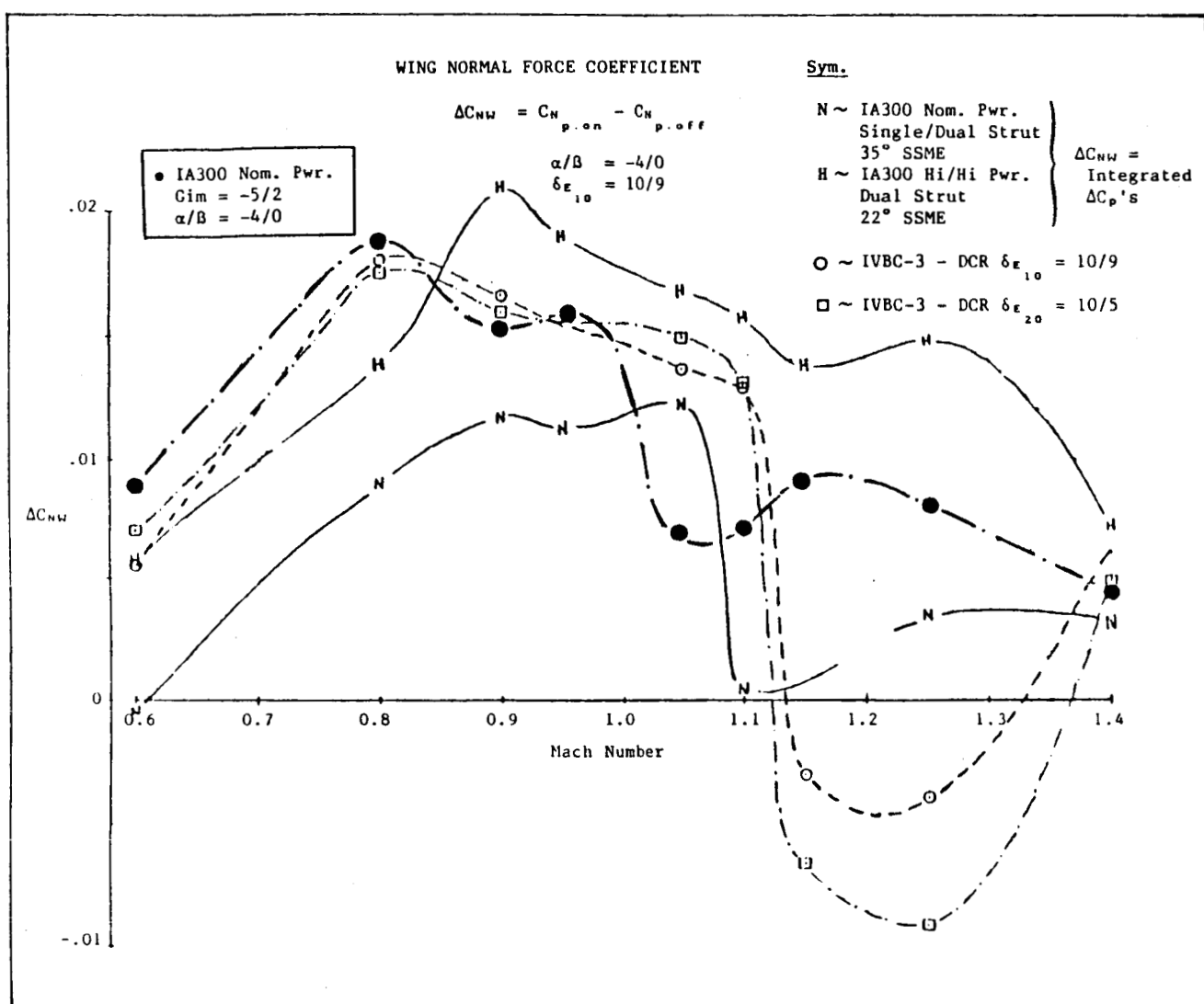


Fig. 7-2 Comparison of Orbiter Wing Normal Force Coefficient Plume Increments with Flight Extracted Data

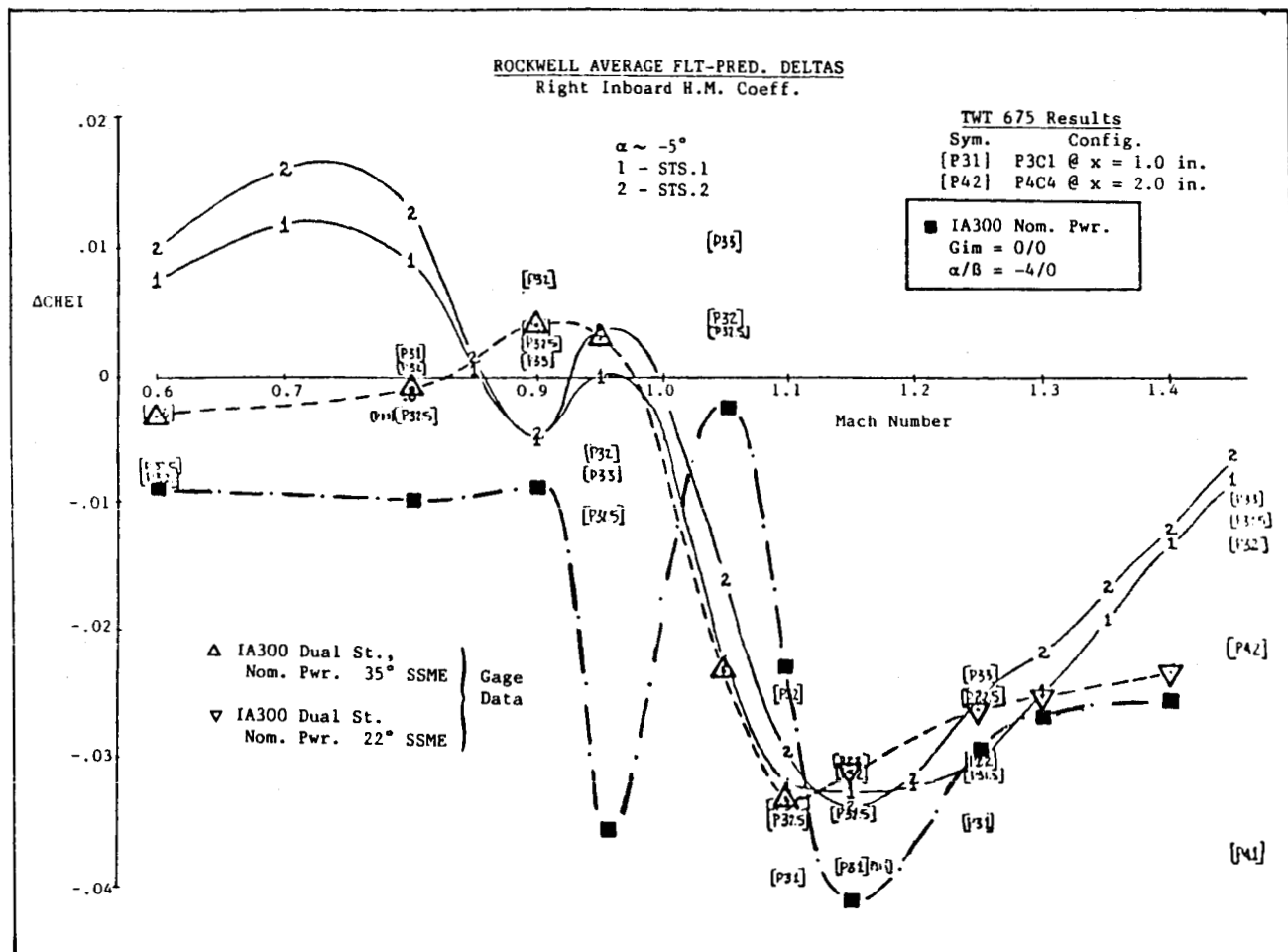


Fig. 7-3 Comparison of Orbiter Wing Hinge Moment Coefficient Plume Increments with Flight Extracted Data

comparision above Mach 1.05 gives conclusive proof of the near simulation of the spacial content of the plume induced pressure field using the IA300 plume simulation.

The close simulation of the flight extracted Orbiter and Orbiter component extracted aerodynamic increments with the IA300 plume induced aerodynamic increments gives verification that the "aerodynamic anomoly" identified on the first flight was due primarily to the plume-induced forebody aerodynamic characteristics being larger than predicted. The significance in the magnitude of the plume-induced aerodynamic characteristic is presented in Fig. 7-4. Figure 7-4 presents estimates of the SSLV, Orbiter, and lower stack normal force coefficient versus angle of attack with and without the influence of the plumes. The data in the figure shows that the plume induced Orbiter normal force coefficient is substantial and has the effect of increasing the Orbiter angle of attack over a degree. Noting that the flight angle of attack is between -2 and -4 deg, the increase in Orbiter normal force due to plume effect is approximately 100 percent. Thus, the plume induced Orbiter aerodynamic characteristics are substantial.

The change in the lower stack normal force coefficient due to the plumes is also presented in Fig. 7-4. Note that the lower stack increment is much smaller than the Orbiter increment. The major contribution of the lower stack normal force increment is due to the plume induced pressure field on the ET. The ET plume increment is presented on Fig. 7-5. The figure shows a good correlation with the flight extracted results. However, the extracted ET data are questionable since there were not enough strut flight measurements made to directly backout the ET and SRB characteristics separately. The positive lower magnitude ET increments are different from what might be expected if one considers a positive pressure field increment in a "channel flow" between Orbiter and ET. Under this condition a negative ET increment of the same order of magnitude might be expected. The plume induced pressure field varies greatly with upstream location, however, the further aft position of the Orbiter Base and Body Flap significantly increase the plume effects on the Orbiter. The ET would have a negative plume increment if it

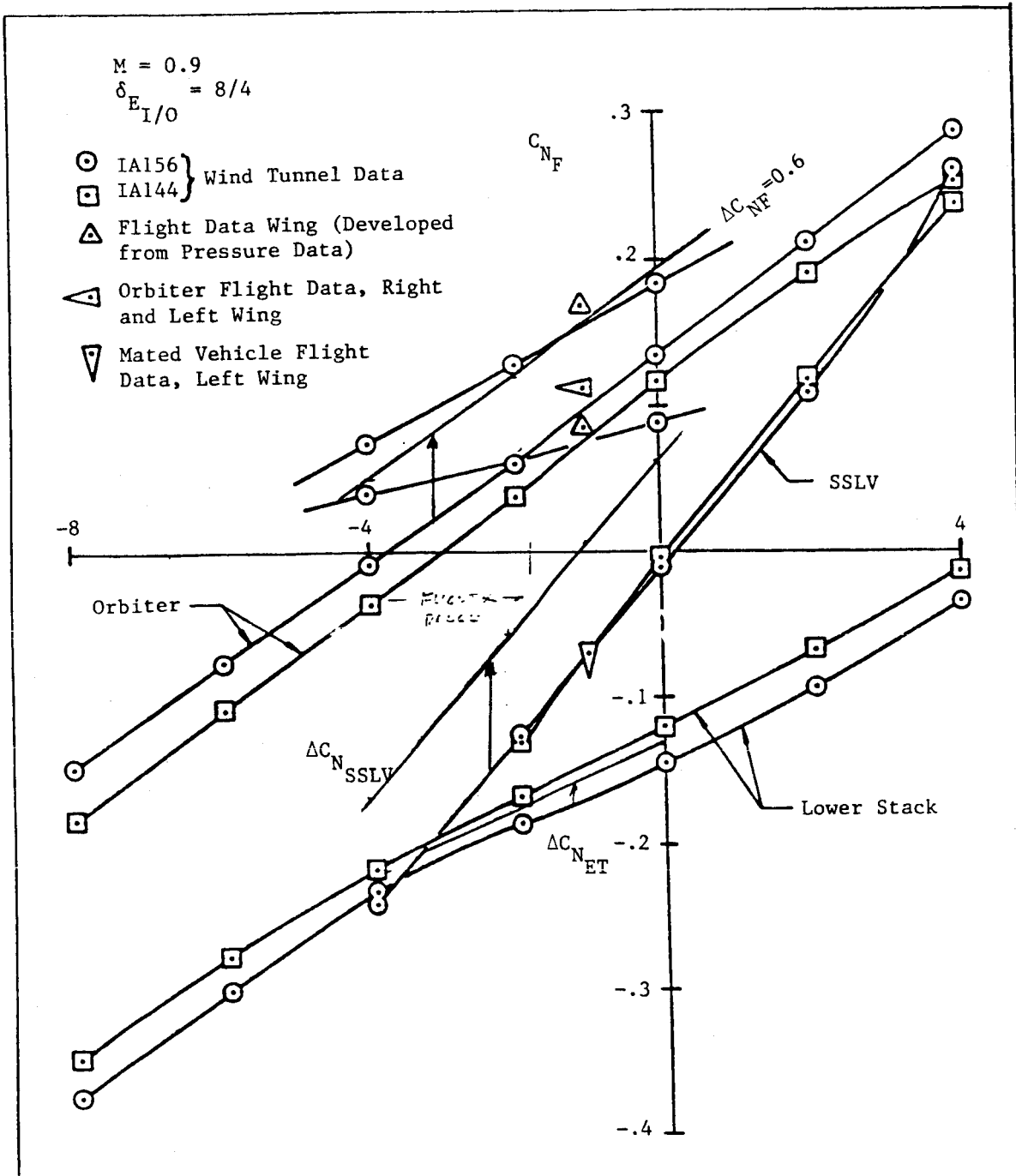


Fig. 7-4 SSLV and Element Normal Force Coefficient Characteristics  
(With and Without Plume Increments)

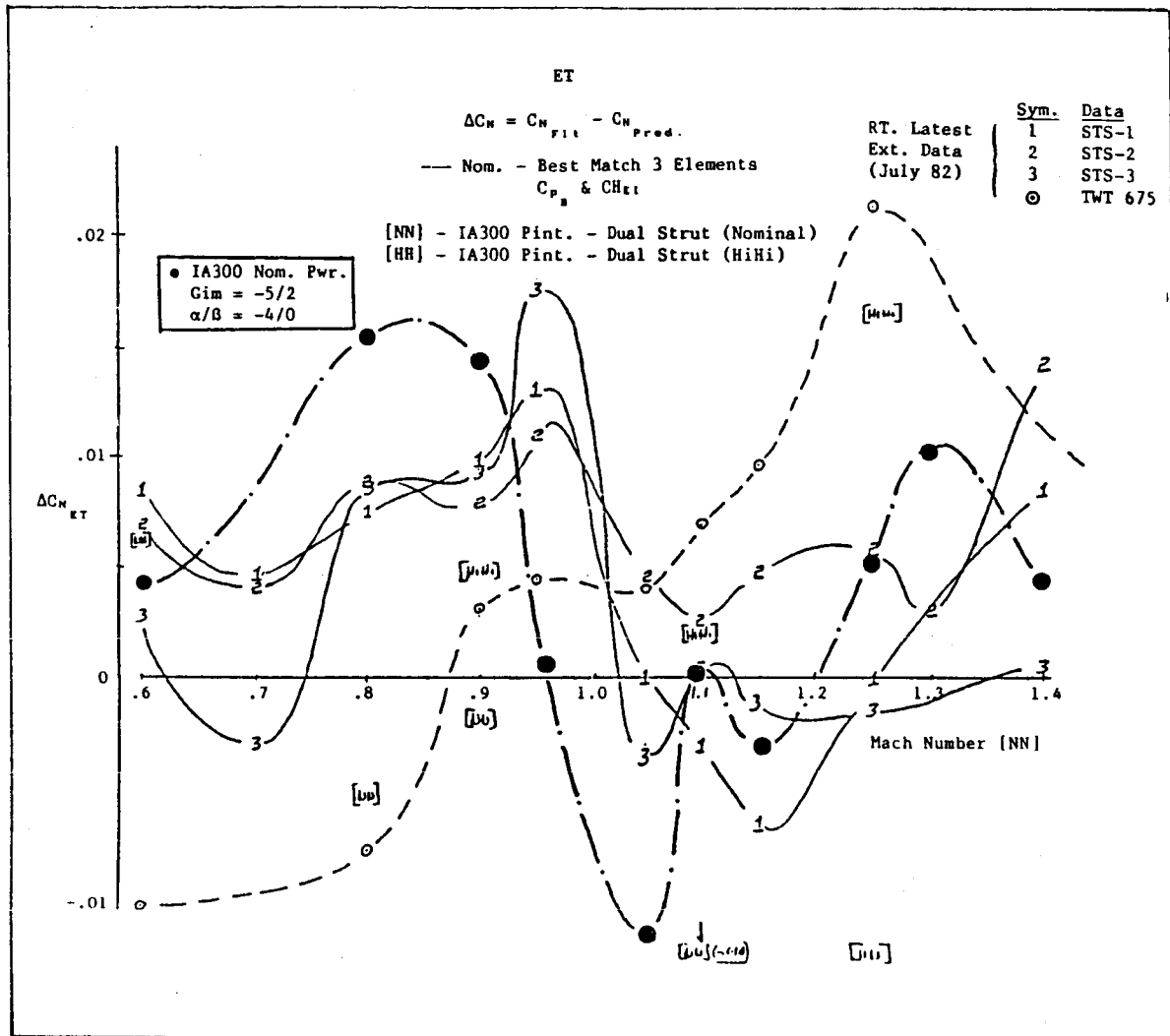


Fig. 7-5 Comparison of ET Normal Force Coefficient Plume Increments (With Flight Extracted Data)

were not for the difference in the plume induced pressure field around the aft attach structure and near the base region. Note in Fig. 7-5 that at certain Mach numbers ET plume induced normal force coefficients are negative.

The net effect of the large Orbiter plume induced normal force coefficient and the lower stack lower magnitude increments results in a substantial change in the SSLV aerodynamic characteristics as shown in Fig. 7-4.

The Orbiter plume induced pitching moment coefficients are presented in Fig. 7-6. These data can be compared to the normal force increment presented in Fig. 7-1 and it is evident that the center of the pressure is near the aft end of the Orbiter since the ratio of pitching moment and normal force approaches 1.0.

The magnitude and Mach trends of the IA300 plume induced forebody aerodynamic increments compare favorably with the flight extracted increments. This comparison provides evidence that the flight "aerodynamic anomaly" was primarily due to the erroneously predicted plume influence on the forebody aerodynamic characteristics. This error is suspected to be manifested in the evaluation of "Prototype Possibility Curves" used to interpret the IA119 and IA138 test results.

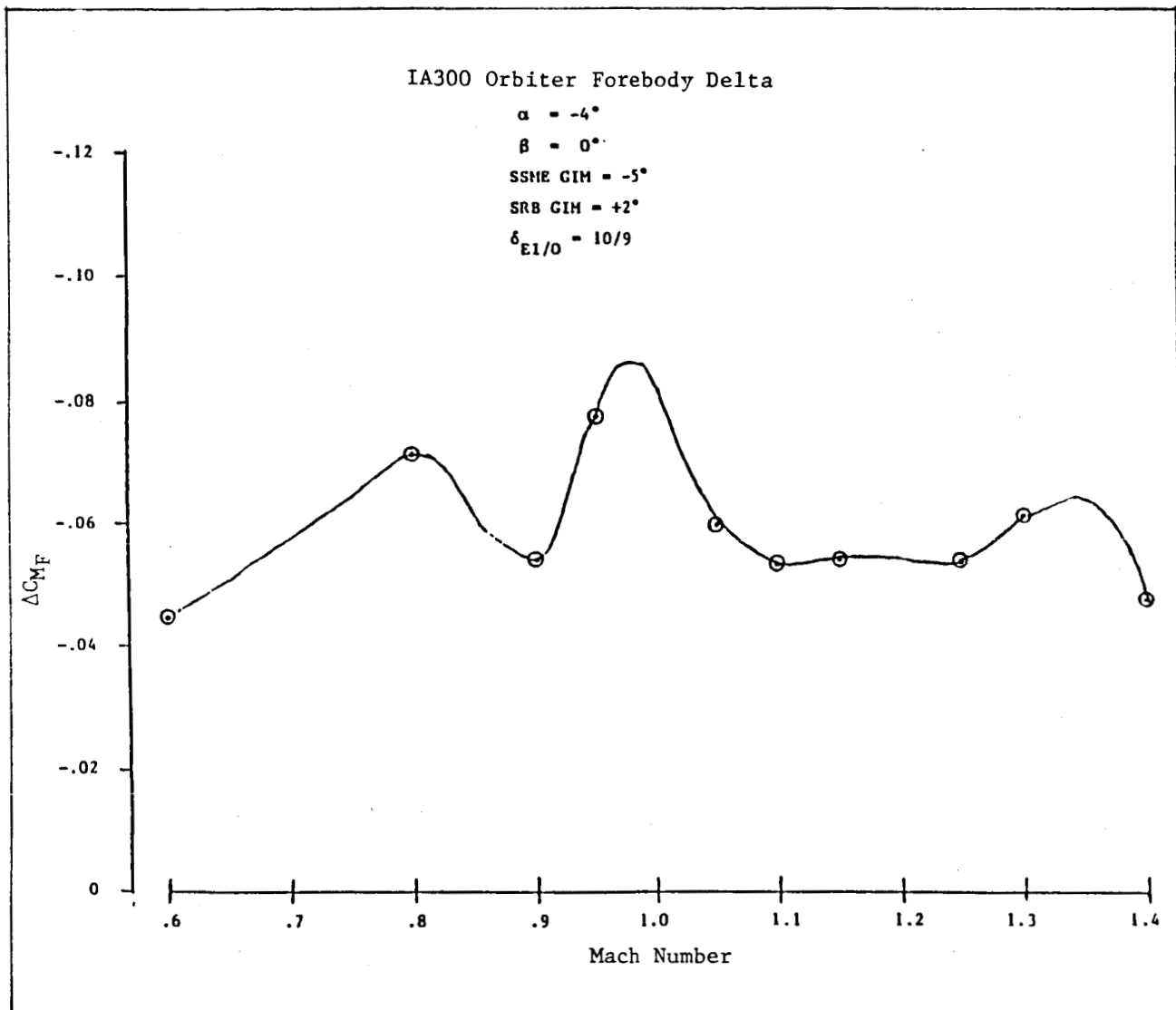


Fig. 7-6 Orbiter Pitching Moment Coefficient Plume Increments

## 8. TEST RESULTS INTEGRATION

The results of the integration of the base pressure and forebody power deltas are presented in tabular and graphical form in the Appendices. The output of the Plume Integration Computer Program contains all the results of the pressure integration including base coefficient increments, forces and moments, and forebody coefficient increments from pressure integration.

An example of the printout from a data set is presented in Fig. 8-1. The data are arranged in nine sections. Section 1 is a header block which identifies the data set according to Mach number, vehicle attitude, and engine gimbal setting. Section 2 presents the element forebody coefficient increments from pressure integration. Section 3 presents the total vehicle coefficient increments from pressure integration. Section 4 presents the results of the pressure integration over the base elements and components. Section 5 presents the total vehicle base forces and moments referenced to the Mission 3A trajectory. Section 6 presents the nozzle gas dynamic properties. Section 7 presents the nozzle gas dynamic similarity parameters for the SSME (SP) and SRB (SP4), respectively. Section 8 presents the average base pressure coefficient for each element. Section 9 presents the Mission 3A reference trajectory dynamic pressure and altitude.

Printouts of each run sequence set are presented in Appendix A. Data sets are grouped for constant engine gimbal angle runs and various elevon deflections. Nominal data are presented first, followed by gimbal angle variations. Each data set is grouped by Mach number, and each Mach number group consists of the various angles of attack and angles of sideslip.

Graphical results of pressure integration are presented in Appendices B through E. Several observations should be made when analyzing these results. The angle of attack will be referred to as alpha and the angle of sideslip

ORIGINAL PAGE IS  
OF POOR QUALITY

(1)	MACH	ALPH	BETA	ELI	ELO	SSME GIM	SRB GIM	***	***	***	***	***
	0.60	-8	-4	10.00	9.00	8.00	8.00	*	*	*	*	*
<hr/>												
(2)	**** FOREBODY PRESSURE INTEGRATION ****											
	CA	CN	CM	CY	CYN	CL						
ORBITER	0.0006	0.0206	-0.0164	0.0112	-0.0089	0.0039						
ORB FUS	0.0001	0.0160	-0.0123	0.0112	-0.0089	0.0031						
ET	0.0000	-0.0271	0.0162	-0.0011	0.0000	0.0000						
L SRB	0.0043	-0.0019	0.0021	-0.0091	0.0060	-0.0004						
R SRB	0.0021	-0.0017	0.0020	0.0101	-0.0096	0.0003						
FBDY TOT	0.0070	-0.0101	0.0040	0.0111	-0.0116	0.0039						
	CFW	CBW	CTW	CHEI	CHEO							
R WING	0.0073	-0.0011	-0.0001	-0.0152	-0.0046							
L WING	-0.0027	0.0012	-0.0007	-0.0043	-0.0020							
	CYVT	CBVT	CTVT									
VT	0.0142	0.0056	-0.0024									
(3)	***** TOTAL VEHICLE (BASE + FBDY) *****											
	CA	CN	CM	CY	CYN	CL						
	0.0000	0.0037	-0.0068	0.0095	-0.0090	0.0040						
(4)	***** BASE COEFFICIENTS *****											
	CA	CN	CM	CY	CYN	CL						
ORBITER	0.0002	0.0002	-0.0061	0.0001	0.0001	0.0001						
ET	0.0009	0.0056	-0.0045	-0.0017	0.0014	0.0000						
L SRB	0.0032	0.0000	-0.0001	0.0000	-0.0006	0.0000						
R SRB	0.0006	0.0000	0.0000	0.0000	0.0017	0.0000						
BASE TOT	0.0010	0.0138	-0.0108	-0.0016	0.0026	0.0001						
(5)	*** BASE FORCES & MOMENTS ***											
	AF	NF	PM	SF	YM	RL						
81834.	13935.	-1169789.	-1619.	279438.	12845.							
(6)	**** NOZZLE CONDITIONS ****											
	SSME						SRB					
PC1	1723.87						PC4	1222.68				
PE	27.54						PE4	21.92				
PC1PE	62.68						PC4PE	55.77				
DELJ	44.57						DELJ4	42.39				
PEPINI	2.39						QINF	2.90				
(7)	***** SIMILARITY PARAMETERS *****											
	SP	111.38					SP4	99.79				
(8)	***** AVERAGE BASE PRESSURE COEF. *****											
	ORBITER	-0.0016					ET	-0.2799				
	LSRB	-0.1927					RSRB	-0.0719				
(9)	***** REFERENCE TRAJECTORY *****											
	DYN PRESS	375.80										
	ALTITUDE	9541.85										

Fig. 8-1 Sample of Data Listing

as beta. In some cases, the coefficient scale has been expanded for easier visibility; therefore, special attention should be paid to scaling parameters on all graphs.

As shown in Fig. 8-2, Appendix B contains results of longitudinal data plotted versus Mach number at -4 deg alpha and 0 degrees beta. Fig. 8-3 shows longitudinal and lateral-directional data plotted versus SSME gimbal for two SRB gimbal configurations, 0 and +2. These results are collected for Mach numbers 0.9, 1.1 and 1.25, and are presented in Appendix C. Appendix D contains results of longitudinal data plotted versus alpha at three betas, -4, 0, and +4 degrees. Fig. 8-4 shows a sample of these results. As beta changes, the alpha origin shifts one unit to the right. Dashed lines are then used to show the variation of the data at  $f(\beta)$ . Fig. 8-5 shows lateral-directional data plotted versus beta at four alphas, -8, -4, 0 and +4 deg. As alpha changes, the beta origin shifts one unit to the right. Dashed lines are once again used to show the variation of the data at different alphas. These results are presented in Appendix E.

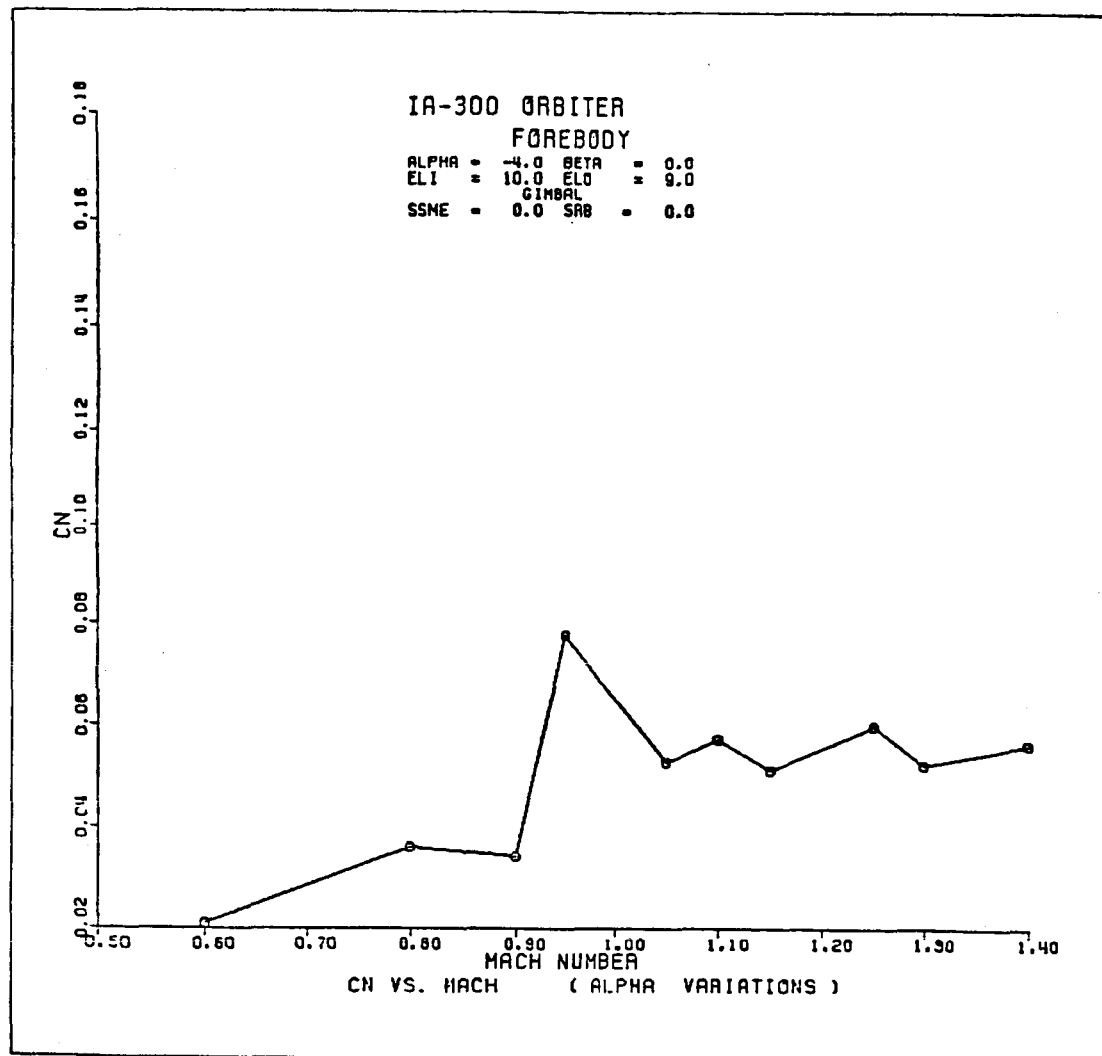


Fig. 8-2 Sample of Analysis Plots in Appendix B

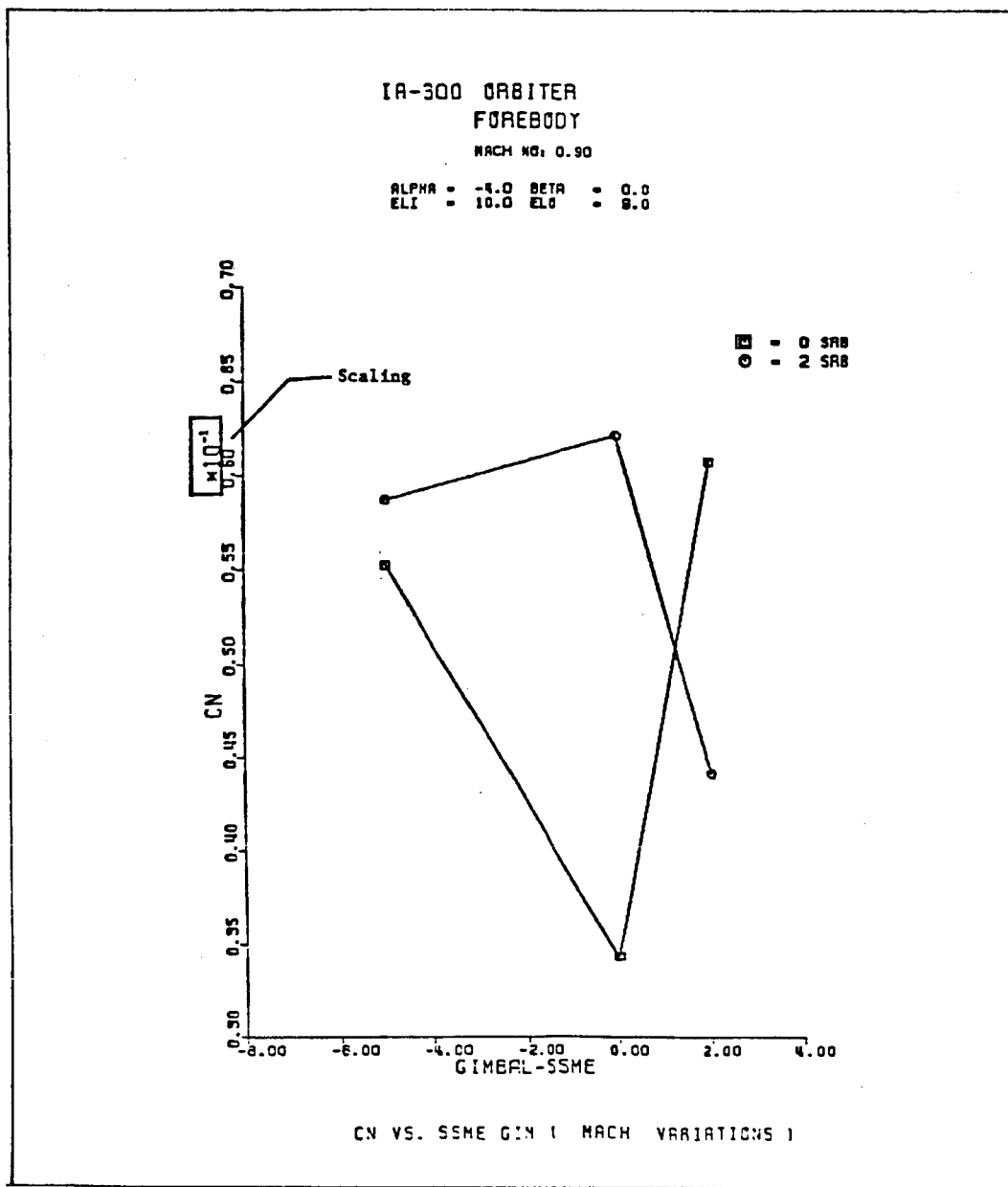


Fig. 8-3 Sample of Analysis Plots in Appendix C

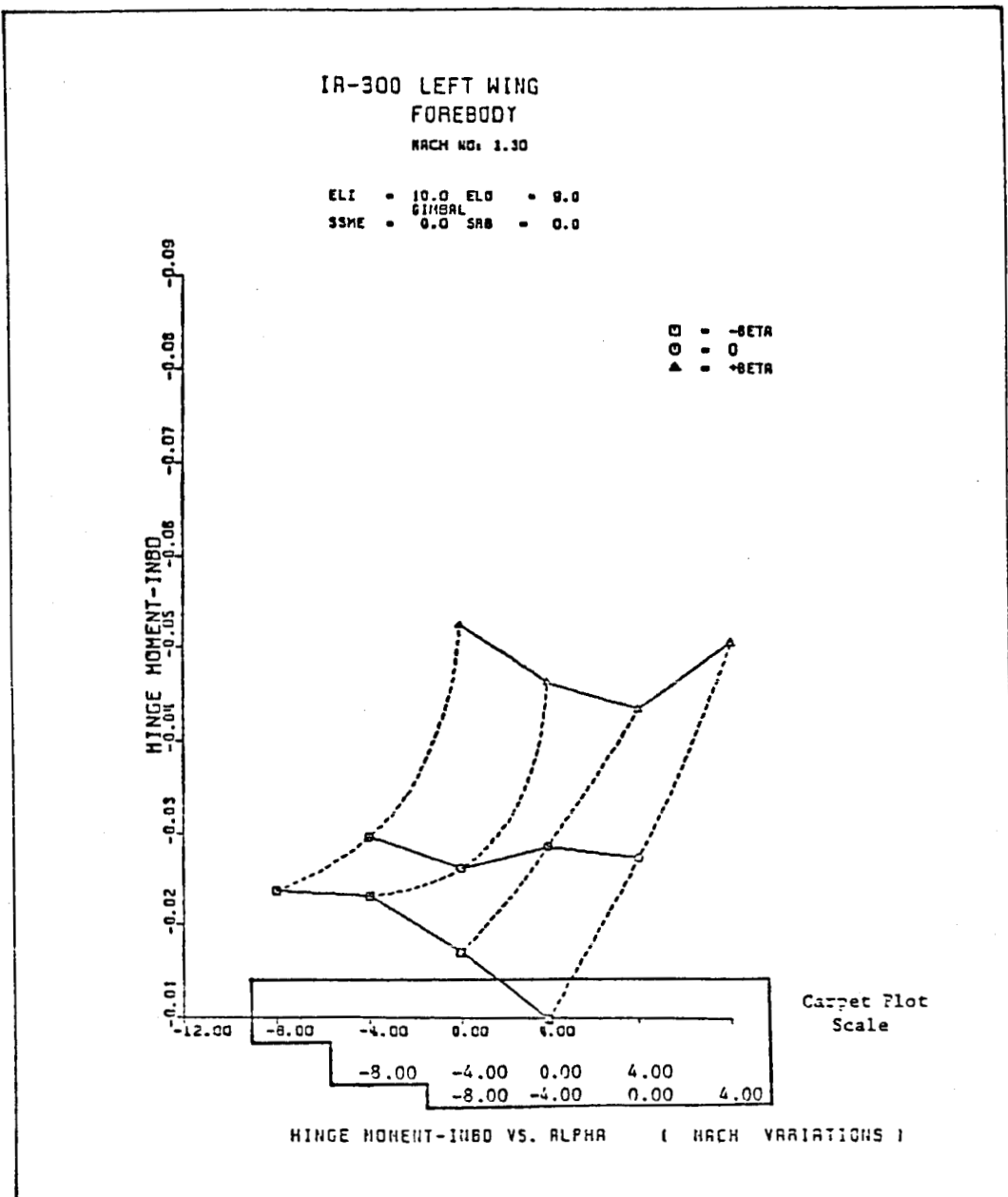


Fig. 8-4 Sample of Analysis Plots in Appendix D

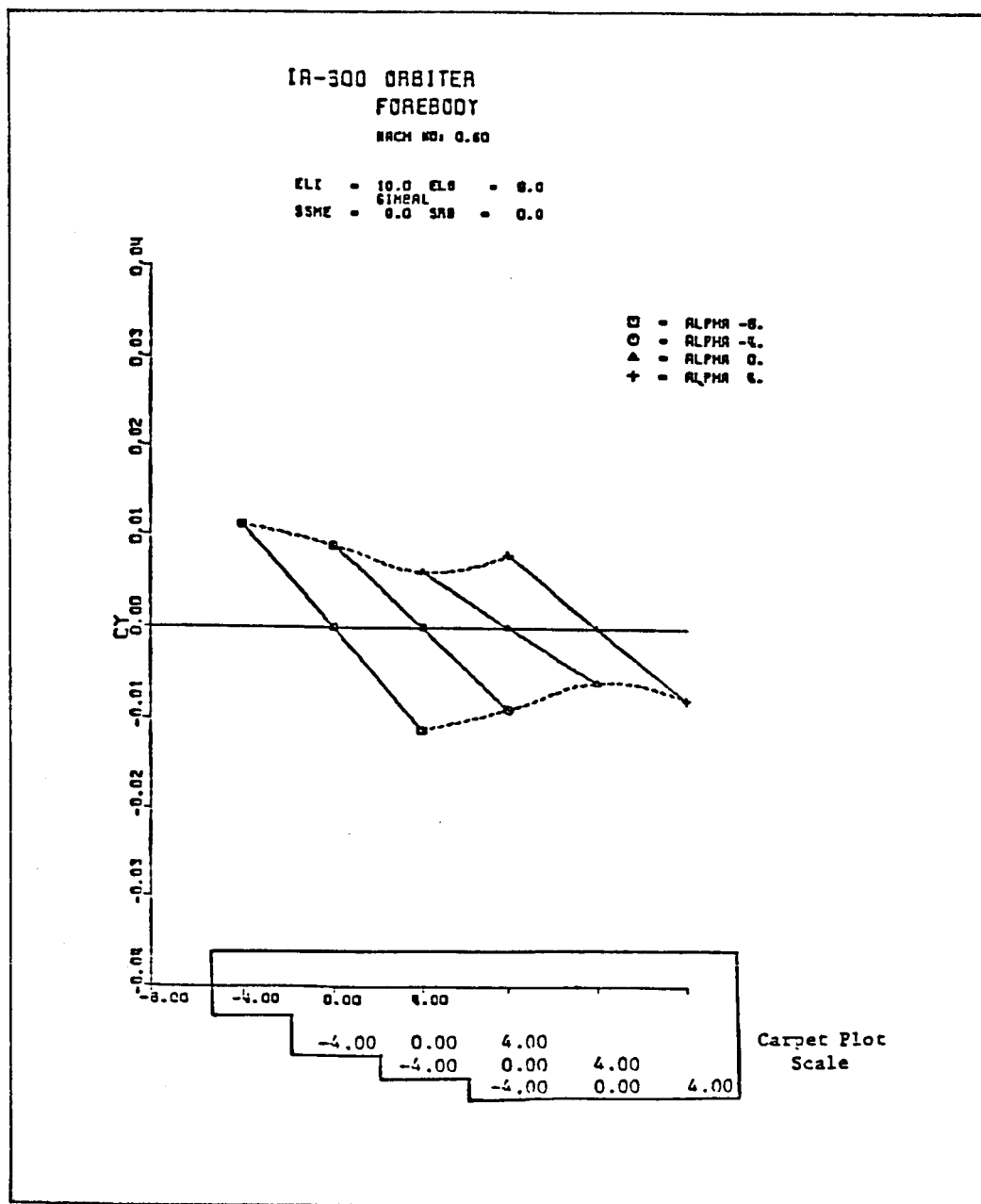


Fig. 8-5 Sample of Analysis Plots in Appendix E

9. REFERENCES

1. Spangler, R.H., "Pretest Information for Test IA300 of the 0.010-Scale 7500TS Cold Plume Space Shuttle Model in the 11-Foot Transonic Leg of the NASA/ARC Unitary Plan Wind Tunnel," Document STS82-0843A, Shuttle Integration and Satellite Systems Division, Rockwell International, January 1983.
2. Gerry, George B., "Flow Tests Results of Prototype SSME and SRB Nozzle Test (TWT-680) and 0.01-Scale SRB and SSME Nozzle Test (TWT-683)," NASA Memo ED32-83-2, February 1983.
3. Boyle, W.W. and B. Conine, "Space Shuttle Plume Simulation Application Final Report, Results and Math Model," Northrop Services, Inc., Huntsville, Ala., 28 July 1978.